Modelling mesoscale evolution of managed sandy shorelines with particular reference to Caribbean small islands

AVIDESH SEENATH

Modelling mesoscale evolution of managed sandy shorelines with particular reference to Caribbean small islands

Volume two
Figures, tables, supporting material, and appendices

Avidesh Seenath

A thesis submitted for the degree of Doctor of Philosophy in Physical Geography

Department of Geography
Durham University

September 2020

Table of contents

List of figures

List of tables

List of abbreviations and acronyms

1DH	One Dimensional Horizontal
2DH	Two Dimensional Horizontal
Bathy$Y$	Bathymetry data with a spatial resolution of Y metres
BSS	Brier Skill Score
CEM	Coastal Evolution Model
COVE	COastal Vector Evolution model
DEM	Digital Elevation Model
FVCOM	Finite Volume Community Ocean Model
GENESIS	GENEralized model for SImulating Shoreline change
IPCC	Intergovernmental Panel on Climate Change
KS	Kolmogorov-Smirnov test
KW	Kruskal-Wallis test
MAC	Mean Absolute Change
MAE	Mean Absolute Error
MNC	Mean Net Change
Mesh$X$	Mesh with a nearshore resolution of X metres
Mesh$X$Bathy$Y$	Mesh$X$ interpolated from Bathy$Y$
MHW	Mean High Water
MIKE21 HD	MIKE 21 FM Hydrodynamic
MIKE21 SM	MIKE 21 FM Shoreline Morphology
MIKE21 ST	MIKE 21 FM Sand Transport
MIKE21 SW	MIKE 21 FM Spectral Wave
MSE	Mean Square Error
NCEI	National Centers for Environmental Information
NDBC	National Data Buoy Center
NGS	National Geodetic Survey
NLD	Net Littoral Drift
NN	Nearest Neighbour
NOAA	National Oceanic and Atmospheric Administration
NSC	Net Shoreline Change
NY	New York test site
PR	Puerto Rico test site
RMSE	Root Mean Square Error
RQ	Research Question
SC	Southern California test site
SD	Standard Deviation
SLR	Sea-Level Rise
SWAN	Simulating WAves Nearshore
USACE	United States Army Corps of Engineers

USGS	United States Geological Survey
UTM	Universal Transverse Mercator
WGS84	World Geodetic System of 1984
WIS	Wave Information Study

List of notations

Symbol	Description	Units
α	Alpha	-
abs	Absolute difference	m
β	Beta	-
c	Number of samples	-
C_w	Weir coefficient	$m^{1/2}/s$
dA_z	Vertical area of the active coastal profile	m^2
D_b	Berm height	m
D_C	Depth of closure	m
$\sum$	Total	-
f	Freeboard	m
h_a	Active height of the coastal profile	m
H_{ds}	The downstream water level relative to MHW	m
H_i	Incoming wave height	m
H_{us}	The upstream water level relative to MHW	m
H_w	Weir level relative to MHW	m
i	Iteration number	-
k	Weir exponential coefficient	-
K_l	Wave loss coefficient	-
K_r	Wave reflection coefficient	-
K_t	Wave transmission coefficient	-
$kurt$	Kurtosis coefficient	-
L	Horizontal distance between D_b and D_c	m
min	Minimum	-
max	Maximum	-
n	Number of samples	-
n_i	Size of sample i	-
N	Sum of the n_i's	-
ΔN	Distance shoreline moves perpendicular to its orientation	m
Q	Discharge over a hard defence structure	m^3
ΔQ	Change in littoral drift gradients	m^3
R	Shoreline retreat	m
R_i	Sum of ranks in the i^{th} sample	
Sh_{int}	Initial shoreline position	x, y (m)
Sh_{obs}	Observed shoreline position	x, y (m)
Sh_{pred}	Predicted shoreline position	x, y (m)
ΔShc_{obs}	Observed net shoreline change	m
ΔShc_{pred}	Predicted net shoreline change	m
$skew$	Skewness coefficient	-

Symbol	Description	Units
SLR	Sea-level rise	m
Δt	Change in time	s
vol	Change in sediment volume	m^3
vol_{error}	Error in deposited/eroded sediment volume	m^3
W	Length (width) of a hard defence structure	m
Δy	Change in shoreline position	m

Operational definitions

Active coastal profile: Area extending from the beach berm to closure depth.

Bathymetry: Seafloor topography relative to MHW (m).

Bathymetry (Initial): Seafloor topography (m) observed at the start of a simulation. The initial bathymetry is the baseline for simulating changes in shoreline morphology.

Bathymetry (Observed): Seafloor topography (m) observed at the end of a simulation. The observed bathymetry is the baseline for quantifying shoreline evolution prediction accuracy.

Beach berm: Area of the beach mostly above water and actively influenced by waves at some point in the tide. The beach berm is the inshore extent of the active coastal profile.

Bed friction: Free parameter specifying flow resistance over the model bathymetry. The optimal bed friction value for modelling shoreline evolution is determined from model calibration, bounded by physically realistic values of Chow (1959) Manning's n ($m^{1/3}/s$).

Boundary conditions: Constraints and values of variables required to simulate shoreline evolution over a defined period. Examples include bathymetry, tides, and waves.

Closure depth: Depth beyond which there is no significant change in bottom elevation and no significant sediment transport between nearshore and offshore. The closure depth is the offshore extent of the active coastal profile.

Cross-shore: Perpendicular to the shoreline orientation.

Cross-shore transport: Sediment transport perpendicular to the shoreline orientation.

Discharge coefficient: Ratio between the true and theoretical flow rate.

Edge map: Map dividing the nearshore into strips of shoreface. Each strip is perpendicular to the shoreline orientation and has one predefined active coastal profile. The edge map assigns each mesh element to a shoreline edge to facilitate MIKE21 one-line theory morphology update.

Grading coefficient: Dimensionless free parameter describing sediment distribution in the coastal system. The optimal grading coefficient for modelling shoreline evolution is determined from model calibration, bounded by physically realistic values defined by Folk and Ward (1957).

Grain size: Free parameter defining the median sand grain size (mm) in the coastal system. The optimal sand grain size (mm) for modelling shoreline evolution is determined from model calibration, bounded by physically realistic values defined by Wentworth (1922).

Initial conditions: Information required at the start of a simulation to define all initial model states. Examples of initial conditions are bathymetry, active coastal profile, and initial shoreline, all of which form the baseline for simulating shoreline evolution.

Littoral drift: Volume of sand (m^3/s) moving past a shoreline edge in the same direction as the longshore current at any point in a simulation.

Littoral drift (gross): Directionless measure of the total sediment volume (m^3) transported past a shoreline edge over a defined period.

Littoral drift (net): Difference between the total sediment volume (m^3) transported to the right and left of a shoreline edge over a defined period. Net littoral drift is of primary concern in shoreline evolution studies because it indicates the predominant direction of sediment transport.

Longshore: Parallel to the shoreline orientation.

Longshore transport: Sediment transport parallel to the shoreline orientation.

Managed sandy shoreline: A shoreline comprising non-cohesive sediments, stabilised by hard defences, such as groynes and breakwaters.

MHW: Average of all high-water levels measured over 19 years.

Mean absolute error: Average absolute difference between observed and predicted net shoreline change.

Mesh: An unstructured grid of triangular elements defining the spatial discretisation for simulating shoreline evolution.

Mesh independence: A mesh is independent if a change in its discretisation has no significant effect on net littoral drift and net shoreline change predictions.

Model calibration: Process of adjusting free parameters' values within known physically realistic values to obtain the best fit between observed and predicted net shoreline change.

Model optimisation: Identifying the parameter and variable set that produces the best fit between observed and predicted net shoreline change.

Model performance: A measure of the accuracy of model predictions relative to related observations (e.g. mean absolute error).

Model sensitivity: Model response to a change in input.

Model verification: A quantitative and objective description of how well a model represents the real system (e.g. Brier skill score).

Net shoreline change (observed): Difference between initial and observed shoreline position (m). A negative (positive) net shoreline change indicates erosion (accretion).

Net shoreline change (predicted): Difference between initial and predicted shoreline position (m). A negative (positive) net shoreline change indicates erosion (accretion).

Nearshore: Area extending from the land boundary to closure depth in the model domain.

Nearshore (Puerto Rico test site): Area extending from the land boundary to seaward boundary of the coral reef network in the model domain.

Offshore: Area extending from the closure depth to sea boundary in the model domain.

Offshore (Puerto Rico test site): Area extending from the seaward boundary of the coral reef network to the sea boundary in the model domain.

Parameter: A constant defined before running a simulation (e.g. bed friction and sediment porosity).

Relative sand density: Dimensionless free parameter describing the ratio of the weight of a given sand volume to the weight of an equal volume of water. Relative sand density is 2.65.

Sea-level rise: Average rise in water level (m) relative to MHW over time.

Sediment porosity: Dimensionless free parameter describing the porosity of sand sediments in the coastal system. The optimal sediment porosity for modelling shoreline evolution is determined from model calibration, bounded by physically realistic values defined by Nimmo (2013).

Shields parameter: Dimensionless parameter defining the initiation of sediment motion in the flow.

Shoreface strip: A shoreface strip defines one cross-shore section in the model domain. Each shoreface strip has a predefined active coastal profile.

Shoreline: Zero-depth contour in the bathymetry (MHW line).

Shoreline edge: An initial shoreline node that moves shore-normal from a change in littoral drift gradients.

Shoreline (initial): Zero-depth contour in the initial bathymetry. The initial shoreline is the baseline for mapping shoreline change.

Shoreline (observed): Zero-depth contour in the observed bathymetry. The observed shoreline is the baseline for quantifying net shoreline change prediction accuracy.

Shoreline (predicted): Shoreline output (x, y) at the end of a simulation.

Significant wave height: Average height (m) of the highest one-third of waves in a year.

Still water depth: Water depths (m) in the model bathymetry.

Surface elevation: Water levels (m) in the model domain relative to the zero-depth contour in the model bathymetry at any point in a simulation.

Tide: Water level (m) above or below MHW at any point in time.

Total water depth: Still water depth (m) + surface elevation (m).

Variable: A condition in the model that changes during a simulation, such as tides, waves, and wind.

Wind direction: Air movement direction (deg) at any point in time.

Wind speed: Air movement rate (m/s) at any point in time.

Wave climate: Wave height (m), period (sec), and direction (deg) at any point in time.

Weir coefficient: A function of the gravitational constant and discharge coefficient and geometry of a hard defence structure. The optimal weir coefficient ($m^{1/2}/s$) for modelling shoreline evolution is determined from model calibration, bounded by known physically realistic values defined by Horton (1906).

01
Introduction and research questions: figures and tables

Table 1.1 External forcings associated with each established scale of shoreline evolution (Stive et al., 2002).

Scale	Natural forcing	Human forcing
Macro *Space dimensions: ≥ 100 km* *Time dimensions: centuries to millennia*	⇒ Sediment availability ⇒ Relative sea-level changes ⇒ Differential bottom changes ⇒ Geological setting ⇒ Long-term climate changes ⇒ Paleomorphology (inherited morphology)	⇒ Human-induced climate change ⇒ Major river regulation ⇒ Major coastal structures ⇒ Major reclamations and closure ⇒ Structural coastal (non)management
Meso *Space dimensions: ~ 10 – 100 km* *Time dimensions: decades to centuries*	⇒ Relative sea-level changes ⇒ Regional climate variations ⇒ Coastal inlet cycles ⇒ Sand waves ⇒ Extreme events	⇒ River regulation ⇒ Coastal structures ⇒ Reclamations and closures ⇒ Coastal (non)management ⇒ Natural resource extraction (subsidence)
Synoptic *Space dimensions: ~ 1 – 5 km* *Time dimensions: years to decades*	⇒ Wave climate variations ⇒ Surf zone bar cycles ⇒ Extreme events	⇒ Surf zone structures ⇒ Shore nourishments
Micro *Space dimensions: ~ 10 m – 1 km* *Time dimensions: hours to years*	⇒ Wave, tide, and surge conditions ⇒ Seasonal climate variations	

02
Test sites and data: figures and tables

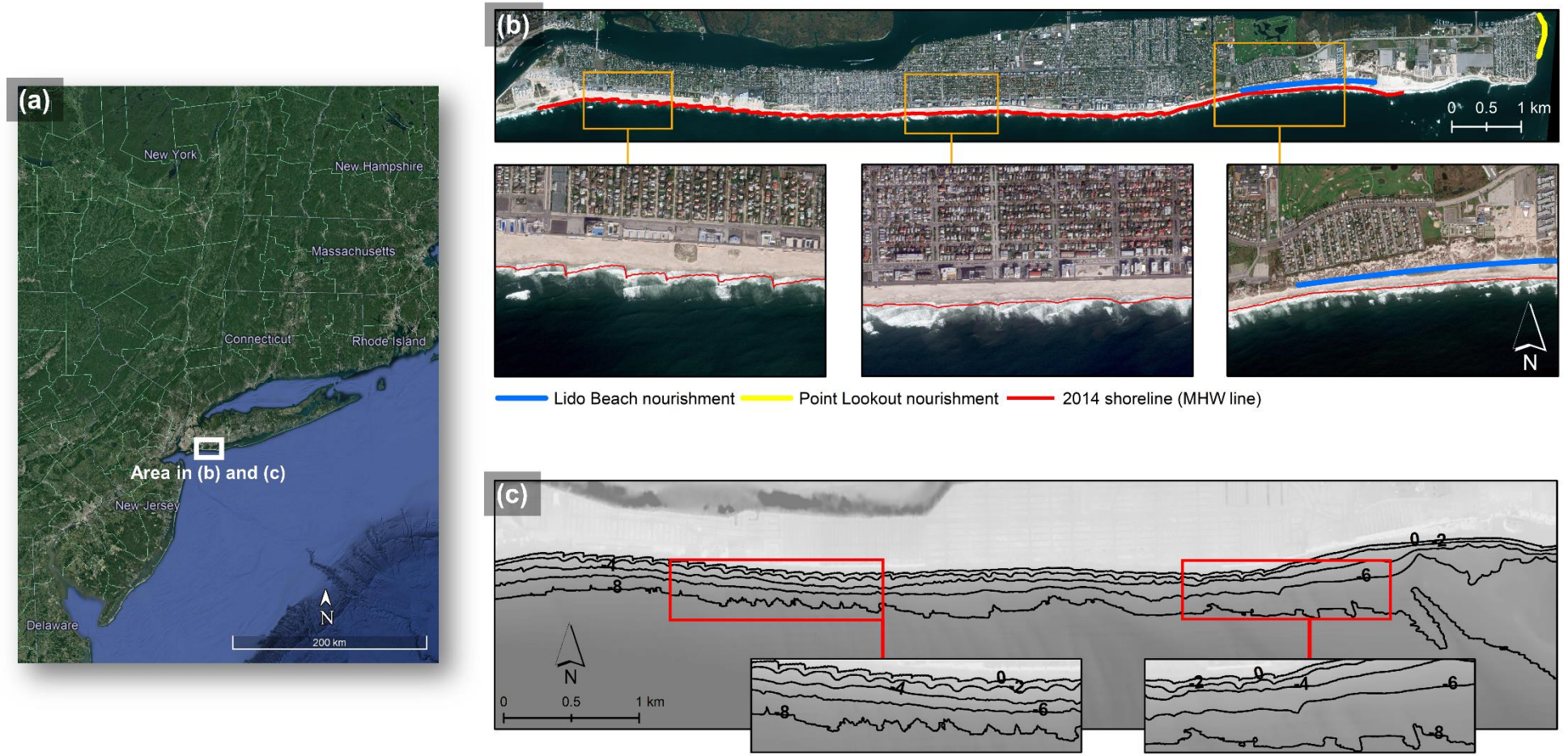

Fig. 2.1 Test site in New York. (a) Location along the United States East Coast. (b) 2012 GeoEye-1 image of the main site features: developed sandy coast, use of groynes for shoreline stabilisation, shoreline deformations around groynes, concave shoreline in the east and west, and a generally straight shoreline elsewhere. (c) Contour map illustrating shore-parallel depth contours in the nearshore. *Credits*: Google Earth (satellite image in a) and LAND INFO Worldwide Mapping (GeoEye-1 image in b).

Fig. 2.2 Test site in Puerto Rico. (a) Location in the Caribbean region. (b) 2013 orthophoto of the main site features: developed sandy coast, cuspate-cape shoreline, coral reefs, use of breakwaters and groynes for shoreline stabilisation, and use of seawalls for private property protection. (c) Contour map illustrating a complex planform morphology in the nearshore, defined by non-parallel depth contours. *Credits*: DigitalGlobe (satellite image in a) and USGS (orthophoto in b).

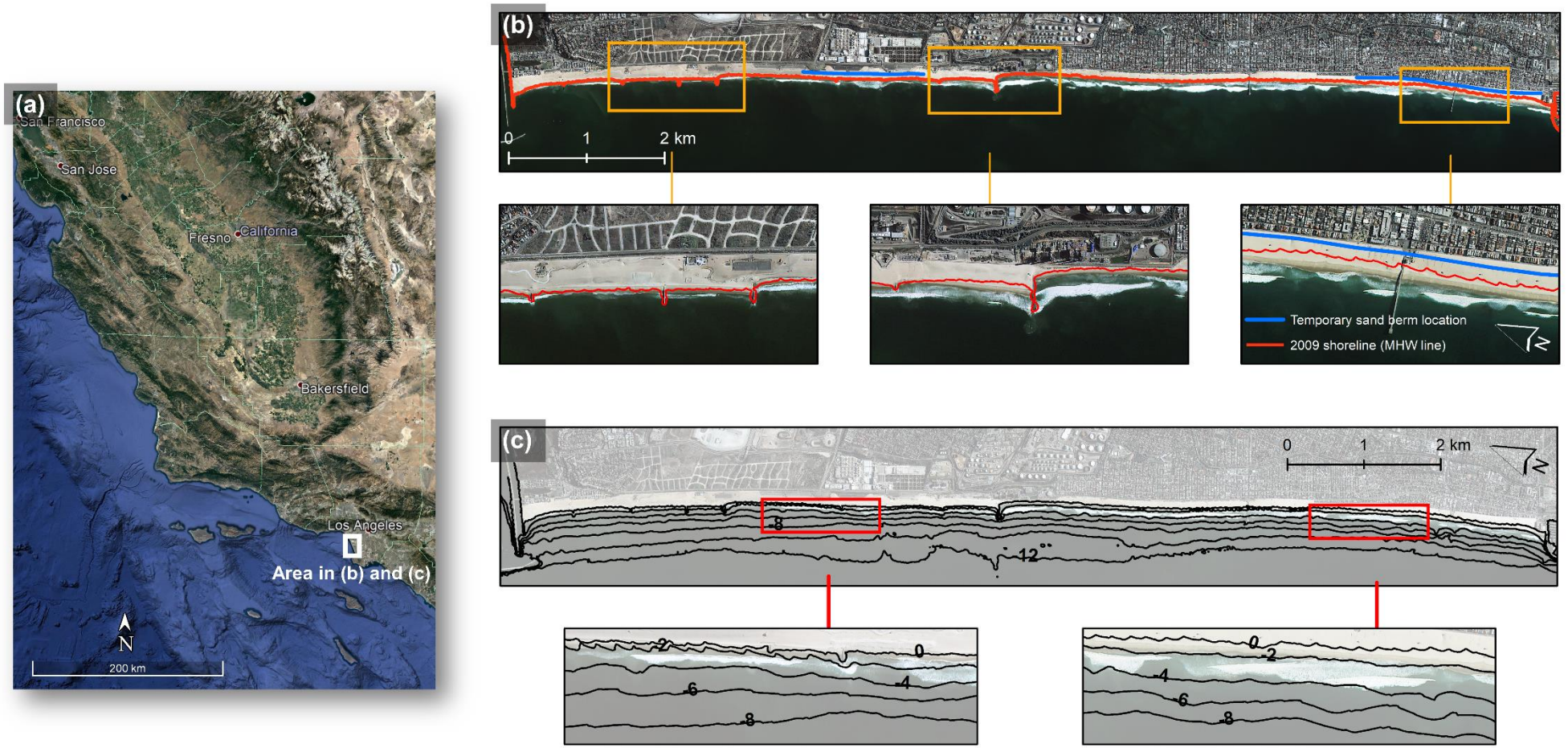

Fig. 2.3 Test site in Southern California. (a) Location along the United States West Coast. (b) 2013 KOMPSAT-2 image of the main site features: developed sandy coast, use of groynes and jetties for shoreline management, and a generally straight shoreline, with deformations mainly around groynes. (c) Contour map illustrating shore-parallel depth contours in the nearshore. *Credits*: DigitalGlobe (satellite image in a) and LAND INFO Worldwide Mapping (KOMPSAT-2 image in b).

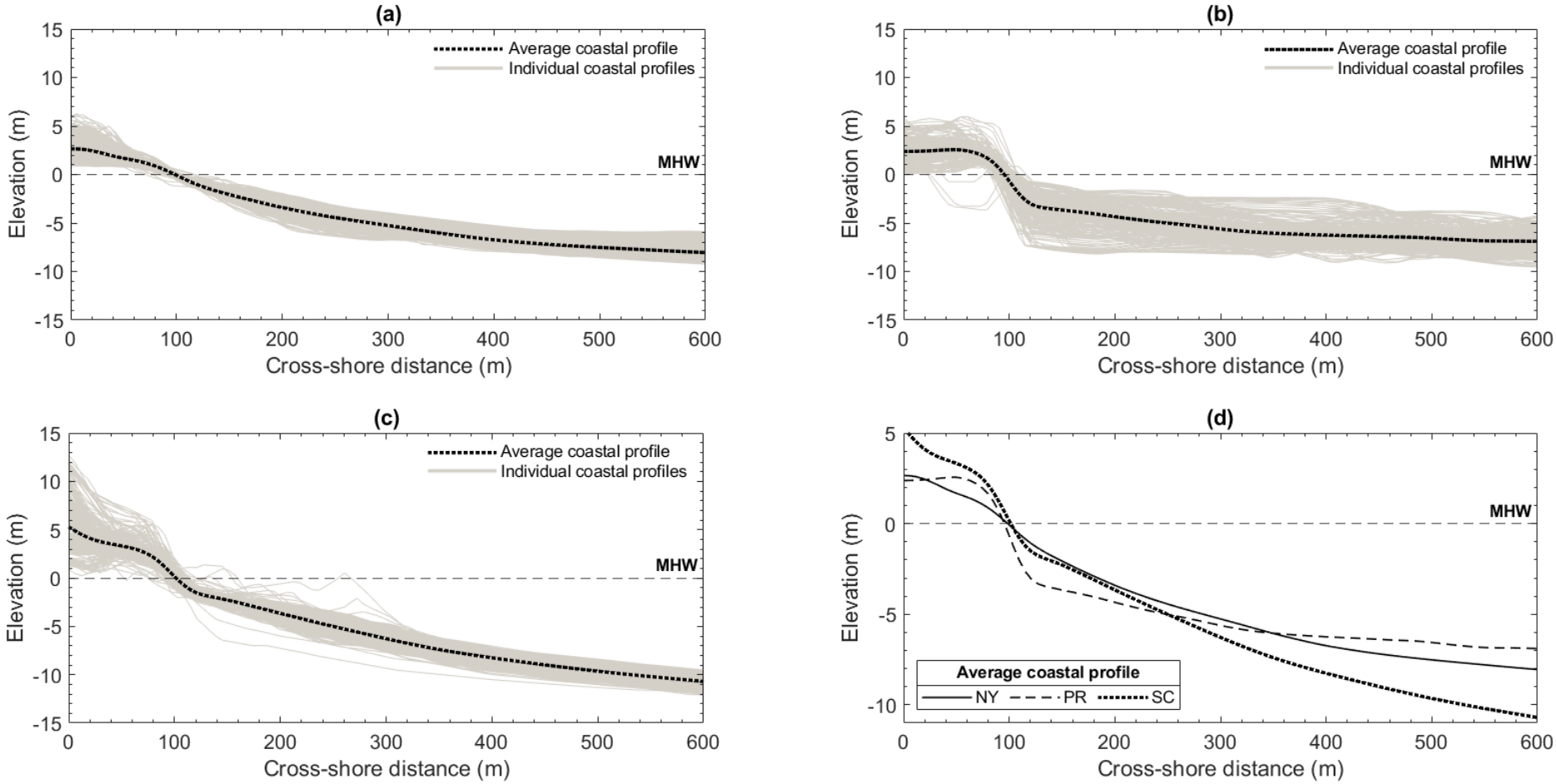

Fig. 2.4 Each test site's coastal profile morphology. (a), (b) and (c) show the coastal profile envelope and average coastal profile in the New York (NY), Puerto Rico (PR), and Southern California (SC) test site, respectively. The coastal profile envelope comprises individual coastal profiles sampled every 15 m longshore. The average coastal profile is the average of the individual coastal profiles. (d) compares each test site's average coastal profile morphology.

Table 2.1 Boundary conditions data for assessing model sensitivity in the New York (NY), Puerto Rico (PR), and Southern California (SC) test site.

Data	Time-period	Horizontal datum	Vertical datum	Units	Resolution	Source
Initial bathymetry	NY: 01-Jan-2014 PR: 01-Oct-2014 SC: 01-Jan-2009	WGS84	MHW	m	NY; PR: 3 m SC: 10 m	NY: NCEI (2017a) PR: NCEI (2019) SC: NCEI (2017b)
Observed bathymetry	NY: 01-Feb-2016 PR: 31-Mar-2016 SC: 02-Aug-2011				NY; PR: 3 m SC: 1 m	NY: NOAA (2017b) PR: NOAA (2019) SC: NOAA (2017a)
Tide	NY: 01-Jan-2014 – 01-Feb-2016 PR: 01-Oct-2014 – 31-Mar-2016 SC: 01-Jan-2009 – 02-Aug-2011	Not applicable	Not applicable		NY; PR; SC: 6 min	NY: NOAA (2017d) PR: NOAA (2017c) SC: NOAA (2017e)
Wind speed				m/s		
Wind direction				deg		
Wave height				m	NY; PR: 60 min SC: 30 min	NY: NDBC (2017a) PR: NDBC (2017b) SC: NDBC (2017c)
Wave direction				deg		
Wave period				s		

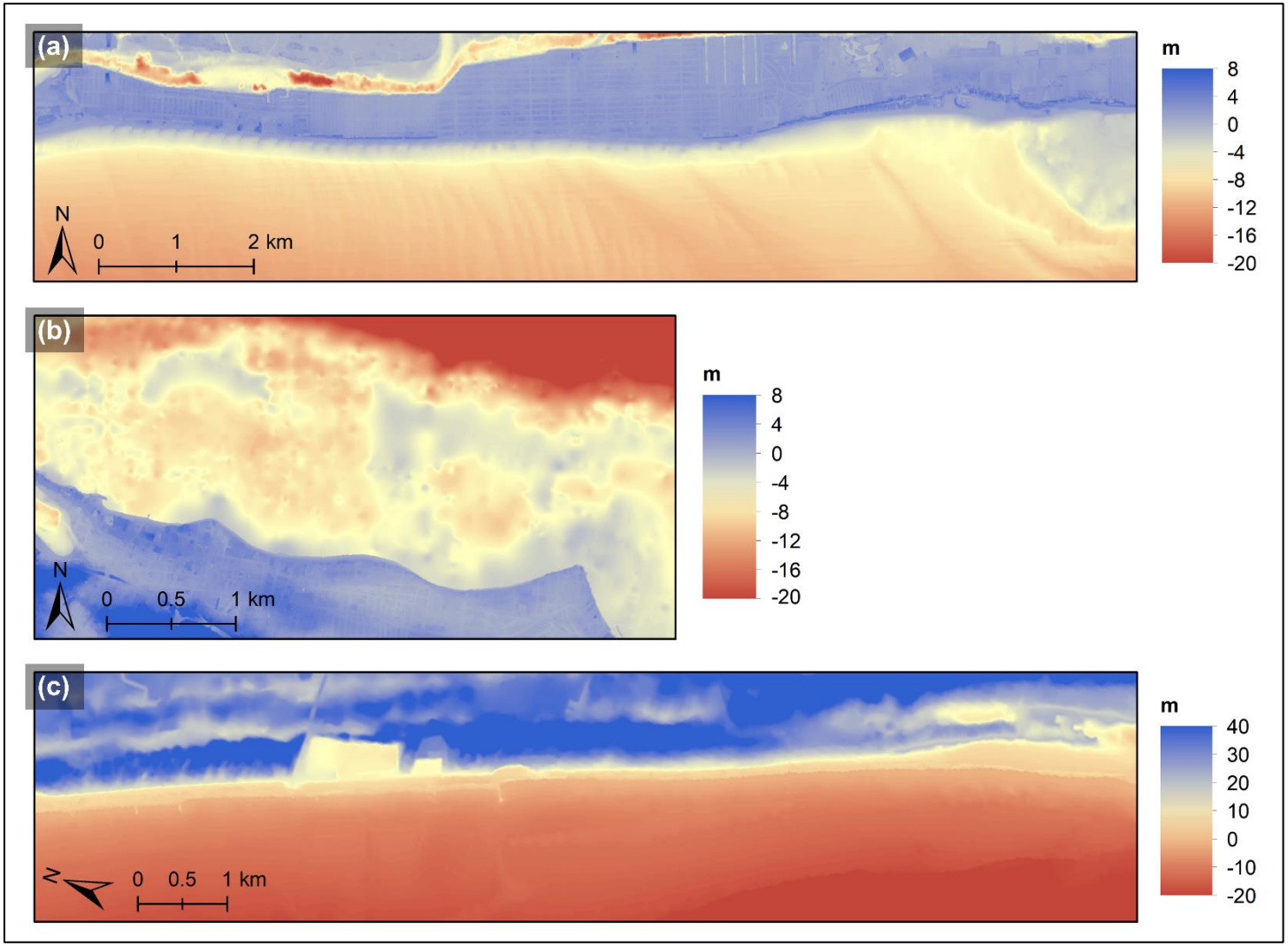

Fig. 2.5 Initial bathymetry data for assessing model sensitivity in the New York (a), Puerto Rico (b), and Southern California (c) test site. (a) and (b) have a spatial resolution of 3 m. (c) has a spatial resolution of 10 m.

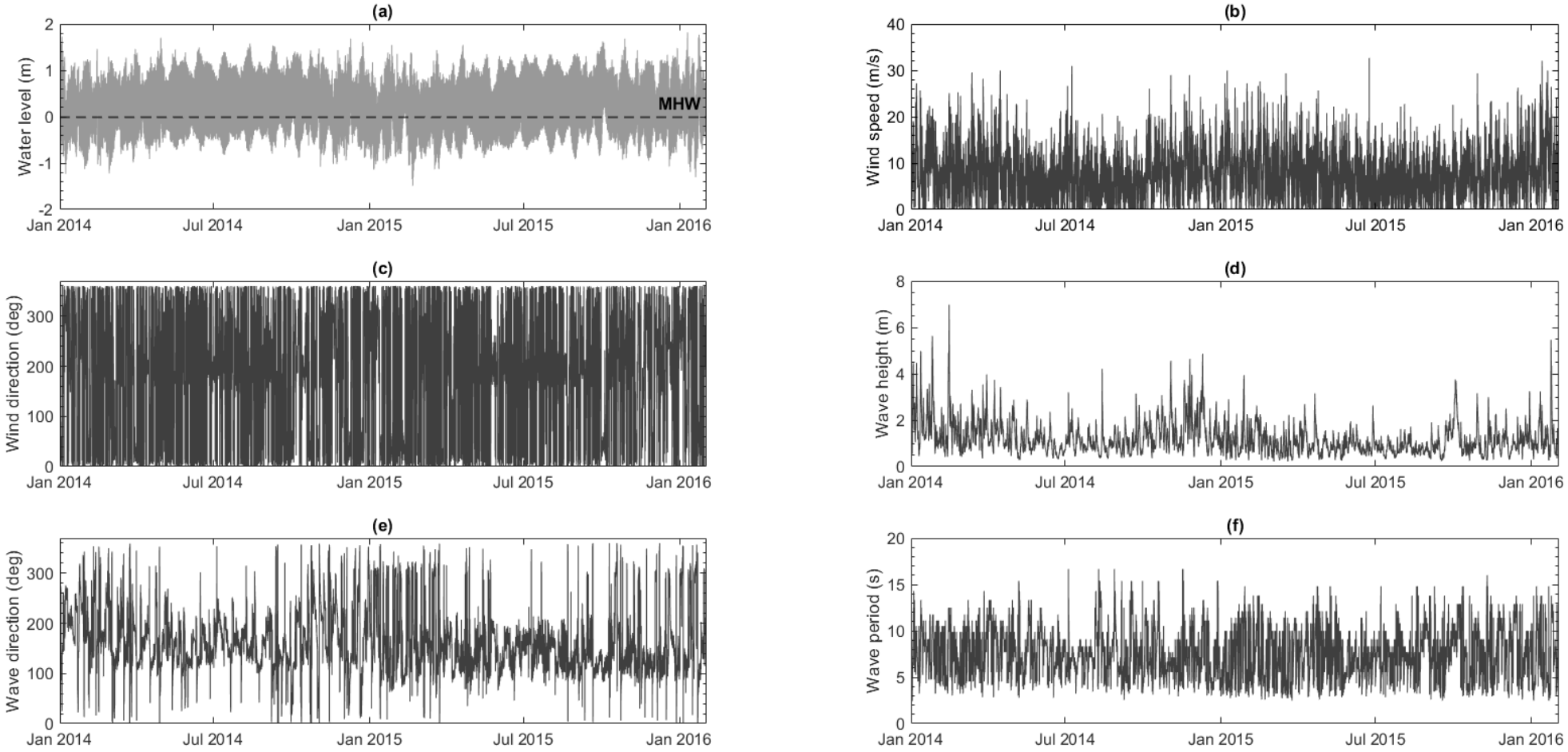

Fig. 2.6 Tide (a), wind speed (b), wind direction (c), wave height (d), wave direction (e), and wave period (f) time series data for assessing model sensitivity in the New York test site. The time series data in (a) to (f) are from 01-Jan-2014 to 01-Feb-2016. (a) to (c) are from NOAA (2017d) and have a 6 min resolution. (d) to (f) are from NDBC (2017a) and have a 60 min resolution.

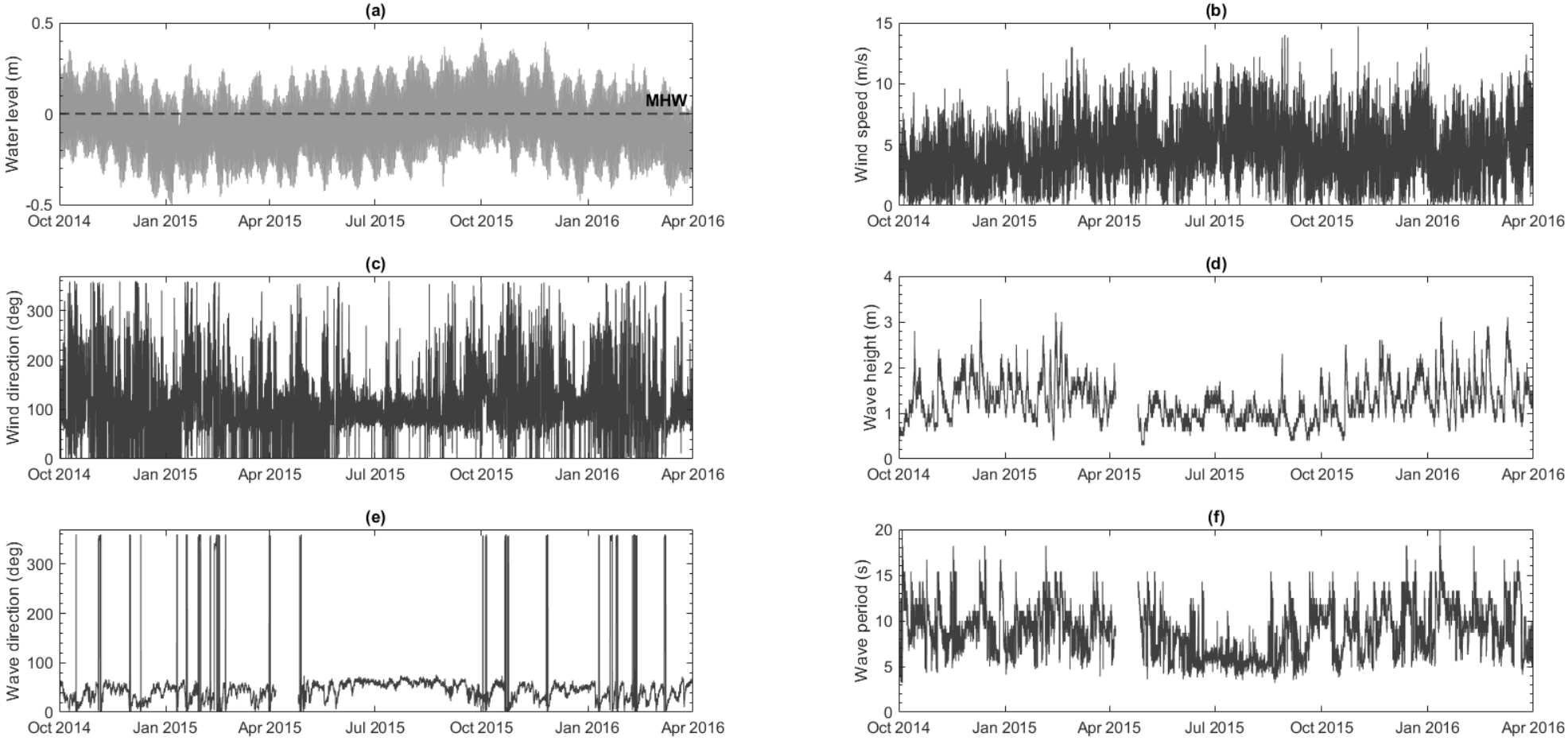

Fig. 2.7 Tide (a), wind speed (b), wind direction (c), wave height (d), wave direction (e), and wave period (f) time series data for assessing model sensitivity in the Puerto Rico test site. The time series data in (a) to (f) are from 01-Oct-2014 to 01-Apr-2016. (a) to (c) are from NOAA (2017c) and have a 6 min resolution. (d) to (f) are from NDBC (2017b) and have a 60 min resolution.

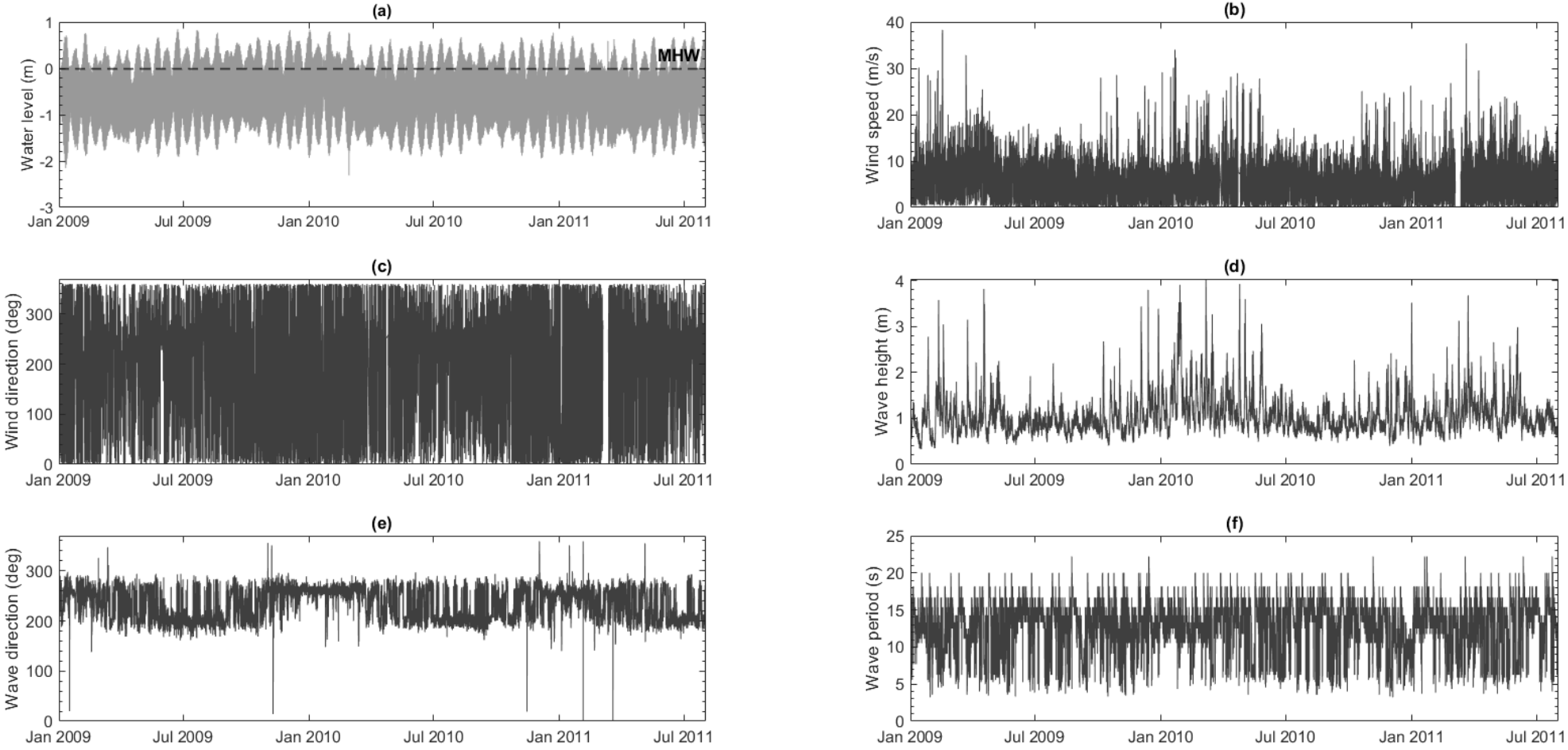

Fig. 2.8 Tide (a), wind speed (b), wind direction (c), wave height (d), wave direction (e), and wave period (f) time series data for assessing model sensitivity in the Southern California test site. The time series data in (a) to (f) are from 01-Jan-2009 to 02-Aug-2011. (a) to (c) are from NOAA (2017e) and have a 6 min resolution. (d) to (f) are from NDBC (2017c) and have a 30-min resolution.

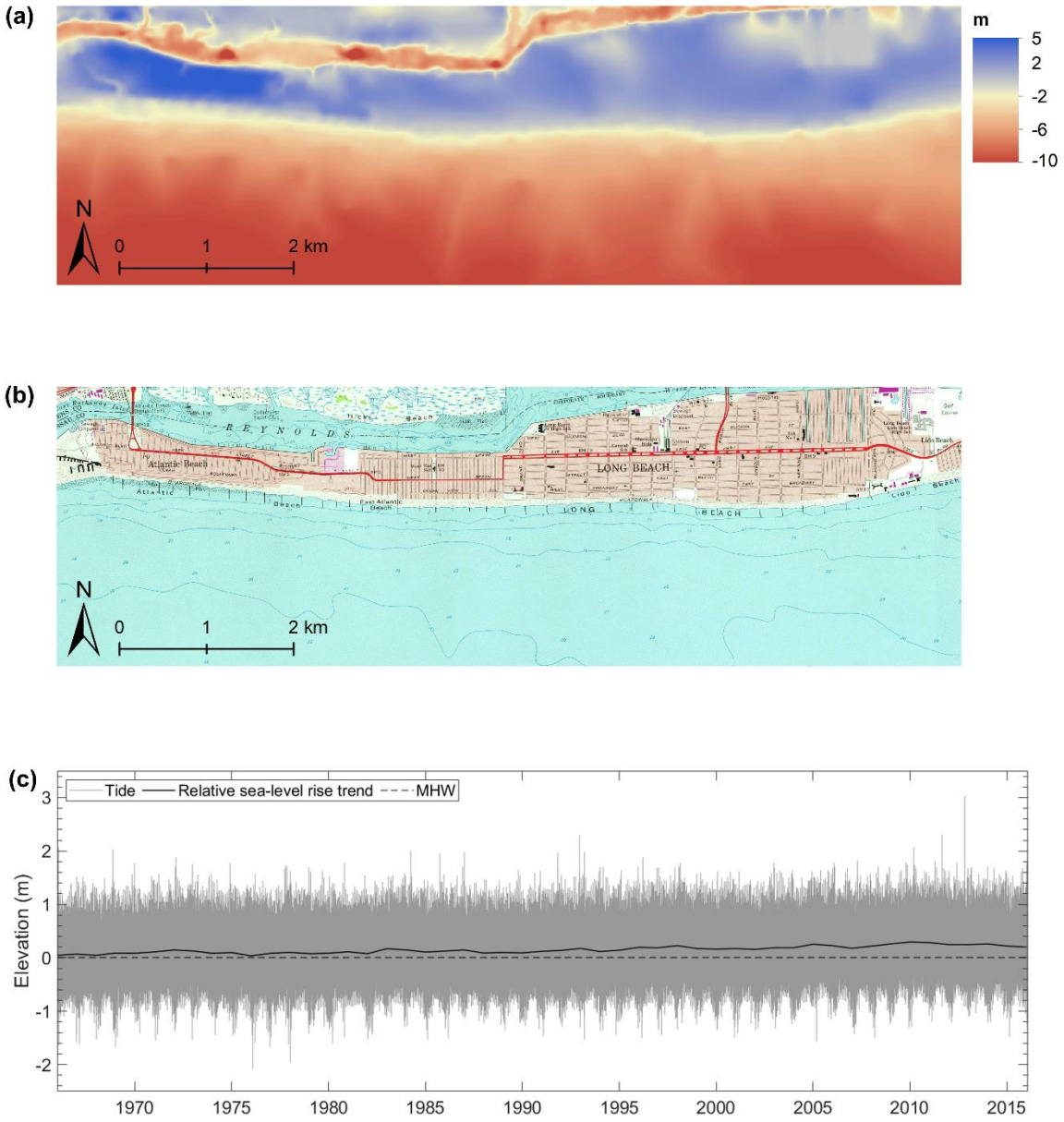

Fig. 2.9 Initial bathymetry and tide data for hindcasting meso timescale shoreline evolution (1966 to 2016) in the New York test site. (a) 10 m resolution 1966 coastal relief model of the New York test site from LAND INFO Worldwide Mapping, the initial bathymetry. (b) 1966 topography map of the New York test site from the USGS, the source of (a). (c) New York test site 1966 to 2016 tide data (60 min resolution) and associated relative sea-level rise trend from NOAA (2017d).

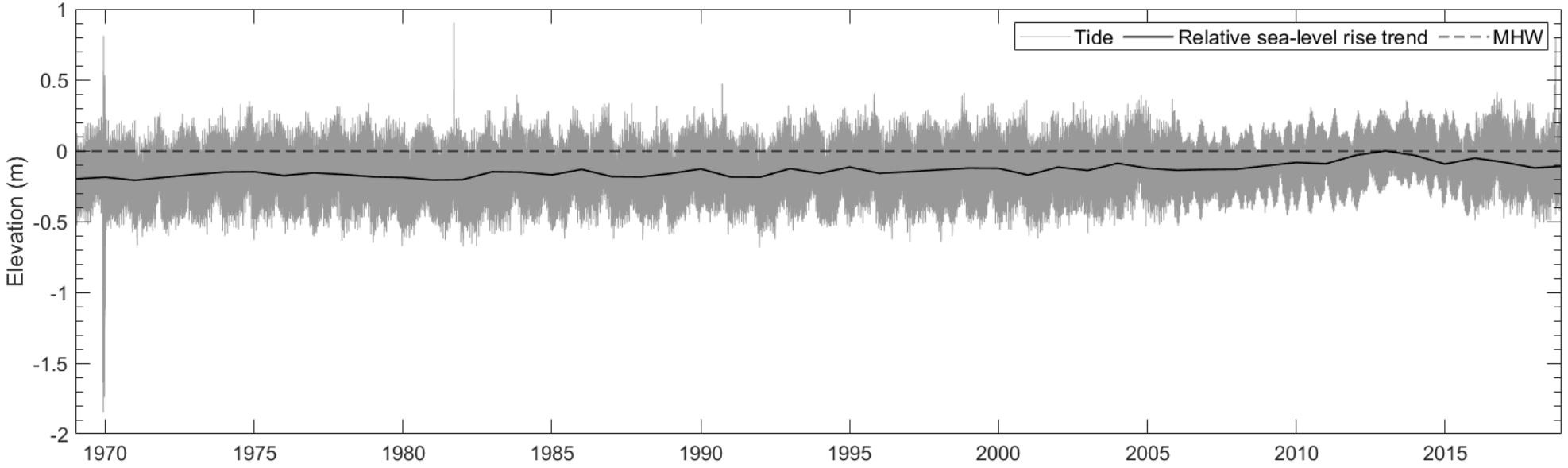

Fig. 2.10 1969 to 2018 tide time series data and associated relative sea-level rise trend for running meso timescale shoreline evolution simulations in the Puerto Rico test site. The tide data are from NOAA (2017c) and have a 60 min resolution.

03
Model selection and approach: figures and tables

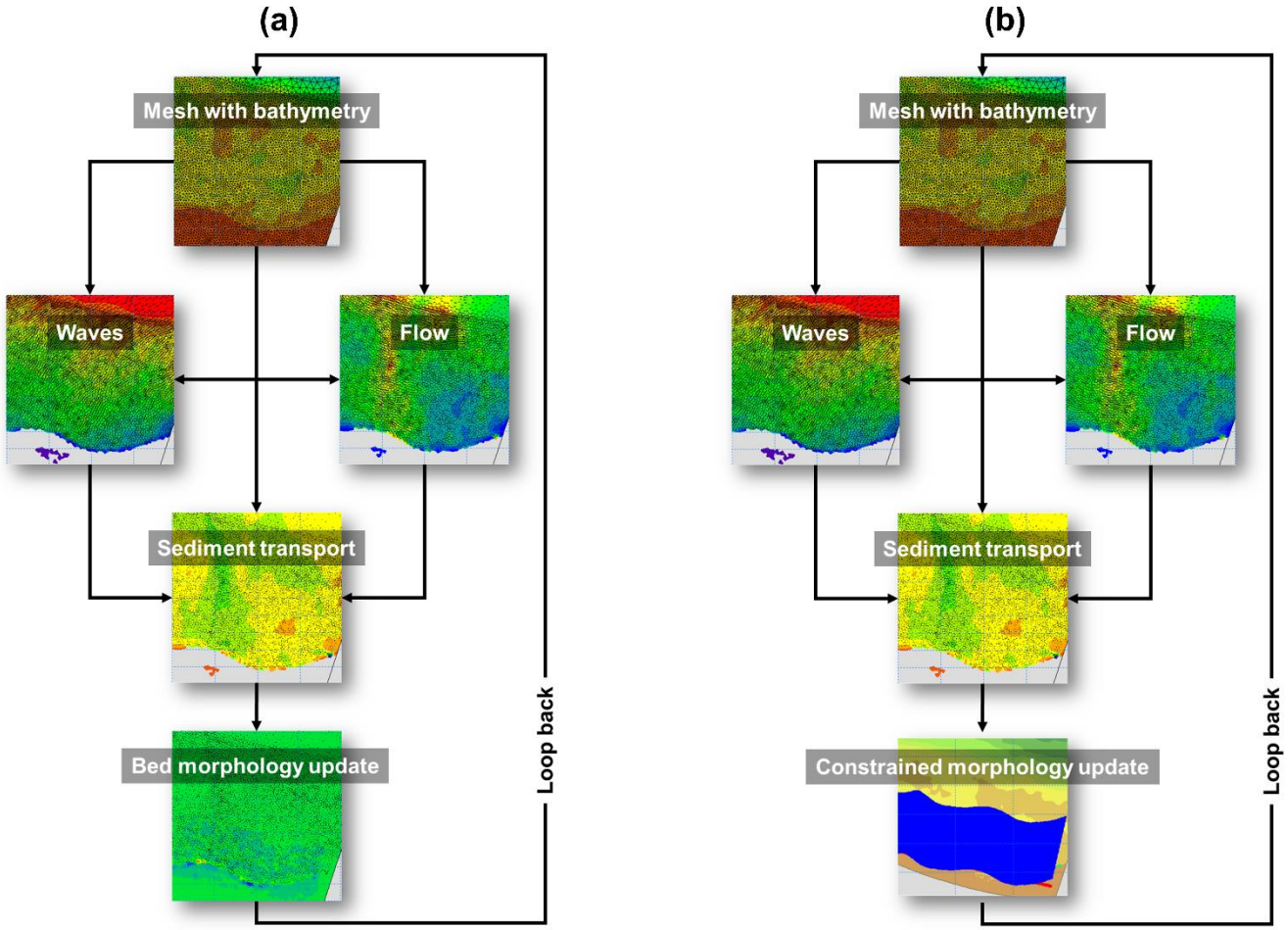

Fig. 3.1 Computational framework of 2DH (a) and hybrid models (b). The main difference between both model types is the morphology update. (a) shows that 2DH models update the morphology in the entire domain at each time-step. The change in morphology from one time-step updates the mesh bathymetry for the next time-step to continue the simulation in 2DH models. (b) shows that hybrid models maintain the same principles but update the morphology within the active coastal profile only.

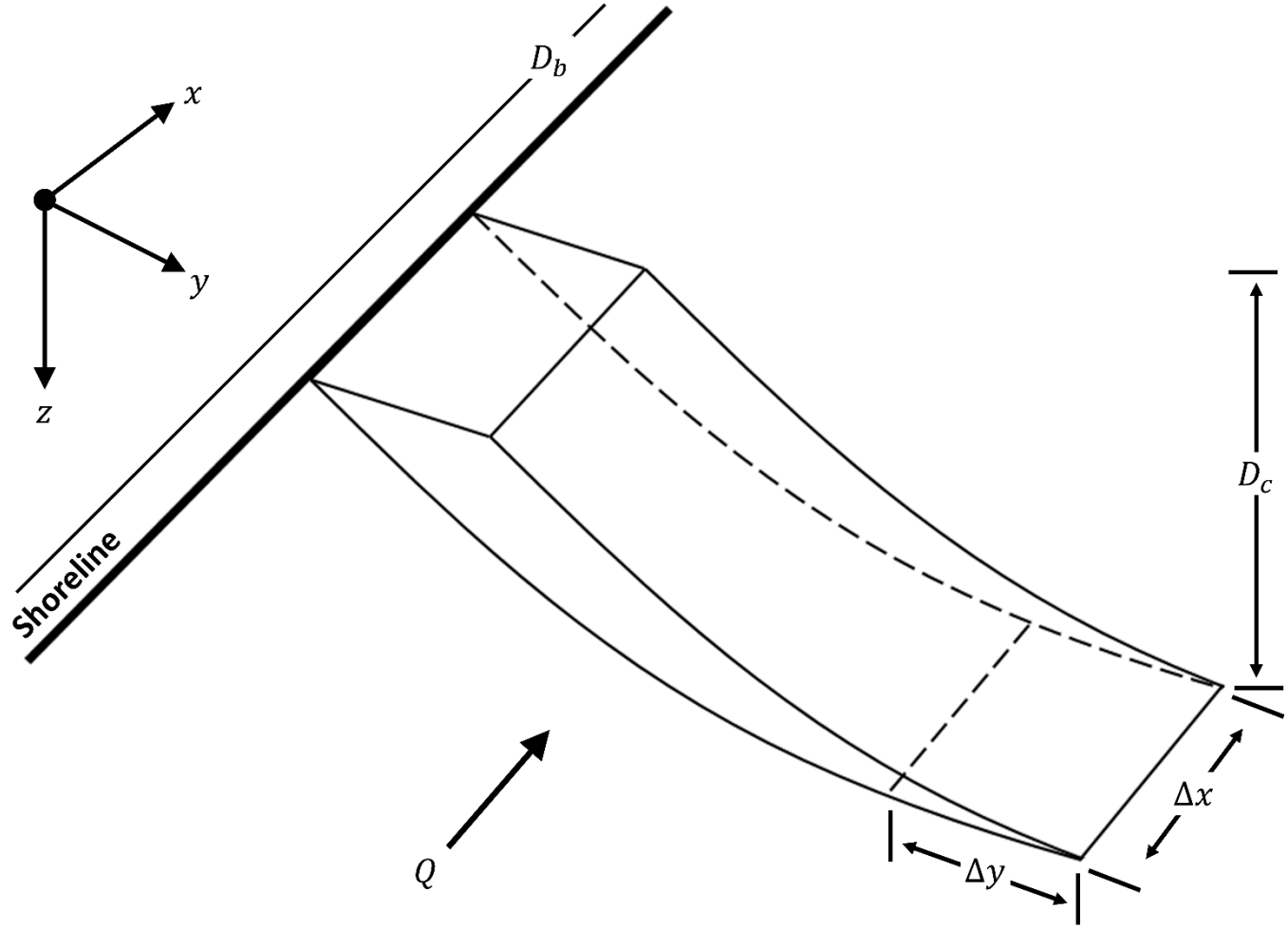

Fig. 3.2 Schematic illustration of the one-line theory, modified from Larson et al. (1987). The one-line theory assumes the active coastal profile, defined as the area extending from beach berm (D_b) to closure depth (D_c), keeps its shape and moves shore-normal (Δy) from a change in longshore sediment transport gradients (Q).

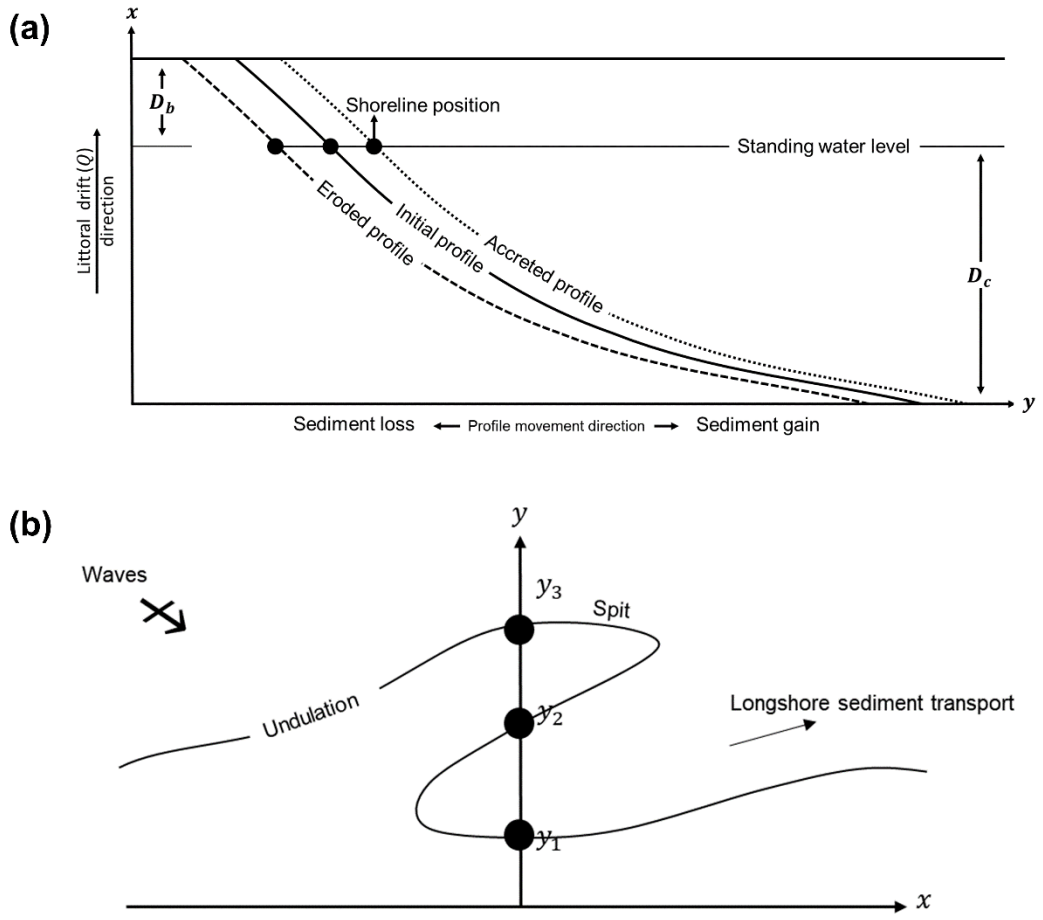

Fig. 3.3 Basic premise and the main limitation of the one-line theory equation. (a) shows that shoreline change is a function of the shore-normal movement of the active coastal profile (D_b to D_c); sediment gain (loss) from Q shifts the active coastal profile seaward (landward). (b) shows an example of a complicated shoreline configuration: an undulation with a spit. The shoreline may have three crossings (y_1, y_2, y_3) in areas with spits for a given x coordinate as in (b). The fixed x, y coordinates in the one-line theory equation prevent one-line models from simulating longshore growth of spits and shoreline deformations from hard defences. *Credits*: (b) modified from Kaergaard and Fredsoe (2013).

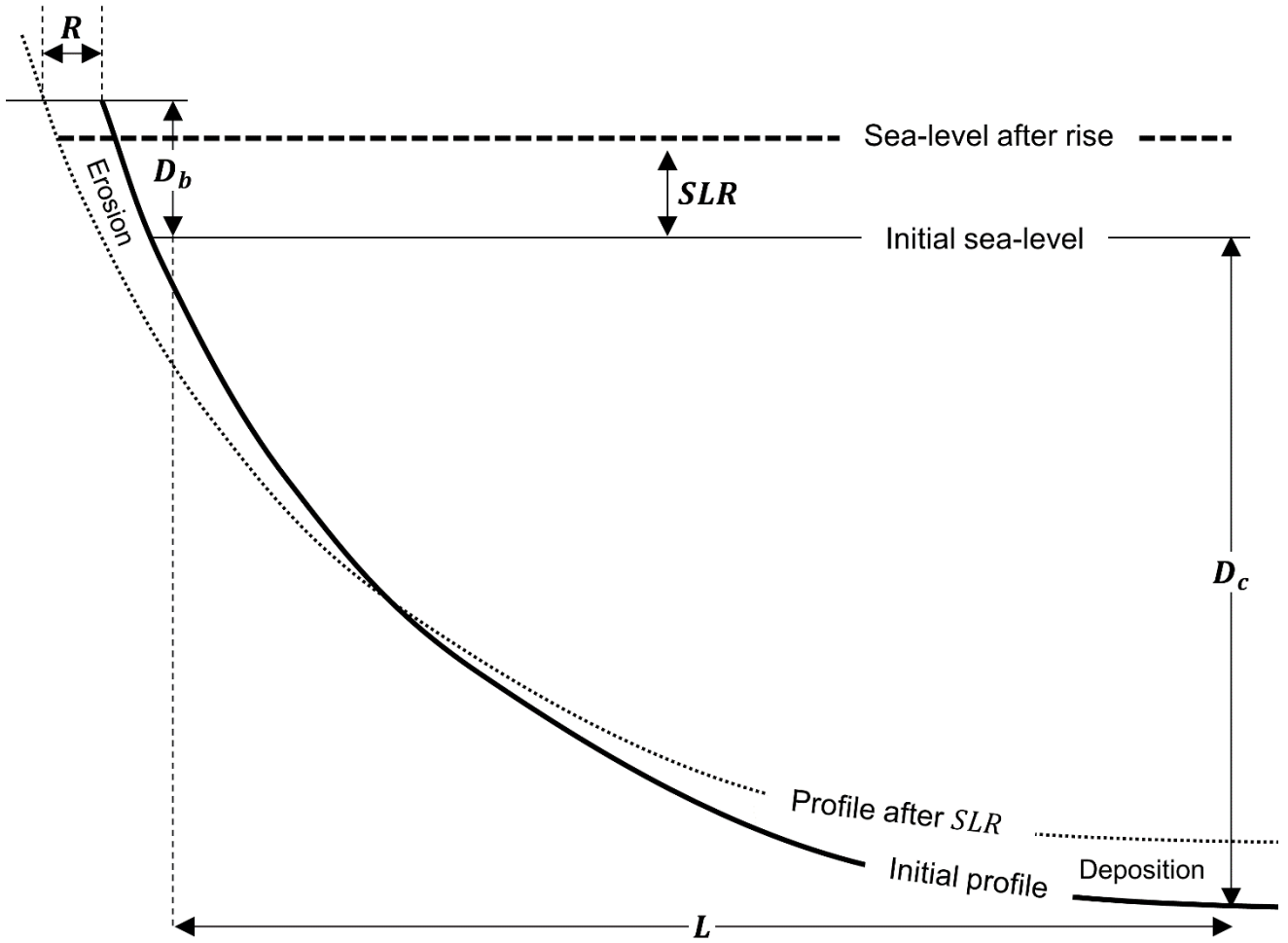

Fig. 3.4 The Bruun Rule model of shoreline retreat, adapted from Bruun (1962). A rise in sea-level (SLR) pushes the active coastal profile (D_b to D_c) upward and landward. This translation causes the upper beach to retreat (R), and the eroded material is deposited offshore. The rise in the nearshore bottom from deposition is equivalent to the increase in sea-level, maintaining a constant water depth offshore.

Table 3.1 Characteristics and capabilities of shoreline evolution models available. Models that can be applied over meso timescales are highlighted in grey. 1DH is one-dimensional horizontal, and 2DH is two-dimensional horizontal. Y means capability included, and N means capability not included. C is cohesive, and NC is non-cohesive.

Model	Capability										Reference
	Timescales[1]	Dimensions	Wave forcing	Wave-current interaction	Tidal forcing	Process sim. over non-parallel depth contours	Sea-level rise effects in shoreline evolution pred.	Sediment	Hard defences	Complex shorelines	
Bruun Rule	Macro	2D	N	N	N	N	Y	NC	N	N	Bruun (1962)
CEM	Macro	1DH, one-line	Y	N	N	N	N	C; NC	Y	Y	Ashton and Murray (2006a); Pye et al. (2017)
CoastalME	Meso	2DH, one-line	Y	N	N	N	N	C; NC	Y	Y	Payo et al. (2017); Pye et al. (2017)
COVE	Macro	1DH, two-line	Y	N	N	N	N	C; NC	Y	Y	Hurst et al. (2015); Payo et al. (2017)
CSHORE	Micro	1DH, 2DH	Y	Y	N	N	N	NC	Y[2]	N	Kobayashi (2016); Pye et al. (2017)
DELFT3D	Micro	2DH, 3D	Y	Y	Y	Y	Y	C; NC	Y	Y	Deltares (2016); Pye et al. (2017)
GENESIS	Synoptic	1DH, one-line	Y	N	N	N	N	NC	Y	N	Thomas and Frey (2013)
LITPACK	Meso	1DH, one-line	Y	Y	Y	N	N	NC	Y	N	Thomas and Frey (2013); DHI (2017a)
MIKE21	Meso	2DH, one-line	Y	Y	Y	Y	N	NC	Y	Y	DHI (2016a); DHI (2016b); DHI (2017b)
TELEMAC2D	Micro	2DH	Y	Y	Y	Y	Y	C; NC	Y	Y	Hervouet (2007); Pye et al. (2017)
UnaLinea	Meso	1DH, one-line	Y	N	N	N	N	C; NC	Y	Y	Pye et al. (2017); Stripling et al. (2017)
UNIBEST	Meso	1DH, one-line	Y	Y	Y	N	N	NC	Y	Y	Roelvink et al. (2012); Thomas and Frey (2013)
XBeach	Micro	1DH, 2DH	Y	Y	Y	Y	Y	NC (sand)	Y	Y	Roelvink et al. (2009); Pye et al. (2017)
XBeach-G	Micro	1DH	Y	Y	Y	Y	Y	NC (gravel)	Y	Y	McCall et al. (2014); Pye et al. (2017)

[1] See Table 1.1 for the definition of each timescale.
[2] Low-crested stone structures only.

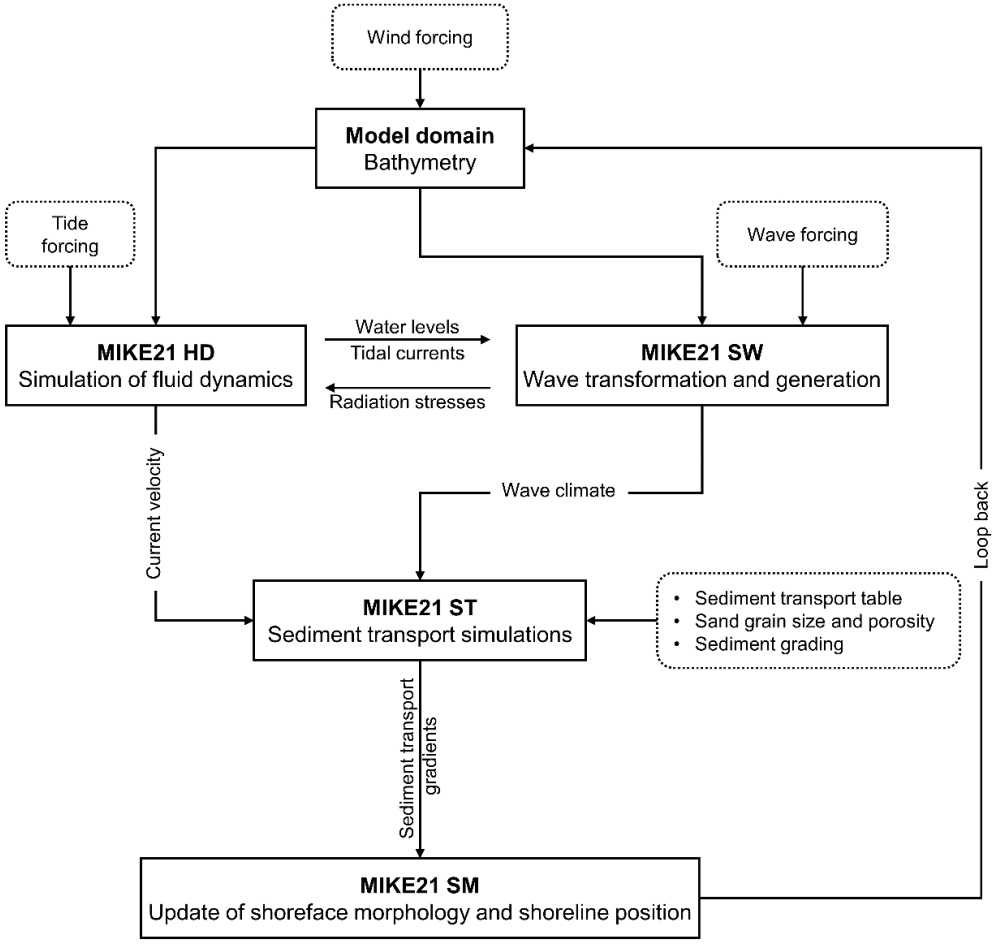

Fig. 3.5 MIKE21 framework. MIKE21 SW and MIKE21 HD simulate the wave and flow field on a finite volume mesh, respectively. MIKE21 ST simulates the sediment transport gradients in response to the wave and flow fields, and MIKE21 SM uses the sediment transport gradients to update the shoreline position at each time-step.

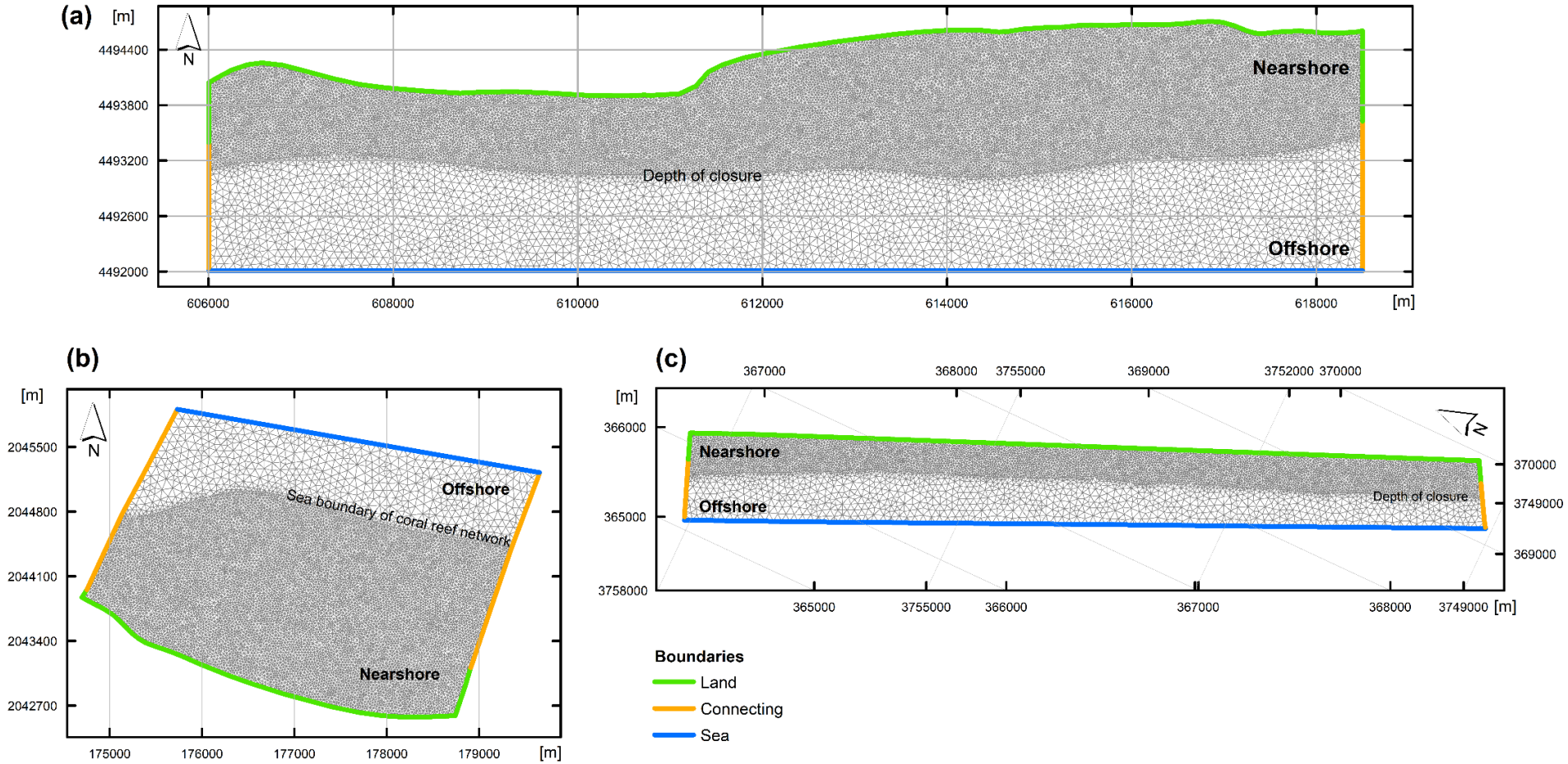

Fig. 3.6 Finite volume mesh for coastal processes simulations in the New York (a), Puerto Rico (b) and Southern California (c) test site. Each mesh is projected in UTM coordinates (m) and has two zones: nearshore and offshore. The closure depth separates these zones in the New York and Southern California test sites, whereas the sea boundary of the reef network separates both zones in the Puerto Rico test site. Each mesh has four boundaries: land, sea, and two connecting boundaries.

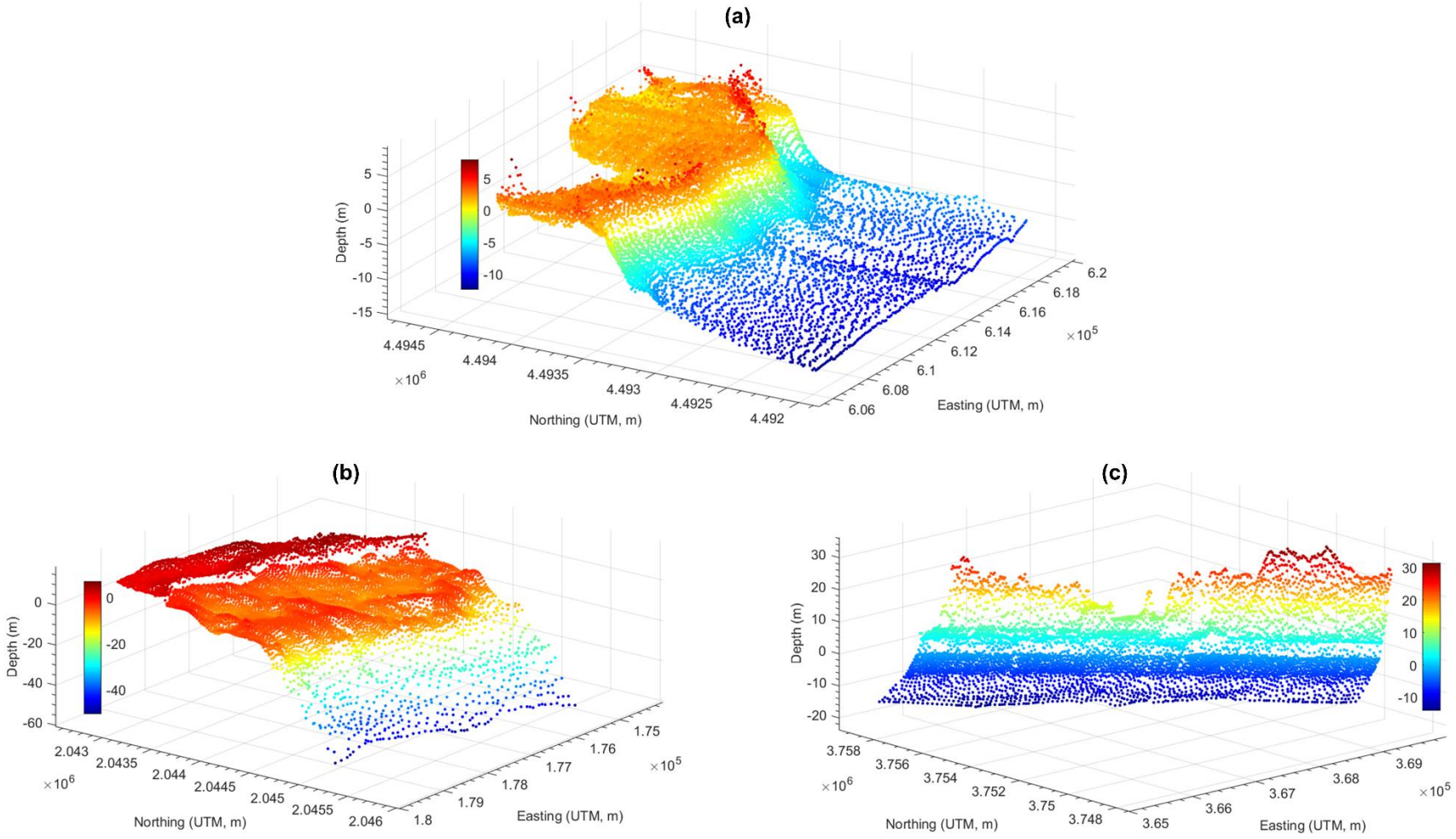

Fig. 3.7 Interpolated nodes in the New York (a), Puerto Rico (b) and Southern California (c) test site's finite volume mesh. Mesh nodes in (a) to (c) are interpolated with the relevant initial bathymetry in Fig. 2.5.

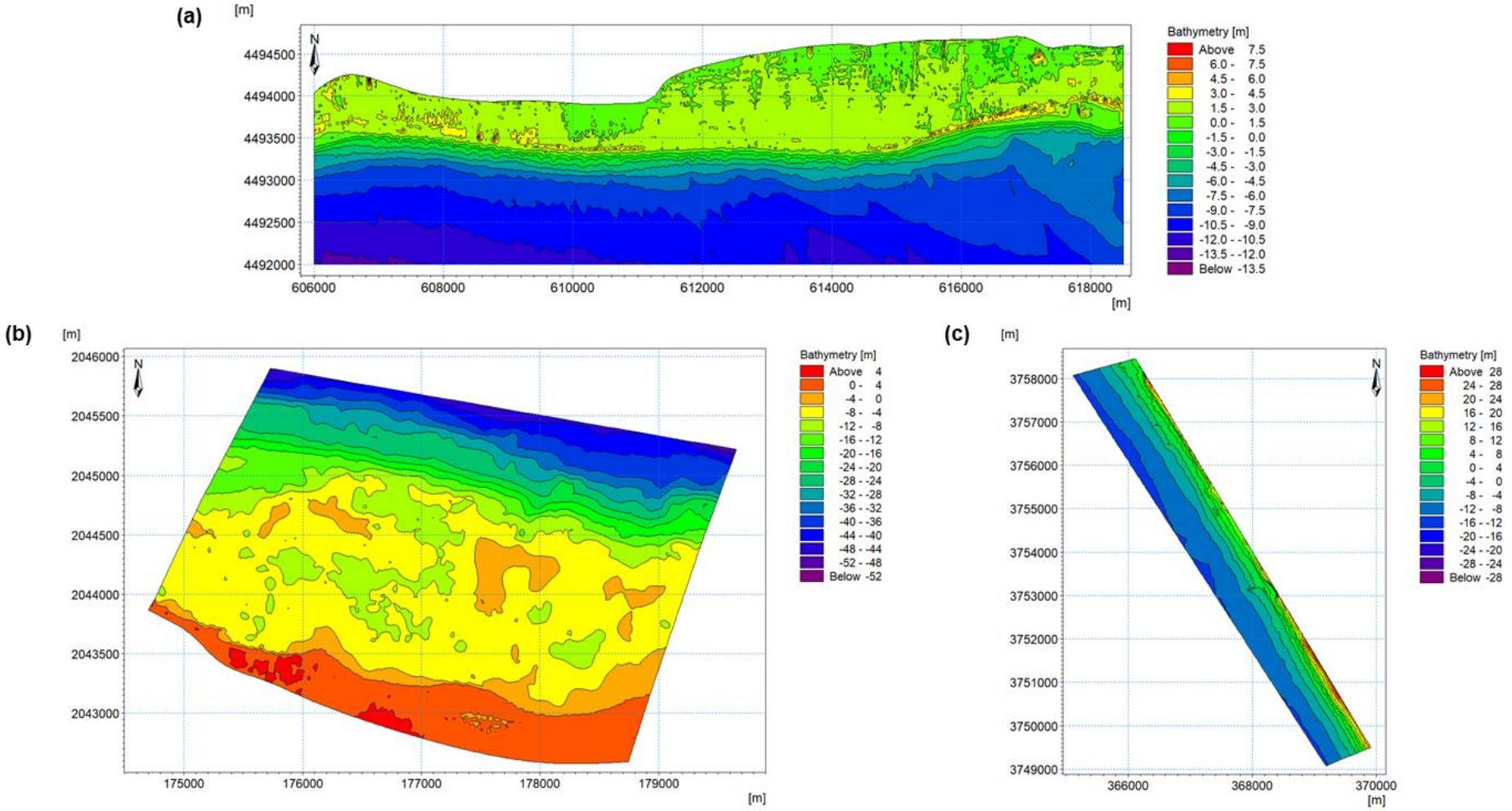

Fig. 3.8 2D planimetric view of the New York (a), Puerto Rico (b), and Southern California (c) test site's interpolated mesh. The mesh in (a) to (c) are interpolated with the relevant initial bathymetry in Fig. 2.5. (a) to (c) are raw outputs of MIKE Zero Mesh Generator. Each mesh is projected in UTM coordinates (m).

Table 3.2 MIKE21 specifications for pre-calibration simulations in each test site. Site-specific specifications are indicated by the acronyms NY (New York test site), PR (Puerto Rico test site) and SC (Southern California test site).

Input	Specifications
General	
Simulation period (model sensitivity testing only)	01-Jan-2014 to 01-Feb-2016 (NY)
	01-Oct-2014 to 31-Mar-2016 (PR)
	01-Jan-2009 to 02-Aug-2011 (SC)
Time step interval (output frequency)	86 400 sec (daily)
MIKE21 HD	
Coriolis forcing	Varying in domain
Courant-Friedrich-Lévy (CFL) number	0.8
Density	Barotropic
Manning's n reciprocal	32 $m^{1/3}/s$
Maximum time step	30 s
Minimum time step	0.01 s
Overtopping discharge[1]	0 $m^3/s/m$
Smagorinsky coefficient (eddy viscosity)	0.28
Wave radiation stresses	Internally transfers from MIKE21 SW
Weir coefficient[2]	1.838 $m^{1/2}/s$
Wind forcing	Wind speed and direction data
Wind friction (varies based on wind speed)	0.001255 to 0.002425
MIKE21 ST	
Critical Shields parameter	0.05
Grading coefficient	1.1
Grain diameter	0.2 mm
Flow/wave forcing	Internally transfers from MIKE21 SW
Maximum bed level change	10 m/day
Porosity	0.4
Relative sand density	2.65
Time step factor	1
MIKE21 SW	
Current conditions (speed and direction)	Internally transfers from MIKE21 HD
Maximum number of iterations	500
Nikuradse roughness	0.04 m
Reflection coefficient (structures)	0.5 (cross-shore structures in each test site)
	1 (longshore structures in PR)
Spectral discretisation	360 degree rose
Water level conditions	Internally transfers from MIKE21 HD
MIKE21 SM	
Berm height	1.14 m (NY); 1.5 m (PR); 2 m (SC)
Closure depth	5.8 m (NY); 5.5 m (PR); 5 m (SC)
Maximum number of iterations	500
Sediment transport gradients	Internally transfers from MIKE21 ST

[1] Used for longshore structures (e.g. seawalls and breakwaters) in the Puerto Rico test site.
[2] Used for each test site's cross-shore structures (e.g. groynes).

Table 3.3 Calibrated sediment transport table for MIKE21 applications in each test site. The first value, spacing, and the number of points in each axis define the range of each condition that may appear during a simulation and influence sediment transport rates in MIKE21 ST. The first value is the minimum value. The second value in each axis, except grain size, is the "First value + Spacing" and so forth. The second value for grain size is the "First value × Spacing" and so on.

Sediment table axis	First value	Spacing	No. of points
New York test site			
Current speed (m/s)	0.01	0.8	5
Wave height (m)	0.19	2	4
Wave period (s)	2.35	2	8
Wave height to water depth ratio	0.01	10	10
Angle between current and waves (deg)	0	30	12
Median grain size (mm)	0.2	2	8
Sediment grading	1.1	0.15	5
Bed slope (current direction)	-0.01	0.7	2
Bed slope (perpendicular to current direction)	-0.02	0.7	2
Puerto Rico test site			
Current speed (m/s)	0.01	0.8	5
Wave height (m)	0.1	1	4
Wave period (s)	3	4	8
Wave height to water depth ratio	0.01	10	10
Angle between current and waves (deg)	0	30	12
Median grain size (mm)	0.2	2	8
Sediment grading	1.1	0.15	5
Bed slope (current direction)	-0.01	0.7	2
Bed slope (perpendicular to current direction)	-0.02	0.7	2
Southern California test site			
Current speed (m/s)	0.01	1	4
Wave height (m)	0.1	1	5
Wave period (s)	3.0	3	8
Wave height to water depth ratio	0.1	11	10
Angle between current and waves (deg)	0	30	12
Median grain size (mm)	0.2	2	8
Sediment grading	1.1	0.15	3
Bed slope (current direction)	-0.01	0.7	2
Bed slope (perpendicular to current direction)	-0.02	0.7	2

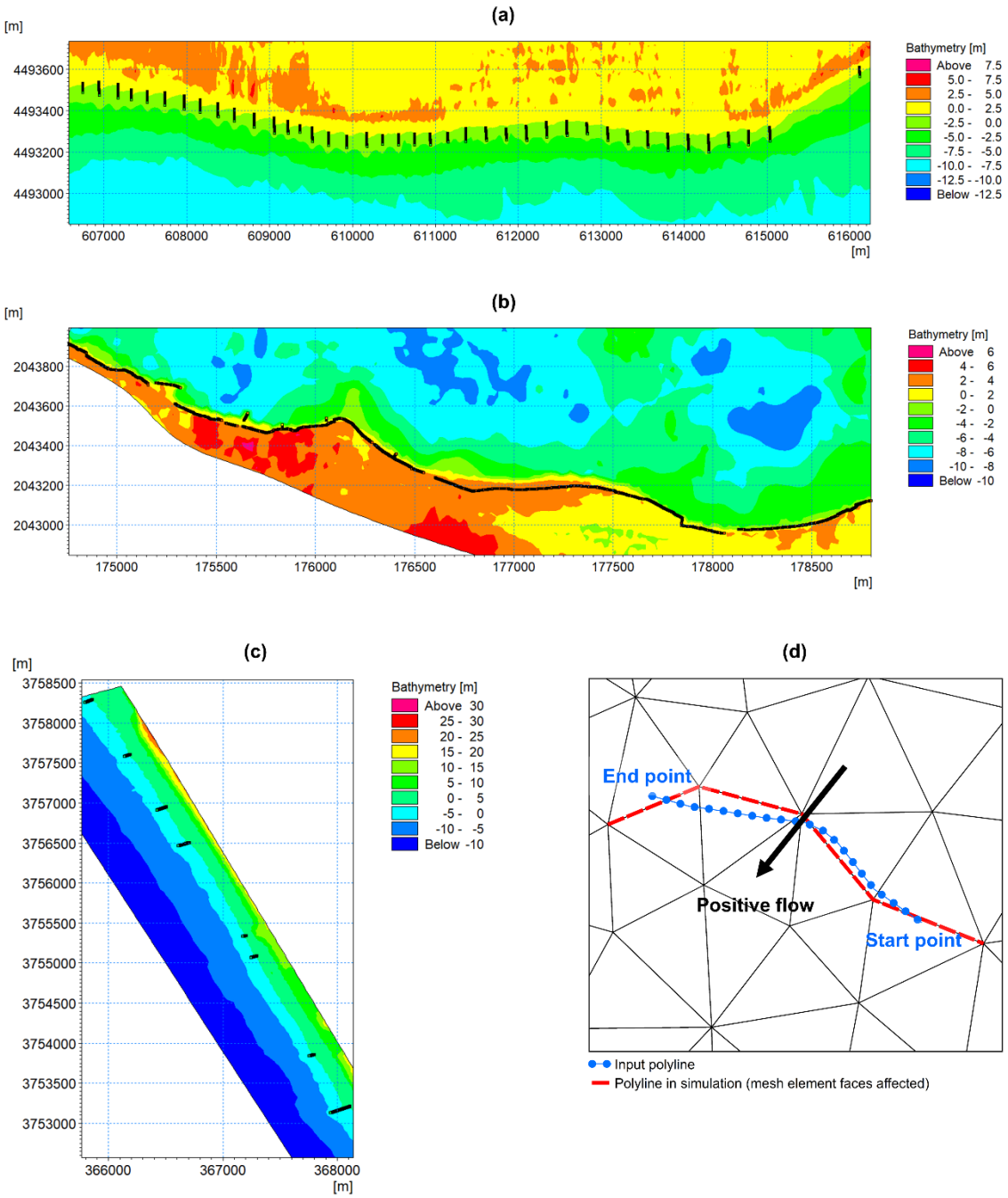

Fig. 3.9 MIKE21 representation and definition of hard defences in a simulation. (a), (b) and (c) show the digitised polylines (with nodes) representing the hard defences in the New York, Puerto Rico, and Southern California test site, respectively. (a), (b) and (c) also show the spatial distribution of hard defences in each test site's finite volume mesh. (d) illustrates how MIKE21 redefines each hard defence polyline as a selection of mesh element faces in a simulation. MIKE21 considers flow moving past a hard defence as positive or negative. Positive flow means movement to the left of a hard defence, whereas negative flow means movement to the right of a hard defence.

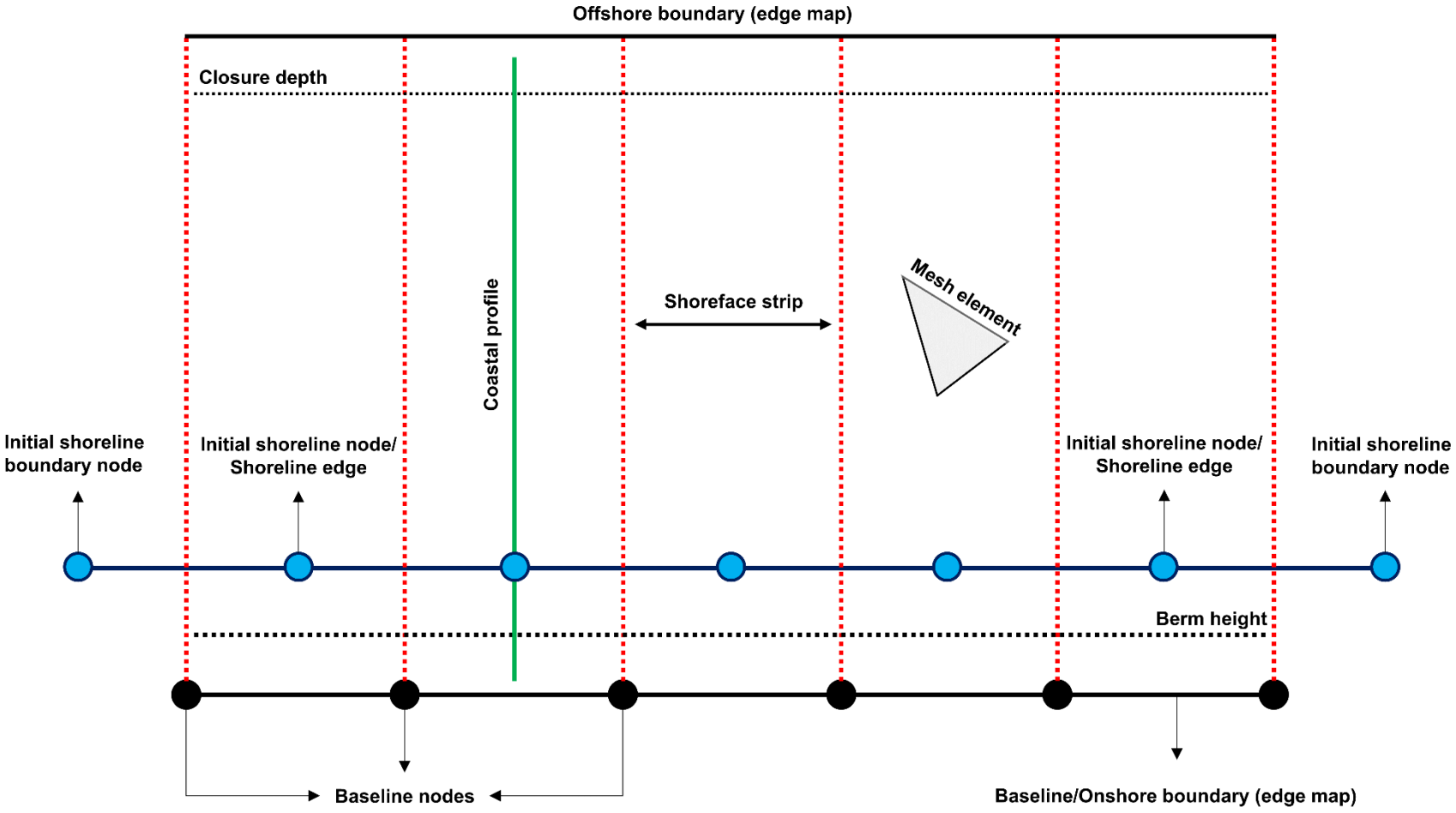

Fig. 3.10 MIKE21 SM domain general setup. MIKE21 SM uses an edge map that divides the shoreface into strips. Each shoreface strip has one active coastal profile and one shoreline edge. The active coastal profile in each shoreface strip moves with the shoreline edge perpendicular to the baseline, based on the total change in sediment volume within the strip. The baseline node spacings determine the initial shoreline resolution and each shoreface strip longshore width. The onshore boundary of the edge map is the baseline, whereas the offshore boundary is the depth contour seaward of the closure depth in the bathymetry.

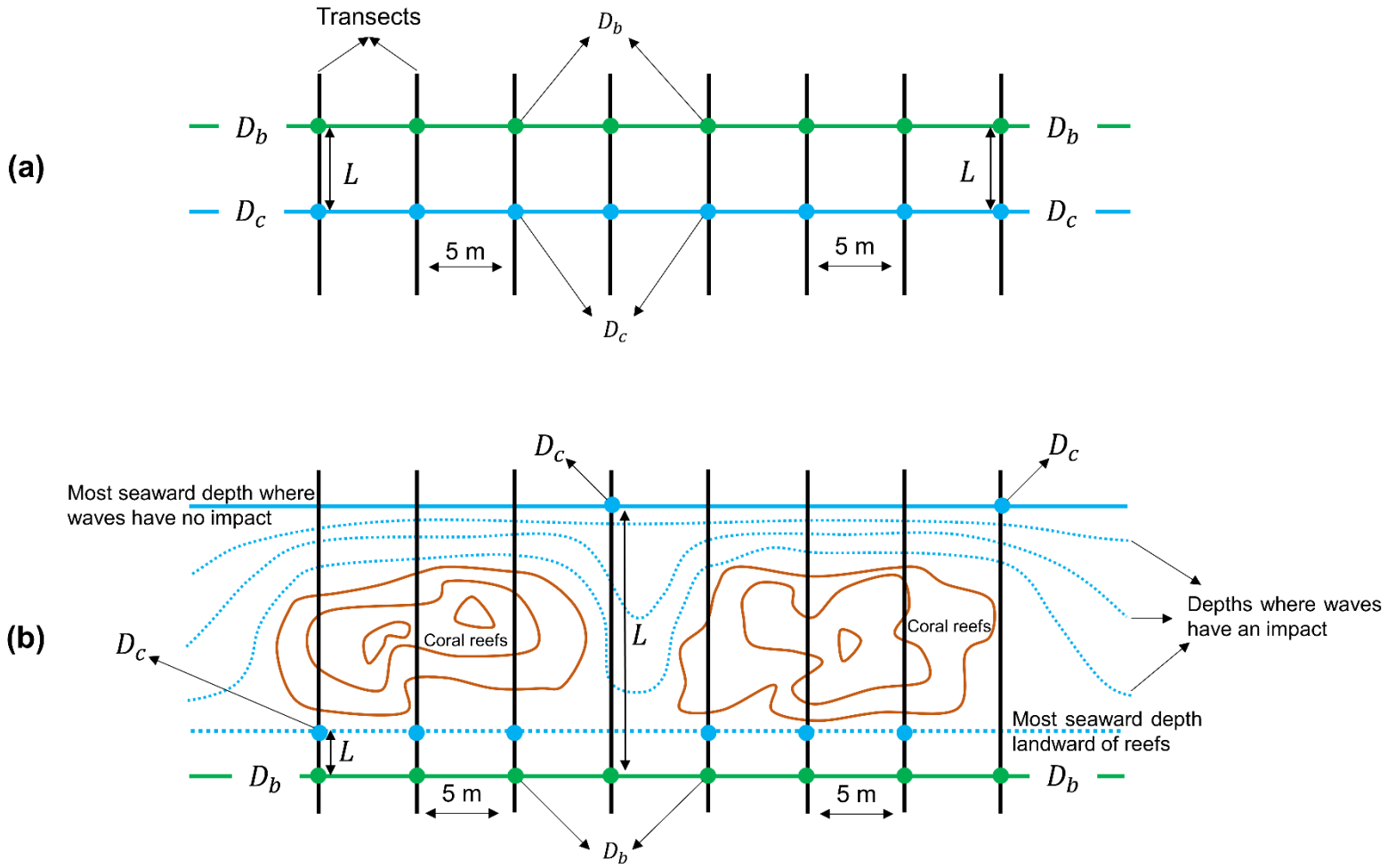

Fig. 3.11 General formulation of the Bruun Rule in the New York and Southern California test sites (a), and the Puerto Rico test site (b). D_c and L are the same in all transects in (a) but vary in each transect according to reef substrate distribution in (b). In all cases, I formulate the Bruun Rule in cross-shore transects every 5 m longshore using the same D_b in each transect.

Table 3.4 Details of all meshes generated in each test site for evaluating MIKE21 sensitivity to nearshore spatial discretisation.

Characteristic	Mesh								
	25	**30**	**35**	**40**	**45**	**50**	**55**	**60**	**65**
Nearshore max. element area (m^2)	625	900	1 225	1 600	2 025	2 500	3 025	3 600	4 225
Offshore max. element area (m^2)	4 900 →								
Nearshore max. resolution (m)	25	30	35	40	45	50	55	60	65
Offshore max. resolution (m)	70 →								
Total nodes									
New York test site	21 456	15 874	12 035	9 684	8 222	7 203	6 396	5 776	5 235
Puerto Rico test site	10 623	7 661	5 706	4 425	3 648	3 089	2 717	2 430	2 191
Southern California test site	6 791	5 061	3 771	3 052	2 670	2 353	2 109	1 957	1 825
Total elements									
New York test site	42 154	31 085	23 547	18 884	15 963	13 934	12 323	11 116	10 010
Puerto Rico test site	20 878	14 974	11 146	8 625	7 071	5 953	5 209	4 635	4 157
Southern California test site	13 032	9 646	7 172	5 755	4 994	4 366	3 889	3 594	3 334

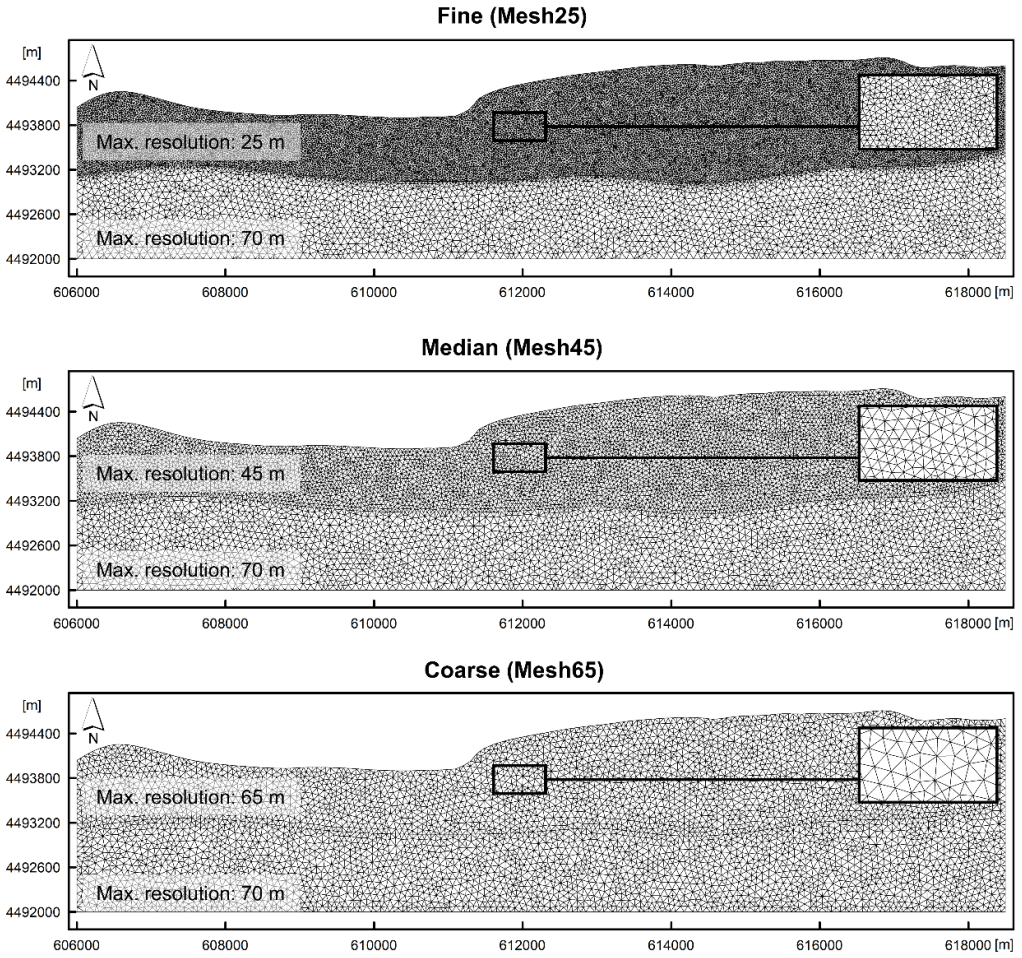

Fig 3.12 The fine, median, and coarse mesh used for evaluating MIKE21 sensitivity to nearshore spatial discretisation in the New York test site. The maximum nearshore resolution is 25 m in the fine mesh, 45 m in the median mesh, and 65 m in the coarse mesh. Each mesh has a maximum offshore resolution of 70 m and is projected in UTM coordinates (m).

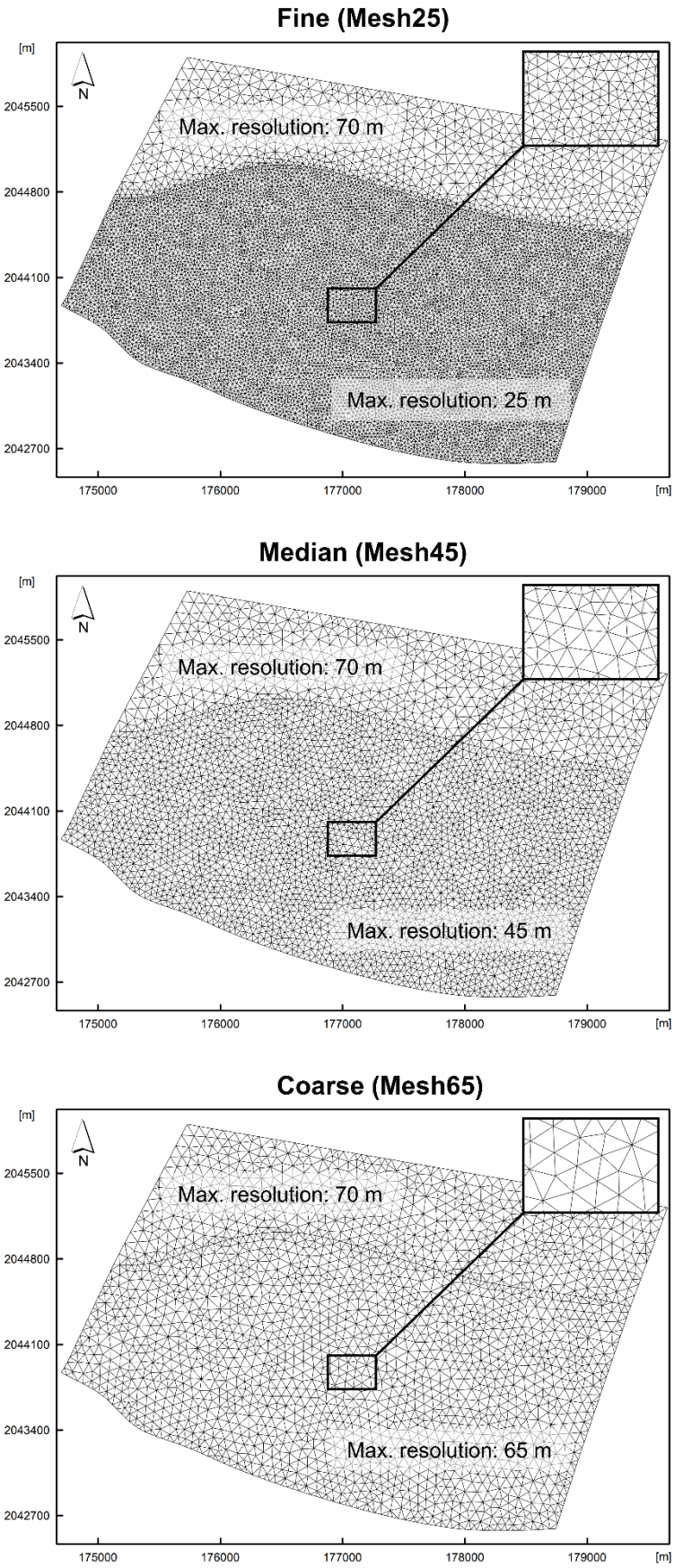

Fig. 3.13 The fine, median, and coarse mesh used for evaluating MIKE21 sensitivity to nearshore spatial discretisation in the Puerto Rico test site. The maximum nearshore resolution is 25 m in the fine mesh, 45 m in the median mesh, and 65 m in the coarse mesh. Each mesh has a maximum offshore resolution of 70 m and is projected in UTM coordinates (m).

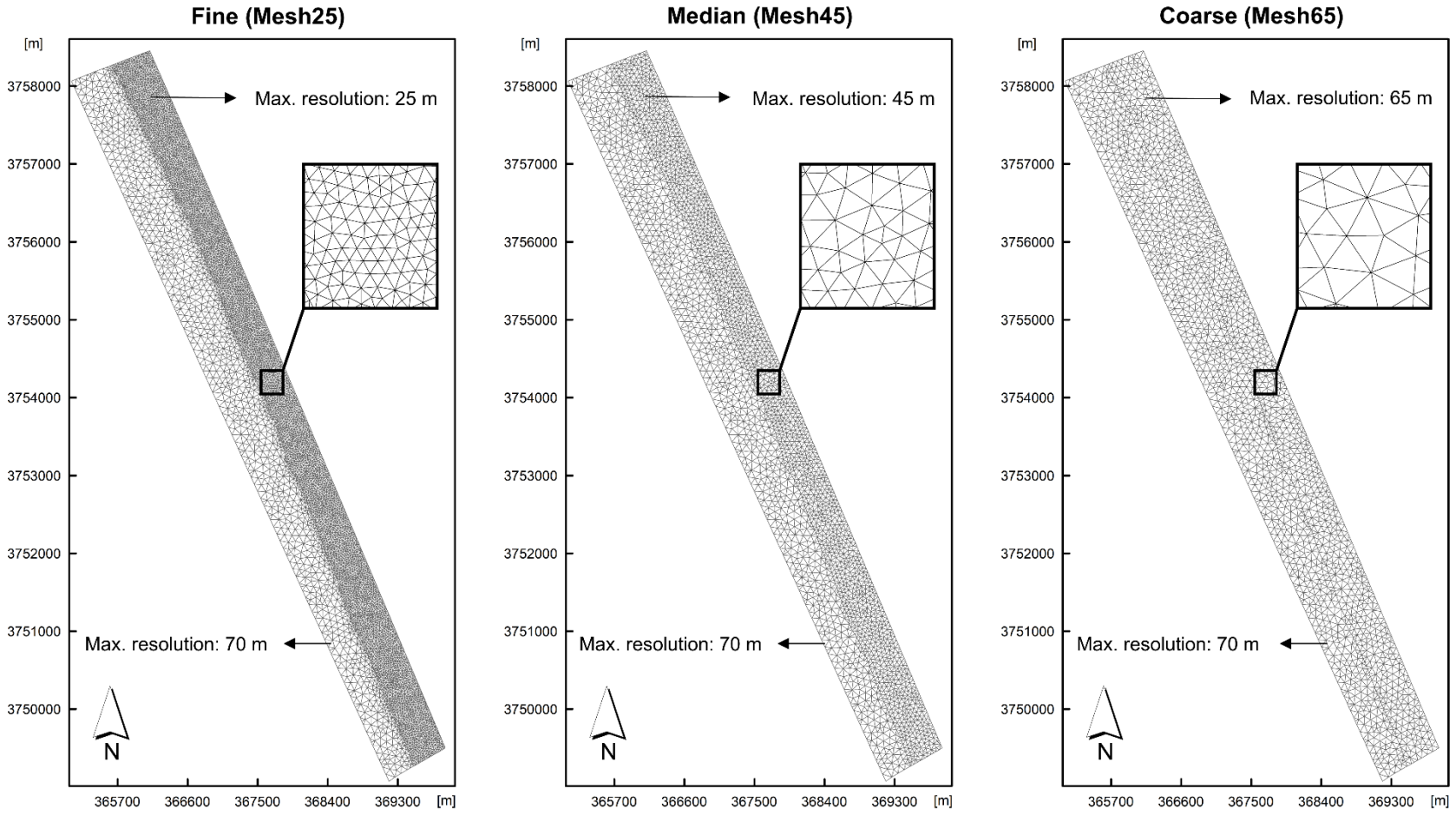

Fig. 3.14 The fine, median, and coarse mesh used for evaluating MIKE21 sensitivity to nearshore spatial discretisation in the Southern California test site. The maximum nearshore resolution is 25 m in the fine mesh, 45 m in the median mesh, and 65 m in the coarse mesh. Each mesh has a maximum offshore resolution of 70 m and is projected in UTM coordinates (m).

Table 3.5 Differences in elevation and slope in the New York test site's bed surfaces resampled using nearest neighbour (NN) and bilinear interpolation (BI). The p value of a two-sample Kolmogorov-Smirnov (KS) test indicates whether bed surfaces resampled from NN and BI are significantly different.

Characteristic		**Original bathymetry**	**Resampling**	**Resampled bathymetry**					
Resolution (m)		3	-	9	27	81	90	100	500
Elevation	Minimum (m)	-12.46	NN	-12.46	-12.45	-12.37	-12.19	-12.19	-12.11
			BI	-12.46	-12.45	-12.36	-12.19	-12.2	-12.12
	Maximum (m)	8.42	NN	8.42	7.89	7.42	5.68	6.25	4.14
			BI	8.37	7.89	7.26	5.68	6.27	4.13
	Mean (m)	-4.3	NN	-4.28	-4.33	-4.32	-4.11	-4.15	-5.26
			BI	-4.29	-4.34	-4.33	-4.11	-4.16	-5.25
	Standard deviation	5.2	NN	5.2	5.2	5.2	5.17	5.19	5.13
			BI	5.2	5.2	5.2	5.17	5.19	5.14
	KS test p value	-	NN						
			BI	1	1	1	1	1	0.997
Slope	Minimum (deg.)	0	NN	0	0	0.01	0.01	0	0.01
			BI	0	0	0	0	0	0.01
	Maximum (deg.)	31.48	NN	15.62	5.21	3.71	5.51	3.89	0.77
			BI	15.44	5.25	3.73	5.51	3.88	0.77
	Mean (deg.)	1.1	NN	0.83	0.56	0.44	0.46	0.45	0.32
			BI	0.82	0.55	0.44	0.46	0.45	0.32
	Standard deviation	1.58	NN	1	0.61	0.52	0.57	0.54	0.21
			BI	1	0.61	0.51	0.57	0.54	0.21
	KS test p value	-	NN						
			BI	1	1	1	1	1	0.999

Table 3.6 Differences in elevation and slope in the Puerto Rico test site's bed surfaces resampled using nearest neighbour (NN) and bilinear interpolation (BI). The p value of a two-sample Kolmogorov-Smirnov (KS) test indicates whether bed surfaces resampled from NN and BI are significantly different.

Characteristic		**Original bathymetry**	**Resampling**	**Resampled bathymetry**					
Resolution (m)		3	-	9	27	81	90	100	500
Elevation	Minimum (m)	-50.52	NN	-50.52	-50.49	-50.67	-49.14	-50.2	-46.7
			BI	-50.53	-50.49	-50.66	-49.07	-50.2	-46.72
	Maximum (m)	7.87	NN	7.67	7.04	6.93	6.12	5.73	4.83
			BI	7.71	7.02	7.02	6.11	5.62	4.77
	Mean (m)	-11.98	NN	-12.08	-12.24	-12.66	-12.22	-12.38	-11.13
			BI	-12.08	-12.24	-12.64	-12.22	-12.38	-11.16
	Standard deviation	12.73	NN	12.81	12.92	13.21	12.87	13.01	12.06
			BI	12.8	12.92	13.2	12.87	13.01	12.08
	KS test p value	-	NN	1	1	1	1	1	0.314
			BI						
Slope	Minimum (deg.)	0	NN	0	0.01	0.03	0.03	0.02	0.03
			BI	0	0.01	0.02	0.03	0.01	0.03
	Maximum (deg.)	50.59	NN	25.72	11.06	5.62	5.16	4.72	2.43
			BI	24.57	10.85	5.59	5.15	4.72	2.44
	Mean (deg.)	2.03	NN	1.89	1.66	1.35	1.3	1.29	0.96
			BI	1.9	1.66	1.35	1.31	1.29	0.96
	Standard deviation	2.16	NN	1.76	1.42	1.11	1.08	1.04	0.77
			BI	1.74	1,42	1.11	1.08	1.04	0.77
	KS test p value	-	NN	1	1	1	1	1	0.341
			BI						

Table 3.7 Differences in elevation and slope in the Southern California test site's bed surfaces resampled using nearest neighbour (NN) and bilinear interpolation (BI). The p value of a two-sample Kolmogorov-Smirnov (KS) test indicates whether bed surfaces resampled from NN and BI are significantly different.

Characteristic		**Original bathymetry**	**Resampling**	**Resampled bathymetry**				
Resolution (m)		10	-	27	81	90	100	500
Elevation	Minimum (m)	-14.06	NN	-14.19	-13.78	-14.09	-13.64	-13
			BI	-14.16	-13.78	-14.12	13.61	-13.01
	Maximum (m)	31.88	NN	28.53	28.81	26.26	31.57	21.79
			BI	28.6	28	26.19	30.84	21.74
	Mean (m)	-3.98	NN	-4.63	-4.16	-5.03	-3.23	-4.08
			BI	-4.63	-4.17	-5.02	-3.23	-4.1
	Standard deviation	8.57	NN	7.92	8.41	7.52	9.37	8.37
			BI	7.92	8.39	7.53	9.34	8.34
	KS test p value	-	NN BI	1	1	1	1	1
Slope	Minimum (deg.)	0	NN	0	0.04	0.02	0.08	0.55
			BI	0.03	0.04	0.02	0.08	0.55
	Maximum (deg.)	32.8	NN	20.21	10.54	9.36	11.32	3.18
			BI	20.1	10.7	9.35	11.31	3.18
	Mean (deg.)	2.06	NN	1.88	1.93	1.76	2.1	1.77
			BI	1.88	1.93	1.76	2.1	1.76
	Standard deviation	2.8	NN	2.25	1.99	1.76	2.1	0.81
			BI	2.24	1.99	1.76	2.09	0.81
	KS test p value	-	NN BI	0.997	1	1	1	1

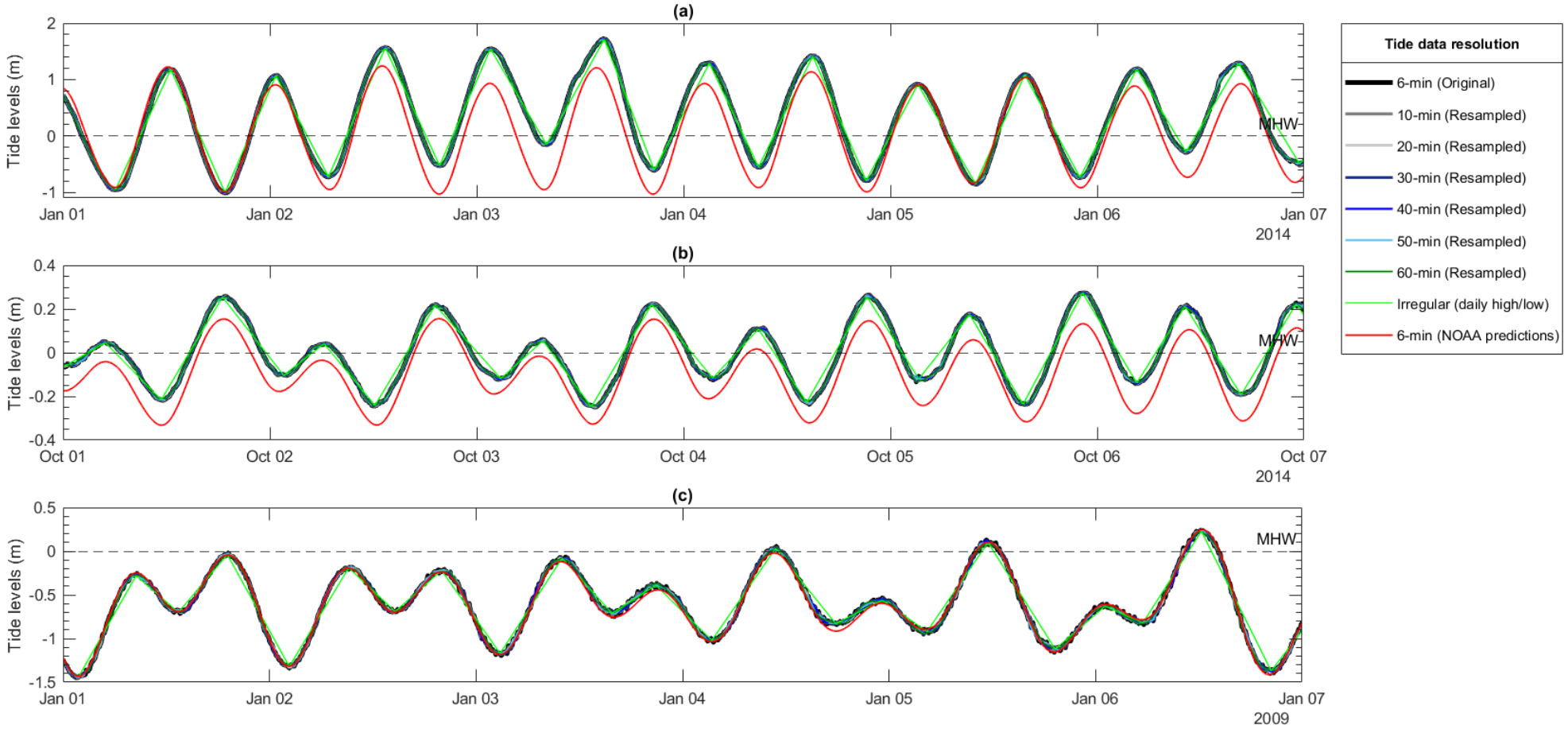

Fig. 3.15 A sample of each tide dataset used for evaluating model sensitivity in the New York (a), Puerto Rico (b), and Southern California (c) test site. All tide datasets comprise verified tidal levels recorded from site-specific tide gauges, except NOAA tide predictions. NOAA tide predictions are expected tidal levels based on harmonic constituents (see NOAA (2020) for details).

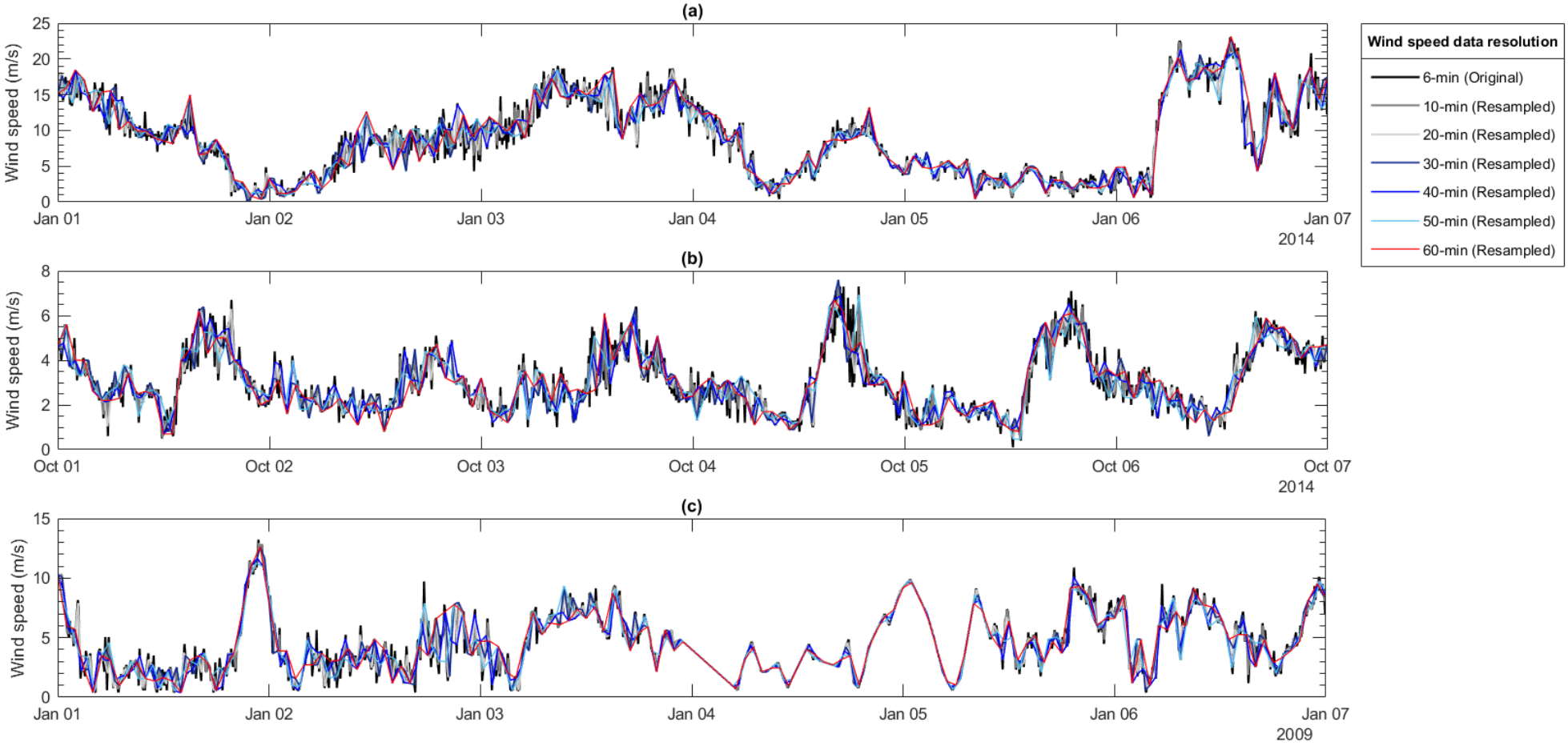

Fig. 3.16 A sample of each wind speed dataset used for evaluating MIKE21 sensitivity in the New York (a), Puerto Rico (b), and Southern California (c) test site.

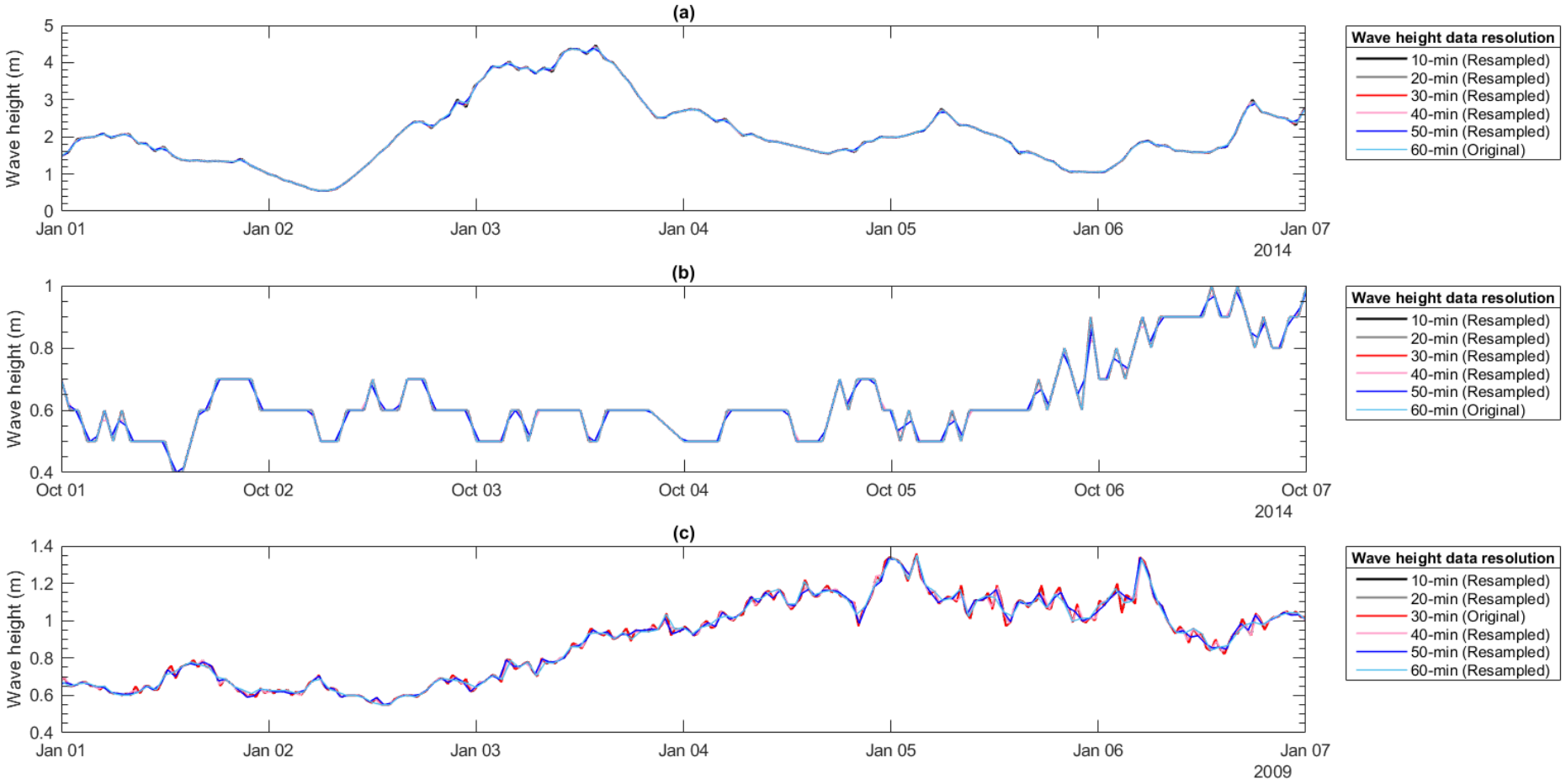

Fig. 3.17 A sample of each wave height dataset used for evaluating MIKE21 sensitivity in the New York (a), Puerto Rico (b), and Southern California (c) test site.

Table 3.8 Combinations of tide, wind and wave climate data resolution used for evaluating MIKE21 sensitivity in each test site.

Simulation	Tide data resolution (min)	Wind data resolution (min)	Wave climate data resolution (min)
1	6		
2	10		
3	20		
4	30	↑	
5	40	6	
6	50	↓	
7	60		↑
8	Infrequent (Daily high/low tides)		10
9	06 (NOAA tide predictions)		↓
10		10	
11		20	
12		30	
13		40	
14	↑	50	
15	6	60	
16	↓		20
17		↑	30
18		6	40
19		↓	50
20			60

Table 3.9 Values used for calibrating Manning's n reciprocal, sand grain diameter, sand porosity, sediment grading coefficient, and the weir coefficient of hard defences. MIKE21 default values are in bold.

Parameter	**Units**	**Established range**	**Reference**	**Selected values (*comments*)**
Manning's n	$m^{1/3}/s$	n values: 0.02 – 0.035 n reciprocals: 28 – 50	Chow (1959)	28, 29, **32**, 33, 40, 50 (*Manning's n reciprocals*)
Sand grain diameter	mm	0.0625 – 0.125 (very fine) 0.0125 – 0.25 (fine) 0.25 – 0.5 (medium) 0.5 – 1 (coarse) 1 – 2 (very coarse)	Wentworth (1922)	0.1, **0.2**, 0.25, 0.5, 1
Sand porosity	-	0.3 – 0.7	Nimmo (2013)	0.3, **0.4**, 0.5, 0.7
Sediment grading coefficient	-	< 1.27 (very well sorted) 1.27 – 1.4 (well sorted) 1.41 – 1.99 (moderately sorted) 2 – 3.99 (poorly sorted) 4 – 15.99 (very poorly sorted) ≥ 16 (extremely poorly sorted)	Folk and Ward (1957)	**1.1**, 1.3, 1.5, and 2 (*Maximum range that MIKE21 can facilitate*)
Weir coefficient	$m^{1/2}/s$	0.11 – 0.27 (Lateral structure) 0.3 – 1.71 (Broad crested structure) 1.77 – 2.26 (Ogee crested structure) 1.71 – 1.82 (Sharp crested structure)	Horton (1906)	0.11, 0.55, 0.77, 0.99, 1.21, 1.44, 1.82, **1.838**, 2.21

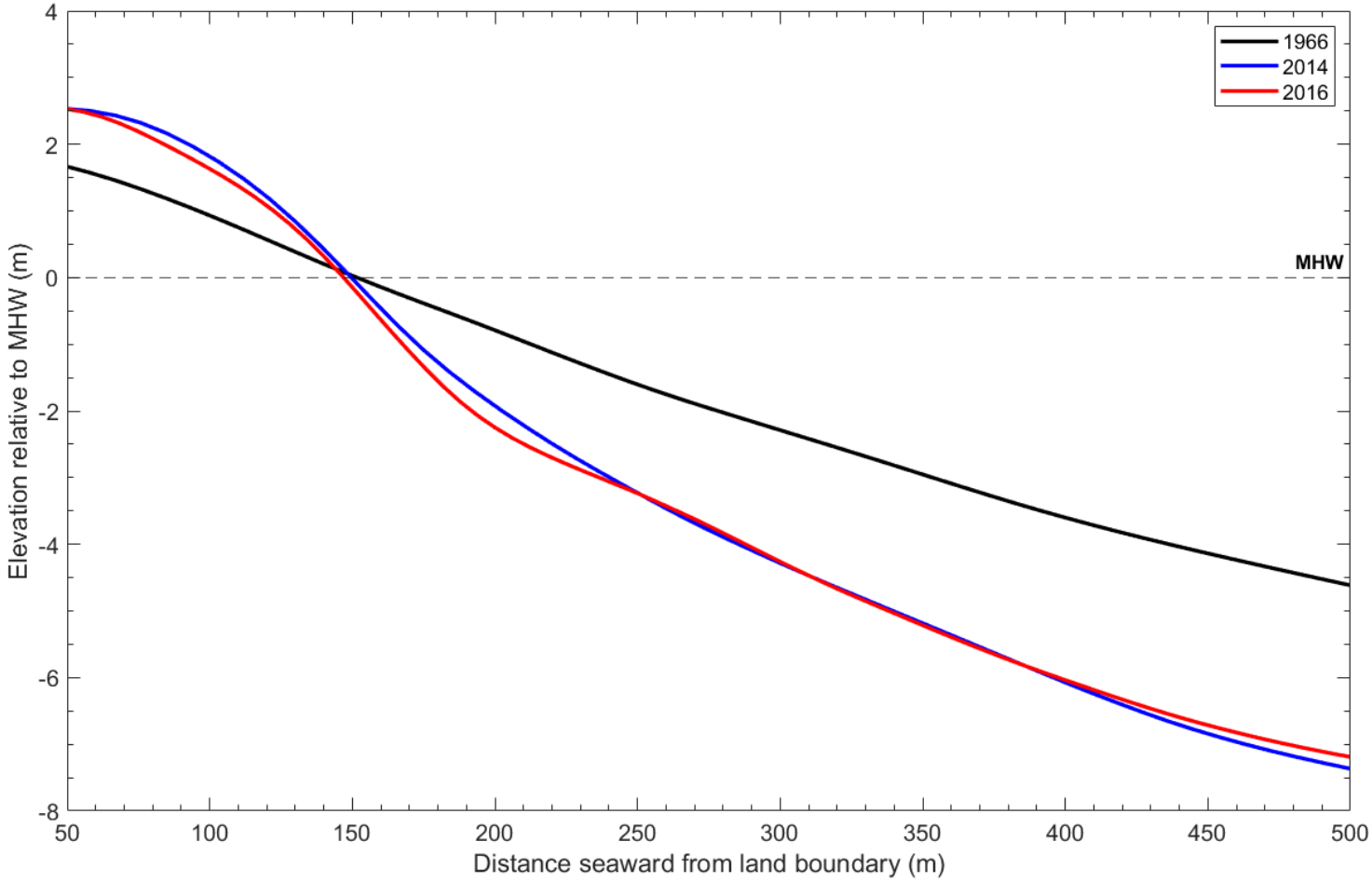

Fig. 3.18 The New York test site's 1966, 2014 and 2016 average coastal profile. The average coastal profile is the average of individual cross-shore profiles sampled every 15 m longshore. Negative (positive) values on the x axis are distances landward (seaward) of the shoreline (zero-depth contour).

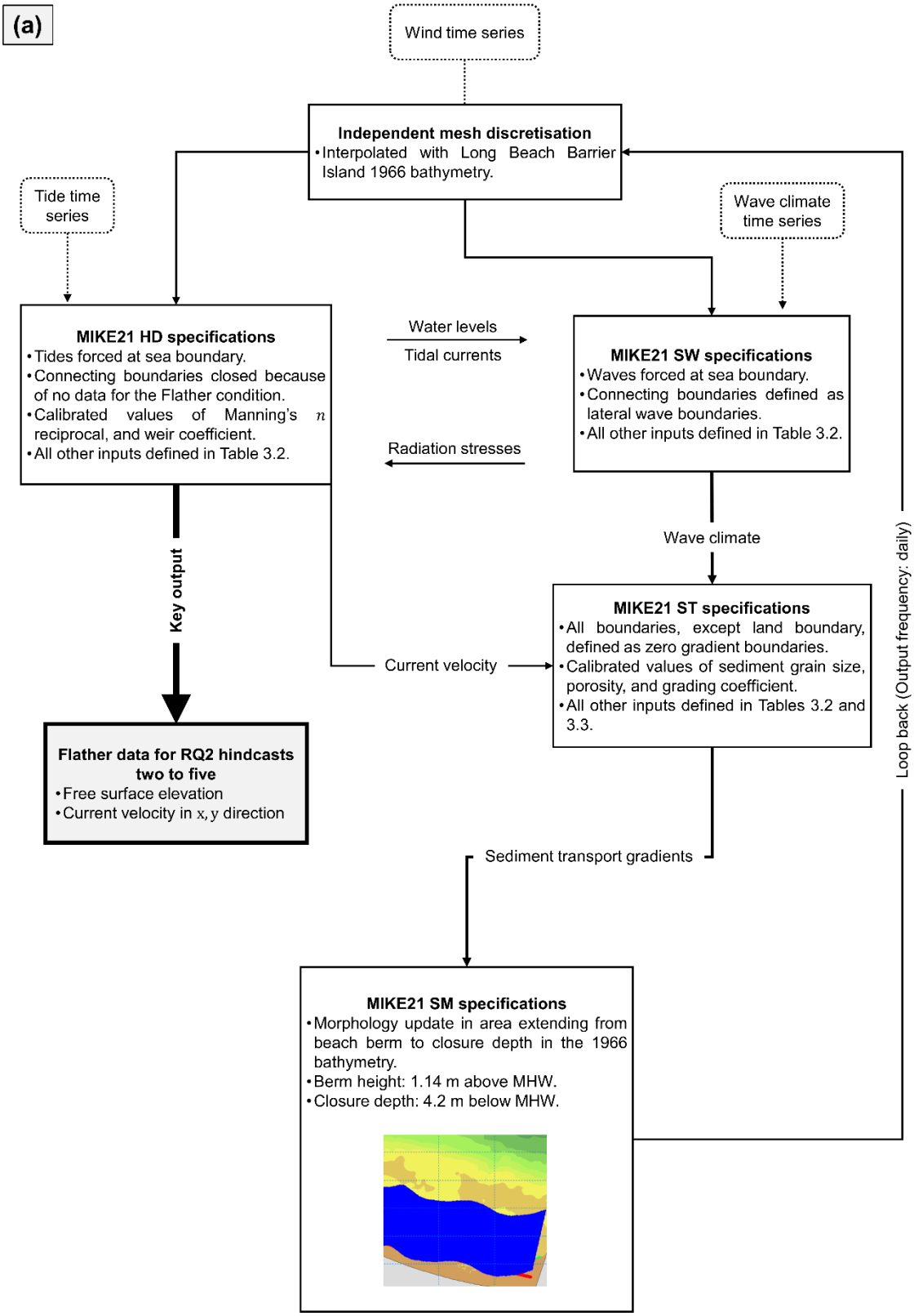

Fig. 3.19 Experimental setup of RQ2 hindcast one (a), two (b), three (c), four (d), and five (e). These are all meso timescale hindcast simulations of shoreline evolution carried out in the New York test site (01-Jan-1966 to 01-Jan-2016) for establishing a method that incorporates a time-varying closure depth in hybrid models.

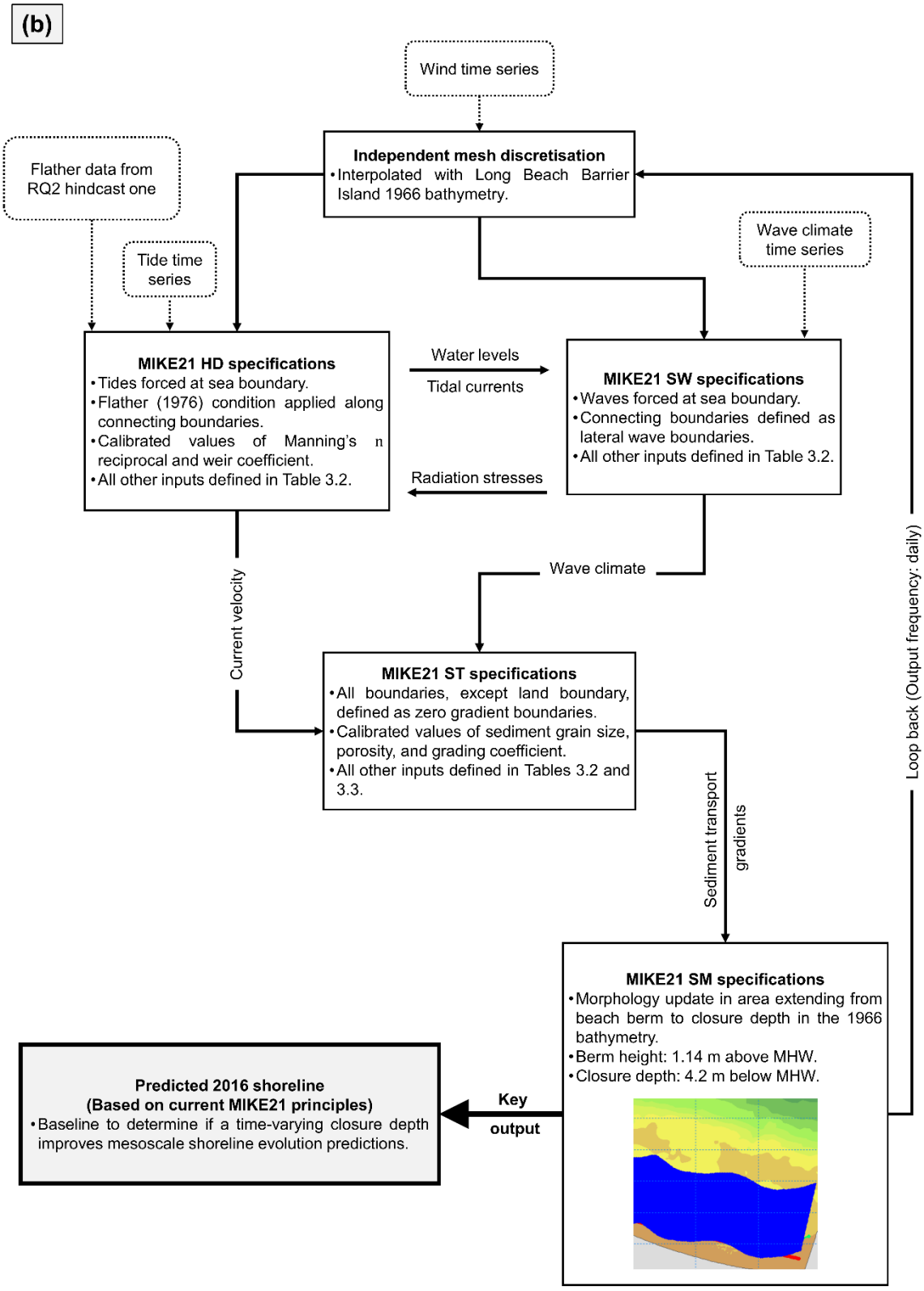

Fig. 3.19 (continued)

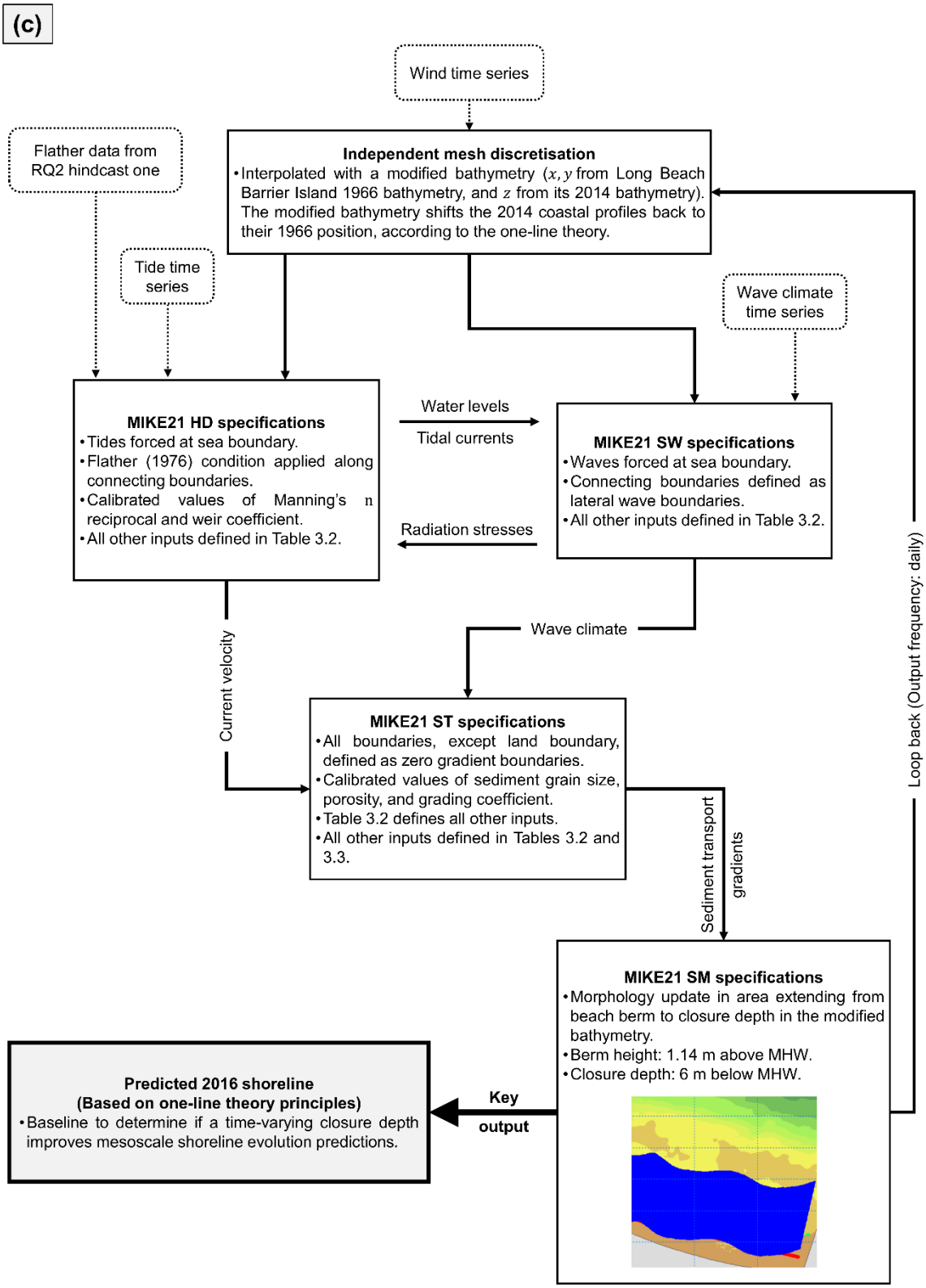

Fig. 3.19 (continued)

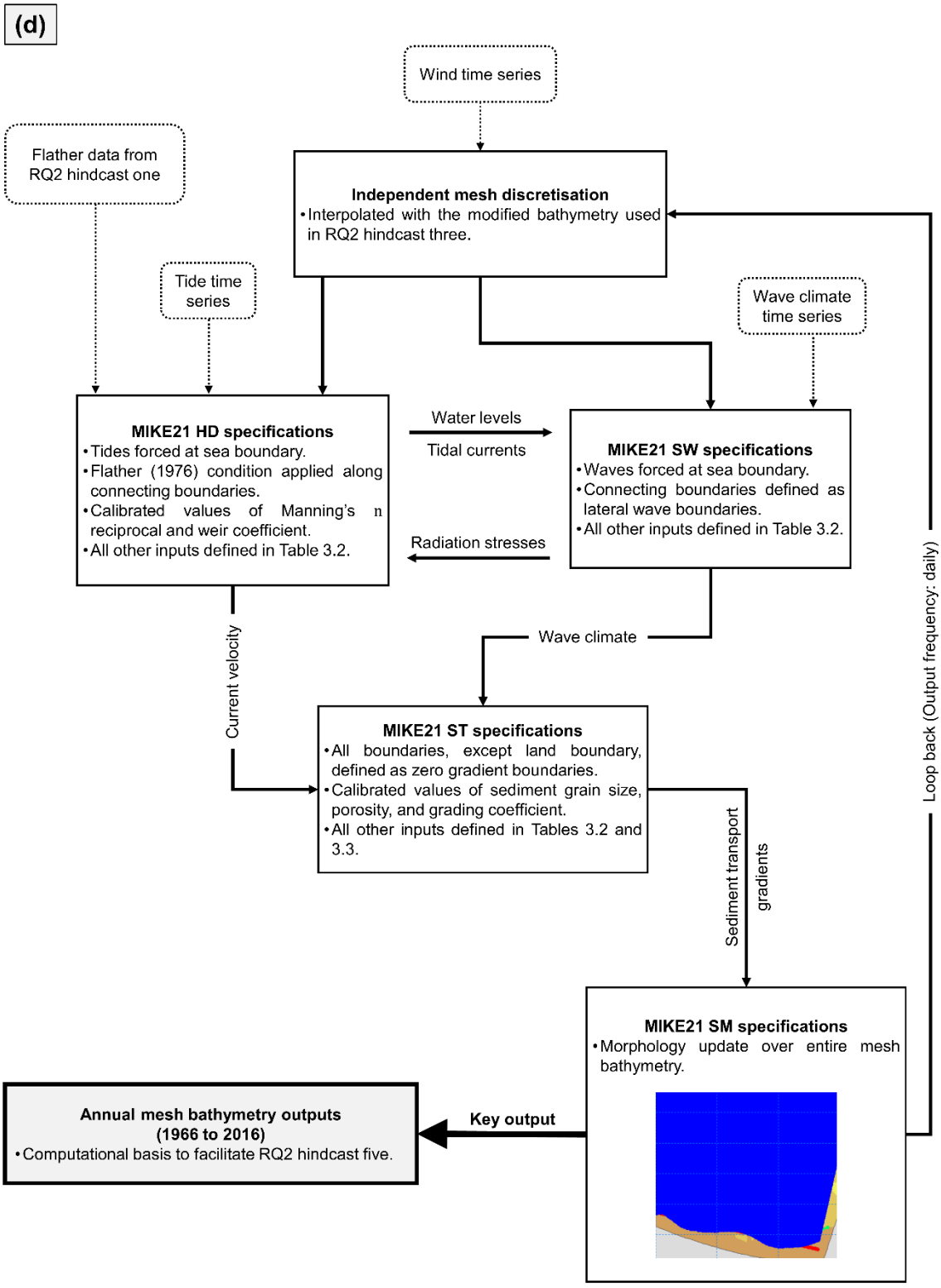

Fig. 3.19 (continued)

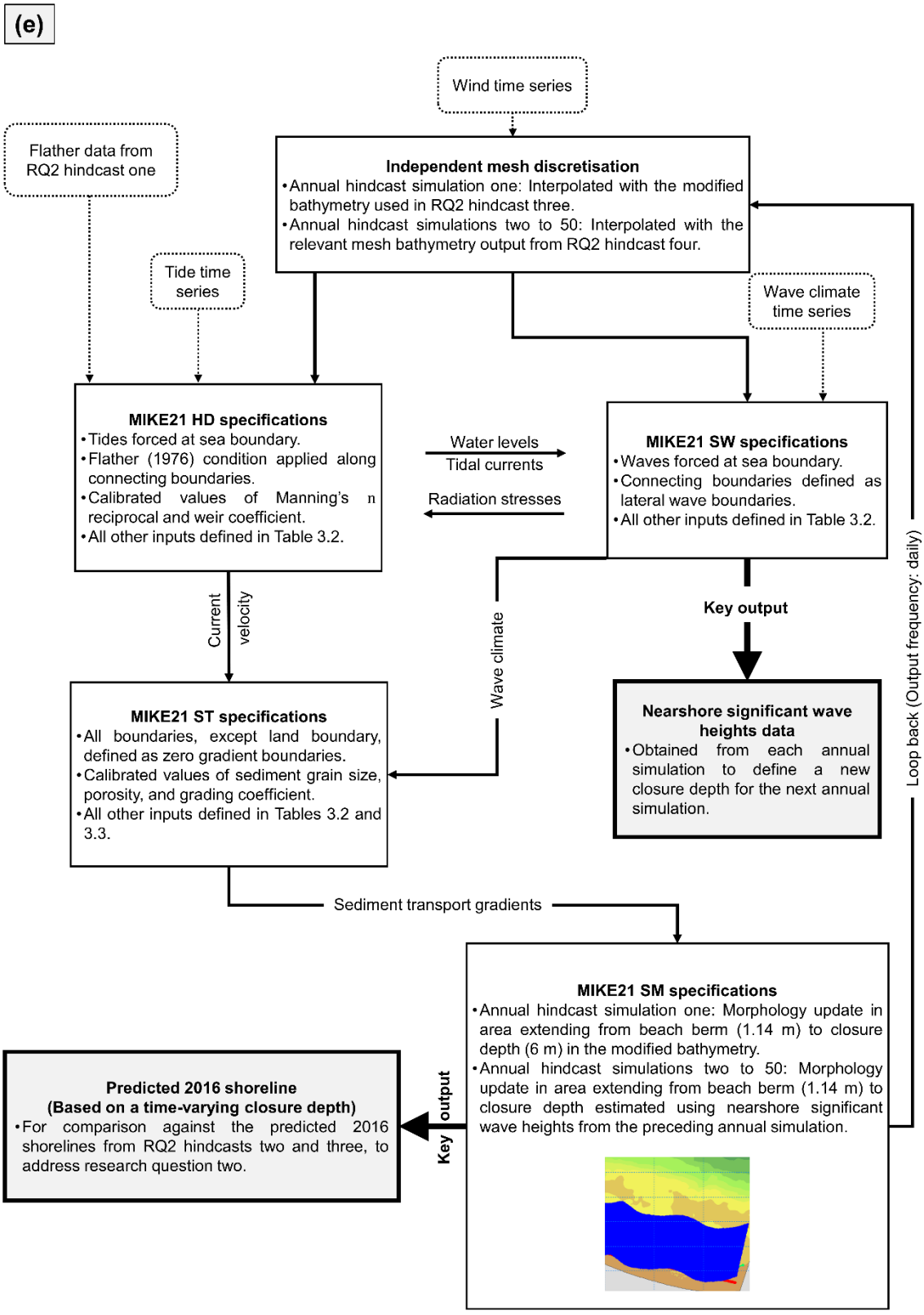

Fig. 3.19 (continued)

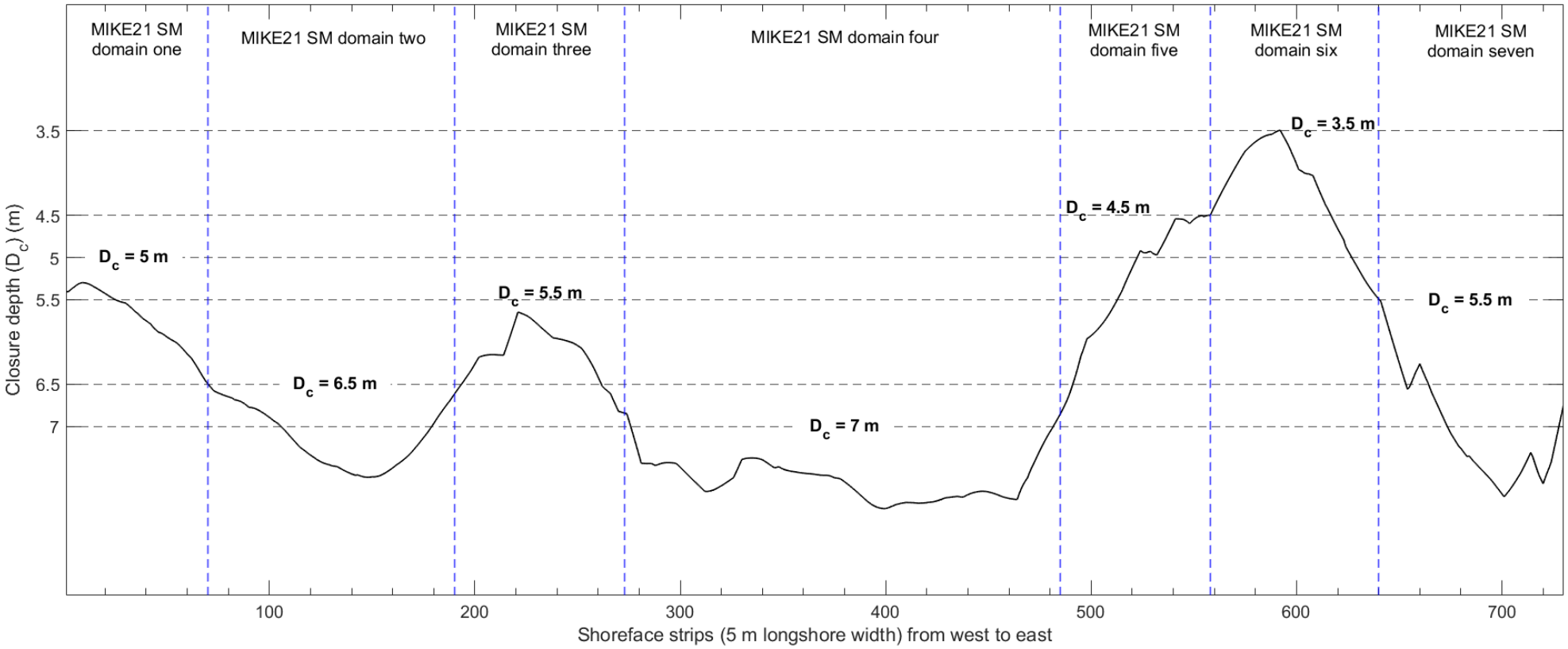

Fig. 3.20 Experimental setup of RQ3 hindcast two. This simulation iteratively hindcasts shoreline evolution in the Puerto Rico test site using a longshore varying closure depth (D_c). The seven MIKE21 SM domains in Fig. 3.20 represent seven (iterative) individual simulations that comprise RQ3 hindcast two. I use the same mesh and specifications for MIKE21 SW, MIKE21 HD and MIKE21 ST in each iterative simulation but apply MIKE21 SM to a continuous coastal stretch with a common depth contour landward of reefs.

Table 3.10 Summary of each MIKE21 simulation carried out for addressing research questions one to four. RQ is research question, NY is the New York test site, PR is the Puerto Rico test site, SC is the Southern California test site, and $intrpl$ is interpolation. Simulations 1 to 57 are carried out in each test site unless otherwise stated. Simulations 58 to 65 are carried out in the New York test site only. Simulations 66 to 71 are carried out in the Puerto Rico test site only. In each simulation, I force tides and waves at the sea boundary, keep the connecting boundaries open unless otherwise stated, and use the specifications in Tables 3.2 and 3.3 for all inputs not specified in Table 3.10.

Simulation	Test site	RQ	Defining specification(s)	Fixed specification(s)	Details
1	↑ NY; PR; SC ↓	↑ One ↓	Nearshore spatial discretisation: 25 m	• Mesh $intrpl$ with relevant bathy. data in Fig. 2.5. • Relevant coastal processes time series in Figs. 2.6 to 2.8.	↑ Section 3.6.1 ↓
2			Nearshore spatial discretisation: 30 m		
3			Nearshore spatial discretisation: 35 m		
4			Nearshore spatial discretisation: 40 m		
5			Nearshore spatial discretisation: 45 m		
6			Nearshore spatial discretisation: 50 m		
7			Nearshore spatial discretisation: 55 m		
8			Nearshore spatial discretisation: 60 m		
9			Nearshore spatial discretisation: 65 m		
10	NY; PR	↑ One ↓	Mesh $intrpl$ with resampled bathy. (9 m)	• Independent mesh discretisation. • Relevant coastal processes time series in Figs. 2.6 to 2.8.	↑ Section 3.6.2 ↓
11	NY; PR; SC		Mesh $intrpl$ with resampled bathy. (27 m)		
12	NY; PR; SC		Mesh $intrpl$ with resampled bathy. (81 m)		
13	NY; PR; SC		Mesh $intrpl$ with resampled bathy. (90 m)		
14	NY; PR; SC		Mesh $intrpl$ with resamp. bathy. (100 m)		
15	NY; PR; SC		Mesh $intrpl$ with resamp. bathy. (500 m)		
16	↑ NY; PR; SC ↓	↑ One ↓	Resampled tide time series (10 min)	• Independent mesh discretisation $intrpl$ with relevant bathy. data in Fig. 2.5. • Relevant coastal processes time series in Figs. 2.6 to 2.8.	↑ Section 3.6.3 ↓
17			Resampled tide time series (20 min)		
18			Resampled tide time series (30 min)		
19			Resampled tide time series (40 min)		
20			Resampled tide time series (50 min)		
21			Resampled tide time series (60 min)		
22			Daily high/low tide time series		
23			NOAA tide predictions (6 min)		

Simulation	Test site	RQ	Defining specification(s)	Fixed specification(s)	Details
24	↑ NY; PR; SC ↓	↑ One ↓	Resampled wind time series (10 min)	• Independent mesh discretisation $intrpl$ with relevant bathy. data in Fig. 2.5. • Relevant coastal processes time series in Figs. 2.6 to 2.8.	↑ Section 3.6.3 ↓
25			Resampled wind time series (20 min)		
26			Resampled wind time series (30 min)		
27			Resampled wind time series (40 min)		
28			Resampled wind time series (50 min)		
29			Resampled wind time series (60 min)		
30	NY; PR; SC	↑ One ↓	Resamp. wave climate time series (10 min)	• Independent mesh discretisation $intrpl$ with relevant bathy. data in Fig. 2.5. • Relevant coastal processes time series in Figs. 2.6 to 2.8.	↑ Section 3.6.3 ↓
31	NY; PR; SC		Resamp. wave climate time series (20 min)		
32	NY; PR		Resamp. wave climate time series (30 min)		
33	NY; PR; SC		Resamp. wave climate time series (40 min)		
34	NY; PR; SC		Resamp. wave climate time series (50 min)		
35	SC		Resamp. wave climate time series (60 min)		
36	↑ NY; PR; SC ↓	↑ One ↓	Manning's n reciprocal: 29 $m^{1/3}/s$	• Independent mesh discretisation $intrpl$ with relevant bathy. data in Fig. 2.5. • Relevant coastal processes time series in Figs. 2.6 to 2.8.	↑ Section 3.6.4 ↓
37			Manning's n reciprocal: 33 $m^{1/3}/s$		
38			Manning's n reciprocal: 40 $m^{1/3}/s$		
39			Manning's n reciprocal: 50 $m^{1/3}/s$		
40	↑ NY; PR; SC ↓	↑ One ↓	Sand grain diameter: 0.1 mm	• Independent mesh discretisation $intrpl$ with relevant bathy. data in Fig. 2.5. • Relevant coastal processes time series in Figs. 2.6 to 2.8. • Calibrated Manning's n reciprocal.	↑ Section 3.6.4 ↓
41			Sand grain diameter: 0.25 mm		
42			Sand grain diameter: 0.5 mm		
43			Sand grain diameter: 1 mm		
44	↑ NY; PR; SC ↓	↑ One ↓	Sand porosity: 0.3	• Independent mesh discretisation $intrpl$ with relevant bathy. data in Fig. 2.5. • Relevant coastal processes time series in Figs. 2.6 to 2.8. • Calibrated Manning's n recip. and sand grain diameter.	↑ Section 3.6.4 ↓
45			Sand porosity: 0.5		
46			Sand porosity: 0.7		
47	↑ NY; PR; SC ↓	↑ One ↓	Sediment grading coefficient: 1.3	• Independent mesh discretisation $intrpl$ with relevant bathy. data in Fig. 2.5. • Relevant coastal processes time series in Figs. 2.6 to 2.8. • Calibrated Manning's n recip., sand grain dia., and por.	↑ Section 3.6.4 ↓
48			Sediment grading coefficient: 1.5		
49			Sediment grading coefficient: 2.0		

Simulation	Test site	RQ	Defining specification(s)	Fixed specification(s)	Details
50	↑ NY; PR; SC ↓	↑ One ↓	Weir coefficient: 0.11 $m^{1/2}/s$	• Independent mesh discretisation $intrpl$ with relevant bathy. data in Fig. 2.5. • Relevant coastal processes time series in Figs. 2.6 to 2.8. • Calibrated Manning's n reciprocal, sand grain diameter, sand porosity, and sediment grading coefficient.	↑ Section 3.6.4 ↓
51			Weir coefficient: 0.55 $m^{1/2}/s$		
52			Weir coefficient: 0.77 $m^{1/2}/s$		
53			Weir coefficient: 0.99 $m^{1/2}/s$		
54			Weir coefficient: 1.21 $m^{1/2}/s$		
55			Weir coefficient: 1.44 $m^{1/2}/s$		
56			Weir coefficient: 1.82 $m^{1/2}/s$		
57			Weir coefficient: 2.21 $m^{1/2}/s$		
58 (RQ2 hindcast one)	↑ NY ↓	↑ Two ↓	• Mesh $intrpl$ with 1966 bathy. (Fig. 2.9a). • 4.2 m closure depth. • Connecting boundaries closed in MIKE21 HD (no Flather data).	• Period: 01-Jan-1966 to 01-Feb-2016 • Independent mesh discretisation. • Tide time series in Fig. 2.9c. • Wind and wave climate time series in Fig. 2.6. • Calibrated Manning's n reciprocal, sand grain diameter, sand porosity, and sediment grading coefficient.	↑ Section 3.8.1 ↓
59 (RQ2 hindcast two)			• Mesh $intrpl$ with 1966 bathy. (Fig. 2.9a). • 4.2 m closure depth.		
60 (RQ2 hindcast three)			• Mesh $intrpl$ with x, y from 1966 bathy., and z from 2014 bathy (modified bathy.). • 6 m closure depth.		
61 (RQ2 hindcast four)			• Mesh $intrpl$ with modified bathy. • Closure depth: most seaward depth in mesh bathy.		
62 (RQ2 hindcast five)			• Annual closure depth variations.		
63 (RQ2 forecast one)	↑ NY ↓	↑ Two ↓	• Mesh $intrpl$ with 2014 bathy. (Fig. 2.5a). • 5.8 m closure depth.	• Period: 01-Jan-2014 to 01-Jan-2064 • Independent mesh discretisation. • Tide time series in Fig. 2.9c superimposed with a sea-level rise of 0.28 m*. • Wind and wave climate time series in Fig. 2.6. • Calibrated Manning's n reciprocal, sand grain diameter, sand porosity, and sediment grading coefficient.	↑ Section 3.8.3 ↓
64 (RQ2 forecast two)			• Mesh $intrpl$ with 2014 bathy. (Fig. 2.5a). • Closure depth: most seaward depth in 2014 bathy.		
65 (RQ2 forecast three)			• Annual closure depth variations.		

Simulation	Test site	RQ	Defining specification(s)	Fixed specification(s)	Details
66 (RQ3 hindcast one)	↑ PR ↓	↑ Three ↓	• Mesh $intrpl$ with 2014 bathy. (Fig. 2.5b). • 5.5 m closure depth.	• Period: 10-Oct-2014 to 31-Mar-2016 • Independent mesh discretisation. • Tide, wind, and wave climate time series in Fig. 2.7. • Calibrated Manning's n reciprocal, sand grain diameter, sand porosity, and sediment grading coefficient.	↑ Section 3.9.1 ↓
67 (RQ3 hindcast two):			• Space varying closure depth.		
68 (RQ4 forecast one)	↑ PR ↓	↑ Four ↓	• Mesh $intrpl$ with 2014 bathy. (Fig. 2.5b). • 5.5 m closure depth. • Connecting boundaries closed in MIKE21 HD.	• Period: 10-Oct-2014 to 10-Oct-2064 • Independent mesh discretisation. • Tide time series in Fig. 2.10 superimposed with a sea-level rise of 0.28 m*. • Wind and wave climate time series in Fig. 2.7. • Calibrated Manning's n reciprocal, sand grain diameter, sand porosity, and sediment grading coefficient.	↑ Section 3.10 ↓
69 (RQ4 forecast two)			• Mesh $intrpl$ with 2014 bathy. (Fig. 2.5b). • Closure depth: most seaward depth in 2014 bathy.		
70 (RQ4 forecast three)			• Time and space-varying closure depth.		
71 (RQ4 forecast four)			• Mesh $intrpl$ with 2014 bathy. (Fig. 2.5b). • 5.5 m closure depth.		

* IPCC global median sea-level rise projection for 2046 to 2065 (Church et al., 2013).

Table 3.11 Summary of each Bruun Rule simulation carried out for addressing research questions one to four. RQ is research question, NY is the New York test site, PR is the Puerto Rico test site, SC is the Southern California test site, L is the distance between beach berm (D_b) and closure depth (D_c), and SLR is sea-level rise.

Simulation	Test site	RQ	Defining specification(s)	Fixed specification(s)	Details
1	NY; PR; SC		L estimated from relevant bathy. data in Fig. 2.5		
2	NY; PR		L estimated from resampled bathy. (9 m)		
3	NY; PR; SC	↑	L estimated from resampled bathy. (27 m)	• Relevant period and D_b in Table 3.2. • Relevant D_c in Table 3.2 (NY; SC). • D_c varies in PR based on reef distribution. • SLR based on relative sea-level rise rate.	↑ Section 3.6.2 ↓
4	NY; PR; SC	One	L estimated from resampled bathy. (81 m)		
5	NY; PR; SC	↓	L estimated from resampled bathy. (90 m)		
6	NY; PR; SC		L estimated from resampled bathy. (100 m)		
7	NY; PR; SC		L estimated from resampled bathy. (500 m)		
8	↑	↑	SLR based on unadjusted tide data.	• Relevant period and D_b in Table 3.2. • Relevant D_c in Table 3.2 (NY; SC). • D_c varies in PR based on reef distribution. • L based on D_b and D_c contours in relevant bathy. data in Fig. 2.5.	↑ Section 3.6.3 ↓
9	NY; PR; SC	One	SLR based on seasonally adjusted tide data.		
10	↓	↓	SLR based on NOAA tide predictions.		
11 (RQ2 hindcast six)	NY	Two	L and D_c derived from 1966 bathy. (Fig. 2.9a).	• Period: 01-Jan-1966 to 01-Jan-2016 • D_b is 1.14 m above MHW. • SLR based on NY sea-level rise rate (0.004 m yr^{-1}).	Section 3.8.2
12 (RQ2 forecast four)	NY	Two	L and D_c derived from 2014 bathy. (Fig. 2.5a).	• Period: 01-Jan-2014 to 01-Jan-2064 • D_b is 1.14 m above MHW. • SLR is 0.28 m*	Section 3.8.3
13 (RQ3 hindcast three)	PR	Three	↑ L and D_c varies based on reef distribution in 2014 bathy. (Fig. 2.5b). ↓	• Period: 10-Oct-2014 to 31-Mar-2016 • D_b is 1.5 m above MHW. • SLR based on PR sea-level rise rate (0.002 m yr^{-1}).	Section 3.9.2
14 (RQ4 forecast five)	PR	Four		• Period: 10-Oct-2014 to 10-Oct-2064 • D_b is 1.5 m above MHW. • SLR is 0.28 m*	Section 3.10

* IPCC global median sea-level rise projection for 2046 to 2065 (Church et al., 2013).

04
Sensitivity to boundary conditions: figures and tables

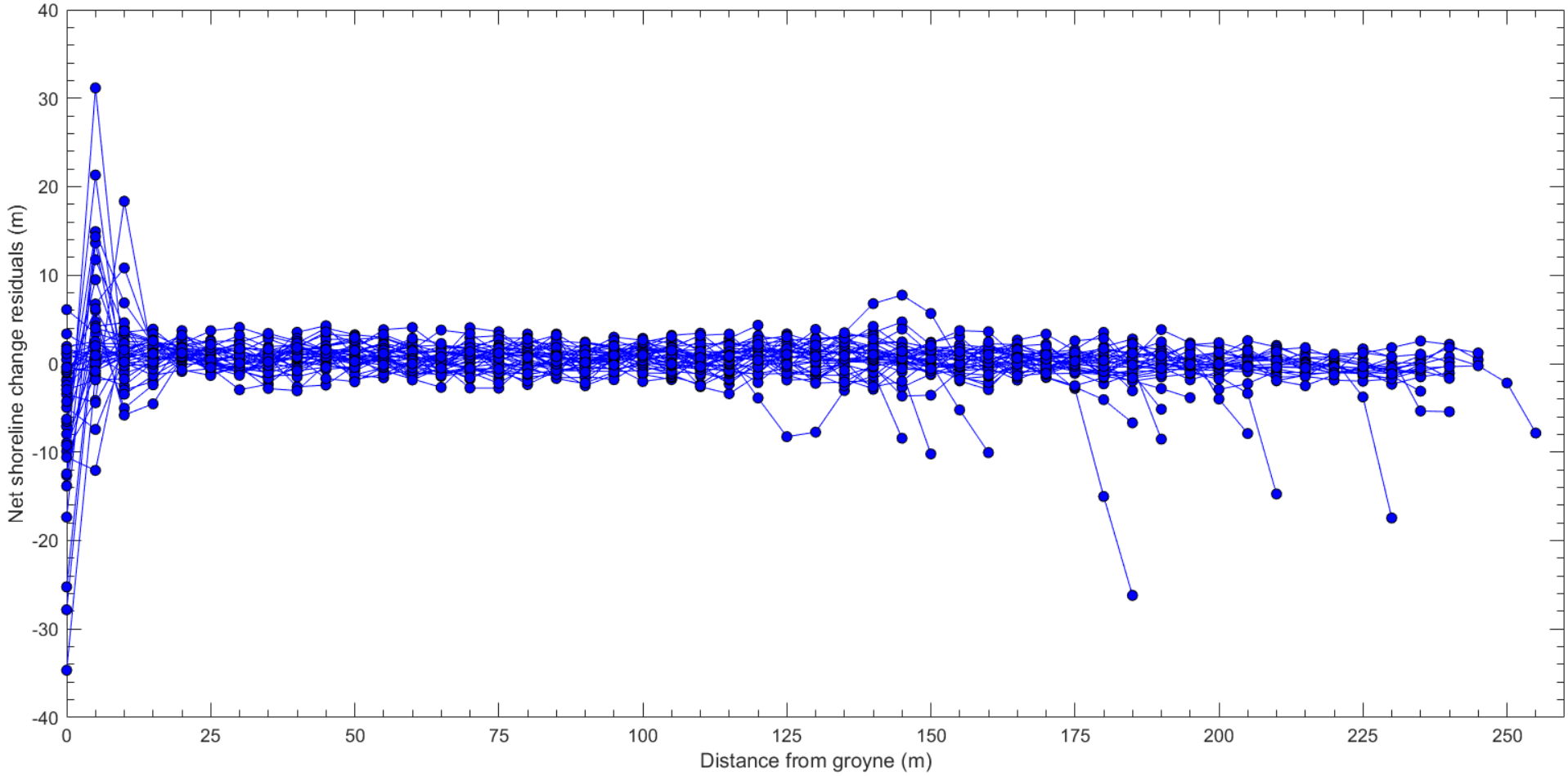

Fig. 4.1 MIKE21 net shoreline change residuals relative to groynes' distance in the New York test site. Net shoreline change residuals above are the difference between net shoreline change observed and predicted from 01-Jan-2014 to 01-Feb-2016. The take-home message from this figure is that the largest residuals occur at or near groyne locations in the New York test site as MIKE21 ignore the bed features over which the active coastal profile migrates.

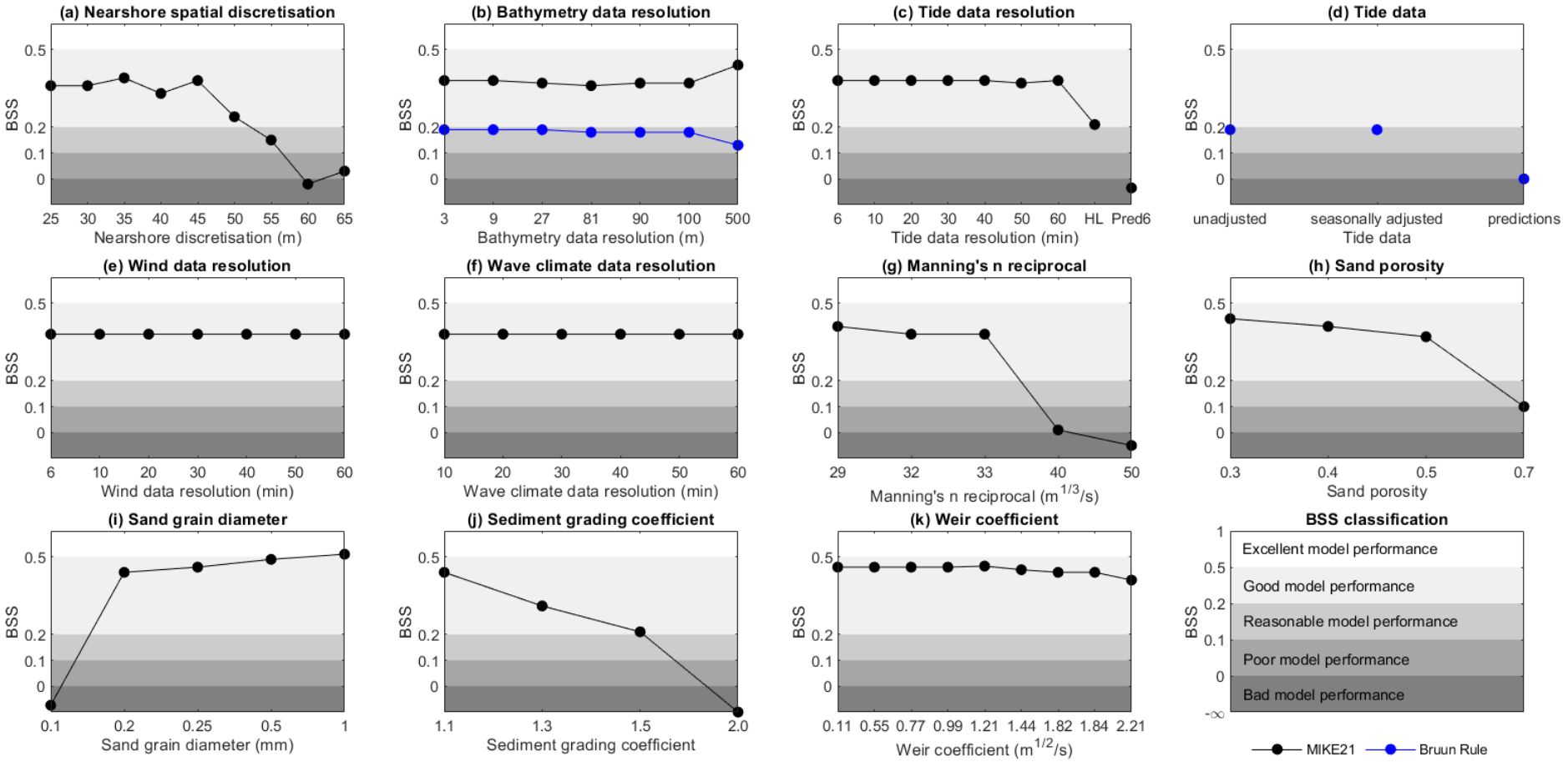

Fig. 4.2 Brier Skill Scores (BSS) estimated from net shoreline change predictions (01-Jan-2014 to 01-Feb-2016) in response to boundary conditions in the New York test site. In (c), HL is daily high/low tide data, and Pred6 is NOAA tide predictions (6 min intervals). In (d), unadjusted is observed tide levels, seasonally adjusted is observed tide levels without the regular seasonal fluctuations in meteorological conditions, and predictions are NOAA calculations of expected tide levels. BSS values < 0 in (c), (i), and (j) are scaled to fall within 0 to -0.1 to better illustrate changes in model accuracy in response to boundary conditions.

Table 4.1 Summary of net shoreline change (01-Jan-2014 to 01-Feb-2016) observed and predicted in response to boundary conditions in the New York test site. M is MIKE21, B is the Bruun Rule, MNC is mean net change, MAC is mean absolute change, MAE is mean absolute error, and BSS is Brier Skill Score. All bolded Kruskal-Wallis p values are less than the 5% significance level, indicating significant differences between net shoreline change predictions. Other bold highlights show samples of net shoreline change predictions significantly different from other samples, based on a Dunn's test. Appendix A contains all spatial distribution plots of net shoreline change associated with statistics in Table 4.1, excluding those incorporated in this chapter.

Input	Specification	MNC (m)	MAC (m)	MAE (m)	BSS	Kruskal-Wallis
Observed net shoreline change	**-**	-0.01	1.16	-	-	-
Nearshore spatial discretisation (m)	25	-0.15	0.87	1.17	0.36	p = 0.863
	30	-0.19	0.87	1.15	0.36	
	35	-0.18	0.88	1.15	0.39	
	40	-0.17	0.89	1.2	0.33	
	45	-0.17	0.88	1.2	0.38	
	50	-0.19	0.96	1.24	0.24	
	55	-0.18	1.01	1.31	0.15	
	60	-0.2	1.17	1.4	-0.02	
	65	-0.21	1.11	1.41	0.03	
Bathymetry data resolution (m)	3	-0.17 (M); -0.32 (B)	0.88 (M); 0.32 (B)	1.2 (M); 1.18 (B)	0.38 (M); 0.19 (B)	p = 0.631 (M) **p < 0.0001 (B)**
	9	-0.17 (M); -0.32 (B)	0.87 (M); 0.32 (B)	1.2 (M); 1.18 (B)	0.38 (M); 0.19 (B)	
	27	-0.16 (M); -0.32 (B)	0.86 (M); 0.32 (B)	1.2 (M); 1.18 (B)	0.37 (M); 0.19 (B)	
	81	-0.18 (M); -0.33 (B)	0.87 (M); 0.33 (B)	1.2 (M); 1.18 (B)	0.36 (M); 0.18 (B)	
	90	-0.17 (M); -0.33 (B)	0.86 (M); 0.33 (B)	1.19 (M); 1.18 (B)	0.37 (M); 0.18 (B)	
	100	-0.19 (M); -0.33 (B)	0.86 (M); 0.33 (B)	1.18 (M); 1.18 (B)	0.37 (M); 0.18 (B)	
	500	-0.2 (M); **-0.55 (B)**	0.82 (M); **0.55 (B)**	1.09 (M); **1.24 (B)**	0.44 (M); **0.13 (B)**	
Tide data resolution (min): MIKE21	6	-0.17	0.88	1.2	0.38	**p = 0.008**
	10	-0.17	0.88	1.2	0.38	
	20	-0.17	0.88	1.2	0.38	
	30	-0.17	0.88	1.2	0.38	
	40	-0.17	0.88	1.2	0.38	
	50	-0.17	0.88	1.2	0.37	
	60	-0.17	0.87	1.2	0.38	
	Daily high/low	-0.12	0.97	1.29	0.21	
	NOAA predictions	**-0.02**	**1.21**	**1.51**	**-0.35**	

Input	Specification	MNC (m)	MAC (m)	MAE (m)	BSS	Kruskal-Wallis
Observed net shoreline change	-	-0.01	1.16	-	-	-
Tide data: Bruun Rule	**Unadjusted**	**-0.31**	**0.31**	**1.18**	**0.19**	**p < 0.0001**
	Seasonally adjusted	**-0.32**	**0.32**	**1.18**	**0.19**	
	NOAA predictions	**0.02**	**0.02**	**1.16**	**0**	
Wind data resolution (min)	6	-0.17	0.88	1.2	0.38	p = 1
	10	-0.17	0.88	1.2	0.38	
	20	-0.18	0.88	1.2	0.38	
	30	-0.17	0.88	1.2	0.38	
	40	-0.17	0.88	1.2	0.38	
	50	-0.17	0.88	1.2	0.38	
	60	-0.18	0.88	1.2	0.38	
Wave climate data resolution (min)	10	-0.17	0.88	1.2	0.38	p = 1
	20	-0.17	0.88	1.2	0.38	
	30	-0.17	0.88	1.2	0.38	
	40	-0.17	0.88	1.2	0.38	
	50	-0.17	0.88	1.2	0.38	
	60	-0.17	0.88	1.2	0.38	
Manning's n reciprocal ($m^{1/3}/s$)	29	-0.17	0.83	1.16	0.41	p = 0.573
	32	-0.17	0.88	1.2	0.38	
	33	-0.17	0.89	1.2	0.38	
	40	-0.17	1.16	1.47	0.01	
	50	-0.21	1.26	1.56	-0.05	
Sand porosity	0.3	-0.17	0.79	1.13	0.44	p = 0.507
	0.4	-0.17	0.83	1.16	0.41	
	0.5	-0.17	0.89	1.2	0.37	
	0.7	-0.16	1.19	1.45	0.1	
Sand grain diameter (mm)	**0.1**	**0.46**	**11.85**	**11.78**	**-73.66**	**p < 0.0001**
	0.2	-0.17	0.79	1.13	0.44	
	0.25	-0.16	0.75	1.1	0.46	
	0.5	-0.17	0.66	1.05	0.49	
	1	-0.19	0.62	1.02	0.51	

Input	Specification	MNC (m)	MAC (m)	MAE (m)	BSS	Kruskal-Wallis
Observed net shoreline change	-	-0.01	1.16	-	-	-
Sediment grading coefficient	1.1	-0.17	0.79	1.13	0.44	p = 0.124
	1.3	-0.15	0.97	1.27	0.31	
	1.5	-0.15	1.41	1.64	-0.21	
	2	1.71	43.33	43.32	-1 169.67	
Weir coefficient ($m^{1/2}/s$)	0.11	-0.16	0.76	1.49	0.46	p = 1
	0.55	-0.16	0.76	1.48	0.46	
	0.77	-0.16	0.76	1.48	0.46	
	0.99	-0.16	0.76	1.48	0.46	
	1.21	-0.16	0.76	1.49	0.46	
	1.44	-0.17	0.77	1.51	0.45	
	1.82	-0.17	0.79	1.52	0.44	
	1.838	-0.17	0.79	1.52	0.44	
	2.21	-0.16	0.82	1.56	0.41	

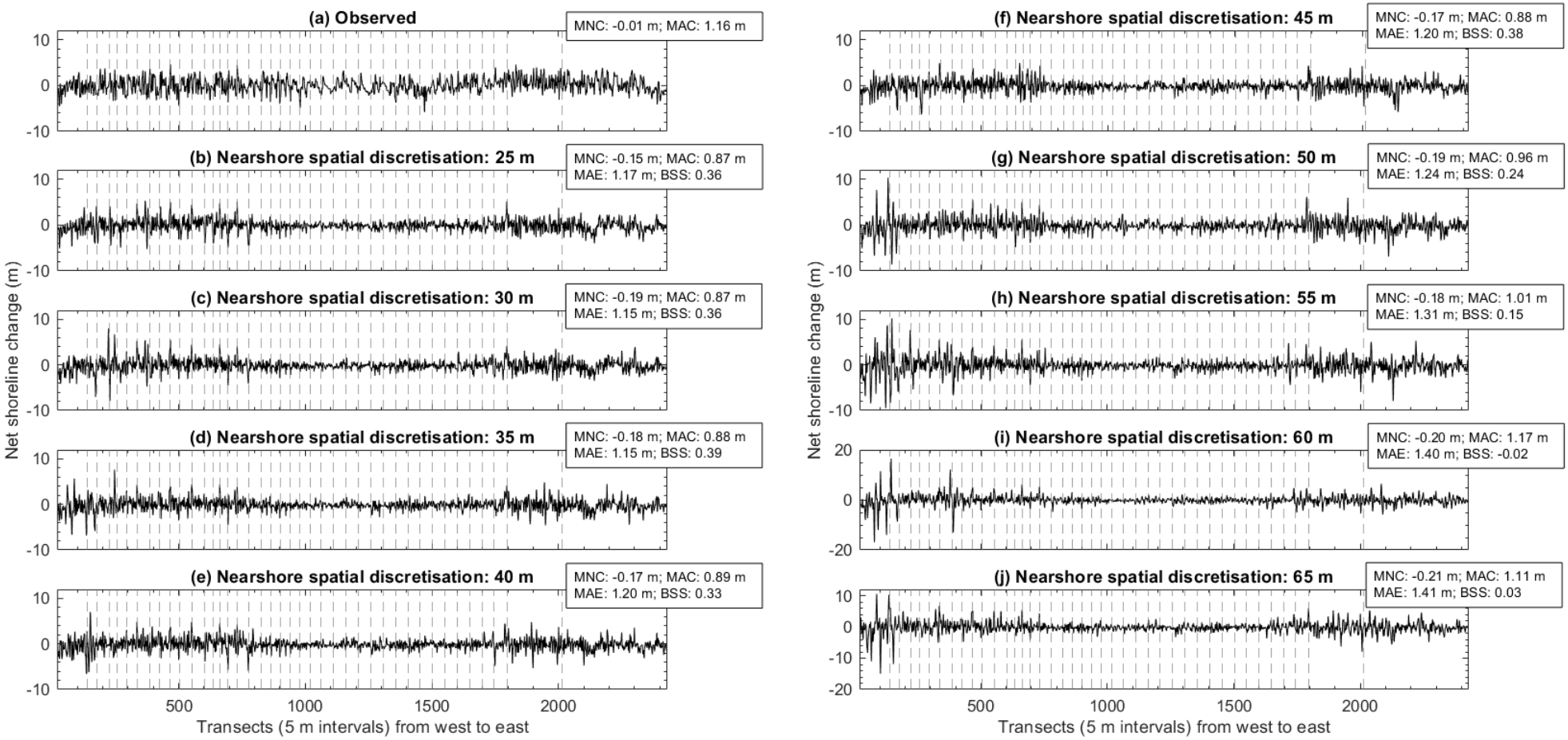

Fig. 4.3 Net shoreline change (01-Jan-2014 to 01-Feb-2016) observed and predicted in response to coarsening nearshore spatial discretisation in the New York test site. Vertical dashed lines indicate groyne locations. MNC is mean net change, MAC is mean absolute change, MAE is mean absolute error, and BSS is Brier Skill Score. Note the difference in y axis in (i) and (j). Net shoreline change observed and predicted in groyne transects are excluded from the above plots and statistics.

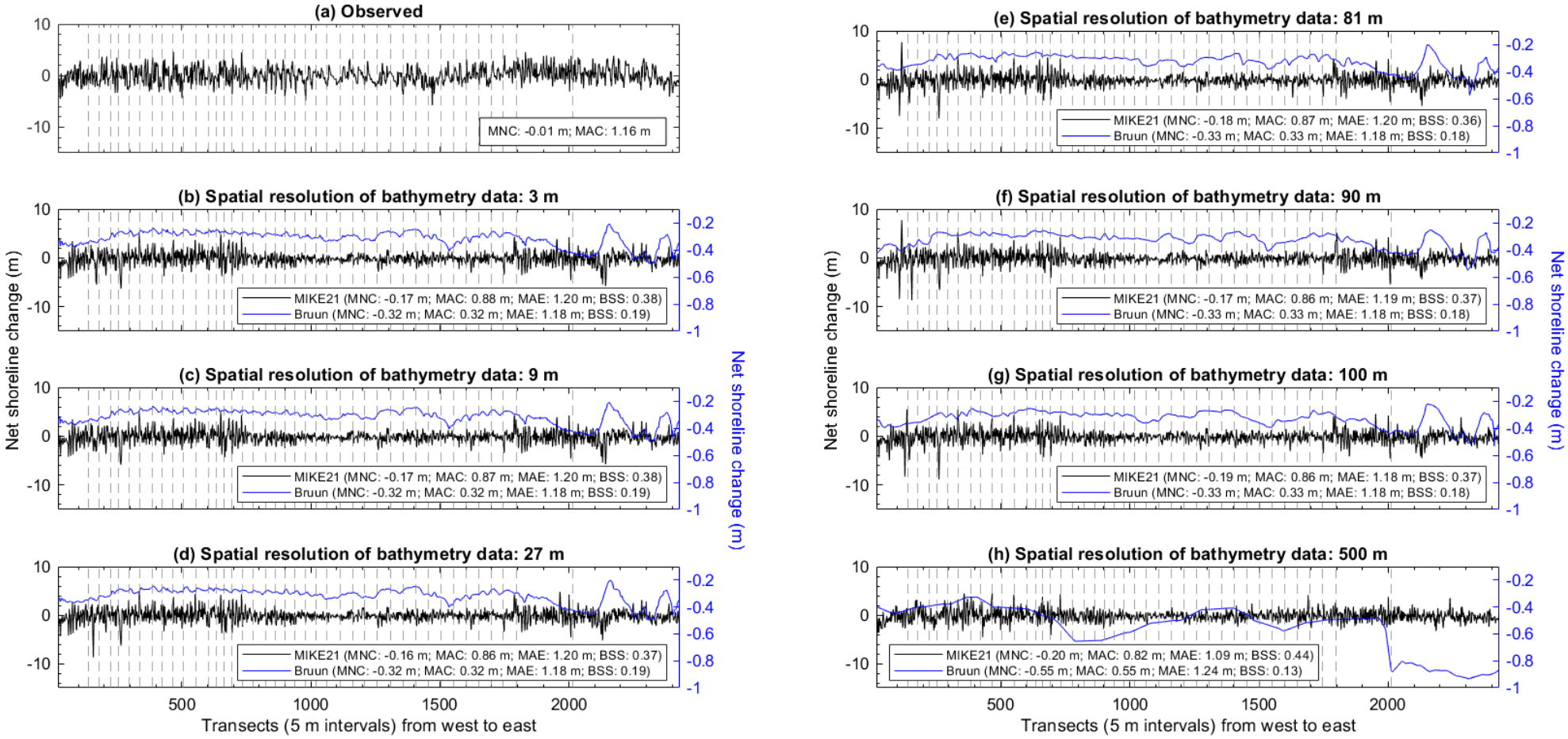

Fig. 4.4 Net shoreline change (01-Jan-2014 to 01-Feb-2016) observed and predicted in response to coarsening bathymetry data in the New York test site. Vertical dashed lines indicate groyne locations. MNC is mean net change, MAC is mean absolute change, MAE is mean absolute error, and BSS is Brier Skill Score. Note there is a separate y axis for MIKE21 and the Bruun Rule predictions in (b) to (h). Net shoreline change observed and predicted in groyne transects are excluded from the above plots and statistics.

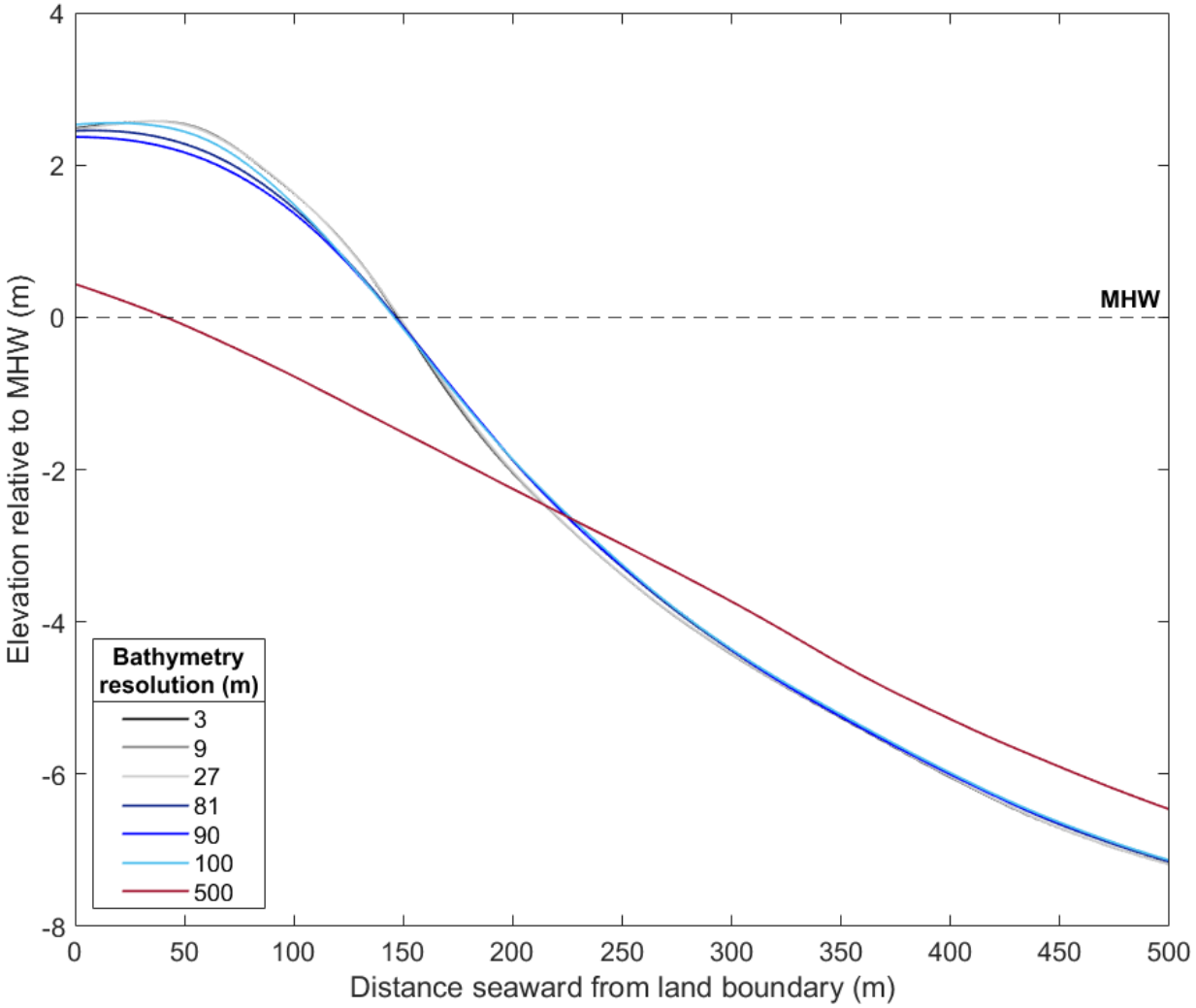

Fig. 4.5 Coarsening bathymetry data effects on the New York test site's average coastal profile.

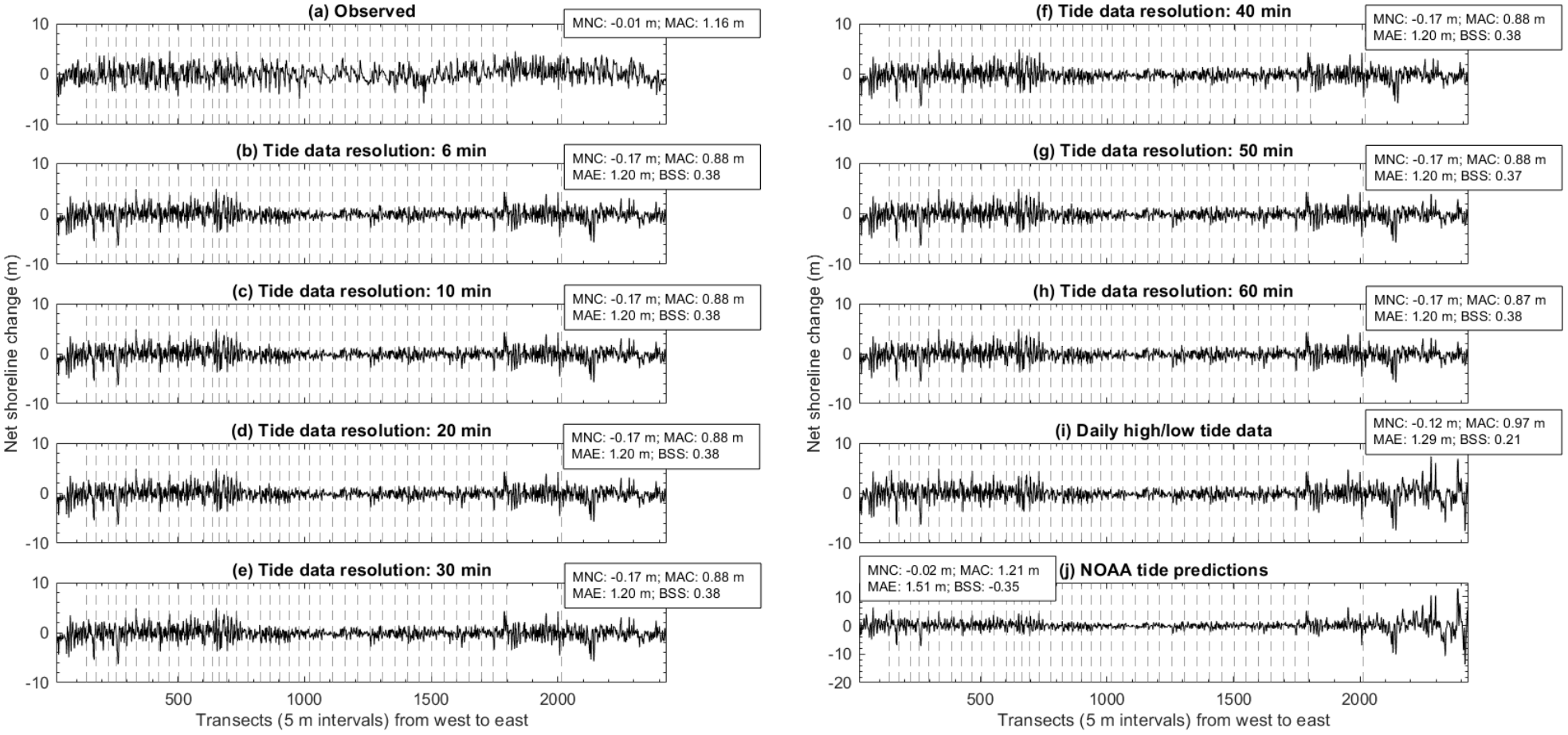

Fig. 4.6 Net shoreline change (01-Jan-2014 to 01-Feb-2016) observed and predicted from MIKE21 in response to tide data resolution in the New York test site. Vertical dashed lines indicate groyne locations. MNC is mean net change, MAC is mean absolute change, MAE is mean absolute error, and BSS is Brier Skill Score. Note the difference in y axis in (j). Net shoreline change observed and predicted in groyne transects are excluded from the above plots and statistics.

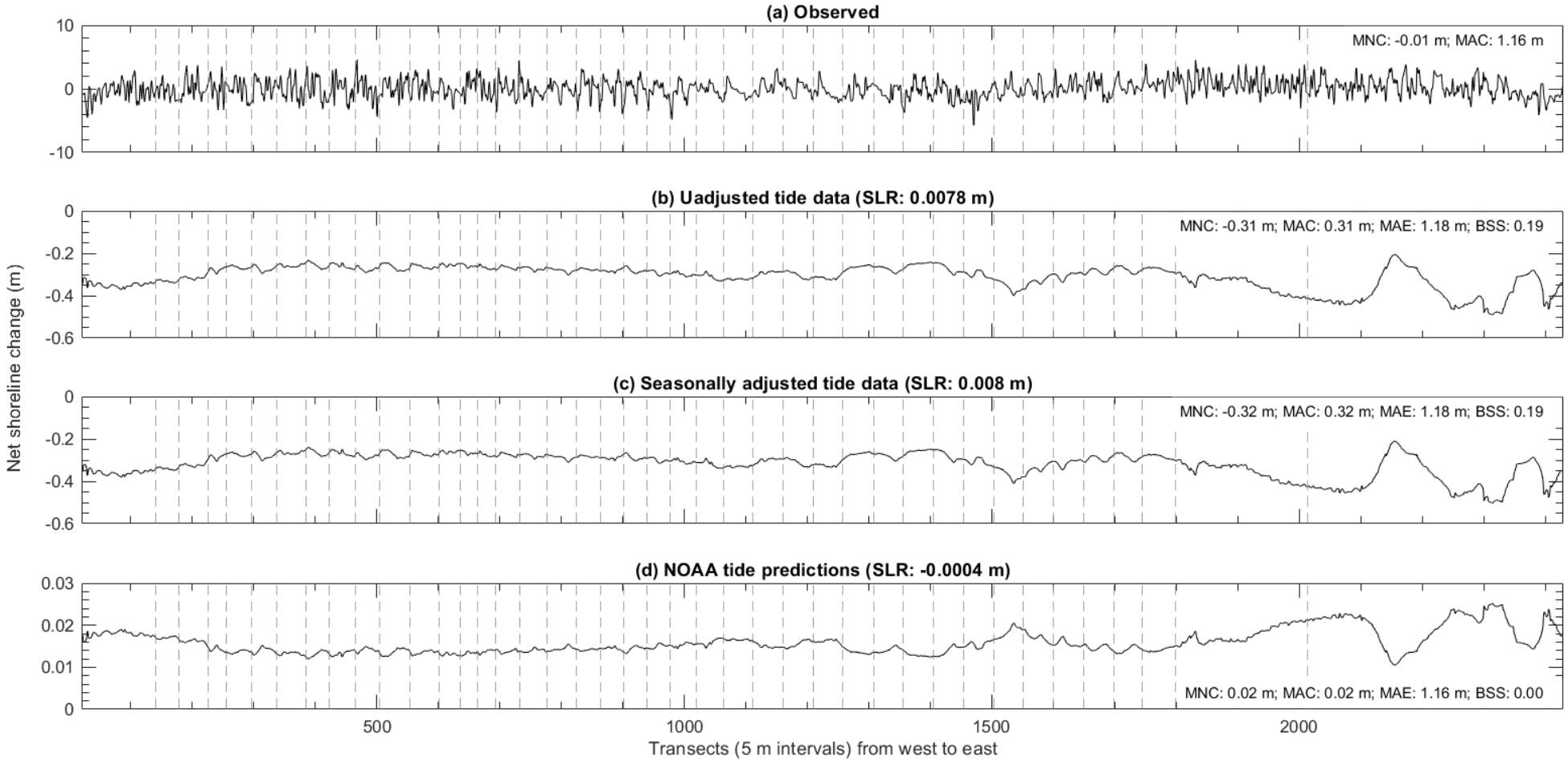

Fig. 4.7 Net shoreline change (01-Jan-2014 to 01-Feb-2016) observed and predicted from the Bruun Rule in response to SLR estimations from different tide datasets in the New York test site. Vertical dashed lines indicate groyne locations. MNC is mean net change, MAC is mean absolute change, MAE is mean absolute error, and BSS is Brier Skill Score. Note the differences in y axis. Net shoreline change observed and predicted in groyne transects are excluded from the above plots and statistics.

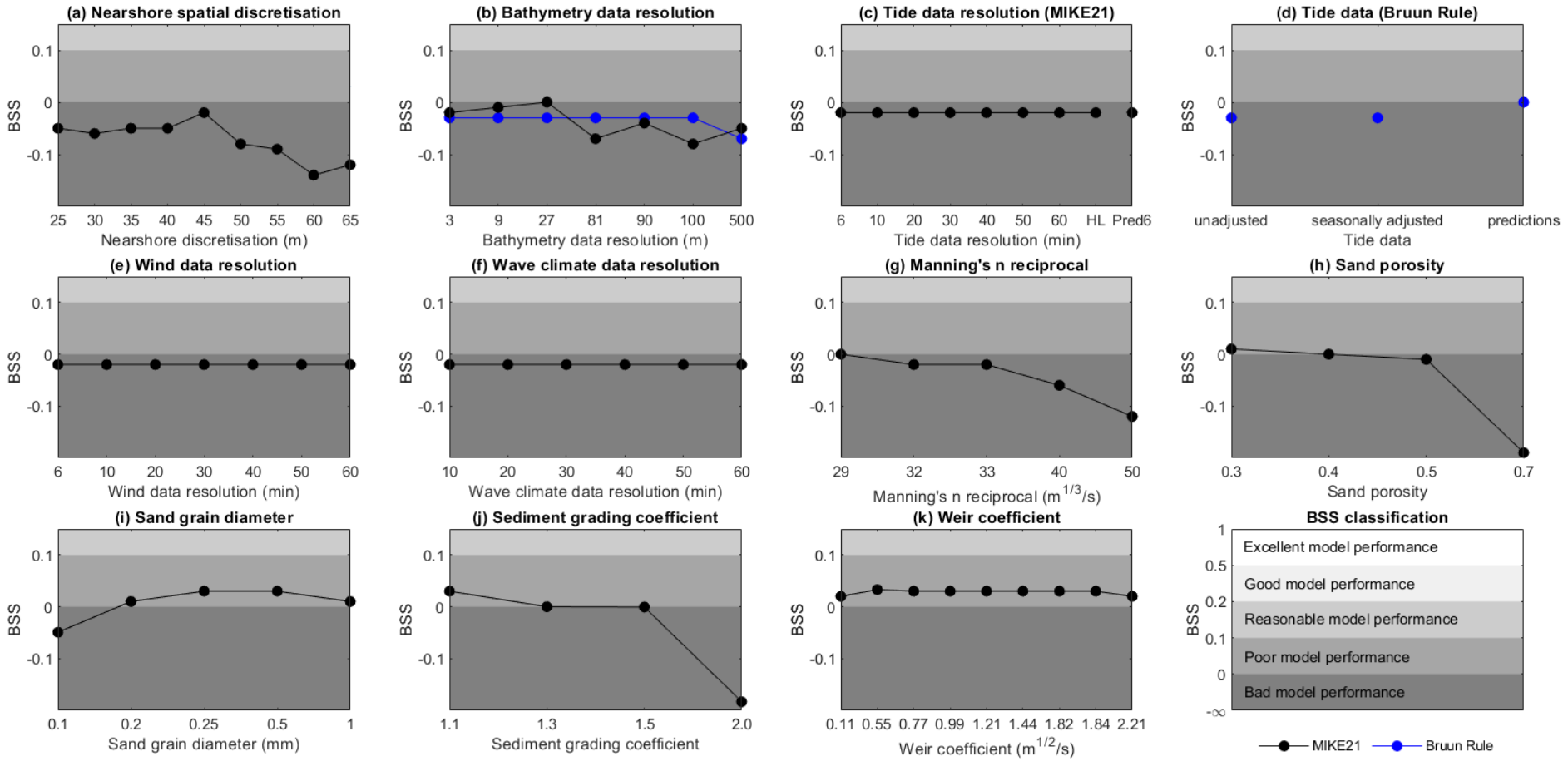

Fig. 4.8 Brier Skill Scores (BSS) estimated from net shoreline change predictions (10-Oct-2014 to 31-Mar-2016) in response to boundary conditions in the Puerto Rico test site. In (c), HL is daily high/low tide data, and Pred6 is NOAA tide predictions (6 min intervals). In (d), unadjusted is observed tide levels, seasonally adjusted is observed tide levels without the regular seasonal fluctuations in meteorological conditions, and predictions are NOAA calculations of expected tide levels. BSS values < 0 in (i) and (j) are scaled to fall within 0 to -0.2 to better illustrate changes in model accuracy in response to boundary conditions.

Table 4.2 Summary of net shoreline change (10-Oct-2014 to 31-Mar-2016) observed and predicted in response to boundary conditions in the Puerto Rico test site. M is MIKE21, B is the Bruun Rule, MNC is mean net change, MAC is mean absolute change, MAE is mean absolute error, and BSS is Brier Skill Score. All bolded Kruskal-Wallis p values are less than the 5% significance level, indicating significant differences between net shoreline change predictions. Other bold highlights show samples of net shoreline change predictions significantly different from other samples, based on a Dunn's test. Appendix A contains all spatial distribution plots of net shoreline change associated with statistics in Table 4.2, excluding those incorporated in this chapter.

Input	Specification	MNC (m)	MAC (m)	MAE (m)	BSS	Kruskal-Wallis
Observed net shoreline change	-	3.22	5.03	-	-	-
Nearshore spatial discretisation (m)	25	0.13	1.18	5.17	-0.05	p = 0.935
	30	0.14	1.23	5.17	-0.06	
	35	0.13	1.25	5.14	-0.05	
	40	0.17	1.23	5.14	-0.05	
	45	0.13	1.25	5.11	-0.02	
	50	0.13	1.41	5.18	-0.08	
	55	0.15	1.29	5.15	-0.09	
	60	0.13	1.41	5.15	-0.14	
	65	0.14	1.41	5.17	-0.12	
Bathymetry data resolution (m)	3	0.13 (M); -0.18 (B)	1.25 (M); 0.18 (B)	5.11 (M); 5.10 (B)	-0.02 (M); -0.03 (B)	p = 0.877 (M) **p < 0.0001 (B)**
	9	0.17 (M); -0.18 (B)	1.21 (M); 0.18 (B)	5.10 (M); 5.10 (B)	-0.01 (M); -0.03 (B)	
	27	0.15 (M); -0.19 (B)	1.13 (M); 0.19 (B)	5.05 (M); 5.11 (B)	0.00 (M); -0.03 (B)	
	81	0.14 (M); **-0.21 (B)**	1.21 (M); **0.21 (B)**	5.24 (M); **5.12 (B)**	-0.07 (M); **-0.03 (B)**	
	90	0.14 (M); **-0.22 (B)**	1.30 (M); **0.22 (B)**	5.14 (M); **5.12 (B)**	-0.04 (M); **-0.03 (B)**	
	100	0.14 (M); **-0.22 (B)**	1.18 (M); **0.22 (B)**	5.17 (M); **5.12 (B)**	-0.08 (M); **-0.03 (B)**	
	500	0.11 (M); **-0.37 (B)**	0.96 (M); **0.37 (B)**	5.10 (M); **5.22 (B)**	-0.05 (M); **-0.07 (B)**	
Tide data resolution (min): MIKE21	6	0.13	1.25	5.11	-0.02	p = 1
	10	0.15	1.27	5.11	-0.02	
	20	0.14	1.27	5.12	-0.02	
	30	0.14	1.27	5.12	-0.02	
	40	0.15	1.27	5.11	-0.02	
	50	0.15	1.27	5.11	-0.02	
	60	0.15	1.27	5.12	-0.02	
	Daily high/low	0.15	1.26	5.11	-0.02	
	NOAA predictions	0.13	1.24	5.1	-0.02	

Input	Specification	MNC (m)	MAC (m)	MAE (m)	BSS	Kruskal-Wallis
Observed net shoreline change	**-**	3.22	5.03	-	-	-
Tide data: Bruun Rule	**Unadjusted**	**-0.21**	**0.21**	**5.11**	**-0.03**	**p < 0.0001**
	Seasonally adjusted	**-0.18**	**0.18**	**5.10**	**-0.03**	
	NOAA predictions	**0**	**0**	**5.03**	**0**	
Wind data resolution (min)	6	0.13	1.25	5.11	-0.02	p = 1
	10	0.14	1.25	5.11	-0.02	
	20	0.14	1.25	5.11	-0.02	
	30	0.15	1.25	5.1	-0.02	
	40	0.15	1.25	5.1	-0.02	
	50	0.15	1.26	5.1	-0.02	
	60	0.15	1.25	5.1	-0.02	
Wave climate data resolution (min)	10	0.14	1.25	5.11	-0.02	p = 1
	20	0.14	1.25	5.11	-0.02	
	30	0.14	1.25	5.11	-0.02	
	40	0.13	1.25	5.11	-0.02	
	50	0.15	1.26	5.11	-0.02	
	60	0.13	1.25	5.11	-0.02	
Manning's n reciprocal ($m^{1/3}/s$)	29	0.12	1.13	5.08	0	p = 0.975
	32	0.13	1.25	5.11	-0.02	
	33	0.16	1.28	5.11	-0.02	
	40	0.18	1.54	5.19	-0.06	
	50	0.19	1.86	5.34	-0.12	
Sand porosity	0.3	0.14	0.99	5.04	0.01	p = 0.960
	0.4	0.13	1.25	5.11	0	
	0.5	0.14	1.3	5.11	-0.01	
	0.7	0.19	2.19	5.49	-0.19	
Sand grain diameter (mm)	**0.1**	**1.13**	**11.76**	**12.55**	**-9.85**	**p = 0.009**
	0.2	0.14	0.99	5.04	0.01	
	0.25	0.11	0.82	5	0.03	
	0.5	0.1	0.51	4.99	0.03	
	1	0.06	0.28	5.02	0.01	

Input	Specification	MNC (m)	MAC (m)	MAE (m)	BSS	Kruskal-Wallis
Observed net shoreline change	-	3.22	5.03	-	-	-
Sediment grading coefficient	1.1	0.11	0.82	5	0.03	p = 0.066
	1.3	0.13	1.255	5.12	-0.02	
	1.5	0.23	2.14	5.44	-0.17	
	2	1.84	27.14	26.80	-55.01	
Weir coefficient ($m^{1/2}/s$)	0.11	0.11	0.82	5	0.02	p = 1
	0.55	0.11	0.82	5	0.03	
	0.77	0.11	0.82	5	0.03	
	0.99	0.11	0.82	5	0.03	
	1.21	0.11	0.82	5	0.03	
	1.44	0.11	0.82	5	0.03	
	1.82	0.11	0.82	5	0.03	
	1.838	0.11	0.82	5	0.03	
	2.21	0.12	0.83	5.01	0.02	

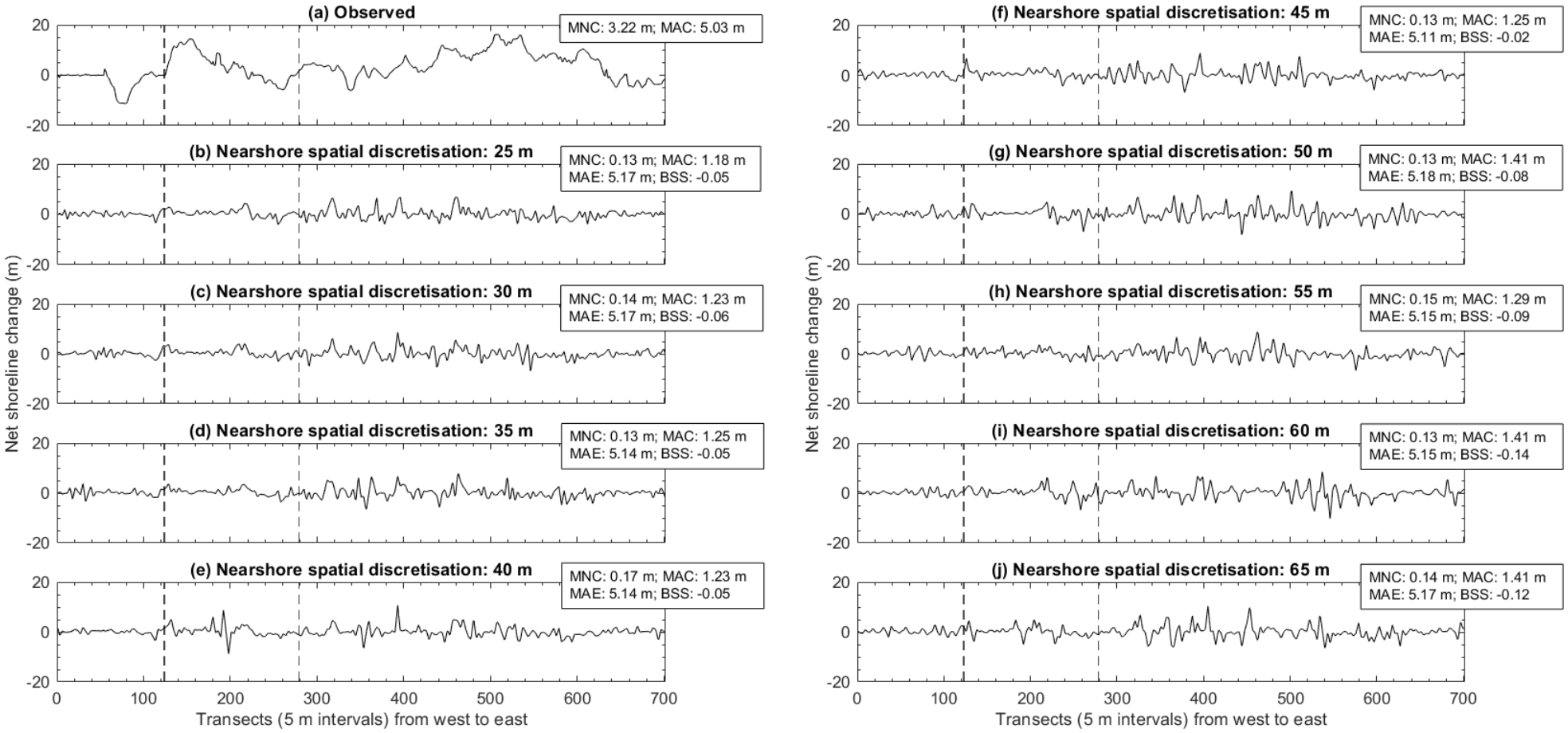

Fig. 4.9 Net shoreline change (10-Oct-2014 to 31-Mar-2016) observed and predicted in response to coarsening nearshore spatial discretisation in the Puerto Rico test site. Vertical dashed lines indicate groyne locations. MNC is mean net change, MAC is mean absolute change, MAE is mean absolute error, and BSS is Brier Skill Score. Net shoreline change observed and predicted in groyne transects are excluded from the above plots and statistics.

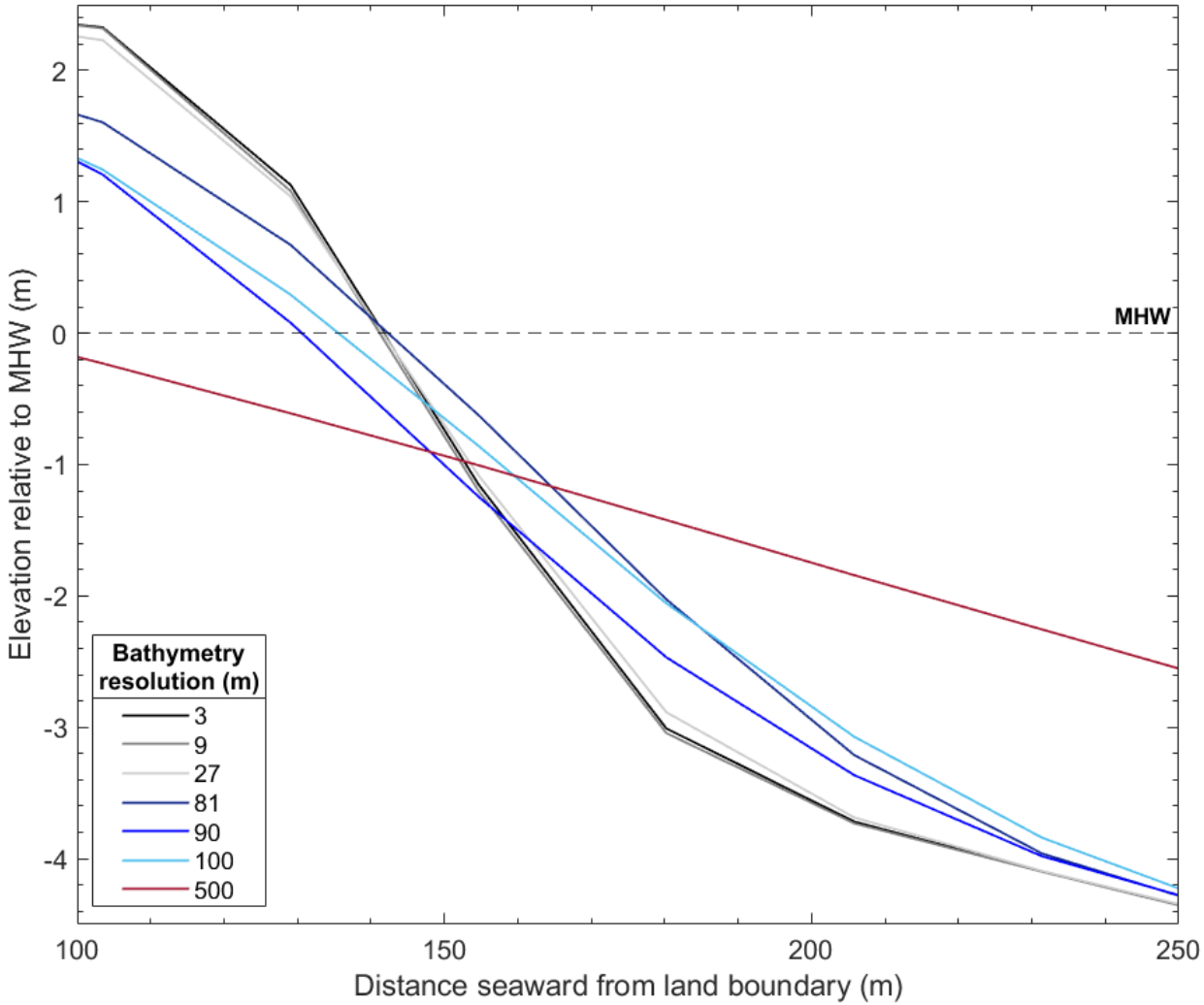

Fig. 4.10 Coarsening bathymetry data effects on the Puerto Rico test site's average upper beach profile.

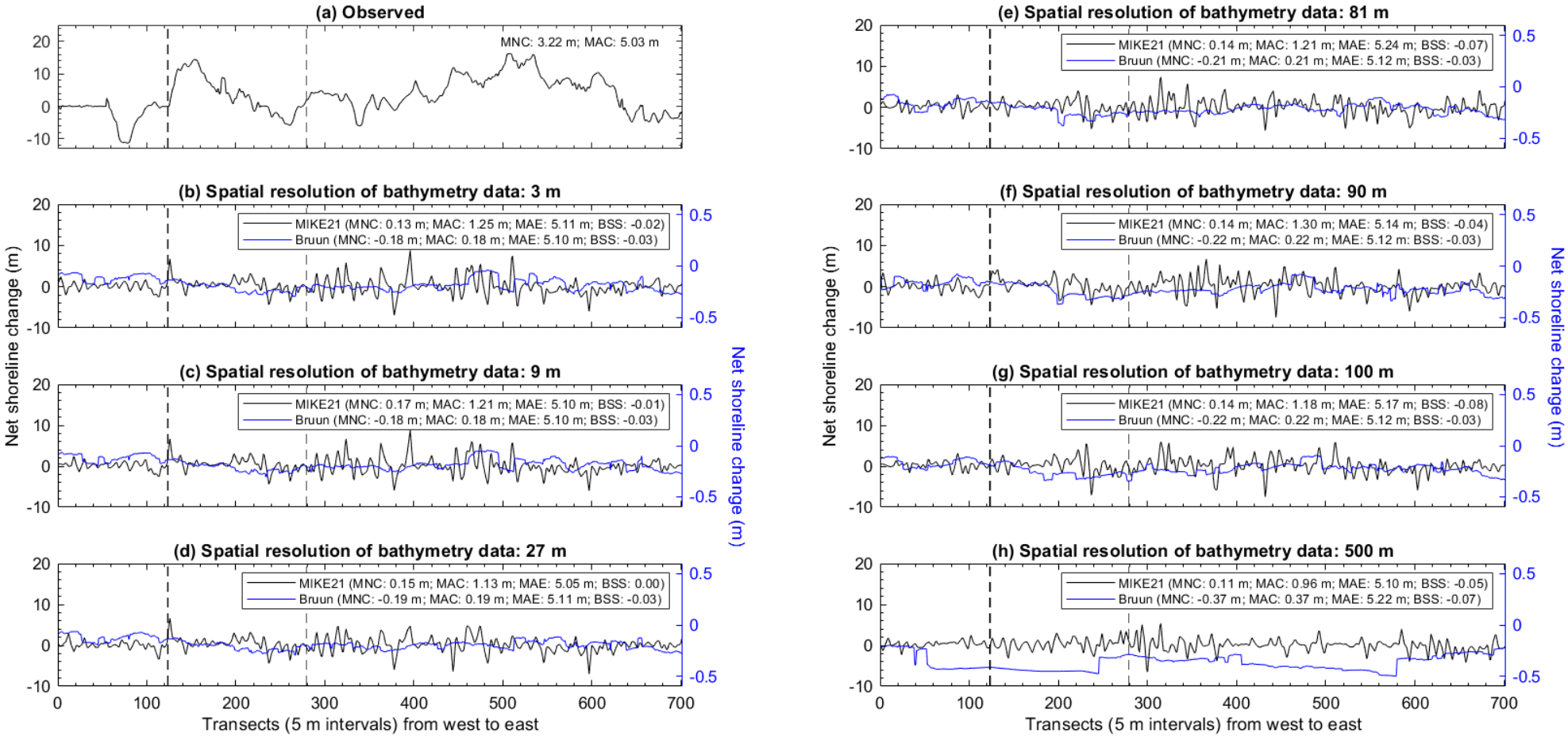

Fig. 4.11 Net shoreline change (10-Oct-2014 to 31-Mar-2016) observed and predicted in response to coarsening bathymetry data in the Puerto Rico test site. Vertical dashed lines indicate groyne locations. MNC is mean net change, MAC is mean absolute change, MAE is mean absolute error, and BSS is Brier Skill Score. Note there is a separate y axis for MIKE21 and the Bruun Rule predictions in (b) to (h). Net shoreline change observed and predicted in groyne transects are excluded from the above plots and statistics.

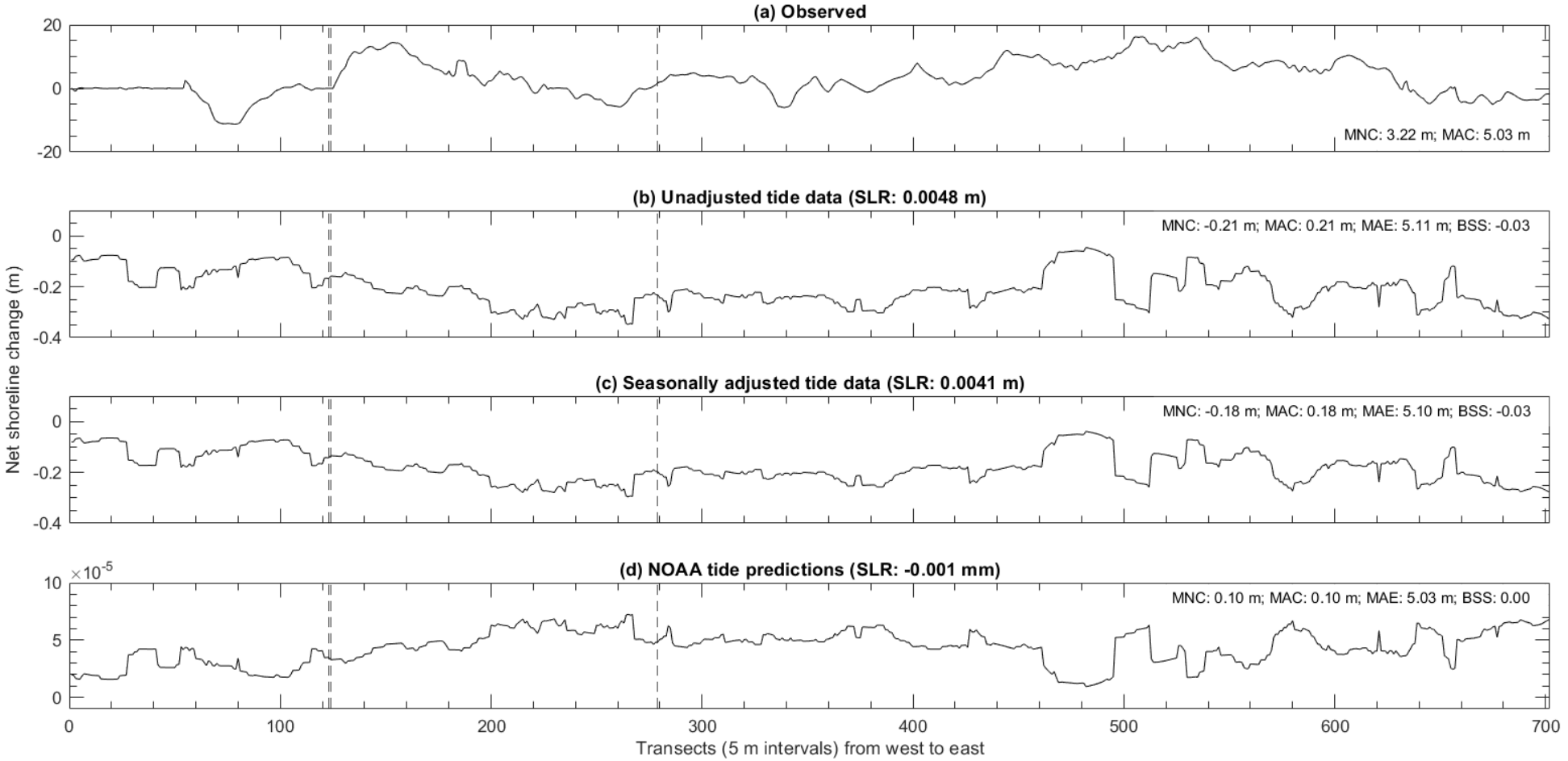

Fig. 4.12 Net shoreline change (10-Oct-2014 to 31-Mar-2016) observed and predicted from the Bruun Rule in response to SLR estimations from different tide datasets in the Puerto Rico test site. Vertical dashed lines indicate groyne locations. MNC is mean net change, MAC is mean absolute change, MAE is mean absolute error, and BSS is Brier Skill Score. Note the differences in y axis. Net shoreline change observed and predicted in groyne transects are excluded from the above plots and statistics.

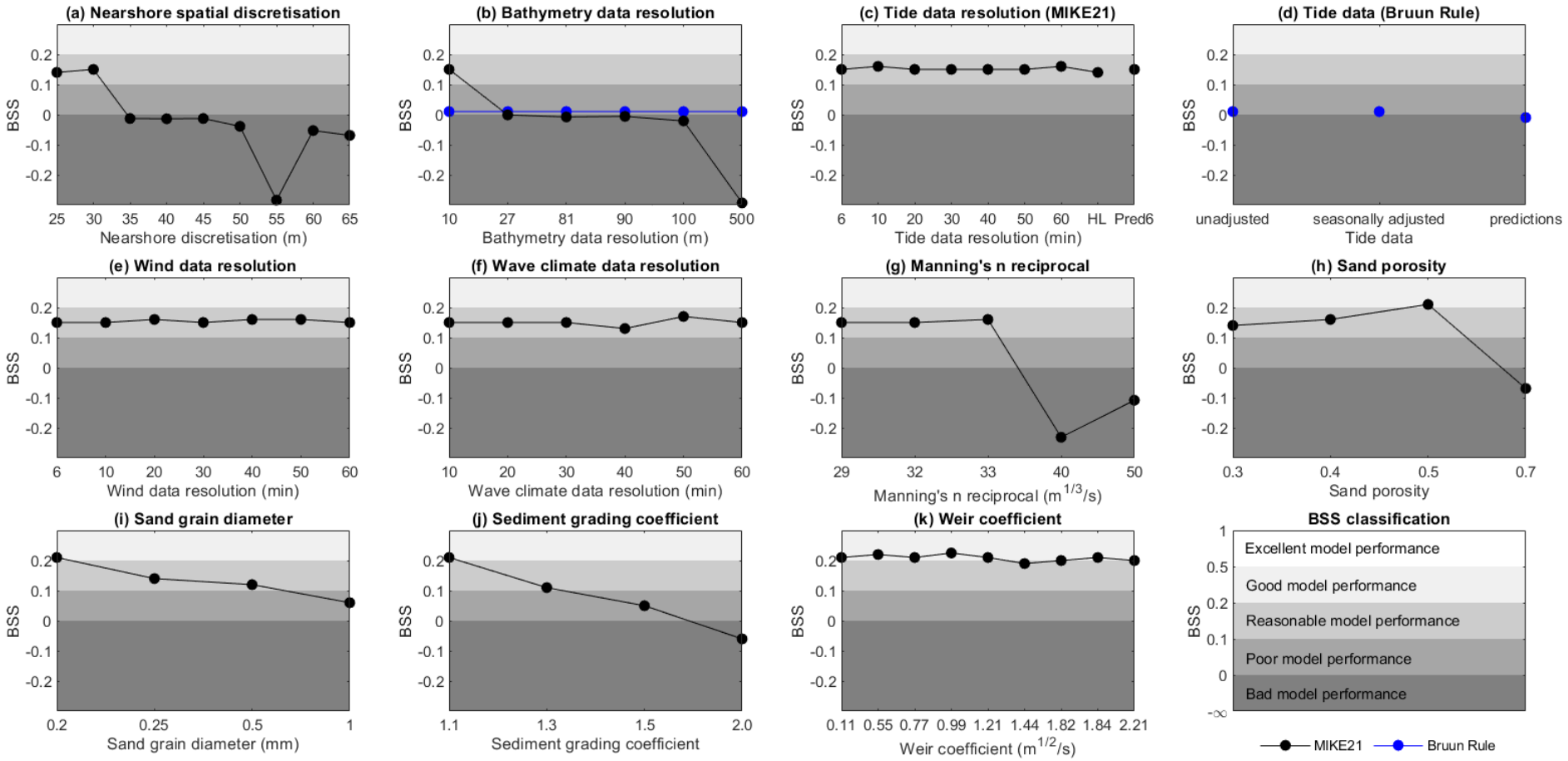

Fig. 4.13 Brier Skill Scores (BSS) estimated from net shoreline change predictions (01-Jan-2009 to 02-Aug-2011) in response to boundary conditions in the Southern California test site. In (c), HL is daily high/low tide data, and Pred6 is NOAA tide predictions (6 min intervals). In (d), unadjusted is observed tide levels, seasonally adjusted is observed tide levels without the regular seasonal fluctuations in meteorological conditions, and predictions are NOAA calculations of expected tide levels. BSS values < 0 in (a), (b), (g), and (h) are scaled to fall within 0 to -0.3 to better illustrate changes in model accuracy in response to boundary conditions.

Table 4.3 Summary of net shoreline change (01-Jan-2009 to 02-Aug-2011) observed and predicted in response to boundary conditions in the Southern California test site. M is MIKE21, B is the Bruun Rule, MNC is mean net change, MAC is mean absolute change, MAE is mean absolute error, and BSS is Brier Skill Score. All bolded Kruskal-Wallis p values are less than the 5% significance level, indicating significant differences between net shoreline change predictions. Other bold highlights show samples of net shoreline change predictions significantly different from other samples, based on a Dunn's test. Appendix A contains all spatial distribution plots of net shoreline change associated with statistics in Table 4.3, excluding those incorporated in this chapter.

Input	Specification	MNC (m)	MAC (m)	MAE (m)	BSS	Kruskal-Wallis
Observed net shoreline change	-	15.15	15.98	-	-	-
Nearshore spatial discretisation (m)	25	0.19	8.14	17.55	0.14	p = 0.057
	30	0.67	8.5	17.02	0.15	
	35	0.42	9.05	18.06	-0.16	
	40	0.40	10.17	18.19	-0.17	
	45	1.09	10.45	17.51	-0.16	
	50	1.35	11.26	18.73	-0.47	
	55	1.7	12.82	20.13	-3.41	
	60	0.93	11.12	19.57	-0.64	
	65	-0.07	10.77	19.74	-0.83	
Bathymetry data resolution (m)	10	0.67 (M); -0.15 (B)	8.5 (M); 0.15 (B)	17.02 (M); 16.09 (B)	0.15 (M); 0.01 (B)	**p < 0.0001 (M; B)**
	27	0.08 (M); -0.15 (B)	7.76 (M); 0.15 (B)	17.73 (M); 16.09 (B)	-0.02 (M); 0.01 (B)	
	81	**-0.24 (M); -0.16 (B)**	**8.11 (M); 0.16 (B)**	**18.18 (M); 16.1 (B)**	**-0.18 (M); 0.01 (B)**	
	90	**-0.22 (M); -0.16 (B)**	**7.98 (M); 0.16 (B)**	**18.01 (M); 16.1 (B)**	**-0.14 (M); 0.01 (B)**	
	100	**-1.18 (M); -0.16 (B)**	**8.43 (M); 0.16 (B)**	**18.56 (M); 16.1 (B)**	**-0.48 (M); 0.01 (B)**	
	500	**-1.93 (M); -0.16 (B)**	**29.76 (M); 0.16 (B)**	**32.04 (M); 16.1 (B)**	**-6.75 (M); 0.01 (B)**	
Tide data resolution (min): MIKE21	6	0.67	8.5	17.02	0.15	p = 1
	10	0.73	8.54	16.97	0.16	
	20	0.7	8.55	17.01	0.15	
	30	0.67	8.56	17.04	0.15	
	40	0.68	8.5	17.03	0.15	
	50	0.68	8.52	17.04	0.15	
	60	0.69	8.55	16.99	0.16	
	Daily high/low	0.65	8.58	17.05	0.14	
	NOAA predictions	0.64	8.54	17.06	0.15	

Input	Specification	MNC (m)	MAC (m)	MAE (m)	BSS	Kruskal-Wallis
Observed net shoreline change	-	15.15	15.98	-	-	-
Tide data: Bruun Rule	**Unadjusted**	**-0.09**	**0.09**	**16.04**	**0.01**	**p < 0.0001**
	Seasonally adjusted	**-0.15**	**0.15**	**16.09**	**0.01**	
	NOAA predictions	**0**	**0**	**15.98**	**-0.01**	
Wind data resolution (min)	6	0.67	8.5	17.02	0.15	p = 1
	10	0.64	8.5	17.03	0.15	
	20	0.67	8.48	17.02	0.16	
	30	0.67	8.51	17.04	0.15	
	40	0.72	8.5	16.98	0.16	
	50	0.7	8.5	16.98	0.16	
	60	0.7	8.48	17	0.15	
Wave climate data resolution (min)	10	0.67	8.48	17.04	0.15	p = 1
	20	0.67	8.48	17.04	0.15	
	30	0.67	8.5	17.02	0.15	
	40	0.6	8.68	17.14	0.13	
	50	0.75	8.54	16.95	0.17	
	60	0.67	8.48	17.04	0.15	
Manning's n reciprocal ($m^{1/3}/s$)	29	0.67	8.38	16.99	0.15	**p < 0.0001**
	32	0.67	8.5	17.02	0.15	
	33	0.89	8.57	16.86	0.16	
	40	**4.39**	**15.16**	**19.96**	**-2.31**	
	50	2.91	13.08	19.02	-1.08	
Sand porosity	0.3	0.63	8.25	17.02	0.14	**p = 0.003**
	0.4	0.89	8.57	16.86	0.16	
	0.5	1.29	9.06	16.69	0.21	
	0.7	**3.46**	**14.52**	**20.12**	**-2.07**	
Sand grain diameter (mm)	0.2	1.29	9.06	16.69	0.21	p = 0.128
	0.25	0.59	8.52	17.1	0.14	
	0.5	0.56	6.77	16.66	0.12	
	1	0.6	6.79	16.7	0.06	

Input	Specification	MNC (m)	MAC (m)	MAE (m)	BSS	Kruskal-Wallis
Observed net shoreline change	**-**	15.15	15.98	-	-	-
Sediment grading coefficient	1.1	1.29	9.06	16.69	0.21	**p = 0.031**
	1.3	0.47	8.55	17.27	0.11	
	1.5	0.4	8.74	17.49	0.05	
	2	**0.25**	**9.7**	**18.18**	**-0.06**	
Weir coefficient ($m^{1/2}/s$)	0.11	1.39	9.06	16.67	0.21	p = 1
	0.55	1.38	8.96	16.53	0.22	
	0.77	1.35	9.08	16.63	0.21	
	0.99	1.37	8.81	16.58	0.22	
	1.21	1.25	9.02	16.66	0.21	
	1.44	1.37	9.27	16.69	0.19	
	1.82	1.38	9.23	16.68	0.2	
	1.838	1.29	9.06	16.69	0.21	
	2.21	1.26	9.2	16.72	0.2	

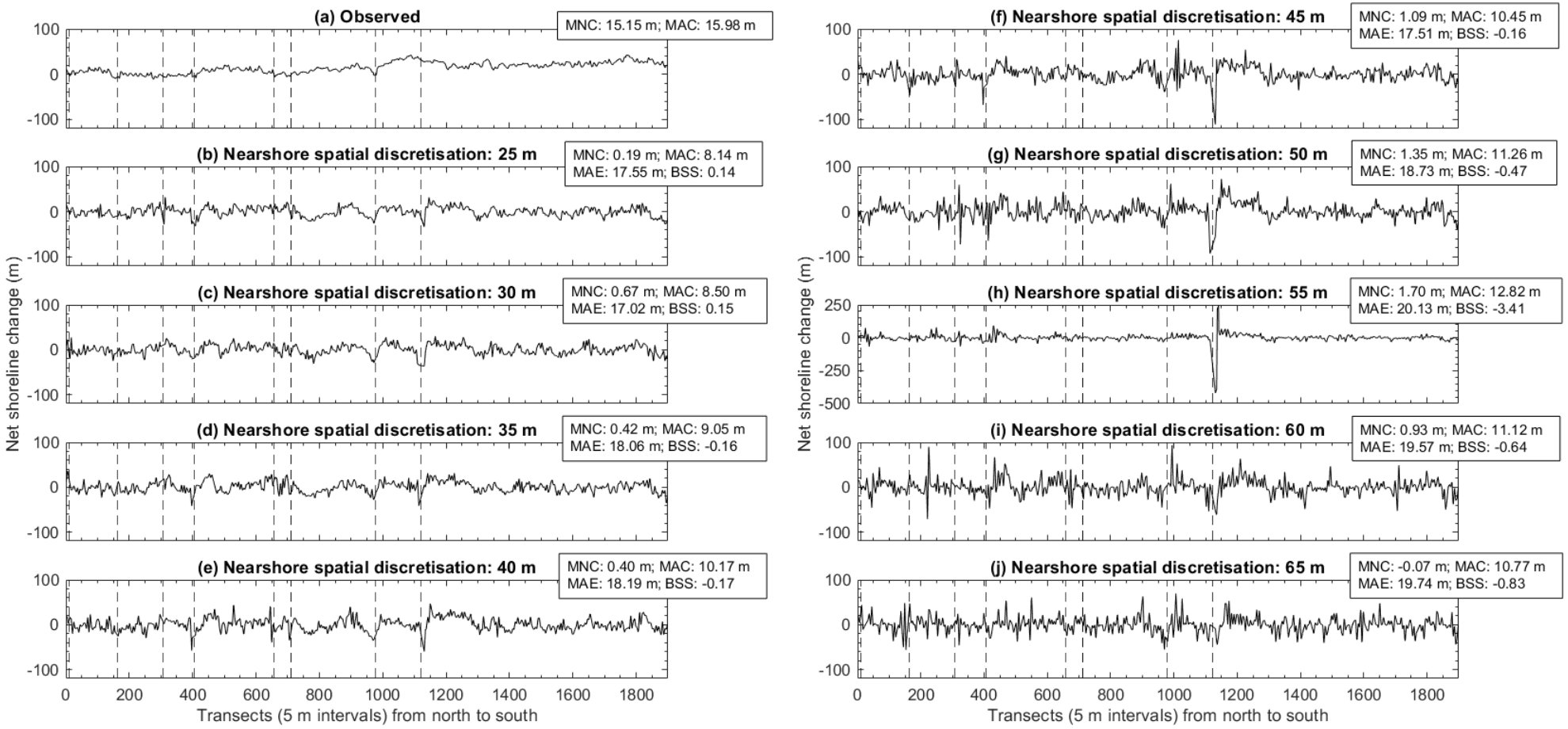

Fig. 4.14 Net shoreline change (01-Jan-2009 to 02-Aug-2011) observed and predicted in response to coarsening nearshore spatial discretisation in the Southern California test site. Vertical dashed lines indicate groyne locations. MNC is mean net change, MAC is mean absolute change, MAE is mean absolute error, and BSS is Brier Skill Score. Note the difference in y axis in (h). Net shoreline change observed and predicted in groyne transects are excluded from the above plots and statistics.

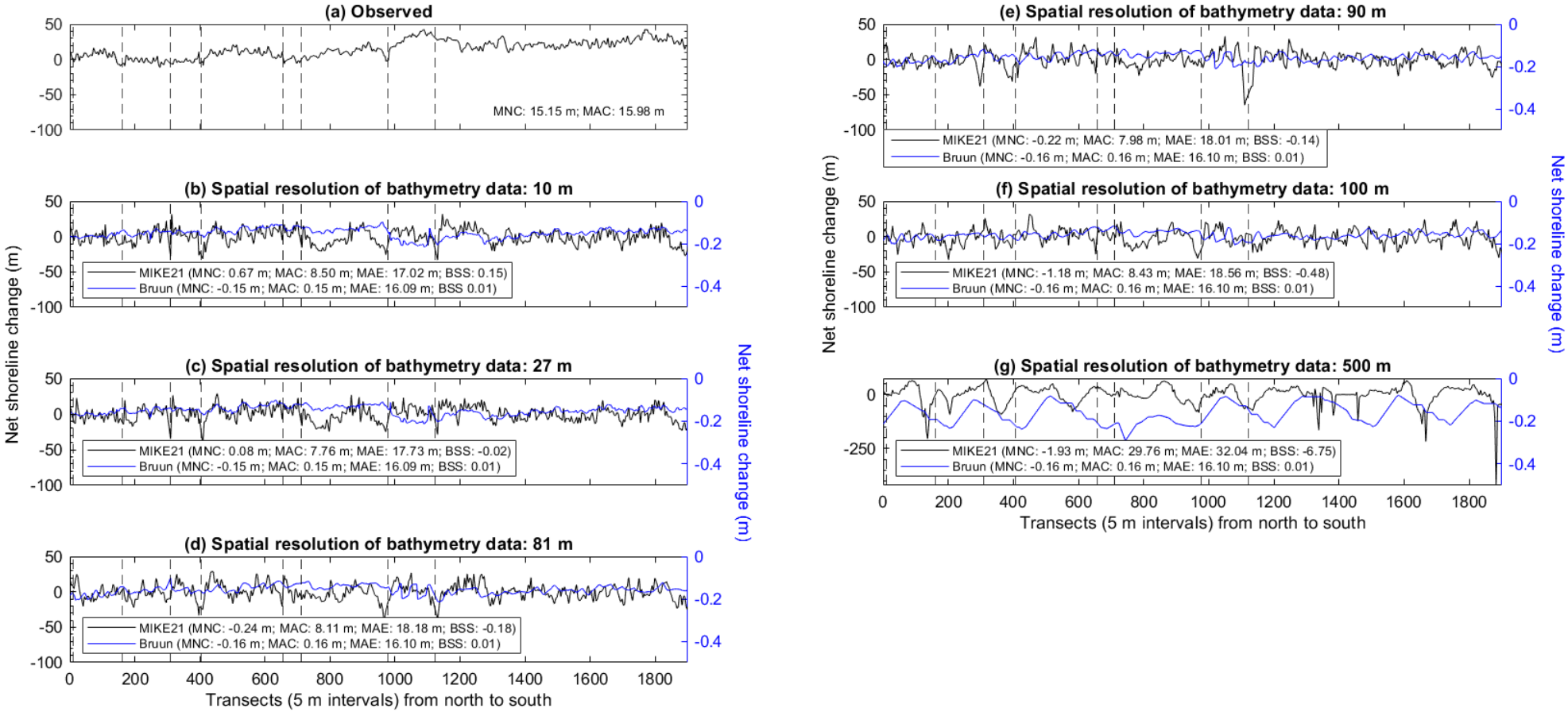

Fig. 4.15 Net shoreline change (01-Jan-2009 to 02-Aug-2011) observed and predicted in response to coarsening bathymetry data in the Southern California test site. Vertical dashed lines indicate groyne locations. MNC is mean net change, MAC is mean absolute change, MAE is mean absolute error, and BSS is Brier Skill Score. Note there is a separate y axis for MIKE21 and the Bruun Rule predictions in (b) to (g), and also note there is a difference in MIKE21 y axis in (g). Net shoreline change observed and predicted in groyne transects are excluded from the above plots and statistics.

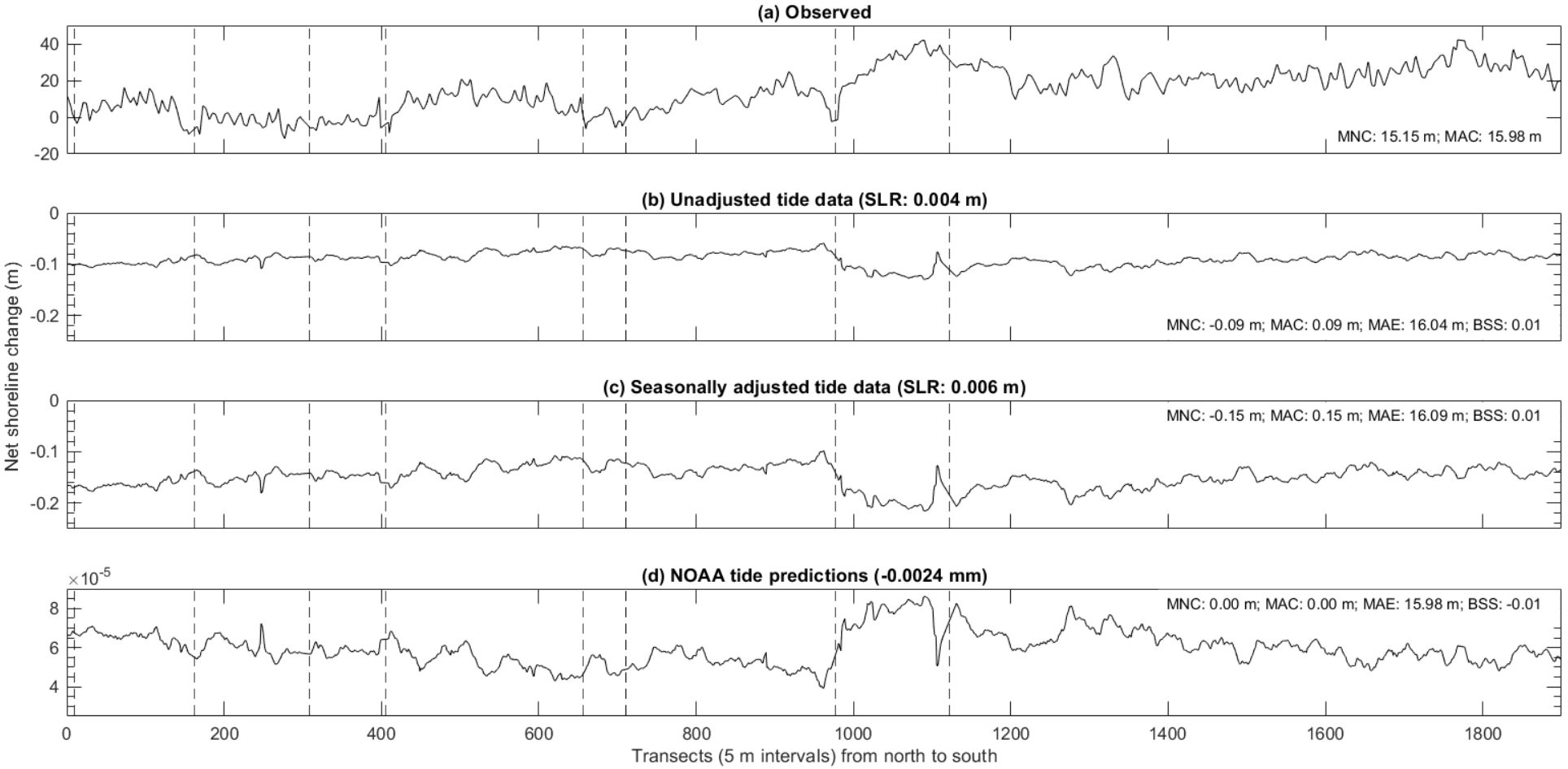

Fig. 4.16 Net shoreline change (01-Jan-2009 to 02-Aug-2011) observed and predicted from the Bruun Rule in response to SLR estimations from different tide datasets in the Southern California test site. Vertical dashed lines indicate groyne locations. MNC is mean net change, MAC is mean absolute change, MAE is mean absolute error, and BSS is Brier Skill Score. Note the differences in y axis. Net shoreline change observed and predicted in groyne transects are excluded from the above plots and statistics.

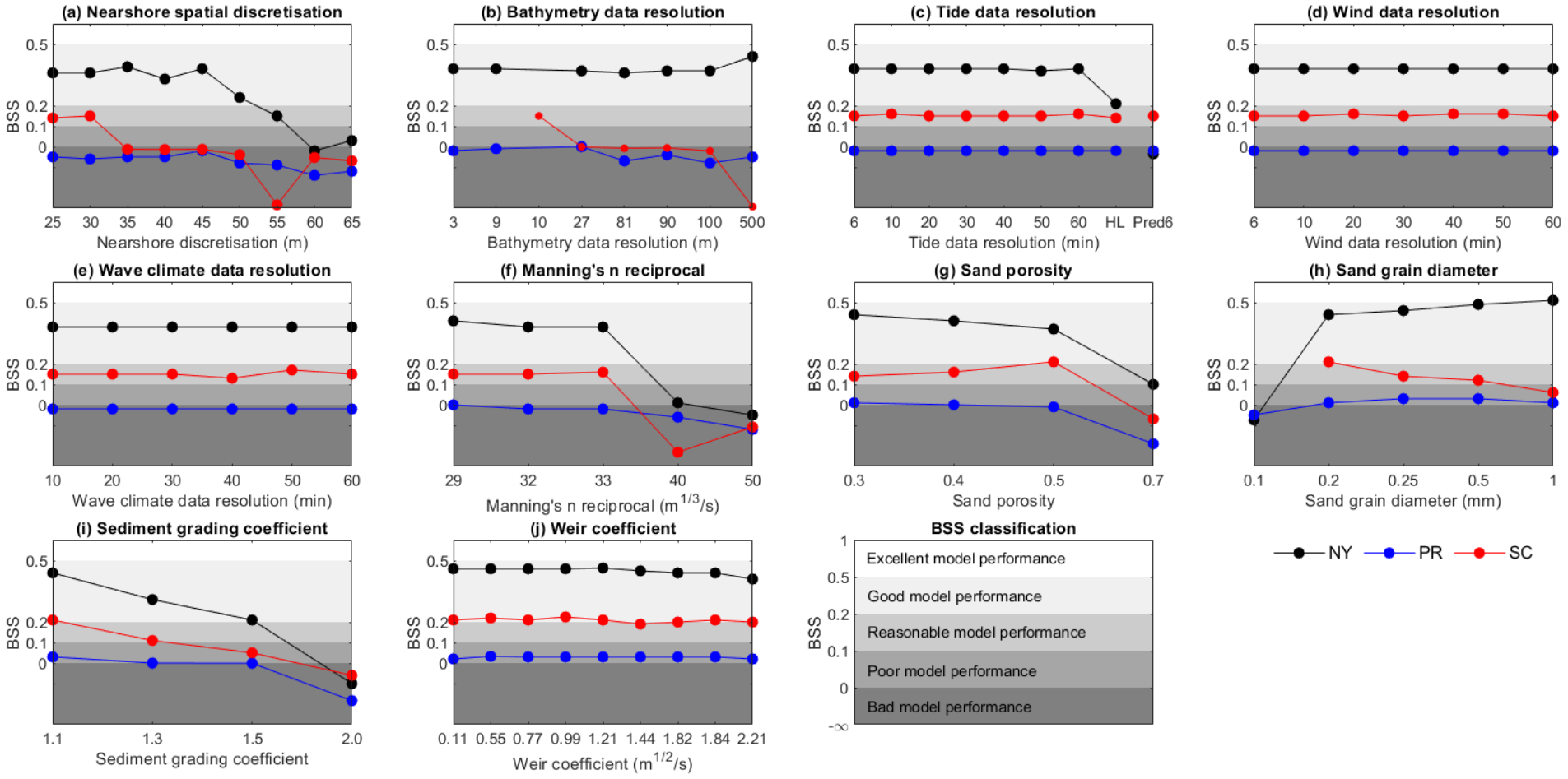

Fig. 4.17 Summary of MIKE21 performance in response to boundary condition variations in the New York (NY), Puerto Rico (PR), and Southern California (SC) test site. In (c), HL is daily high/low tide data, and Pred6 is NOAA tide predictions (6 min intervals). BSS values < 0 in (a) to (c) and (f) to (h) are scaled as before to better illustrate changes in model accuracy in response to boundary conditions. Tables 4.1 to 4.3 list all BSS estimations from evaluating model sensitivity in each test site.

Table 4.4 Optimal boundary condition specifications for simulating shoreline evolution in each test site. Highlighted cells indicate boundary conditions that have no apparent optimal specifications. I select and use the original or base values of boundary conditions with no defined optimal specifications in further simulations (where applicable).

Input (units)	Specification		
	New York test site	**Puerto Rico test site**	**Southern California test site**
Nearshore spatial discretisation (m)	45	45	30
Bathymetry data resolution (m): MIKE21 and Bruun Rule *****	≤ 100 (selected: 3 m)	≤ 27 (selected: 3 m)	≤ 10 (selected: 10 m)
Tide data resolution (min): MIKE21	6 min (original)	6 min (original)	6 min (original)
Tide data: Bruun Rule	Seasonally adjusted (original)	Seasonally adjusted (original)	Seasonally adjusted (original)
Wind data resolution (min)	6 min (original)	6 min (original)	6 min (original)
Wave climate data resolution (min)	60 min (original)	60 min (original)	30 min (original)
Manning's n reciprocal ($m^{1/3}/s$)	29	29	33
Sand porosity	0.3	0.3	0.5
Sand grain diameter (mm)	0.2	0.25; 0.5 (selected: 0.25) ******	0.2
Sediment grading coefficient	1.1	1.1	1.1
Weir coefficient ($m^{1/2}/s$) *******	1.21	0.55	0.99
BSS	**0.46**	**0.03**	**0.22**

***** I select the original bathymetry data in each test site for further simulations. This selection guarantees the best model representation of the observed coastal profile morphology.
****** Using a sand grain diameter of 0.25 mm instead of 0.5 mm results in less net shoreline change under-prediction in the Puerto Rico test site (Table 4.2; Fig. A8.3).
******* Weir coefficients in Table 4.4 provide a marginal improvement in MIKE21 performance, which may become more significant over meso timescale simulations.

Table 4.5 Characteristics of the active coastal profile slope in each test site. Descriptive statistics in Table 4.5 are based on the active coastal profile slope in transects every 5 m longshore, excluding those in groyne areas.

Slope (%)	New York test site	Puerto Rico test site	Southern California test site
Minimum	1.19	1.13	2.08
Maximum	2.42	2.28	4
Mean	1.82	1.75	2.68
Standard deviation	0.22	0.26	0.42

Table 4.6 Descriptive summary of tide levels observed over the associated sensitivity testing period in each test site.

Tide levels relative to MHW (m)	New York test site	Puerto Rico test site	Southern California test site
Minimum	-1.49	-0.5	-2.31
Maximum	1.82	0.42	0.92
Mean	0.24	-0.06	-0.55
Standard deviation	0.55	0.15	0.5

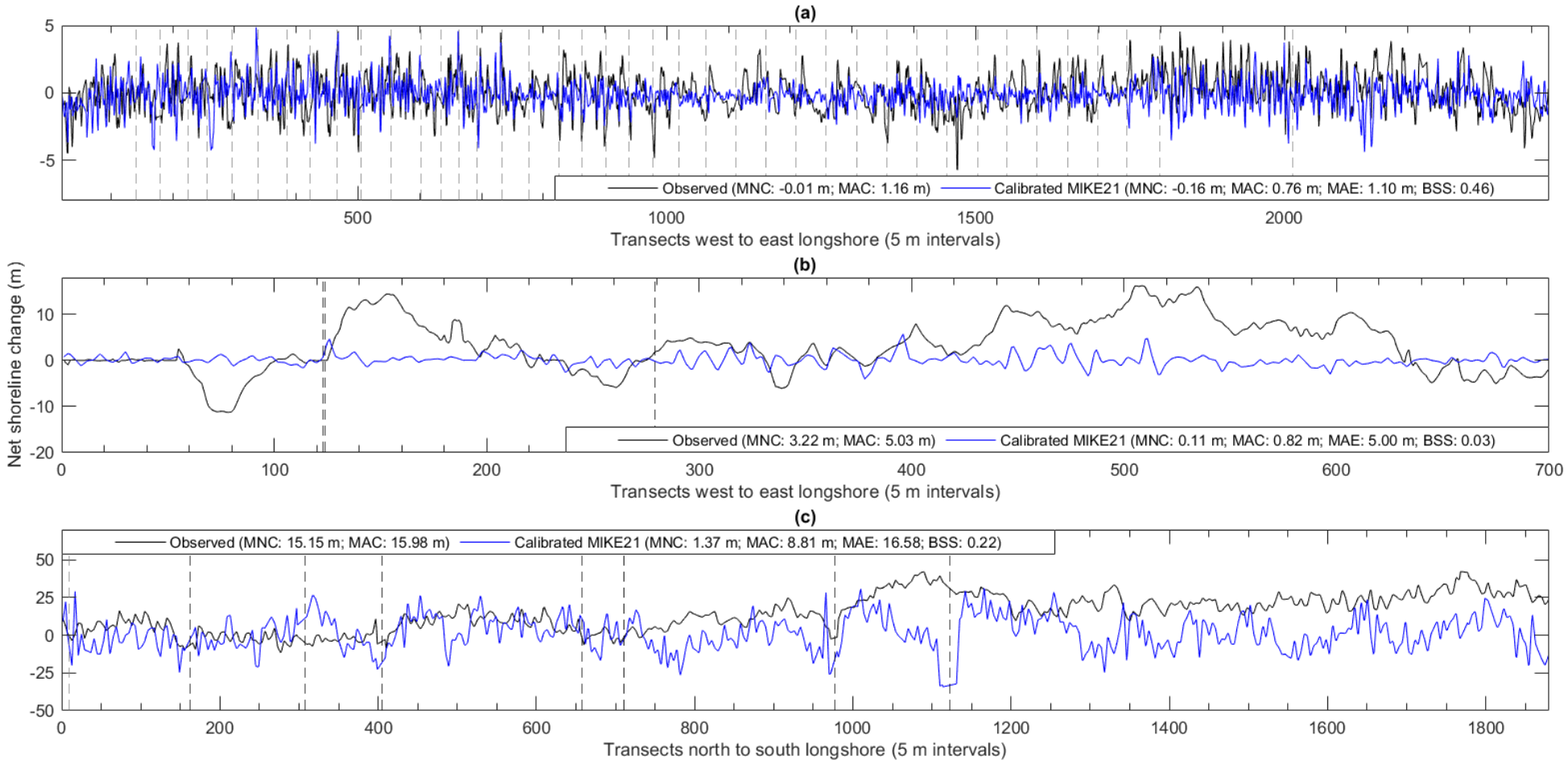

Fig. 4.18 Net shoreline change observed and predicted from the New York (01-Jan-2014 to 01-Feb-2016) (a), Puerto Rico (10-Oct-2014 to 31-Mar-2016) (b), and Southern California (01-Jan-2009 to 02-Aug-2011) (c) test site's calibrated MIKE21 model. Vertical dashed lines in (a) to (c) indicate groyne locations. MNC is mean net change, MAC is mean absolute change, MAE is mean absolute error, and BSS is Brier Skill score. Note the differences in axes. Net shoreline change observed and predicted in groyne transects are excluded from the above plots and statistics.

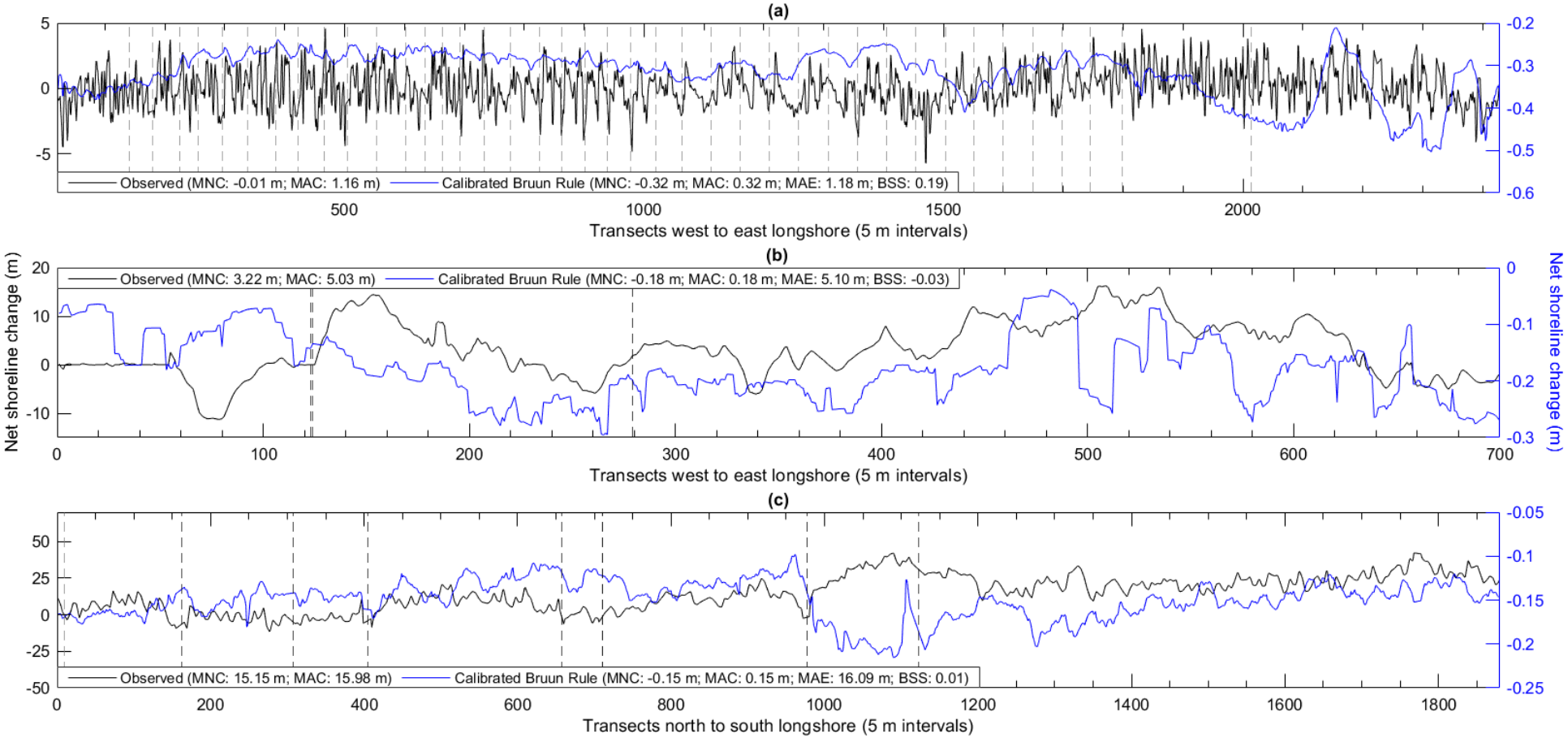

Fig. 4.19 Net shoreline change observed and predicted from the New York (01-Jan-2014 to 01-Feb-2016) (a), Puerto Rico (10-Oct-2014 to 31-Mar-2016) (b), and Southern California (01-Jan-2009 to 02-Aug-2011) (c) test site's calibrated Bruun Rule model. Vertical dashed lines in (a) to (c) indicate groyne locations. MNC is mean net change, MAC is mean absolute change, MAE is mean absolute error, and BSS is Brier Skill score. Note there is a separate y axis for net shoreline change observed and predicted from the calibrated Bruun Rule in (a) to (c). Net shoreline change observed and predicted in groyne transects are excluded from the above plots and statistics.

05
Incorporating sea-level rise: figures and tables

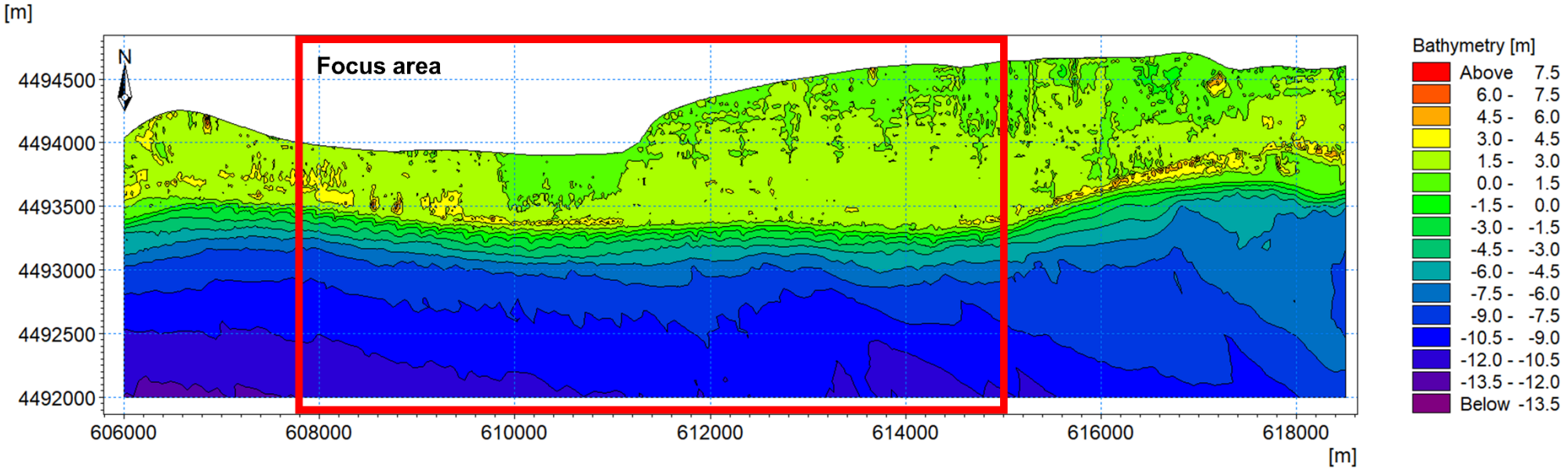

Fig. 5.1 The New York test site's model domain area used to quantify and compare meso timescale shoreline evolution predictions. MIKE21 net shoreline change predictions outside this area are sensitive to the Flather condition data applied at the west and east boundaries.

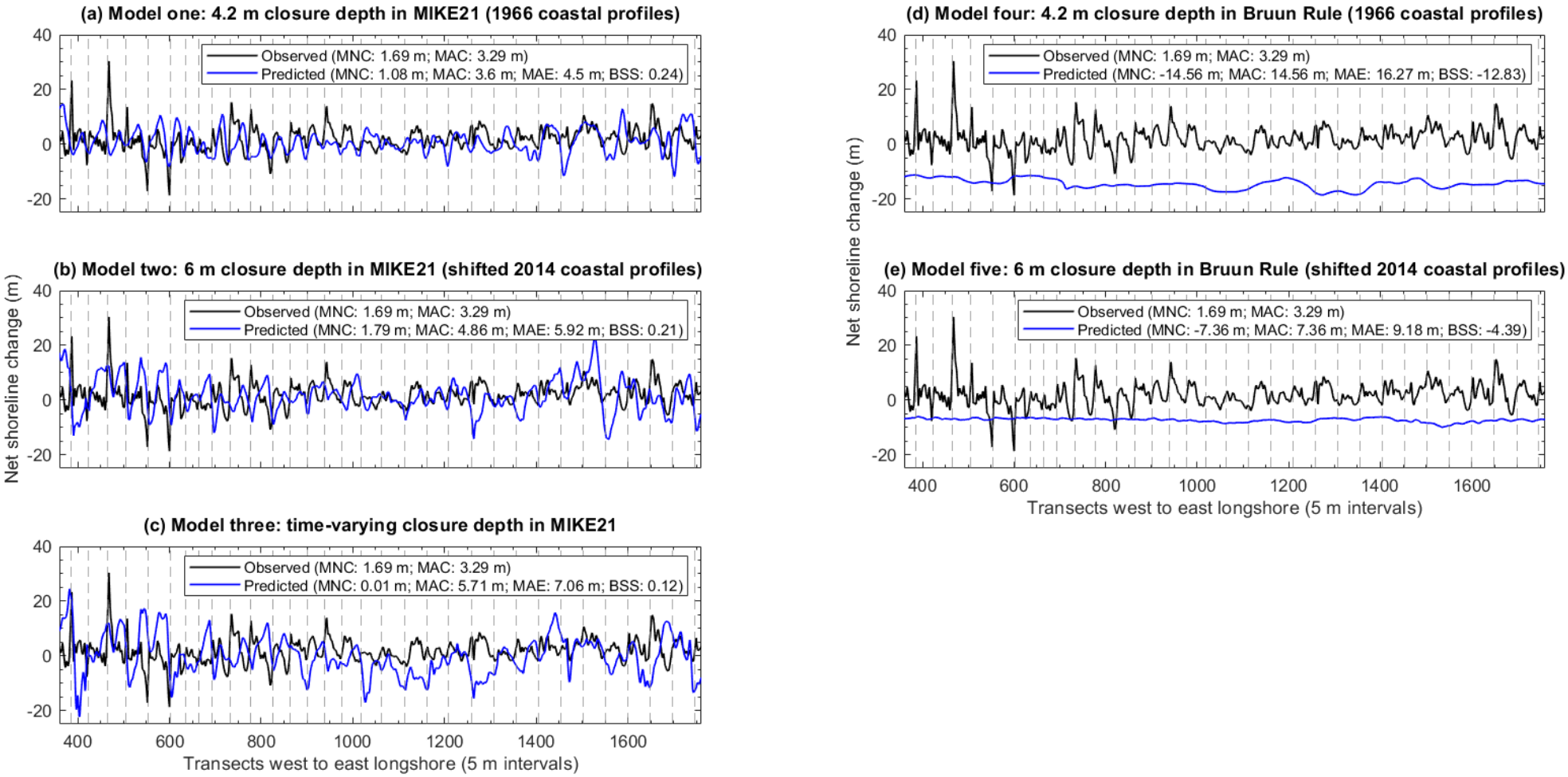

Fig. 5.2 Net shoreline change observed and predicted (01-Jan-1966 to 01-Feb-2016) in the New York test site. Vertical dashed lines indicate groyne locations. MNC is mean net change, MAC is mean absolute change, MAE is mean absolute error, and BSS is Brier Skill Score. Net shoreline change observed and predicted in groyne transects are excluded from the above plots and statistics.

Table 5.1 Closure depth time series estimates used to hindcast meso timescale shoreline evolution (1966 to 2016) in the New York test site compared against corresponding observations. Closure depth estimations are derived from Birkemeier (1985) formula using nearshore significant wave heights calculated by MIKE21. Closure depth observations are from USACE Wave Information Study (WIS) station 63124 (USACE, 2020). Net difference (m) = estimated closure depth – observed closure depth. Grey rows indicate non-verifiable closure depth estimations, yellow rows indicate closure depth overestimation, and non-highlighted rows indicate closure depth underestimation.

Year	Estimated (m below MHW)	Observed (m below MHW)	Net difference (m)
1966	6		
1967	7.93		
1968	5.45		
1969	7.82		
1970	5.8		
1971	7.39		
1972	6.36	No observed closure depth data	
1973	7.4		
1974	6.24		
1975	7.32		
1976	6.09		
1977	7.18		
1978	6.42		
1979	7.29		
1980	6.55	6.67	-0.12
1981	7.29	6.96	0.34
1982	6.85	6.31	0.54
1983	7.22	7	0.22
1984	6.98	8.21	-1.23
1985	6.95	6.67	0.28
1986	7.15	6.61	0.54
1987	6.78	5.45	1.33
1988	7.24	5.7	1.54
1989	6.19	5.53	0.66
1990	7.66	4.43	3.23
1991	5.23	6.41	-1.18
1992	7.93	8.76	-0.83
1993	5.45	7.99	-2.54
1994	7.74	7.25	0.48
1995	5.89	6.47	-0.58
1996	7.48	7.9	-0.41
1997	6.27	5.2	1.08
1998	7.4	6.41	1
1999	6.23	6.08	0.15
2000	7.4	5.62	1.78
2001	6.09	5.93	0.16
2002	7.28	5.06	2.23
2003	6.43	8.2	-1.76
2004	7.29	5.31	1.99
2005	6.55	6.58	-0.03
2006	7.29	7.17	0.12
2007	6.85	6.56	0.29
2008	7.21	7.17	0.03
2009	7	8.93	-1.93
2010	6.95	8.32	-1.37
2011	7.25	7.74	-0.49
2012	6.78	10.49	-3.71
2013	7.24		
2014	6.27	No observed closure depth data	
2015	7.75		

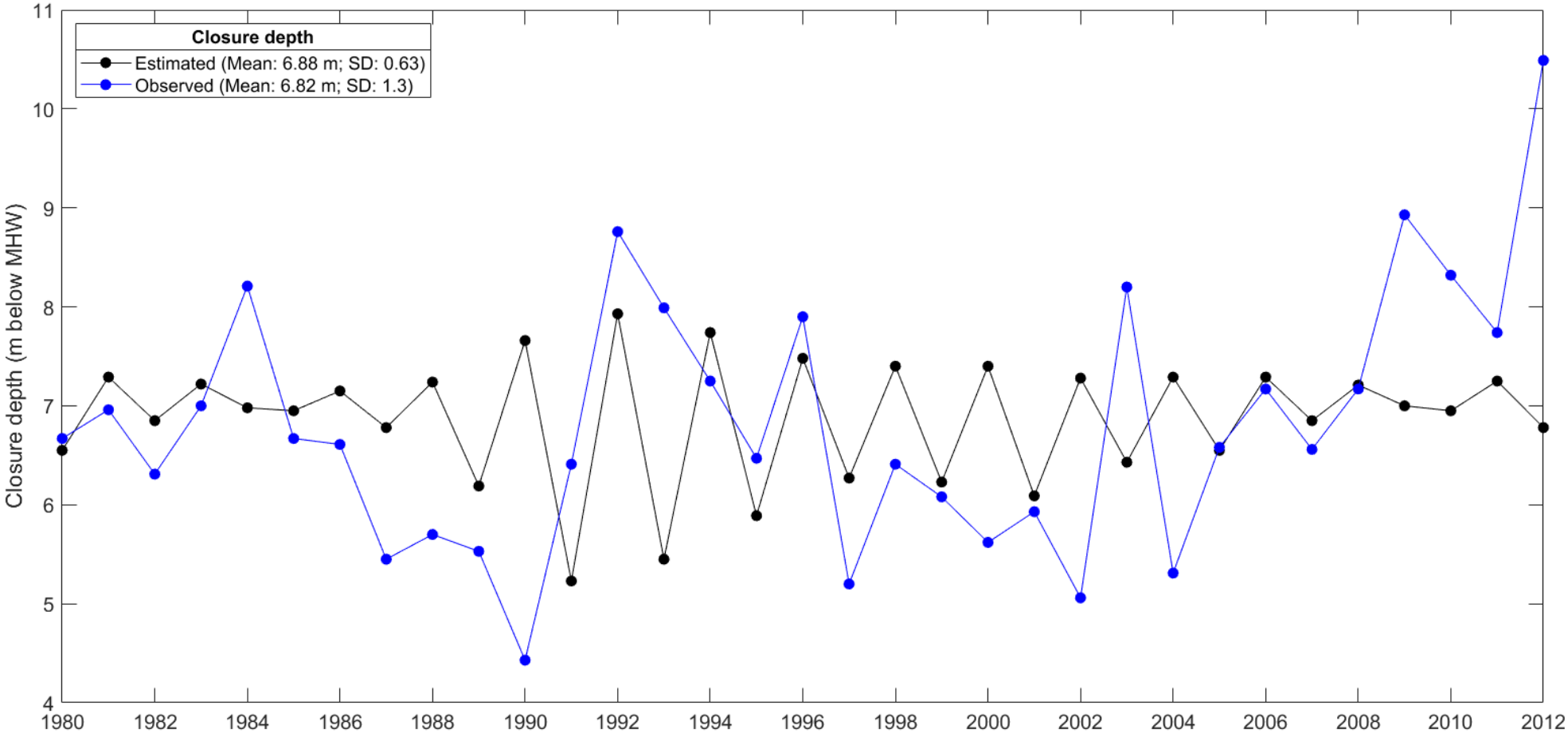

Fig. 5.3 Comparing closure depth (m below MHW) observations and estimations (1980 to 2012) in the New York test site. SD is the standard deviation. All closure depth estimations are derived from Birkemeier (1985) formula using nearshore significant wave heights calculated by MIKE21. All closure depth observations are from USACE WIS station 63124 (USACE, 2020).

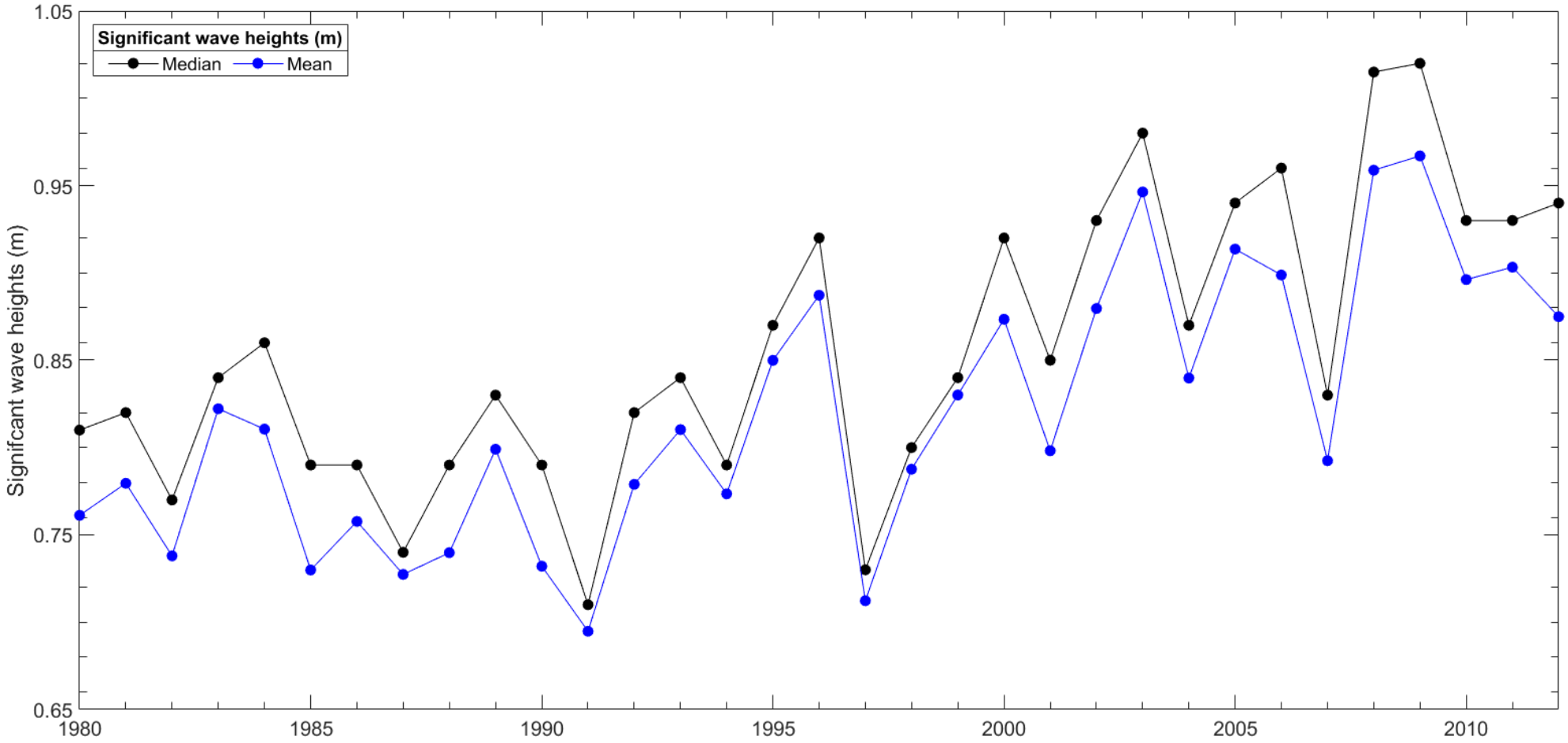

Fig. 5.4 Annual median and mean significant wave height statistics (1980 to 2012) in the New York test site. Annual significant wave height statistics in the above plots are from USACE WIS station 63124 (USACE, 2020).

Table 5.2 Summary of all meso timescale shoreline evolution hindcasts (01-Jan-1966 to 01-Feb-2016) in the New York test site. MNC is mean net change, MAC is mean absolute change, MAE is mean absolute error, and BSS is Brier Skill Score.

Hindcast (Relative sea-level rise: +0.2 m)	Modelling approach	MNC (m)	MAC (m)	MAE (m)	BSS
Observed		1.69	3.29		
Model one	4.2 m closure depth in MIKE21 (1966 coastal profiles)	1.08	3.6	4.5	0.24
Model two	6 m closure depth in MIKE21 (shifted 2014 coastal profiles)	1.79	4.86	5.92	0.21
Model three	Time-varying closure depth in MIKE21	0.01	5.71	7.06	0.12
Model four	4.2 m closure depth in Bruun Rule (1966 coastal profiles)	-14.56	14.56	16.27	-12.83
Model five	6 m closure depth in Bruun Rule (shifted 2014 coastal profiles)	-7.36	7.36	9.18	-4.39

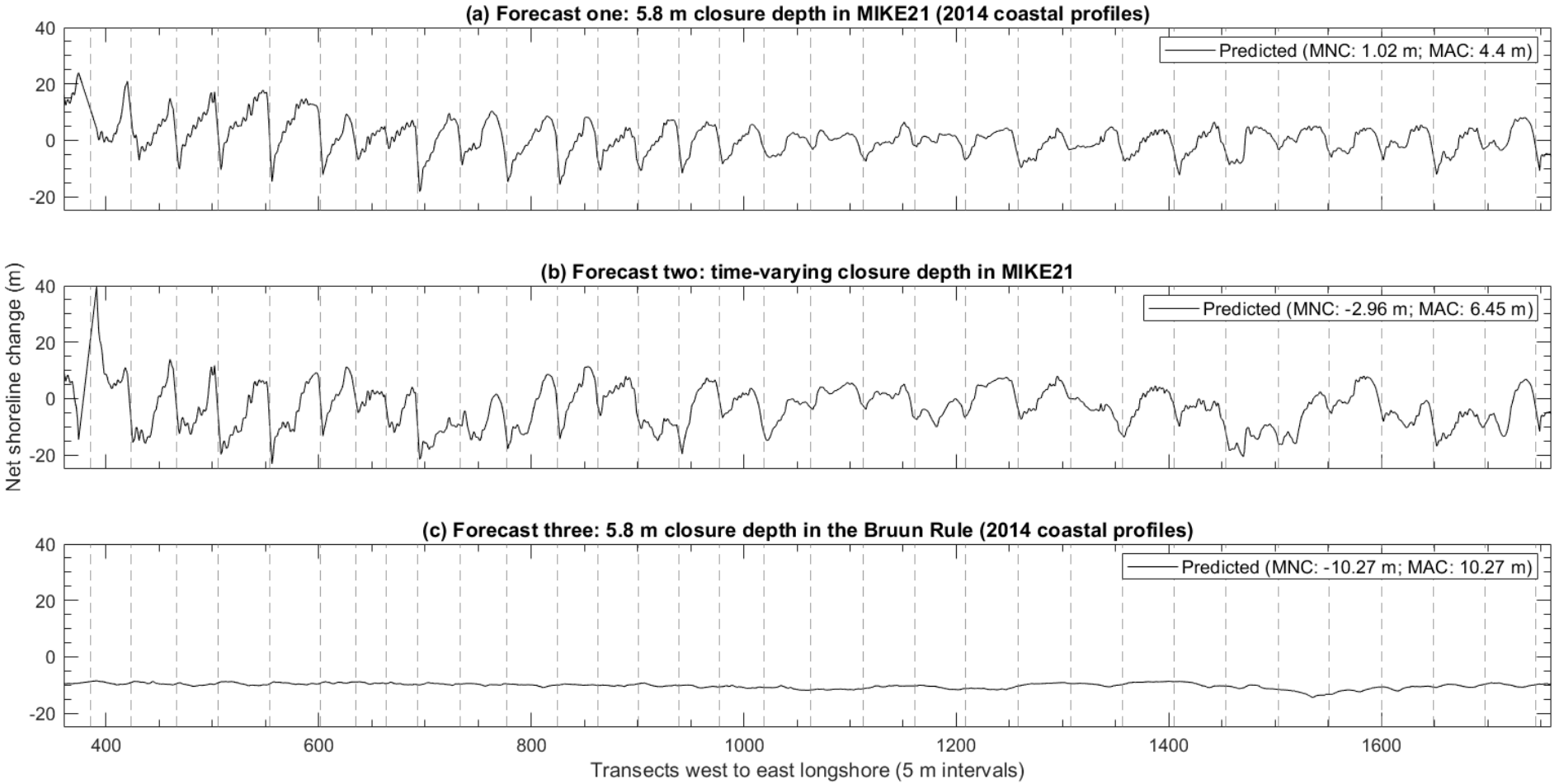

Fig. 5.5 Net shoreline change forecasted (01-Jan-2014 to 01-Jan-2064) in the New York test site. Vertical dashed lines indicate groyne locations. MNC is mean net change, and MAC is mean absolute change. Net shoreline change predictions in groyne transects are excluded from the above plots and statistics.

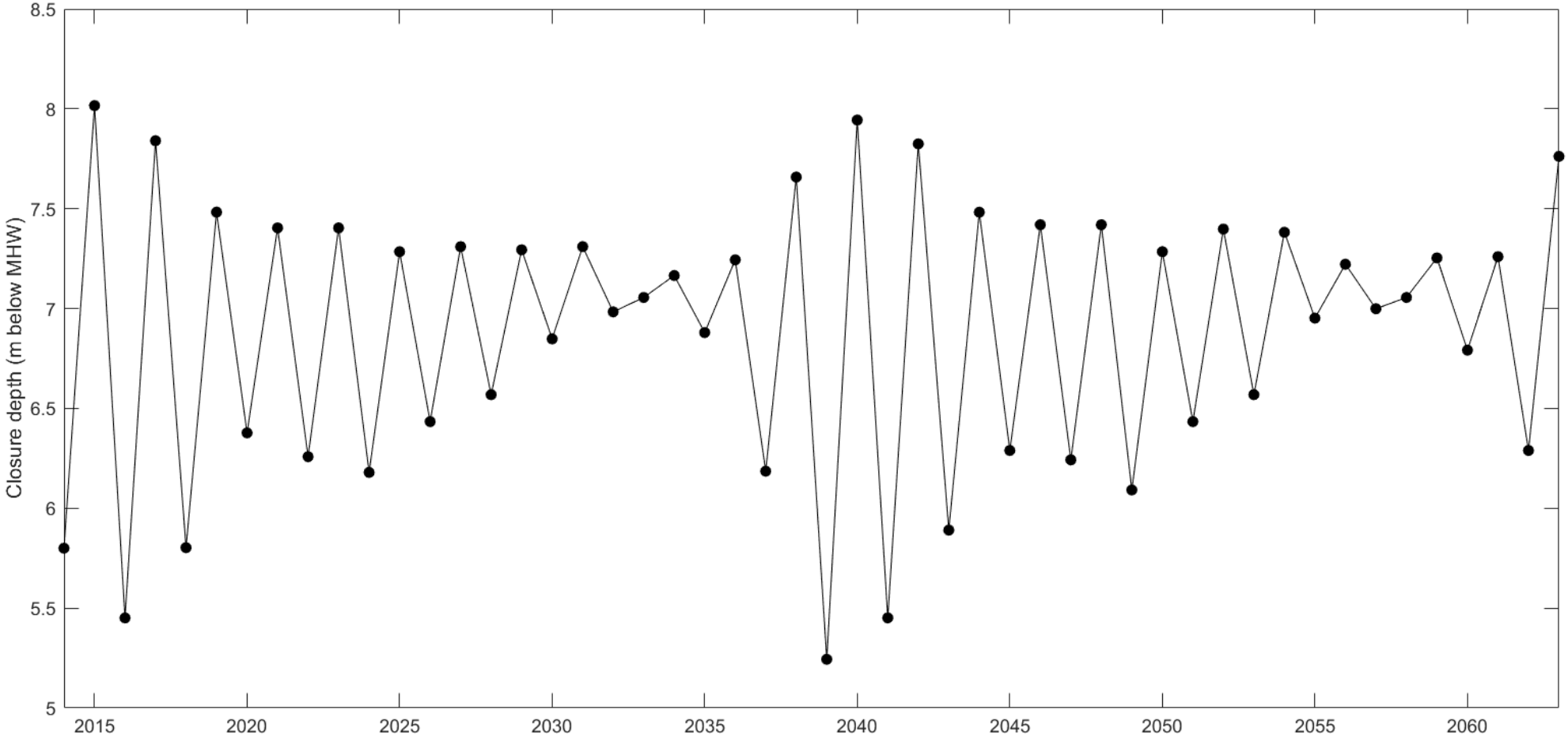

Fig. 5.6 Closure depth estimations used to forecast meso timescale shoreline evolution (2014 to 2064) in the New York test site with a time-varying closure depth in MIKE21. All closure depth estimations are derived from Birkemeier (1985) formula using nearshore significant wave heights calculated by MIKE21.

06
Handling complex planform morphologies: figures and tables

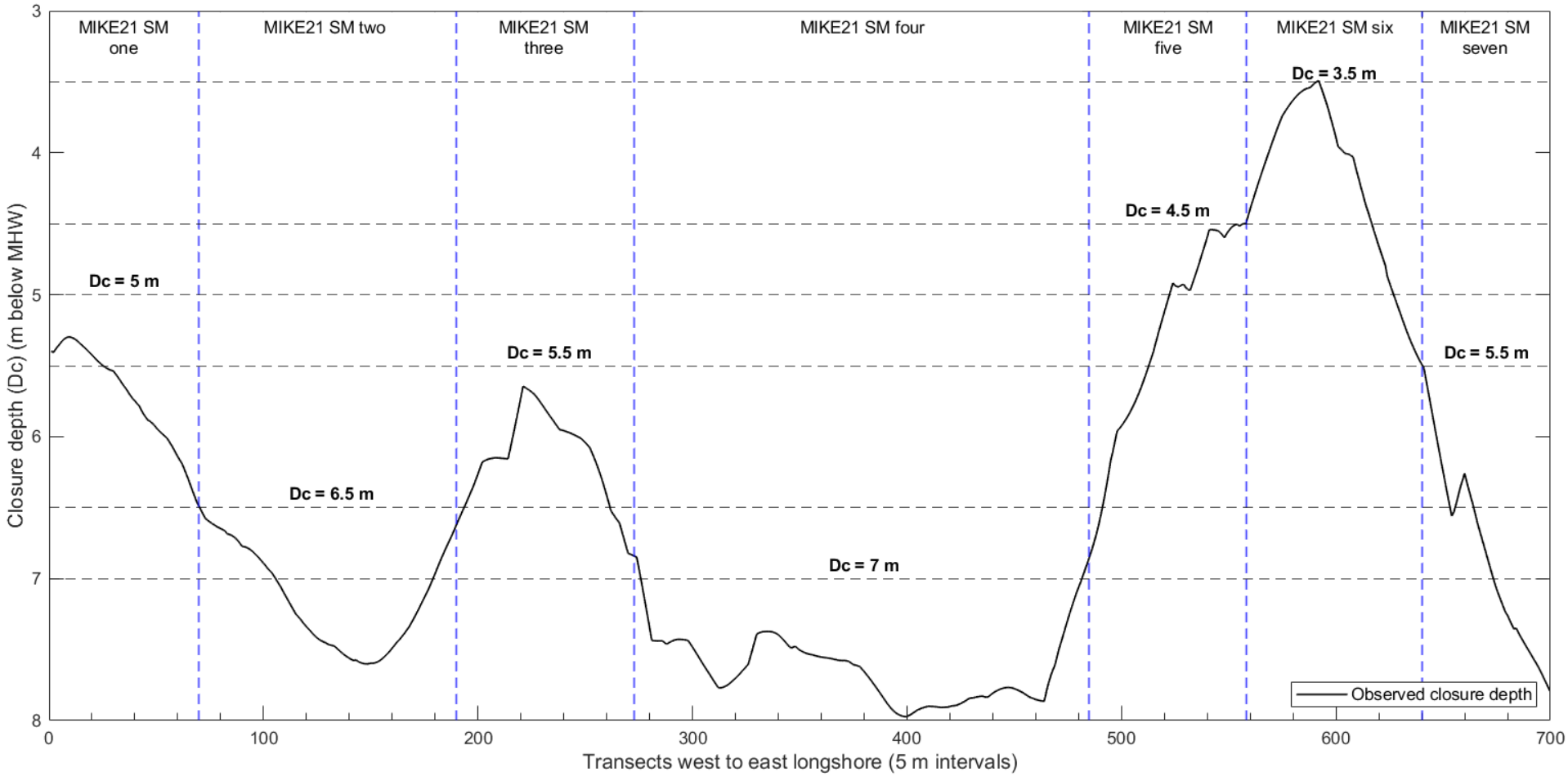

Fig. 6.1 Closure depths observed and applied to hindcast shoreline evolution over irregular spatial intervals in the Puerto Rico test site. Blue vertical dashed lines indicate the boundaries of each MIKE21 SM domain.

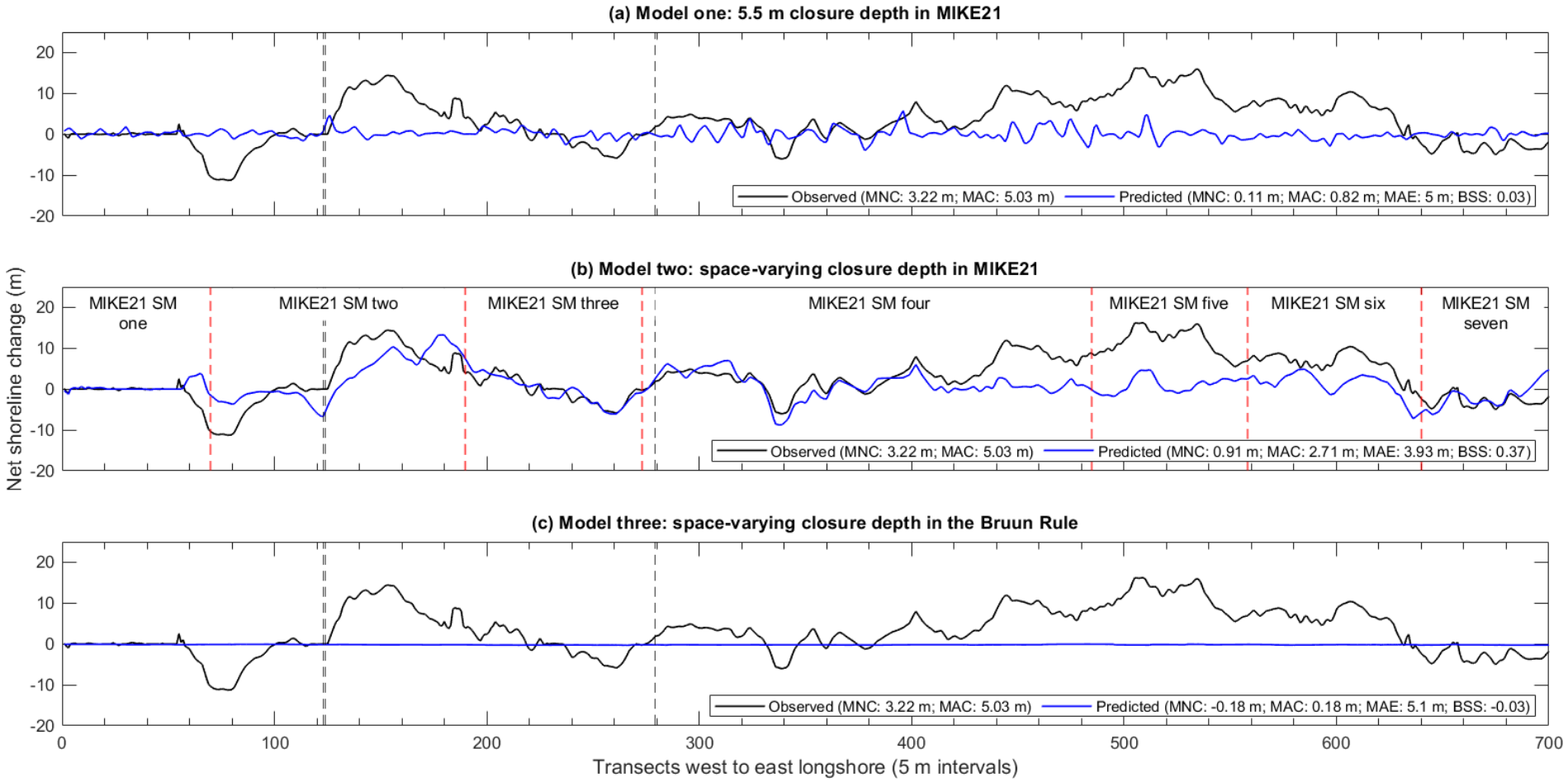

Fig. 6.2 Net shoreline change observed and predicted (10-Oct-2014 to 31-Mar-2016) in the Puerto Rico test site. Black vertical dashed lines indicate groyne locations. Red vertical dashed lines in (b) indicate the boundaries of each MIKE21 SM domain. MNC is mean net change, MAC is mean absolute change, MAE is mean absolute error, and BSS is Brier Skill Score. Net shoreline change observed and predicted in groyne transects are excluded from the above plots and statistics.

Table 6.1 Closure depth observations and specifications in each MIKE21 SM domain used for hindcasting shoreline evolution (10-Oct-2014 to 31-Mar-2016) with a space-varying closure depth in the Puerto Rico test site.

MIKE21 SM Domain (Each defined in Fig. 6.1)	Observed closure depth			Closure depth specified (m)
	Range (m)	Mean (m)	Standard deviation	
One	5.3 to 6.5 (1.2 m range)	5.7	0.4	5
Two	6.5 to 7.7 (1.2 m range)	7.2	0.4	6.5
Three	5.5 to 7 (1.6 m range)	6.1	0.3	5.5
Four	7 to 8 (1 m range)	7.7	0.2	7
Five	4.5 to 7 (2.5 m range)	5.3	0.7	4.5
Six	3.3 to 5.6 (2.3 m range)	4.2	0.7	3.5
Seven	5.6 to 7.8 (2.2 m range)	6.8	0.7	5.5

Table 6.2 Summary of all shoreline evolution hindcasts (10-Oct-2014 to 31-Mar-2016) in the Puerto Rico test site. MNC is mean net change, SD is the standard deviation, MAC is mean absolute change, MAE is mean absolute error, and BSS is Brier Skill Score.

Hindcast	Modelling approach	MNC (m)	SD	MAC (m)	MAE (m)	BSS
Observed		3.22	5.7	5.03		
Model one	5.5 m closure depth in MIKE21	0.11	1.17	0.82	5	0.03
Model two	Space-varying closure depth in MIKE21	0.91	3.63	2.71	3.93	0.37
Model three	Space-varying closure depth in the Bruun Rule	-0.18	0.06	0.18	5.1	-0.03

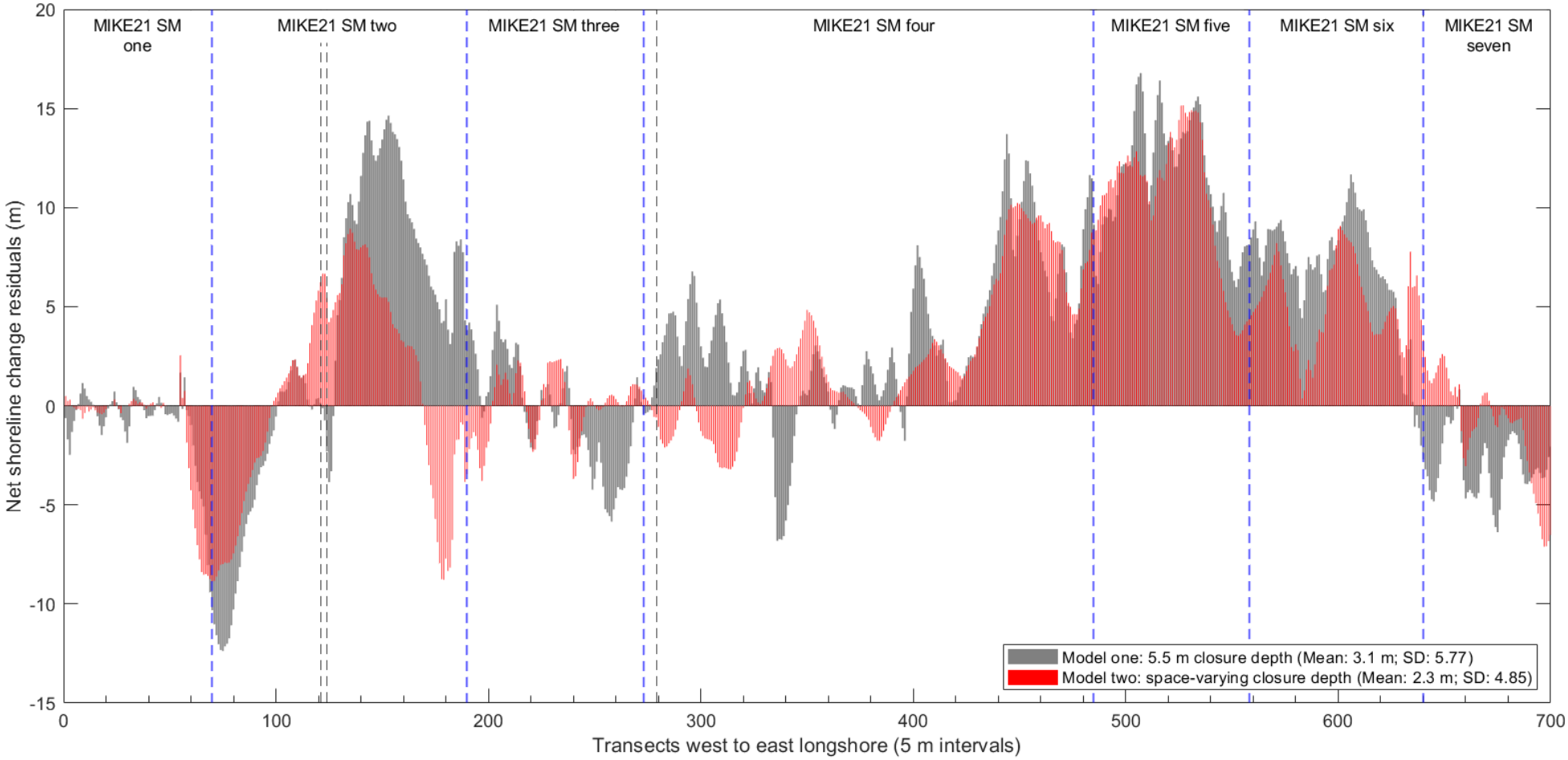

Fig. 6.3 Net shoreline change residuals obtained from using a 5.5 m (model one) and space-varying closure depth (model two) in MIKE21 to hindcast shoreline evolution in the Puerto Rico test site (10-Oct-2014 to 31-Mar-2016). Net shoreline change residuals are the difference between net shoreline change observed and predicted. Blue vertical dashed lines indicate the boundaries of each MIKE21 SM domain, and black vertical dashed lines indicate groyne locations. SD is the standard deviation. Net shoreline change residuals in groyne transects are excluded from the above plots and statistics.

07
Accounting for sea-level rise and complex planform morphologies: figures and tables

Table 7.1 Closure depth time and space variations used to forecast meso timescale shoreline evolution in the Puerto Rico test site (2014 to 2064). 2014 closure depths are based on reef substrate distribution. 2015 to 2063 closure depths are derived from Birkemeier (1985) formula using nearshore significant wave heights calculated by MIKE21. SD is the standard deviation.

Year	MIKE21 SM Domain (see defined areas in Fig. 6.1)							Mean	SD
	One	Two	Three	Four	Five	Six	Seven		
2014	5	6.5	5.5	7	4.5	3.5	5.5	5.36	1.18
2015	4.95	4.69	4.36	4.2	3.65	5.1	4.17	4.45	0.5
2016	5.37	5.07	4.73	4.45	3.71	5.54	4.36	4.75	0.64
2017	5.06	4.78	4.47	4.2	3.66	5.21	4.19	4.51	0.54
2018	4.95	4.69	4.36	3.96	3.57	5.12	4.08	4.39	0.56
2019	5.28	5.07	4.73	4.45	3.72	5.54	4.28	4.72	0.63
2020	5.14	4.88	4.57	4.3	3.76	5.31	4.29	4.61	0.54
2021	4.97	4.69	4.38	4.2	3.68	5.21	4.19	4.47	0.52
2022	5.39	5.07	4.84	4.54	3.81	5.64	4.33	4.8	0.63
2023	5.07	4.79	4.57	4.3	3.76	5.31	4.29	4.59	0.52
2024	4.95	4.69	4.36	4.2	3.66	5.12	4.1	4.44	0.51
2025	5.39	5.16	4.84	4.54	3.81	5.64	4.44	4.83	0.63
2026	5.06	4.79	4.48	4.22	3.76	5.29	4.27	4.55	0.53
2027	4.95	4.69	4.36	4.19	3.57	5.1	4.08	4.42	0.53
2028	5.37	5.07	4.73	4.54	3.71	5.62	4.36	4.77	0.65
2029	5.06	4.79	4.48	4.22	3.76	5.31	4.2	4.55	0.54
2030	4.95	4.69	4.36	4.2	3.68	5.21	4.19	4.47	0.52
2031	5.39	5.07	4.75	4.45	3.72	5.54	4.35	4.75	0.64
2032	5.07	4.79	4.57	4.22	3.76	5.31	4.29	4.57	0.53
2033	4.95	4.69	4.36	4.11	3.66	5.1	4.08	4.42	0.52
2034	5.39	5.07	4.75	4.54	3.81	5.62	4.36	4.79	0.62
2035	5.14	4.79	4.57	4.3	3.76	5.31	4.29	4.6	0.54
2036	4.97	4.69	4.38	4.22	3.68	5.21	4.19	4.47	0.52
2037	5.47	5.18	4.84	4.54	3.82	5.73	4.45	4.86	0.65
2038	5.16	4.88	4.57	4.3	3.87	5.31	4.29	4.63	0.52
2039	4.95	4.69	4.38	4.2	3.68	5.21	4.19	4.47	0.52
2040	5.39	5.18	4.84	4.54	3.82	5.64	4.45	4.84	0.62
2041	5.07	4.79	4.57	4.3	3.78	5.31	4.29	4.59	0.52
2042	4.95	4.69	4.36	4.11	3.68	5.1	4.08	4.43	0.51
2043	5.39	5.09	4.75	4.56	3.82	5.64	4.36	4.8	0.62
2044	5.14	4.79	4.57	4.3	3.87	5.31	4.29	4.61	0.51
2045	4.95	4.69	4.36	4.2	3.68	5.12	4.19	4.45	0.5
2046	5.39	5.09	4.84	4.54	3.84	5.64	4.36	4.81	0.62
2047	5.06	4.79	4.55	4.22	3.78	5.29	4.27	4.57	0.52
2048	4.95	4.69	4.38	4.2	3.78	5.21	4.19	4.48	0.49
2049	5.47	5.18	4.84	4.56	3.93	5.73	4.45	4.88	0.63
2050	5.16	4.9	4.57	4.32	3.88	5.31	4.39	4.65	0.5

Year	MIKE21 SM Domain (see defined areas in Fig. 6.1)							Mean	SD
	One	Two	Three	Four	Five	Six	Seven		
2051	4.97	4.69	4.38	4.2	3.78	5.21	4.19	4.49	0.5
2052	5.39	5.09	4.75	4.54	3.84	5.64	4.36	4.8	0.62
2053	5.06	4.79	4.48	4.22	3.78	5.21	4.19	4.53	0.51
2054	5.06	4.78	4.38	4.2	3.78	5.21	4.19	4.51	0.52
2055	5.49	5.18	4.84	4.56	3.94	5.64	4.45	4.87	0.61
2056	5.16	4.79	4.57	4.22	3.88	5.31	4.29	4.6	0.52
2057	5.06	4.79	4.47	4.22	3.78	5.21	4.29	4.54	0.5
2058	5.49	5.19	4.85	4.57	3.96	5.74	4.48	4.9	0.62
2059	5.16	4.9	4.58	4.32	3.99	5.31	4.39	4.66	0.48
2060	5.06	4.79	4.47	4.3	3.88	5.29	4.29	4.58	0.49
2061	5.39	5.18	4.84	4.56	3.94	5.64	4.54	4.87	0.58
2062	5.16	4.81	4.57	4.32	3.9	5.31	4.3	4.62	0.5
2063	5.06	4.79	4.38	4.22	3.8	5.21	4.2	4.52	0.51
Min.	4.95	4.69	4.36	3.96	3.57	3.5	4.08		
Max.	5.49	6.5	5.5	7	4.5	5.74	5.5		
Mean	5.16	4.91	4.59	4.38	3.79	5.33	4.31		
SD	0.18	0.29	0.22	0.41	0.14	0.33	0.21		

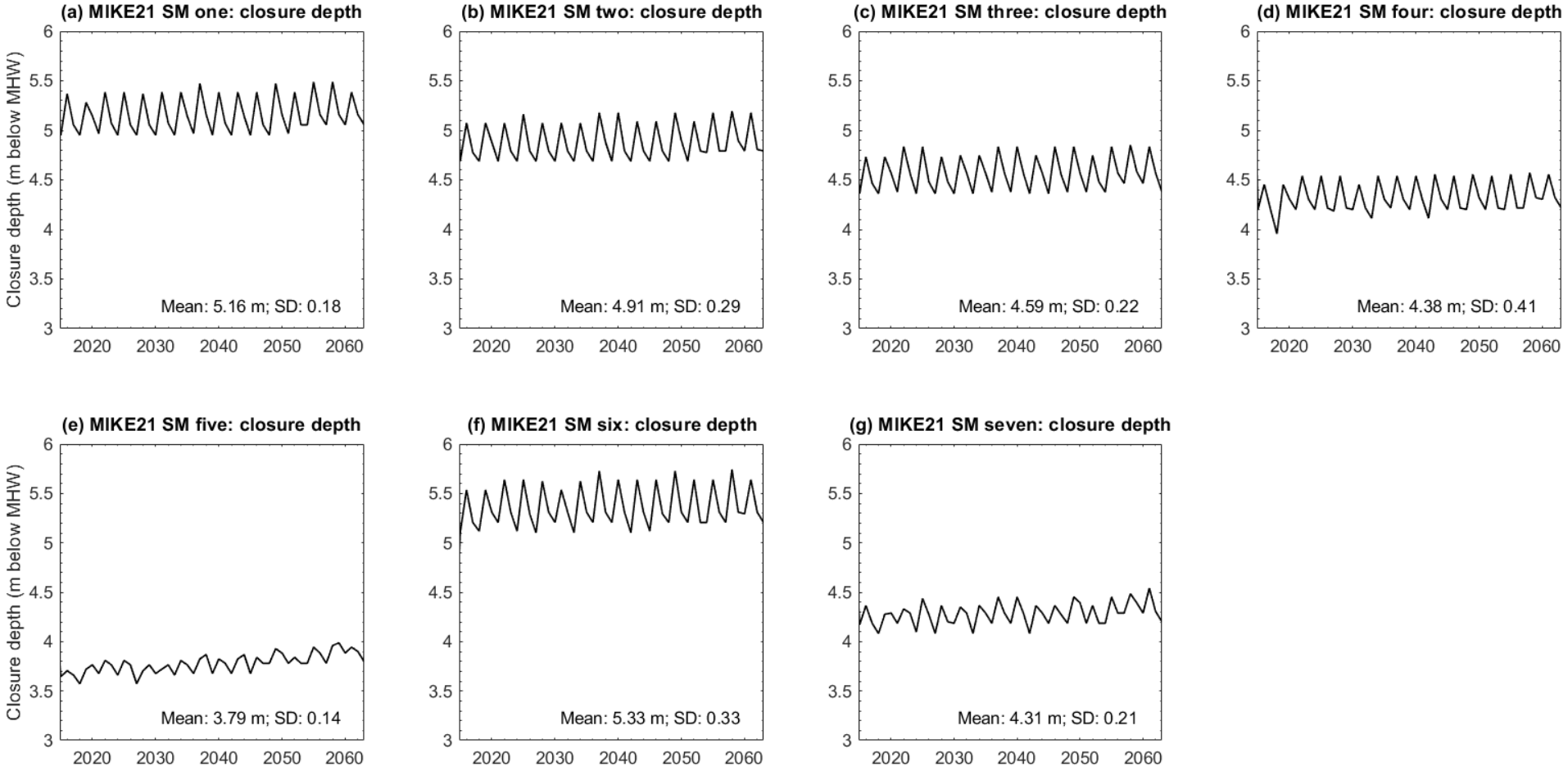

Fig. 7.1 Estimated closure depths (2015 to 2063) applied in all MIKE21 SM domains used to forecast meso timescale shoreline evolution (10-Oct-2014 to 10-Oct-2064) in the Puerto Rico test site with a time and space-varying closure depth. Closure depth estimations in each MIKE21 SM domain are derived from Birkemeier (1985) formula using significant wave heights calculated by MIKE21 in their respective nearshore area.

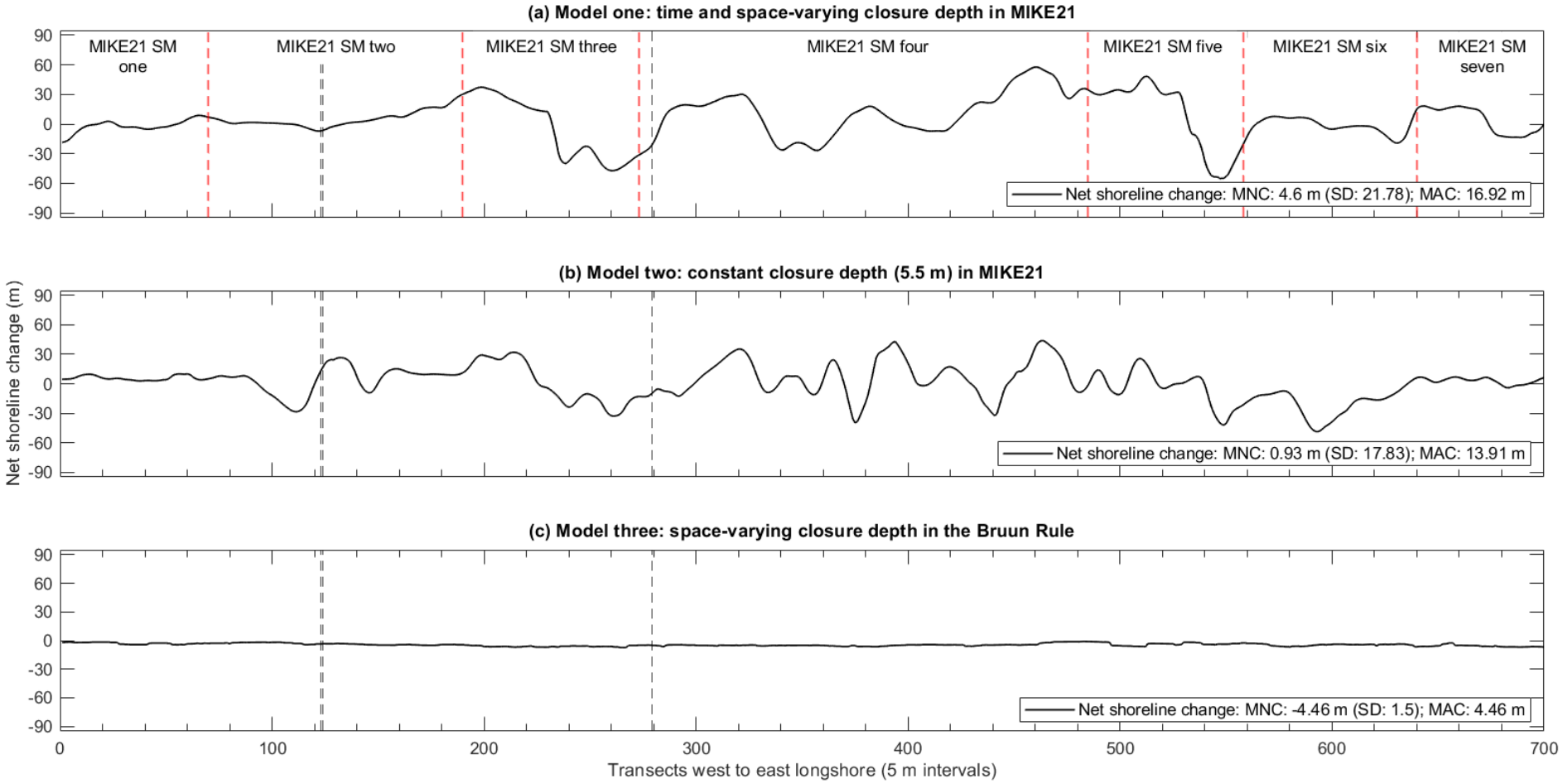

Fig. 7.2 Net shoreline change forecasted in the Puerto Rico test site (10-Oct-2014 to 10-Oct-2064) using a time and space-varying closure depth in MIKE21 (a), a 5.5 m constant closure depth in MIKE21 (b), and a space-varying closure depth in the Bruun Rule (c). Black vertical dashed lines indicate groyne locations. Red vertical dashed lines in (a) indicate the boundaries of each MIKE21 SM domain. MNC is mean net change, SD is the standard deviation, and MAC is mean absolute change. Net shoreline change observed and predicted in groyne transects are excluded from the above plots and statistics.

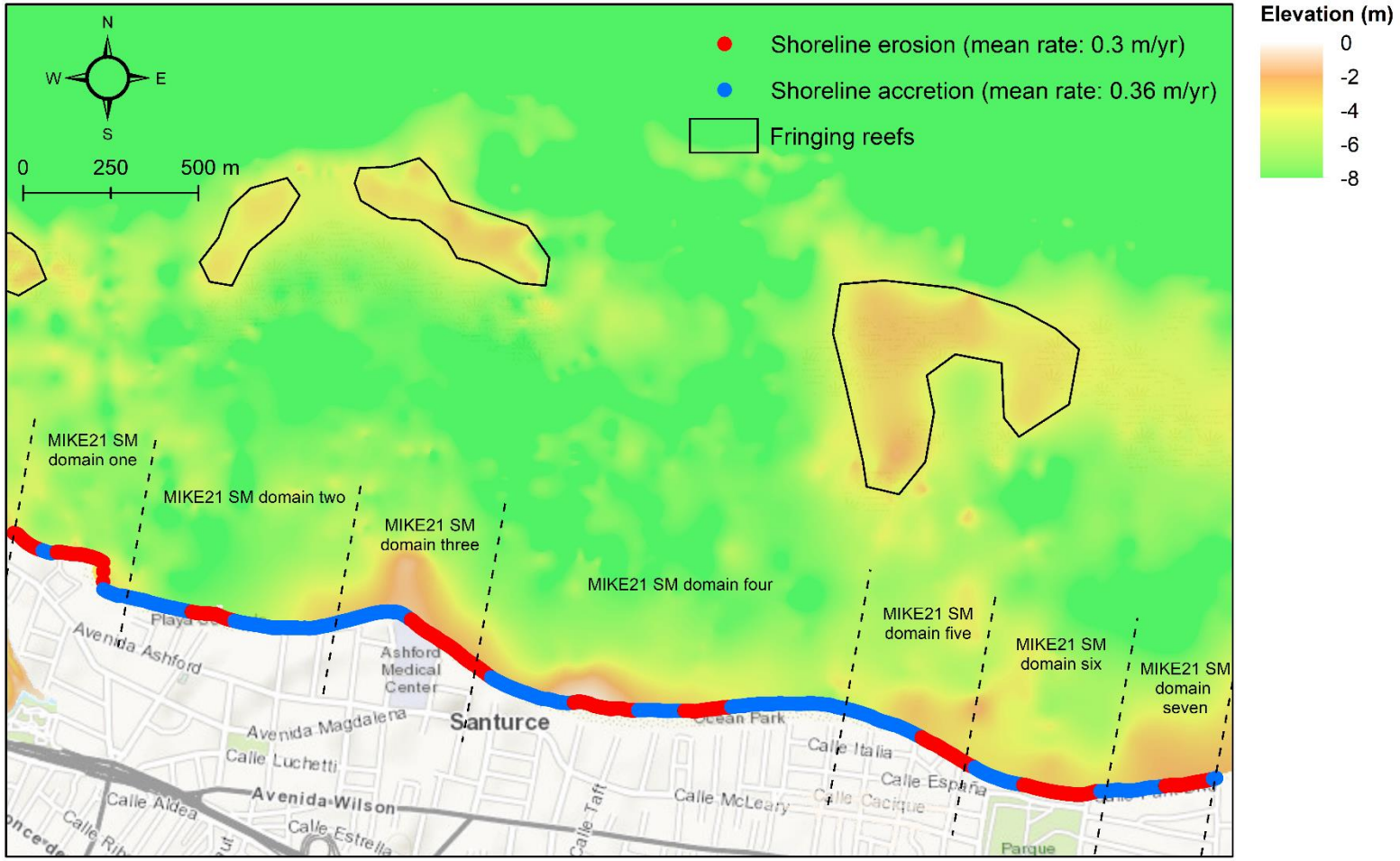

Fig. 7.3 Longshore variations in net shoreline change (accretion vs erosion) forecasted in the Puerto Rico test site (10-Oct-2014 to 10-Oct-2064) using a time and space-varying closure depth in MIKE21. *Credits* (streetmap): ESRI (2020)

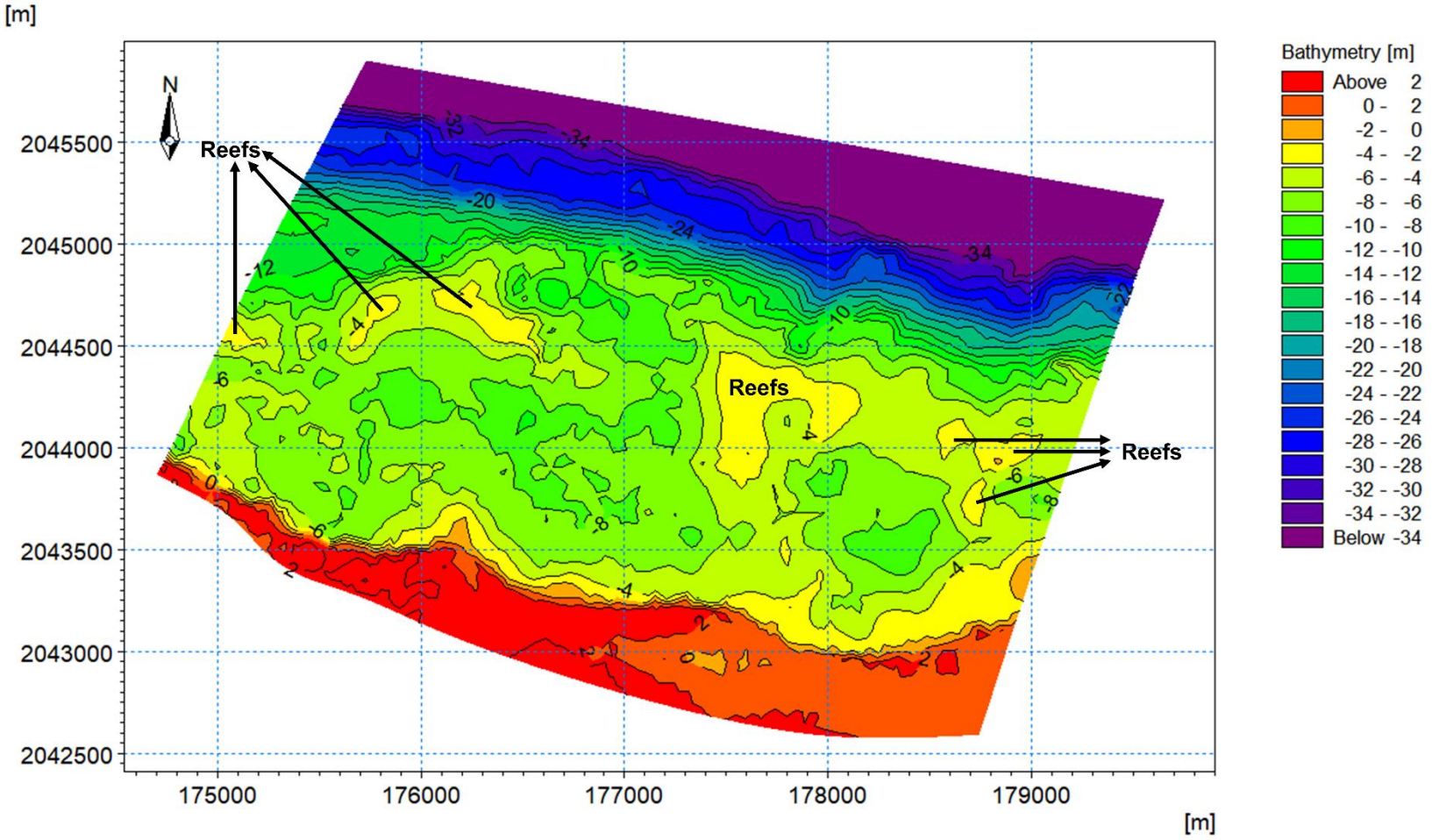

Fig. 7.4 Coral reefs present in the Puerto Rico test site's mesh bathymetry.

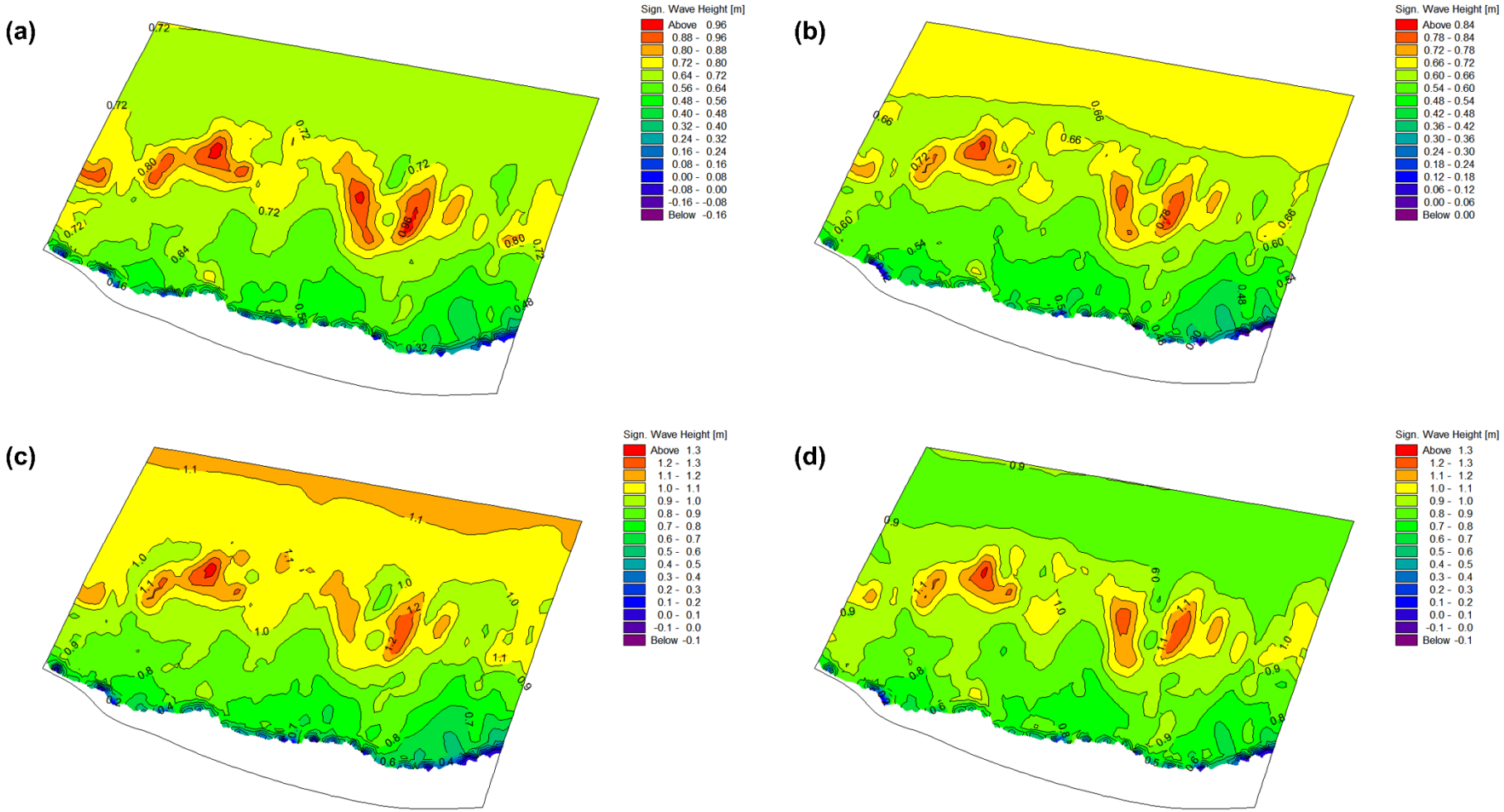

Fig. 7.5 Significant wave heights at different timesteps in MIKE21 meso timescale shoreline evolution simulation (10-Oct-2014 to 10-Oct-2064) in the Puerto Rico test site: 10-Oct-2015 00:00:00 (a), 10-Oct-2024 00:00:00 (b), 10-Oct-2034 00:00:00 (c), and 10-Oct-2054 00:00:00 (d). The key take-home message of this figure is that the highest significant wave heights occur in the coral reefs vicinity (see coral reef areas in Figs. 7.3 and 7.4).

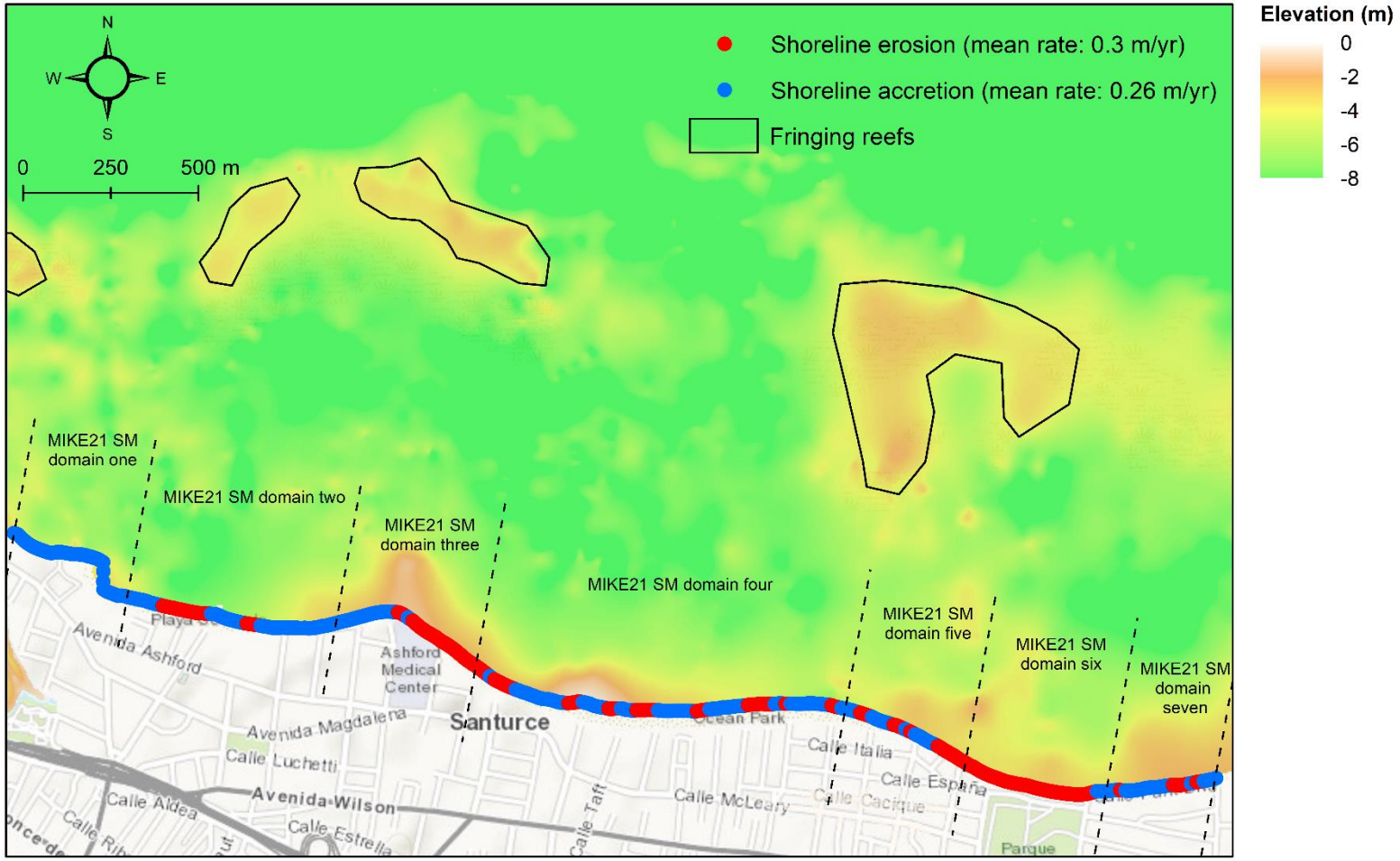

Fig. 7.6 Longshore variations in net shoreline change (accretion vs erosion) forecasted in the Puerto Rico test site (10-Oct-2014 to 10-Oct-2064) using a 5.5 m constant closure depth in MIKE21. *Credits* (streetmap): ESRI (2020)

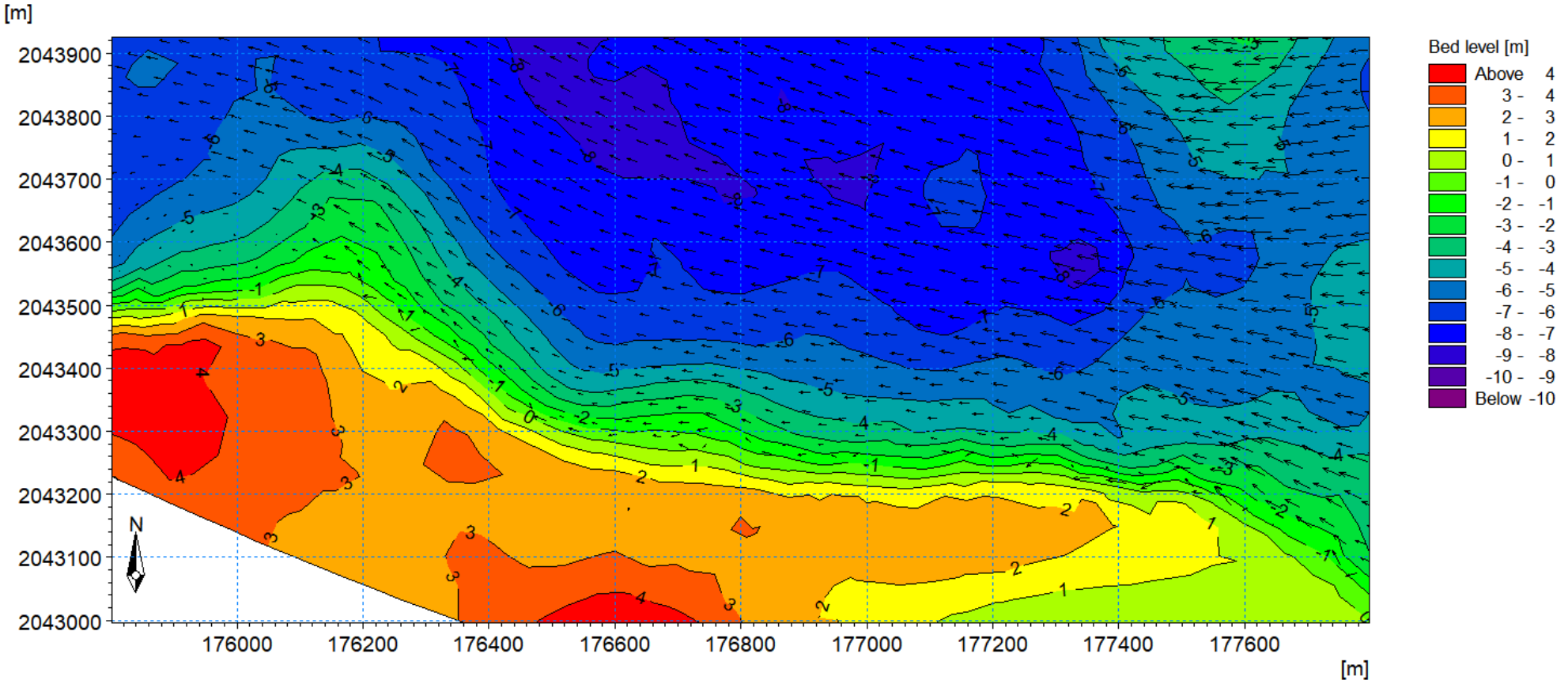

Fig. 7.7 Predominant direction of littoral drift in the Puerto Rico test site (indicated by arrows).

Table 7.2 Summary of MIKE21 and the Bruun Rule performance in their various applications in preceding chapters. All Bruun Rule modelling applications and statistics are highlighted in grey.

Chapter	Test site	Model	Timescale	BSS	MAE (m)
4	New York	Calibrated MIKE21	2014 to 2016	0.46	1.1
		Calibrated Bruun Rule		0.19	1.18
	Puerto Rico	Calibrated MIKE21	2014 to 2016	0.03	5
		Calibrated Bruun Rule		-0.03	5.10
	Southern California	Calibrated MIKE21	2009 to 2011	0.22	16.58
		Calibrated Bruun Rule		0.01	16.09
5	New York	4.2 m constant closure depth in MIKE21	1966 to 2016	0.24	4.5
		6 m constant closure depth in MIKE21		0.21	5.92
		Time-varying closure depth in MIKE21		0.12	7.06
		4.2 m constant closure depth in Bruun Rule		-12.83	16.27
		6 m constant closure depth in Bruun Rule		-4.39	9.18
6	Puerto Rico	5.5 constant closure depth in MIKE21	2014 to 2016	0.03	5
		Space-varying closure depth in MIKE21		0.37	3.93
		Space-varying closure depth in Bruun Rule		-0.03	5.1

Table 7.3 Summary of all meso timescale shoreline evolution forecasts (10-Oct-2014 to 10-Oct-2064) in the Puerto Rico test site. MNC is mean net change, SD is the standard deviation, and MAC is mean absolute change.

Forecast (Relative sea-level rise: +0.28 m)	Modelling approach	MNC (m)	SD	MAC (m)
Model one	Time and space-varying closure depth in MIKE21	4.6	21.78	16.92
Model two	5.5 m closure depth in MIKE21	0.93	17.83	13.91
Model three	Space-varying closure depth in the Bruun Rule	-4.46	1.5	4.46

08
Discussion and conclusions – On modelling mesoscale evolution of managed sandy shorelines: figures and tables

Table. 8.1 Quantitative summary of meso timescale net shoreline change observed and predicted (01-Jan-1966 to 01-Feb-2016) in the New York test site. MNC is mean net change, MAC is mean absolute change, MAE is mean absolute error, and BSS is Brier Skill Score.

Model	Modelling approach	Shoreline change statistics				Longshore trends in shoreline morphology				
		MNC (m)	MAC (m)	MAE (m)	BSS	Range (m)	% Erosion	% Accretion	Mean erosion (m)	Mean accretion (m)
-	Observed	1.69	3.29	-	-	-18.76 to 30.37	33	67	2.46	3.69
One	4.2 m closure depth in MIKE21 (1966 coastal profiles)	1.08	3.6	4.5	0.24	-11.88 to 14.58	40	60	3.08	3.96
Two	6 m closure depth in MIKE21 (shifted 2014 coastal profiles)	1.79	4.86	5.92	0.21	-14.44 to 23.06	38	62	4.03	5.38
Three	Time-varying closure depth in MIKE21	0.01	5.71	7.06	0.12	-22.42 to 24.5	51	49	5.6	5.83
Four	4.2 m closure depth in Bruun Rule (1966 coastal profiles)	-14.56	14.56	16.27	-12.83	-18.57 to -11.28	100	-	14.56	-
Five	6 m closure depth in Bruun Rule (shifted 2014 coastal profiles)	-7.36	7.36	9.18	-4.39	-10.02 to -6.08	100	-	7.36	-

Table. 8.2 Quantitative summary of micro timescale net shoreline change observed and predicted (10-Oct-2014 to 31-Mar-2016) in the Puerto Rico test site. MNC is mean net change, MAC is mean absolute change, MAE is mean absolute error, and BSS is Brier Skill Score.

Modelling approach	Shoreline change statistics				Longshore trends in shoreline morphology				
	MNC (m)	MAC (m)	MAE (m)	BSS	Range (m)	% Erosion	% Accretion	Mean erosion (m)	Mean accretion (m)
Observed	3.22	5.03	-	-	-11.26 to 16.23	31	69	2.96	5.94
Space-varying closure depth in MIKE21	0.91	2.71	3.93	0.37	-8.76 to 13.27	39	61	2.32	2.95
5.5 m closure depth in MIKE21	0.11	0.82	5	0.03	-4 to 5.74	47	53	0.76	0.88
Bruun Rule	-0.18	0.18	5.1	-0.03	-0.3 to -0.04	100	-	0.18	-

Table. 8.3 Quantitative summary of meso timescale net shoreline change observed and predicted (10-Oct-2014 to 10-Oct-2064) in the Puerto Rico test site. MNC is mean net change, MAC is mean absolute change, and SD is the standard deviation.

Shoreline change statistics	Modelling approach			
	Historical trends (1936 to 2017)	Time and space-varying closure depth in MIKE21	5.5 m closure depth in MIKE21	Bruun Rule
MNC (m)	-	4.6	0.93	-4.46
MAC (m)	-	16.92	13.91	4.46
Range (m)	-	-55.21 to 57.72	-48.88 to 43.9	-7.39 to -0.97
% Accretion	-	59	57	-
Accretion range (m)	-	0.03 to 57.72	0.01 to 43.9	-
Mean accretion (m)	-	18.16	12.92	-
SD (accretion)		14.3	10.65	-
Accretion rate per year (m)	0.3 to 0.5 (range)	0.36 (mean)	0.26 (mean)	-
% Erosion	-	41	43	100
Erosion range (m)	-	0.05 to 55.21	0.17 to 48.88	-7.39 to -0.97
Mean erosion (m)	-	15.12	15.23	4.46
SD (erosion)		14.52	11.77	1.5
Erosion rate per year (m)	0.2 to 1.21 (range)	0.3 (mean)	0.3 (mean)	0.09

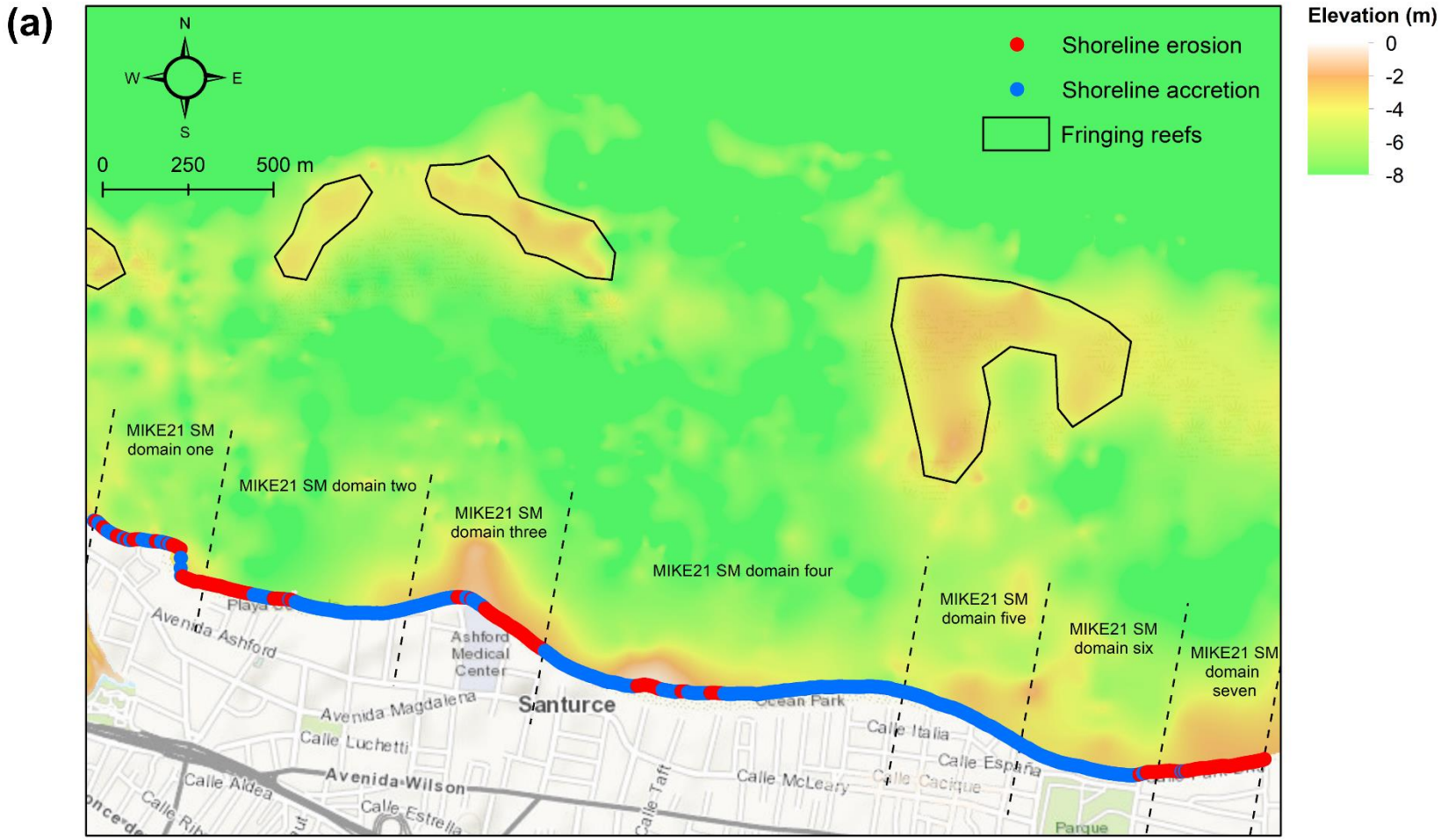

Fig. 8.1 Longshore trends (accretion versus erosion) in shoreline evolution observed (a) and predicted in the Puerto Rico test site (10-Oct-2014 to 31-Mar-2016) using a space-varying closure depth in MIKE21 (b), a 5.5 m constant closure depth in MIKE21 (c), and a space-varying closure depth in the Bruun Rule (d).

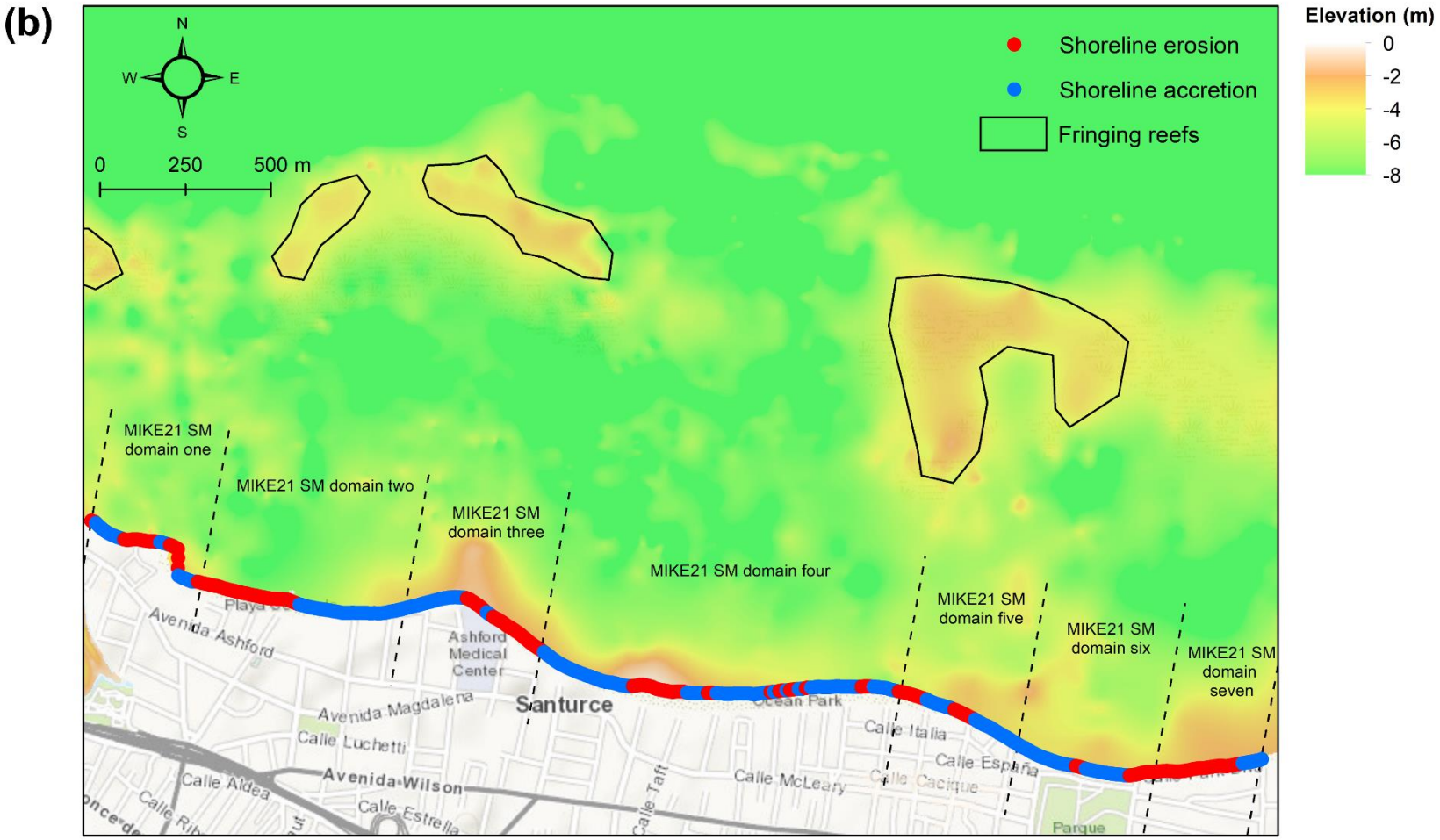

Fig. 8.1 (continued)

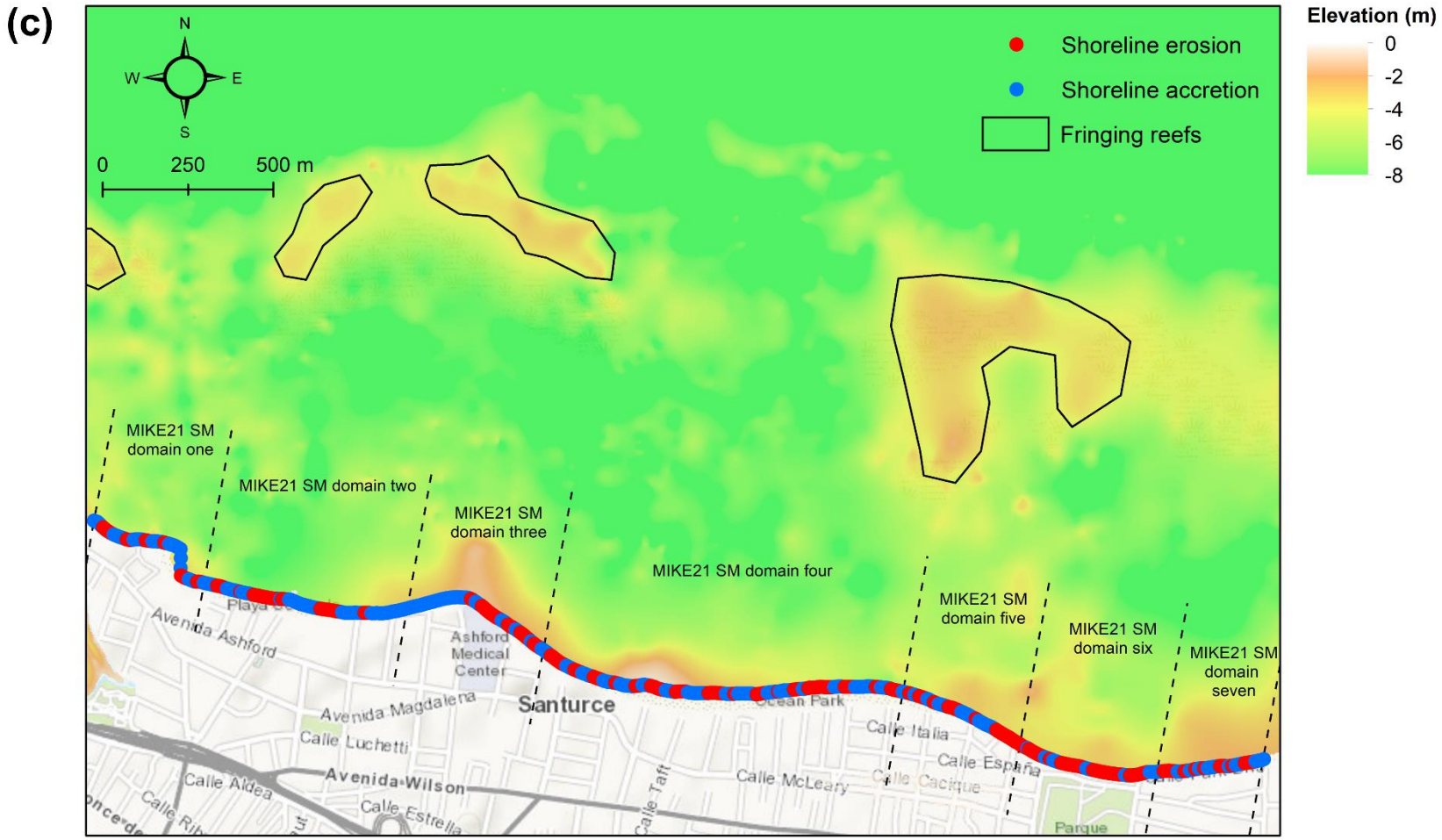

Fig. 8.1 (continued)

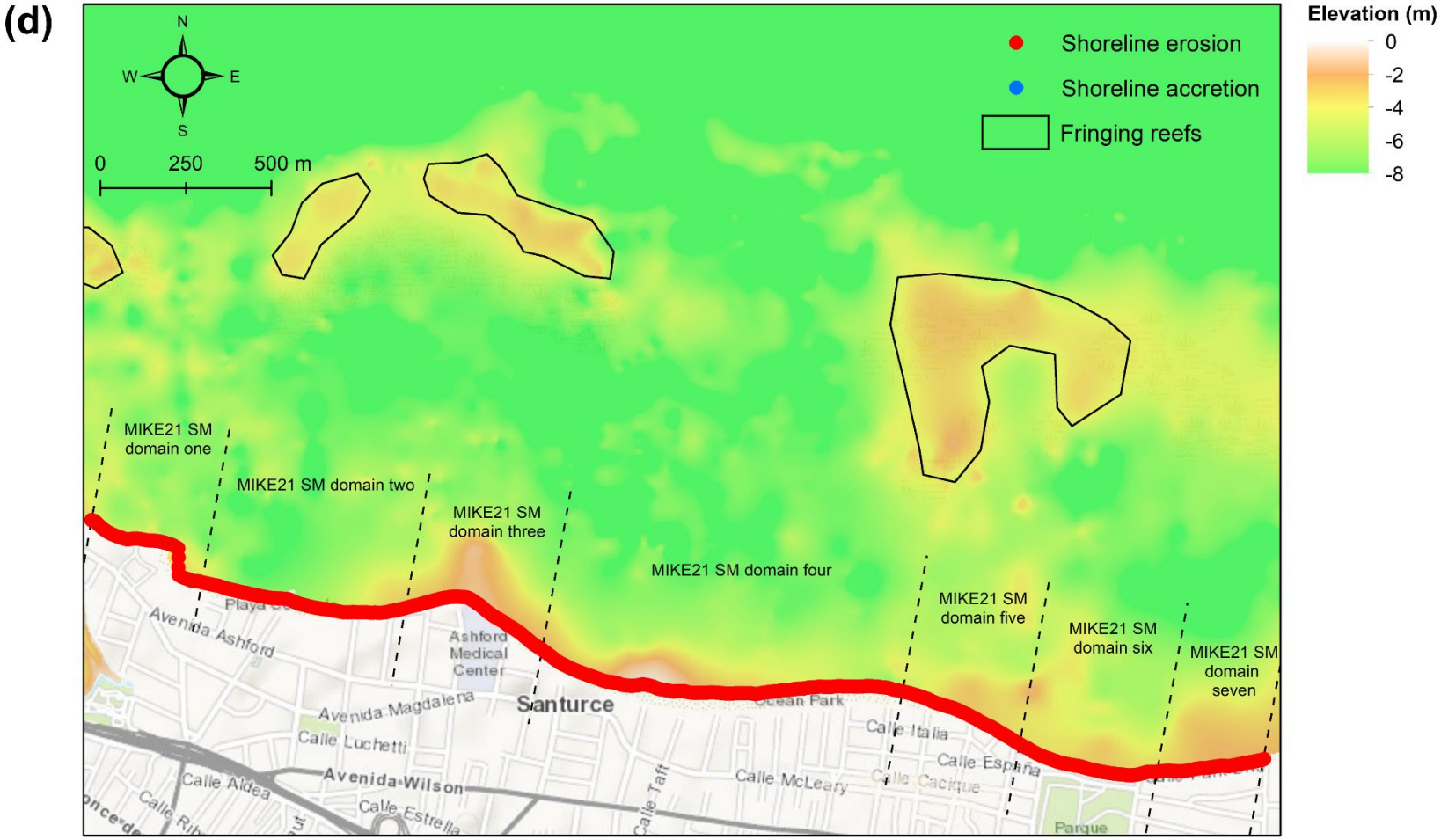

Fig. 8.1 (continued)

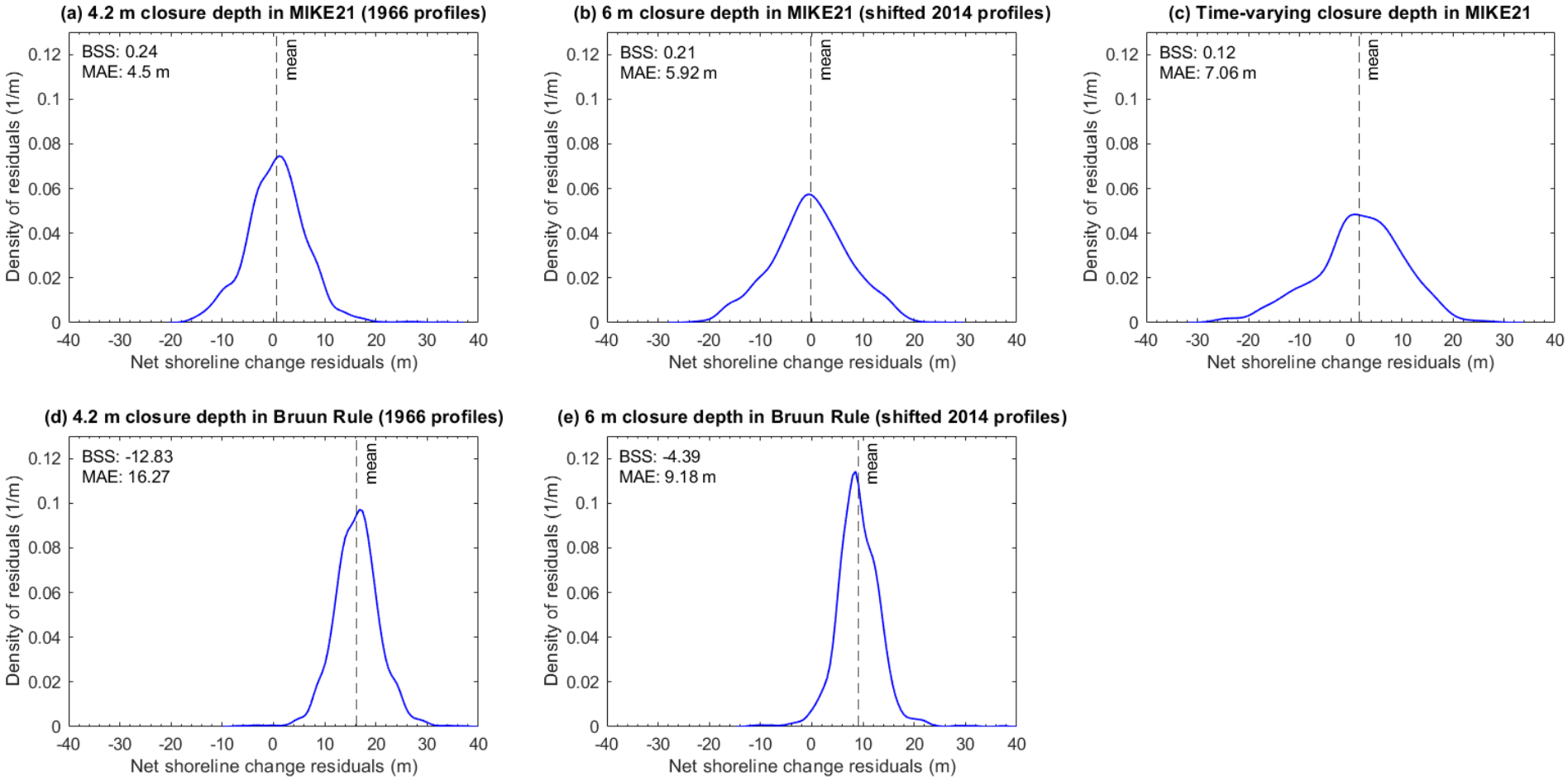

Fig. 8.2 Kernel density plots of net shoreline change residuals derived from hindcasting meso timescale shoreline evolution in the New York test site (01-Jan-1966 to 01-Feb-2016). Net shoreline change residuals are the difference between net shoreline change observed and predicted. BSS is Bier Skill Score, and MAE is mean absolute error.

Appendix A
Graphical representation of model sensitivity in each test site

A1 MIKE21 sensitivity to nearshore spatial discretisation

A1 graphically illustrates the sensitivity of MIKE21 net littoral drift and net shoreline change predictions to coarsening nearshore spatial discretisation in each test site.

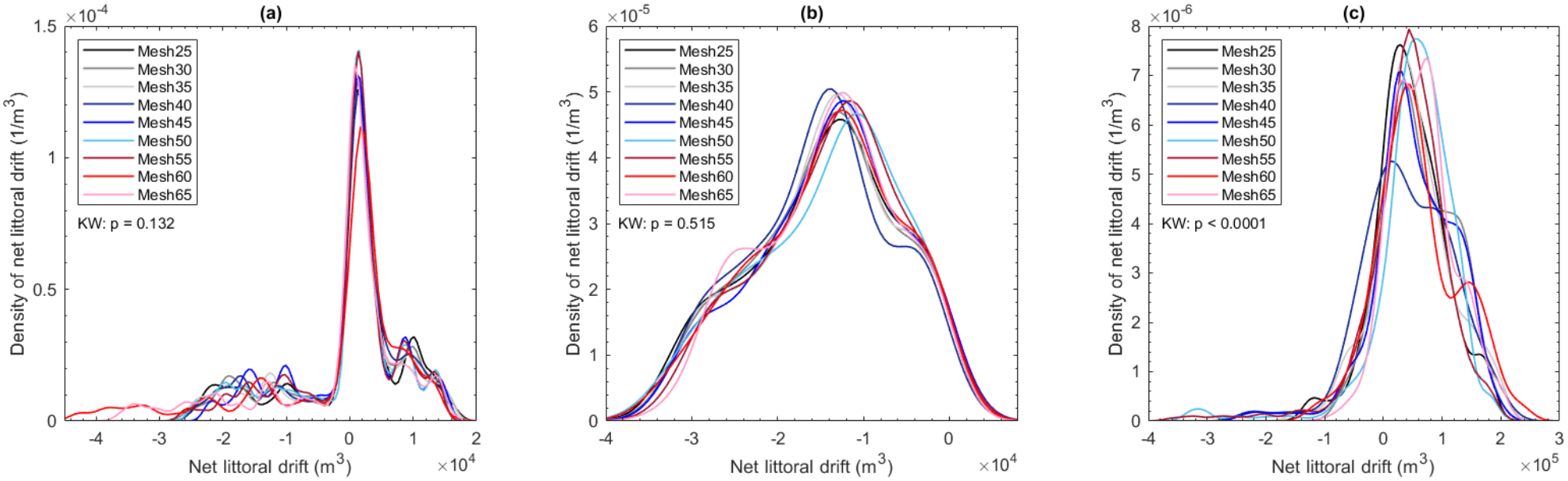

Fig. A1.1 Kernel density plots of net littoral drift predictions in response to coarsening nearshore spatial discretisation in the New York (a), Puerto Rico (b), and Southern California (c) test site. In (a), (b), and (c), Mesh$X$ refers to a mesh with a nearshore spatial discretisation of X resolution (m). Net littoral drift predictions in Fig. A1.1 are from 01-Jan-2014 to 01-Feb-2016 in the New York test site, 10-Oct-2014 to 31-Mar-2016 in the Puerto Rico test site, and 01-Jan-2009 to 02-Aug-2011 in the Southern California test site. The Kruskal-Wallis (KW) test indicates that coarsening nearshore spatial discretisation significantly affects net littoral drift predictions in the Southern California test site only. A post hoc Dunn's test reveals that net littoral drift predictions are consistent from all meshes in the Southern California test site, except Mesh30, Mesh50, and Mesh65.

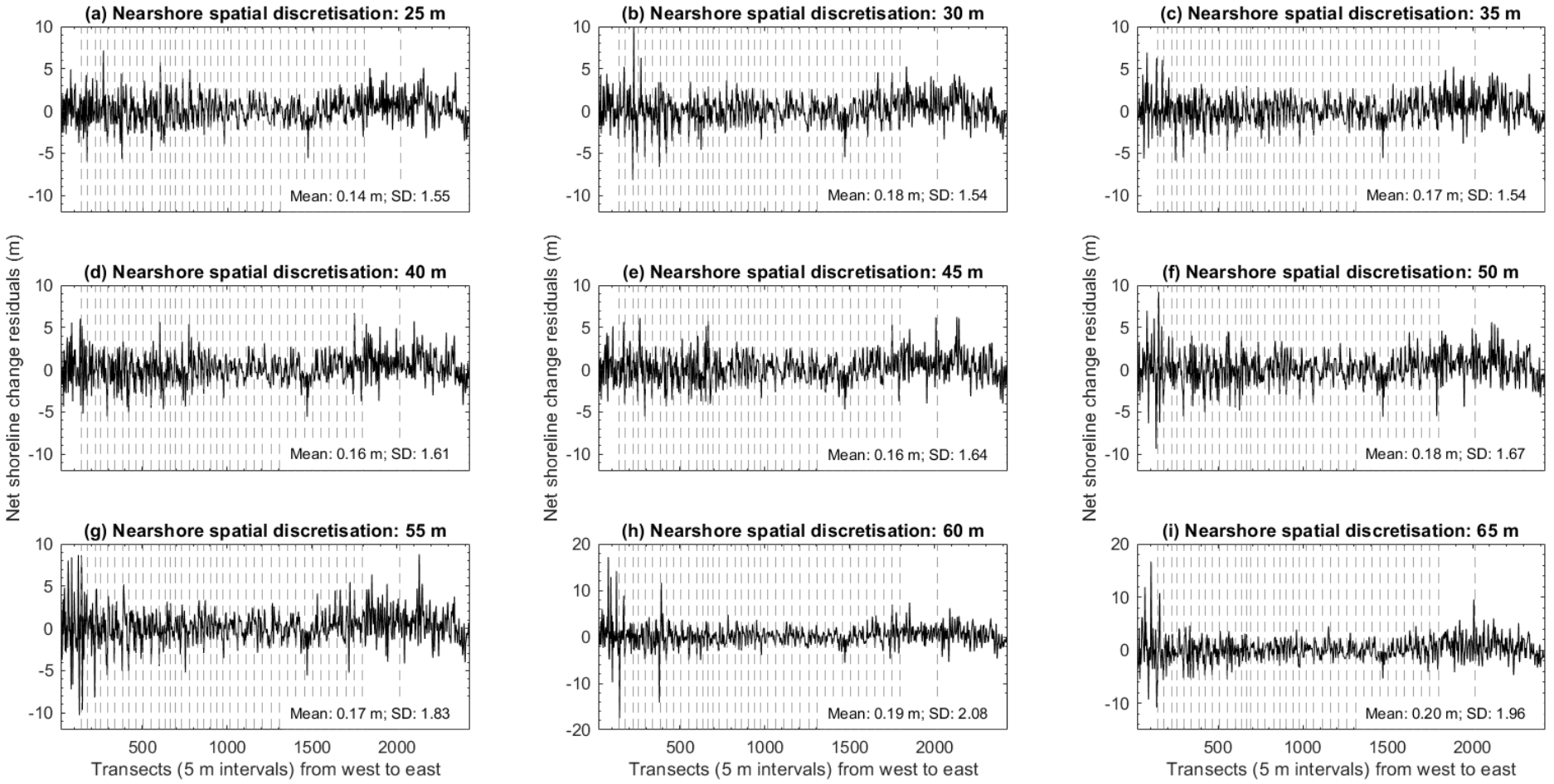

Fig. A1.2 Net shoreline change residuals from coarsening nearshore spatial discretisation in the New York test site. Vertical dashed lines indicate groyne locations. SD is the standard deviation. Net shoreline change residuals in (a) to (i) are the difference between net shoreline change observed and predicted from 01-Jan-2014 to 01-Feb-2016. Note the difference in y axis in (h) and (i). Net shoreline change residuals obtained in groyne transects are excluded from the above plots and statistics.

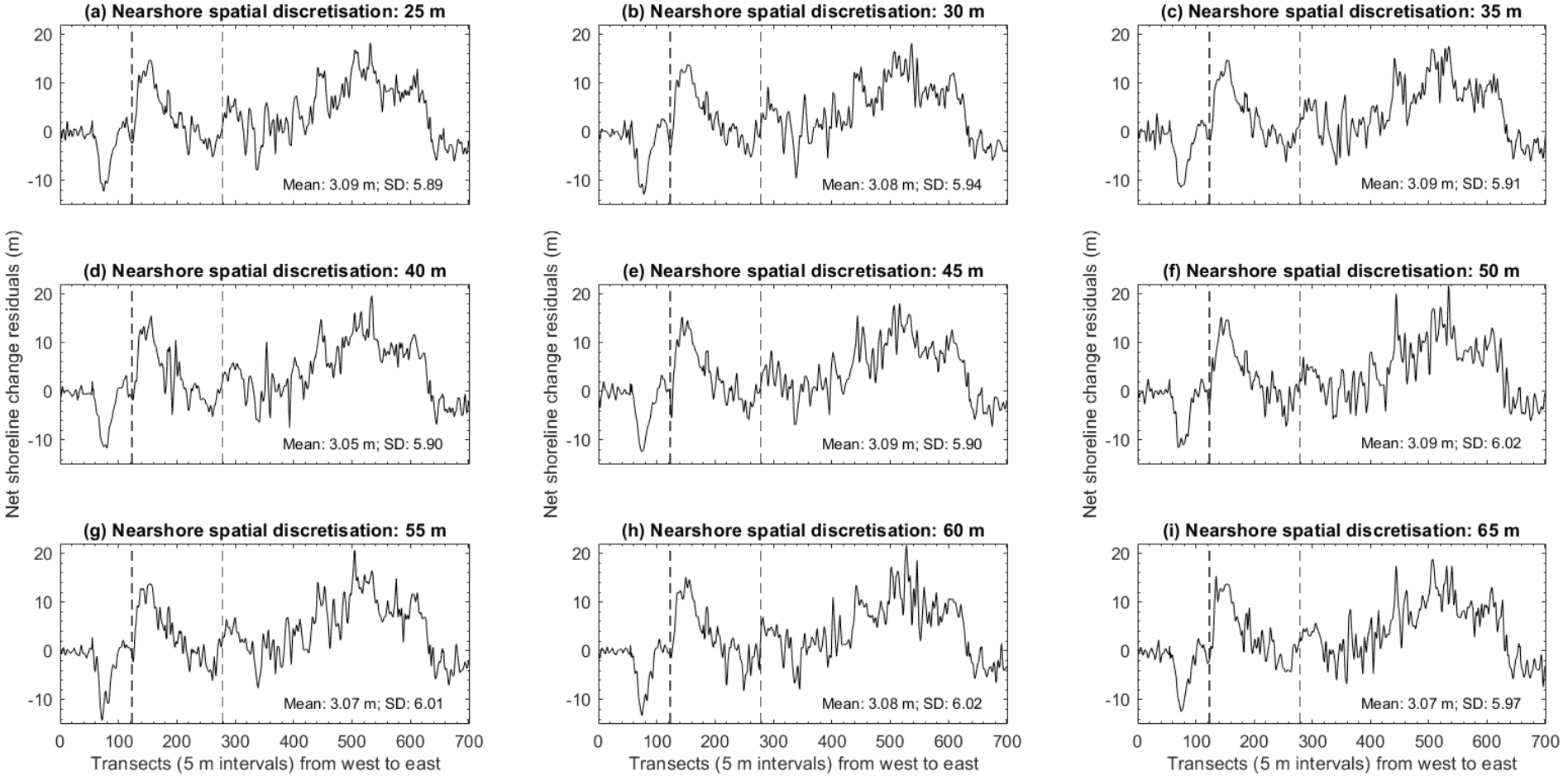

Fig. A1.3 Net shoreline change residuals from coarsening nearshore spatial discretisation in the Puerto Rico test site. Vertical dashed lines indicate groyne locations. SD is the standard deviation. Net shoreline change residuals in (a) to (i) are the difference between net shoreline change observed and predicted from 10-Oct-2014 to 31-Mar-2016. Net shoreline change residuals obtained in groyne transects are removed from the above plots and statistics.

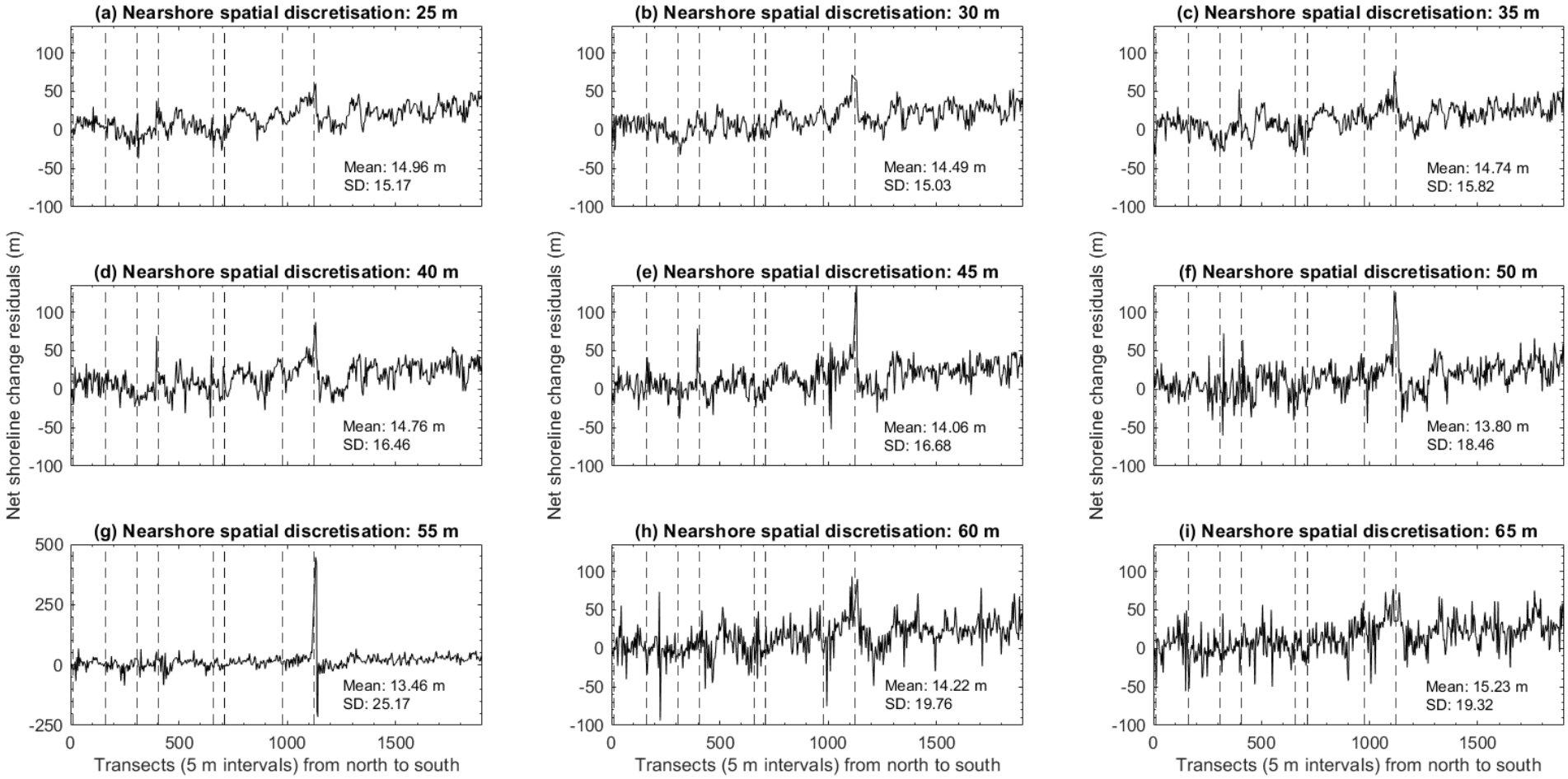

Fig. A1.4 Net shoreline change residuals from coarsening nearshore spatial discretisation in the Southern California test site. Vertical dashed lines indicate groyne locations. SD is the standard deviation. Net shoreline change residuals in (a) to (i) are the difference between net shoreline change observed and predicted from 01-Jan-2009 to 02-Aug-2011. Note the difference in y axis in (g). Net shoreline change residuals obtained in groyne transects are removed from the above plots and statistics.

A2 MIKE21 and the Bruun Rule sensitivity to bathymetry data spatial resolution

A2 graphically illustrates the sensitivity of MIKE21 and the Bruun Rule to coarsening bathymetry data in each test site.

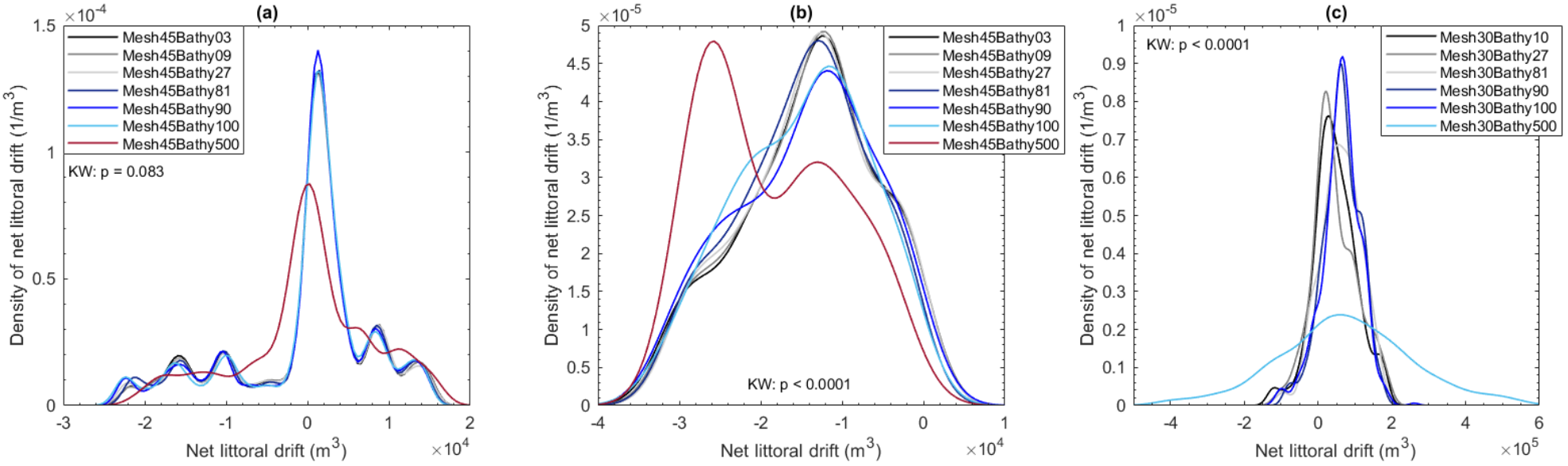

Fig. A2.1 Kernel density plots of net littoral drift predictions in response to coarsening bathymetry data in the New York (a), Puerto Rico (b), and Southern California (c) test site. In (a) to (c), Mesh$X$Bathy$Y$ refers to a mesh with a nearshore discretisation of X resolution (m) interpolated with bathymetry data of Y resolution (m). Net littoral drift predictions in Fig. A2.1 are from 01-Jan-2014 to 01-Feb-2016 in the New York test site, 10-Oct-2014 to 31-Mar-2016 in the Puerto Rico test site, and 01-Jan-2009 to 02-Aug-2011 in the Southern California test site. The Kruskal-Wallis (KW) test indicates that coarsening bathymetry data significantly affects net littoral drift predictions in the Puerto Rico and Southern California test sites only. A post hoc Dunn's test reveals net littoral drift predictions are not significantly different from bathymetry data resolutions ≤ 100 m in the Puerto Rico test site and ≤ 27 m in the Southern California test site.

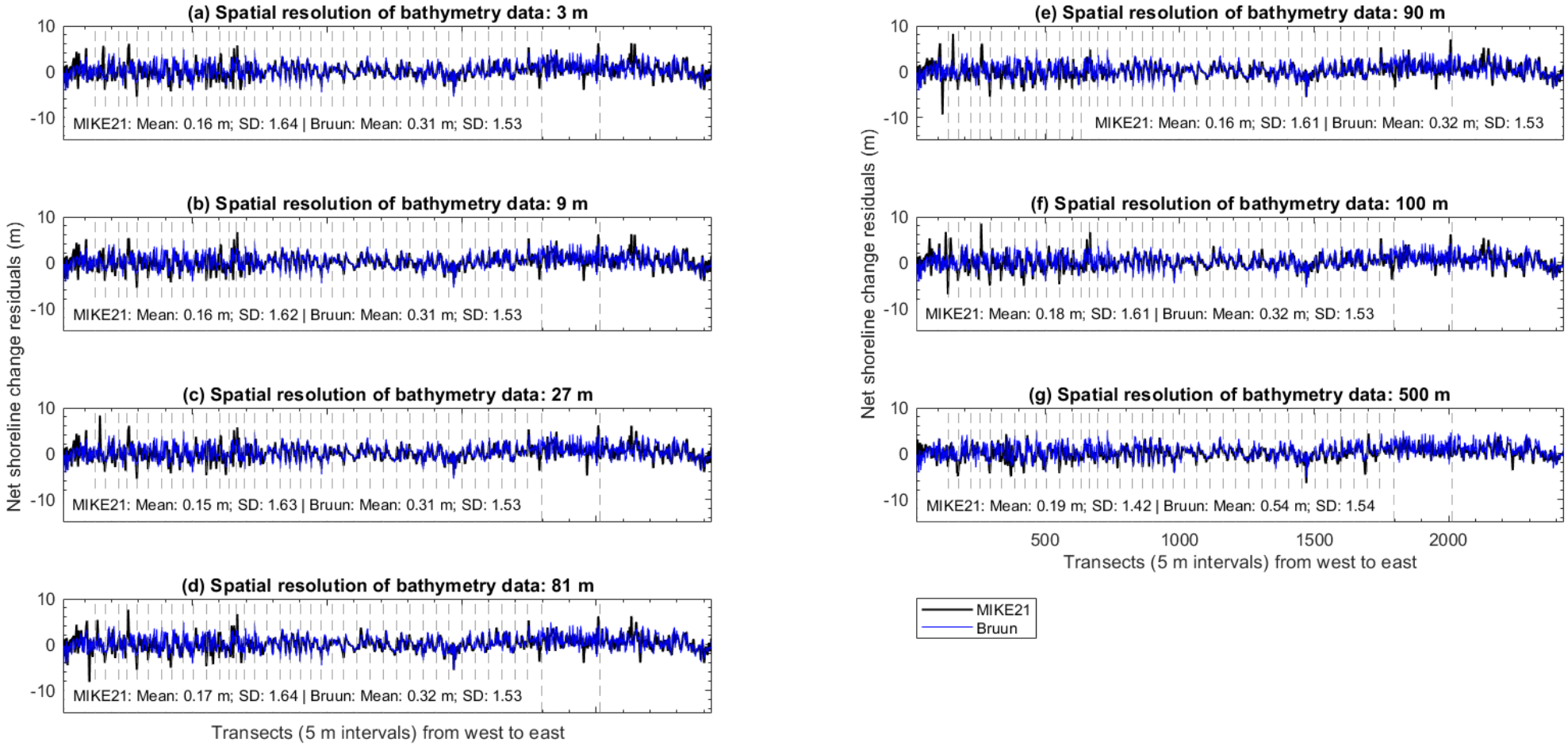

Fig. A2.2 Net shoreline change residuals from coarsening bathymetry data in the New York test site. Vertical dashed lines indicate groyne locations. SD is the standard deviation. Net shoreline change residuals in (a) to (g) are the difference between net shoreline change observed and predicted from 01-Jan-2014 to 01-Feb-2016. Net shoreline change residuals obtained in groyne transects are removed from the above plots and statistics.

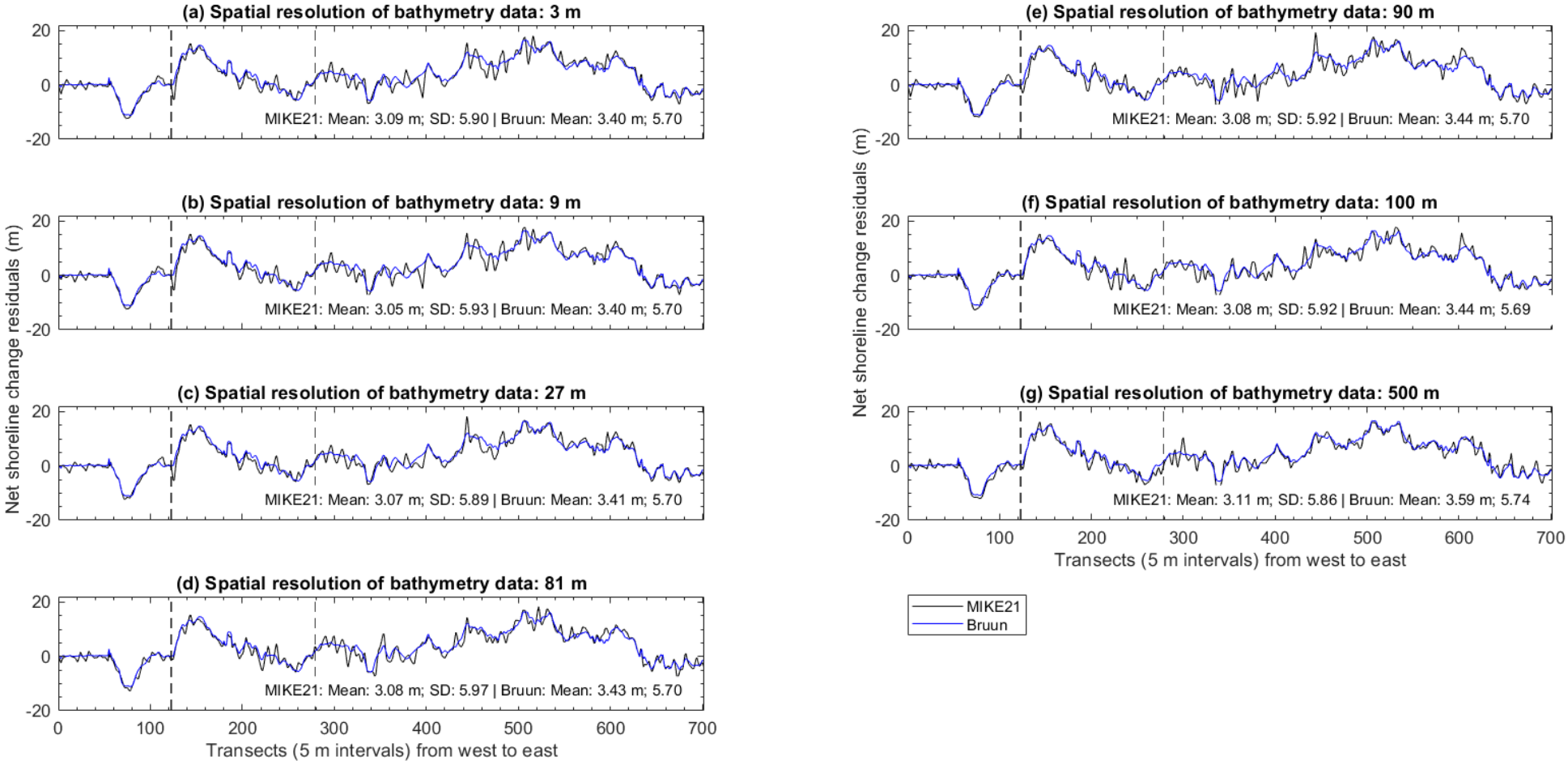

Fig. A2.3 Net shoreline change residuals from coarsening bathymetry data in the Puerto Rico test site. Vertical dashed lines indicate groyne locations. SD is the standard deviation. Net shoreline change residuals in (a) to (g) are the difference between net shoreline change observed and predicted from 10-Oct-2014 to 31-Mar-2016. Net shoreline change residuals obtained in groyne transects are excluded from the above plots and statistics.

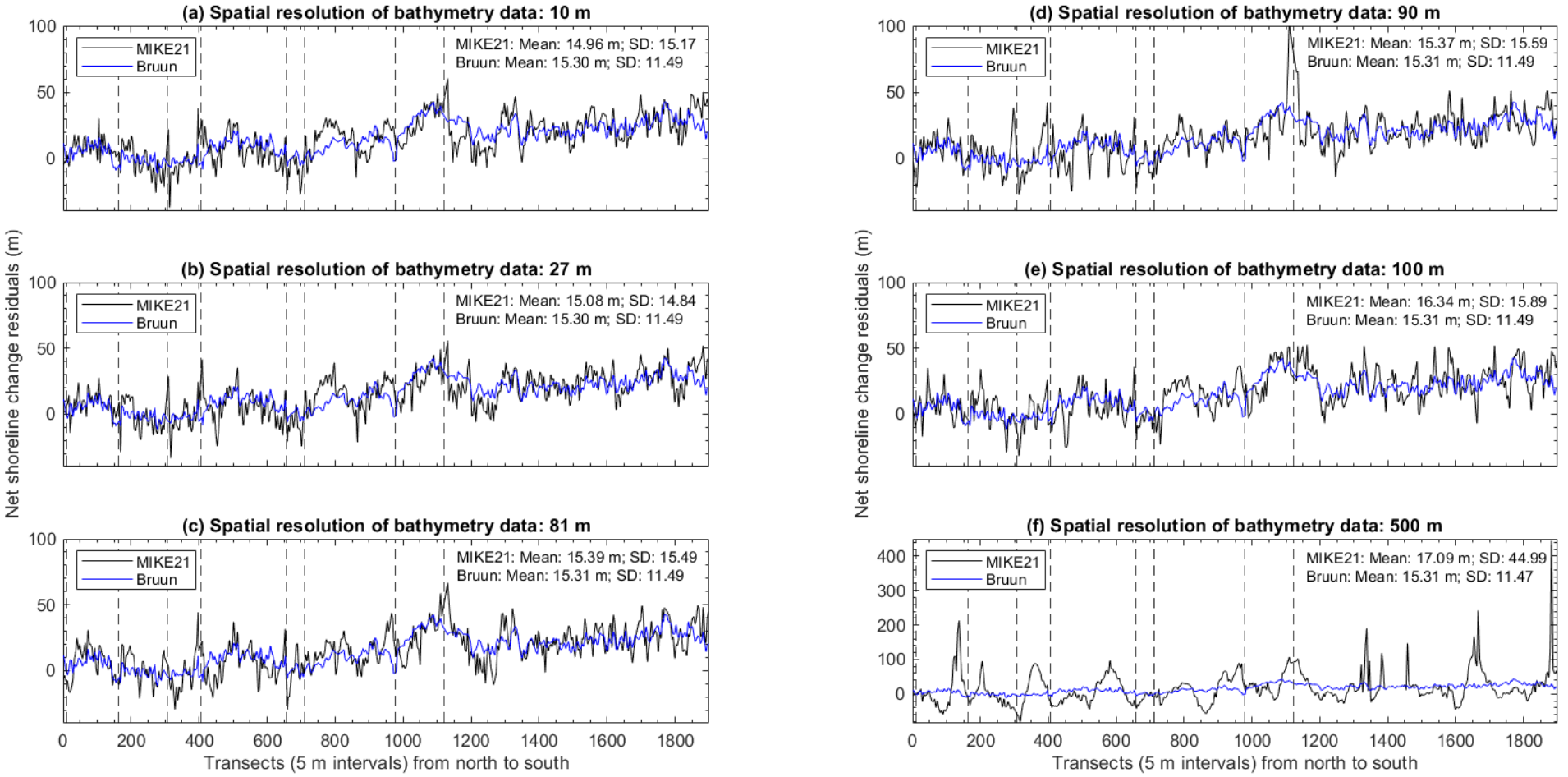

Fig. A2.4 Net shoreline change residuals from coarsening bathymetry data in the Southern California test site. Vertical dashed lines indicate groyne locations. SD is the standard deviation. Net shoreline change residuals in (a) to (f) are the difference between net shoreline change observed and predicted from 01-Jan-2009 to 02-Aug-2011. Note the difference in y axis in (f). Net shoreline change residuals obtained in groyne transects are excluded from the above plots and statistics.

A3 MIKE21 and the Bruun Rule sensitivity to tide data

A3 graphically illustrates the sensitivity of MIKE21 and the Bruun Rule to tide time series data resolution in each test site.

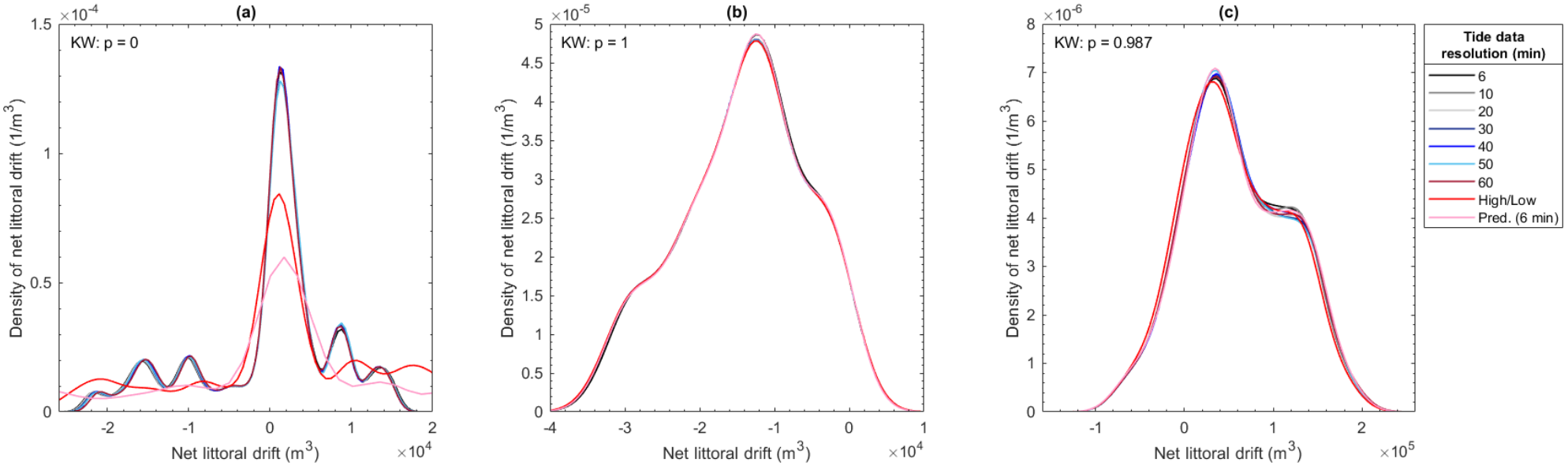

Fig. A3.1 Kernel density plots of net littoral drift predictions in response to tide data resolution in the New York (a), Puerto Rico (b), and Southern California (c) test site. Pred is NOAA tide predictions. Net littoral drift predictions in Fig. A3.1 are from 01-Jan-2014 to 01-Feb-2016 in the New York test site, 10-Oct-2014 to 31-Mar-2016 in the Puerto Rico test site, and 01-Jan-2009 to 02-Aug-2011 in the Southern California test site. The Kruskal-Wallis (KW) test indicates that tide data variations significantly affect net littoral drift predictions in the New York test site only. A post hoc Dunn's test reveals that net littoral drift predictions in the New York test site are significantly affected by NOAA tide predictions only.

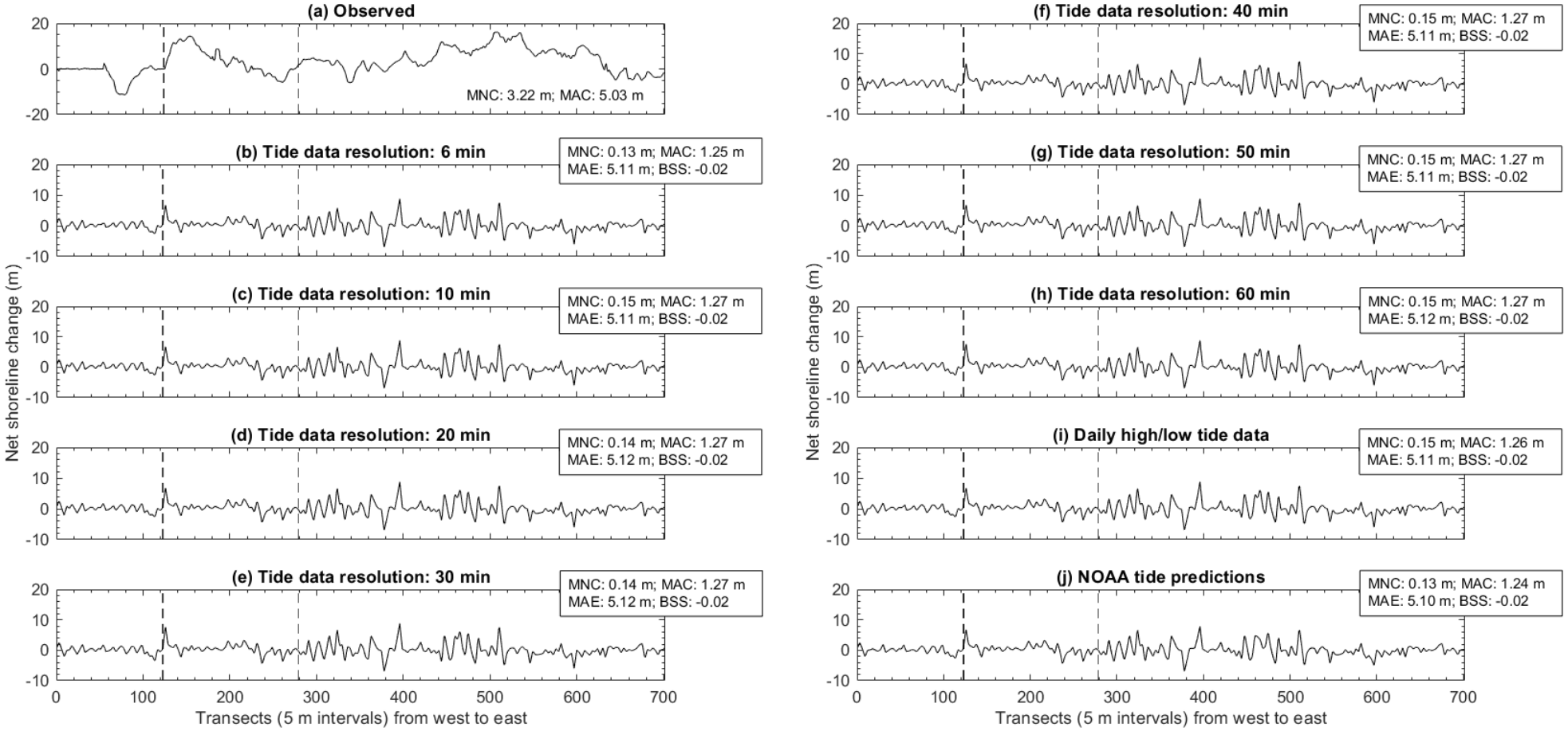

Fig. A3.2 Net shoreline change (10-Oct-2014 to 31-Mar-2016) observed and predicted from MIKE21 in response to tide data resolution in the Puerto Rico test site. Vertical dashed lines indicate groyne locations. MNC is mean net change, MAC is mean absolute change, MAE is mean absolute error, and BSS is Brier Skill Score. Note (a) has a different y axis from (b) to (j). Net shoreline change observed and predicted in groyne transects are excluded from the above plots and statistics.

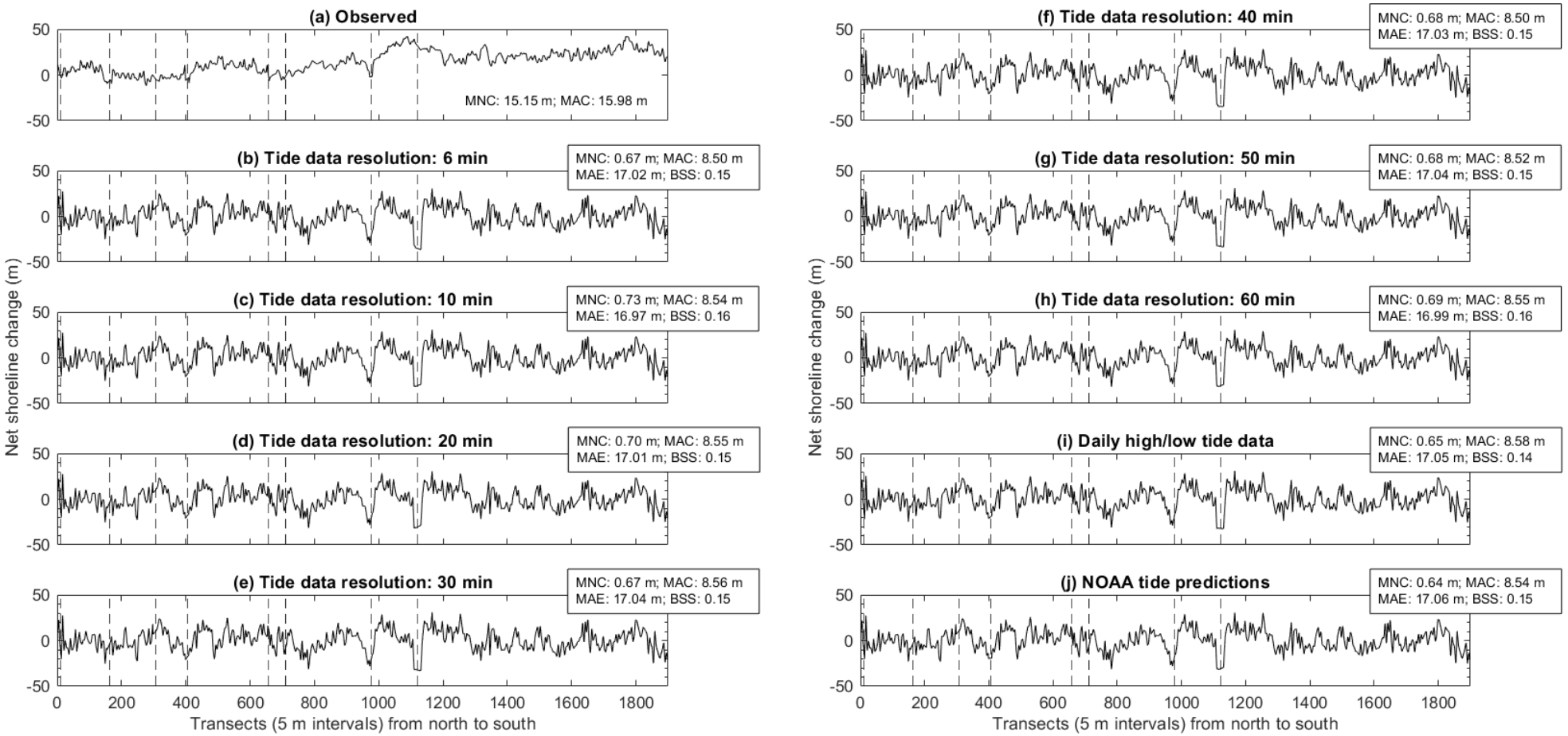

Fig. A3.3 Net shoreline change (01-Jan-2009 to 02-Aug-2011) observed and predicted from MIKE21 in response to tide data resolution in the Southern California test site. Vertical dashed lines indicate groyne locations. MNC is mean net change, MAC is mean absolute change, MAE is mean absolute error, and BSS is Brier Skill Score. Net shoreline change observed and predicted in groyne transects are excluded from the above plots and statistics.

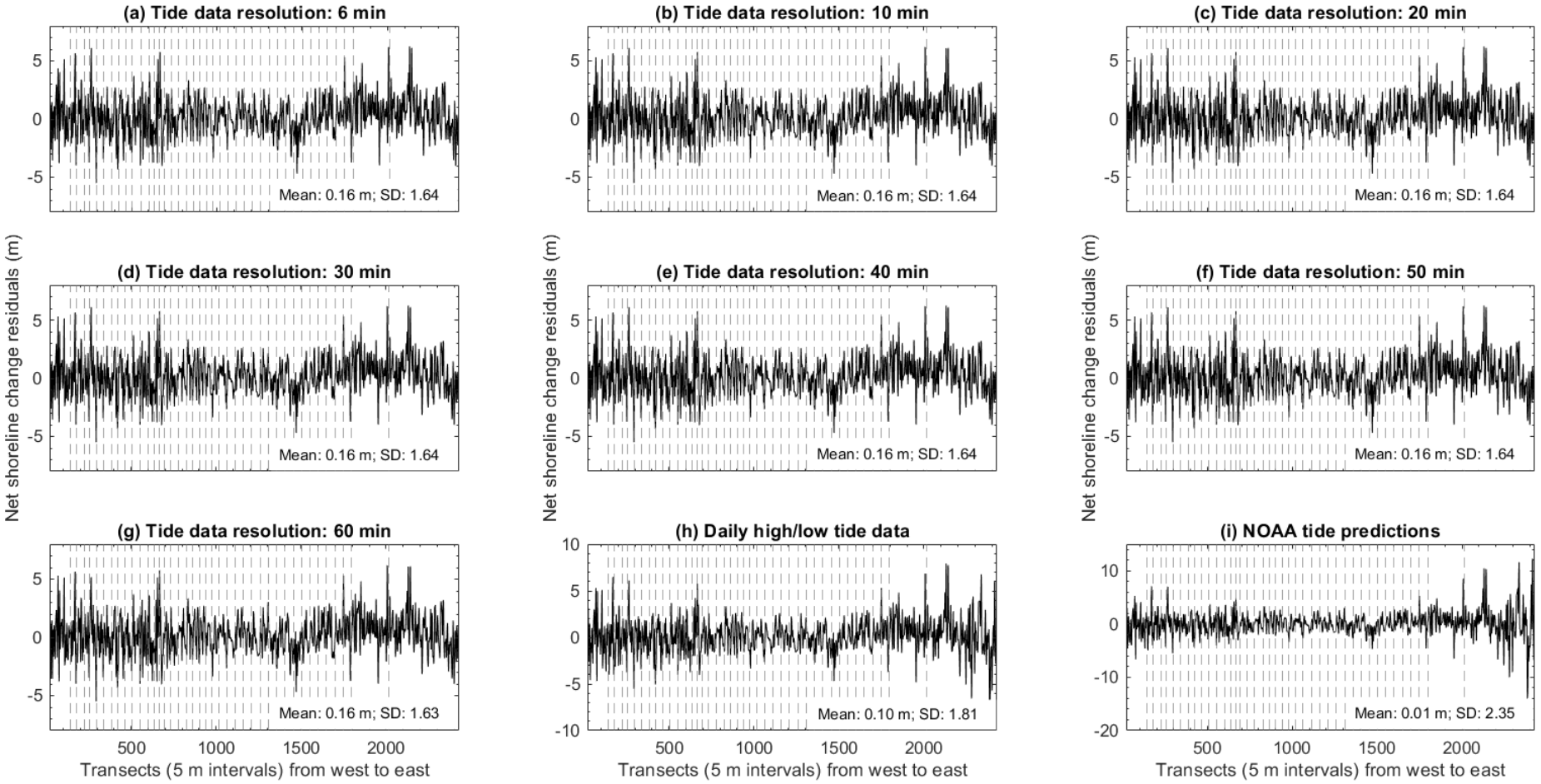

Fig. A3.4 MIKE21 net shoreline change residuals from variations in tide data resolution in the New York test site. Vertical dashed lines indicate groyne locations. SD is the standard deviation. Net shoreline change residuals in (a) to (i) are the difference between net shoreline change observed and predicted from 01-Jan-2014 to 01-Feb-2016. Note the difference in y axis in (h) and (i). Net shoreline change residuals obtained in groyne transects are excluded from the above plots and statistics.

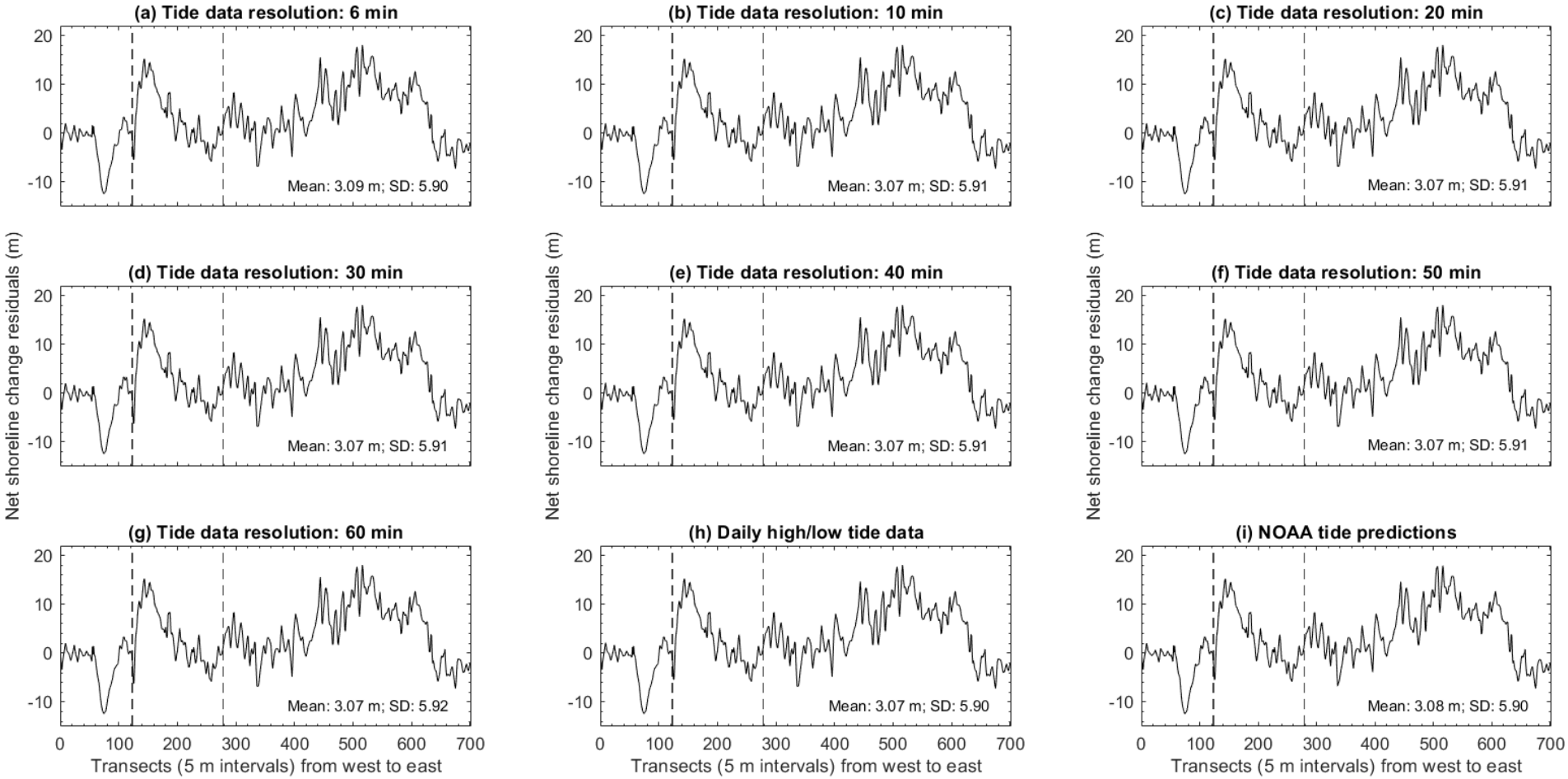

Fig. A3.5 MIKE21 net shoreline change residuals from variations in tide data resolution in the Puerto Rico test site. Vertical dashed lines indicate groyne locations. SD is the standard deviation. Net shoreline change residuals in (a) to (i) are the difference between net shoreline change observed and predicted from 10-Oct-2014 to 31-Mar-2016. Net shoreline change residuals obtained in groyne transects are excluded from the above plots and statistics.

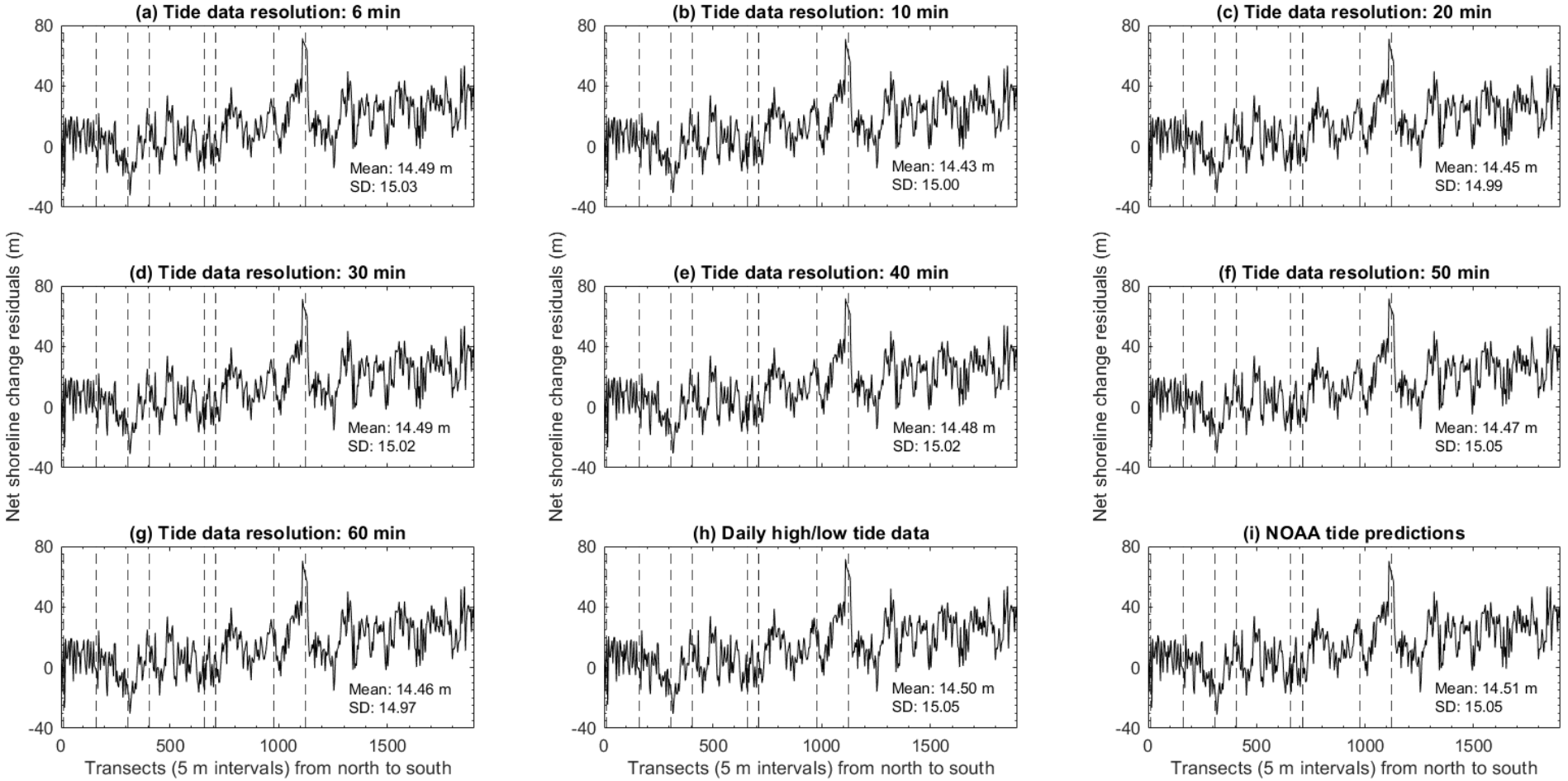

Fig. A3.6 MIKE21 net shoreline change residuals from variations in tide data resolution in the Southern California test site. Vertical dashed lines indicate groyne locations. SD is the standard deviation. Net shoreline change residuals in (a) to (i) are the difference between net shoreline change observed and predicted from 01-Jan-2009 to 02-Aug-2011. Net shoreline change residuals obtained in groyne transects are removed from the above plots and statistics.

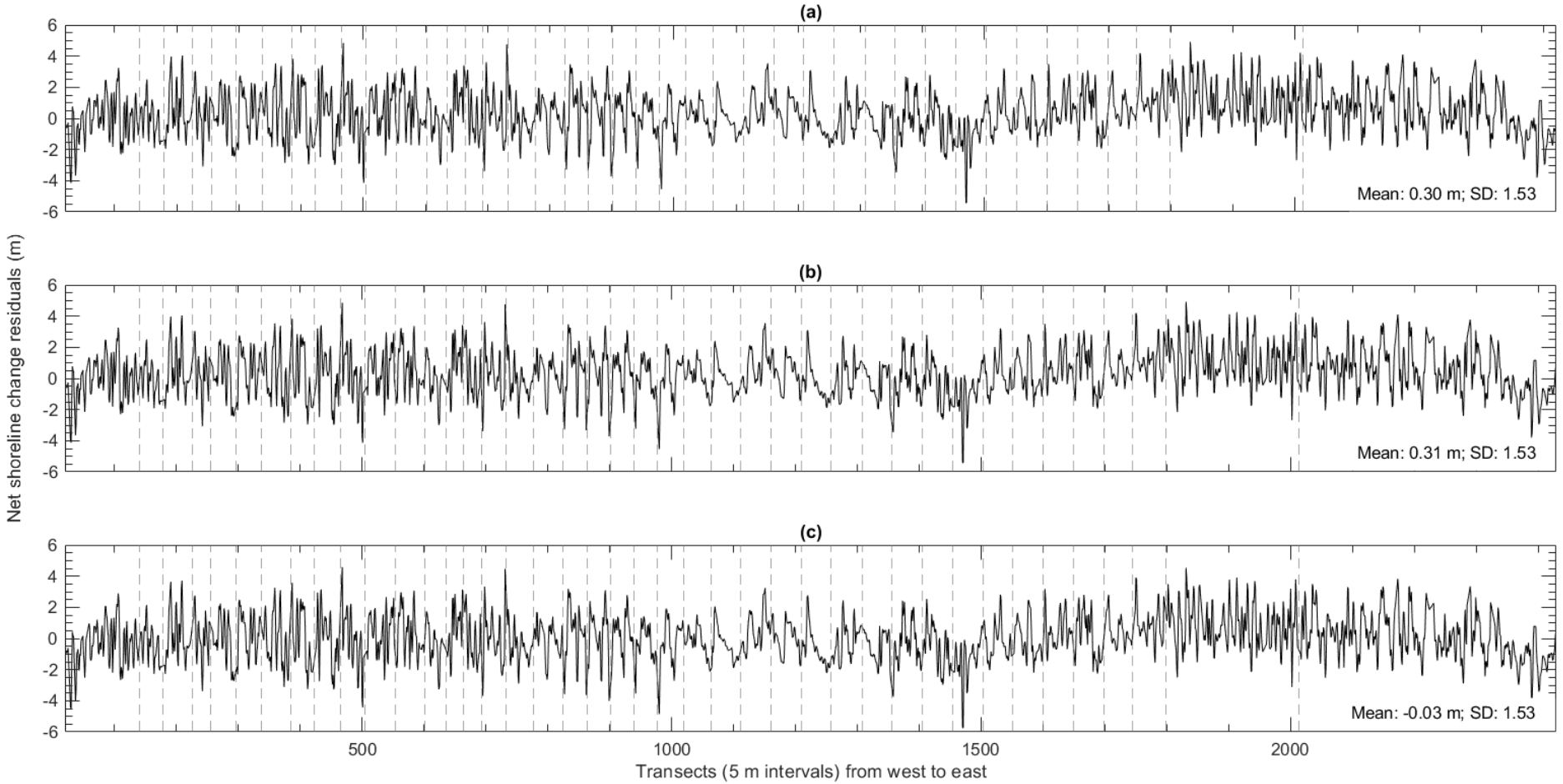

Fig. A3.7 The Bruun Rule net shoreline change residuals in response to SLR estimations from unadjusted tide data (a), seasonally adjusted tide data (b), and NOAA tide predictions (c) in the New York test site. Vertical dashed lines indicate groyne locations. SD is the standard deviation. Net shoreline change residuals in (a) to (c) are the difference between net shoreline change observed and predicted from 01-Jan-2014 to 01-Feb-2016. Net shoreline change residuals obtained in groyne transects are removed from the above plots and statistics.

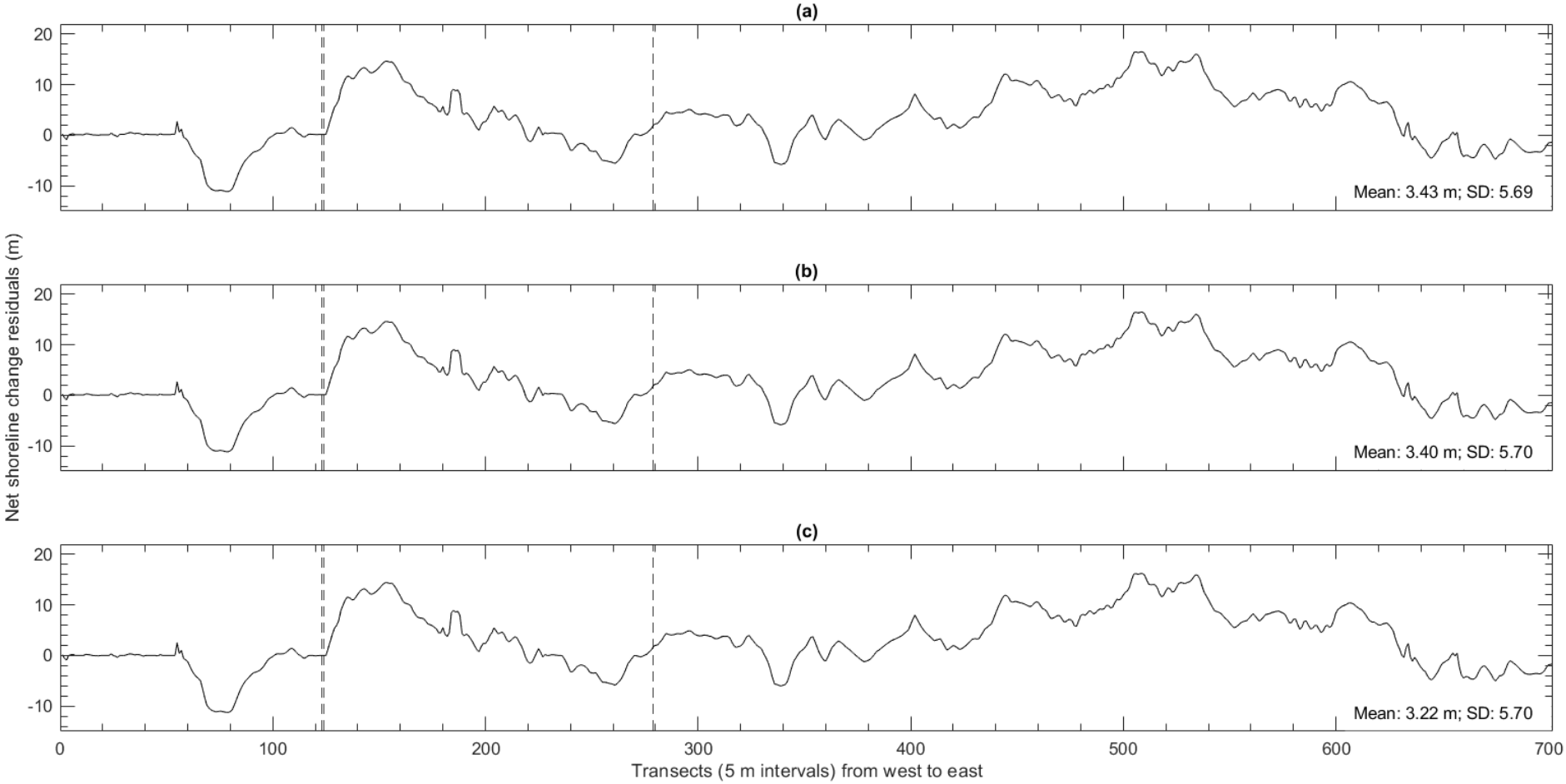

Fig. A3.8 The Bruun Rule net shoreline change residuals in response to SLR estimations from unadjusted tide data (a), seasonally adjusted tide data (b), and NOAA tide predictions (c) in the Puerto Rico test site. Vertical dashed lines indicate groyne locations. SD is the standard deviation. Net shoreline change residuals in (a) to (c) are the difference between net shoreline change observed and predicted from 10-Oct-2014 to 31-Mar-2016. Net shoreline change residuals obtained in groyne transects are removed from the above plots and statistics.

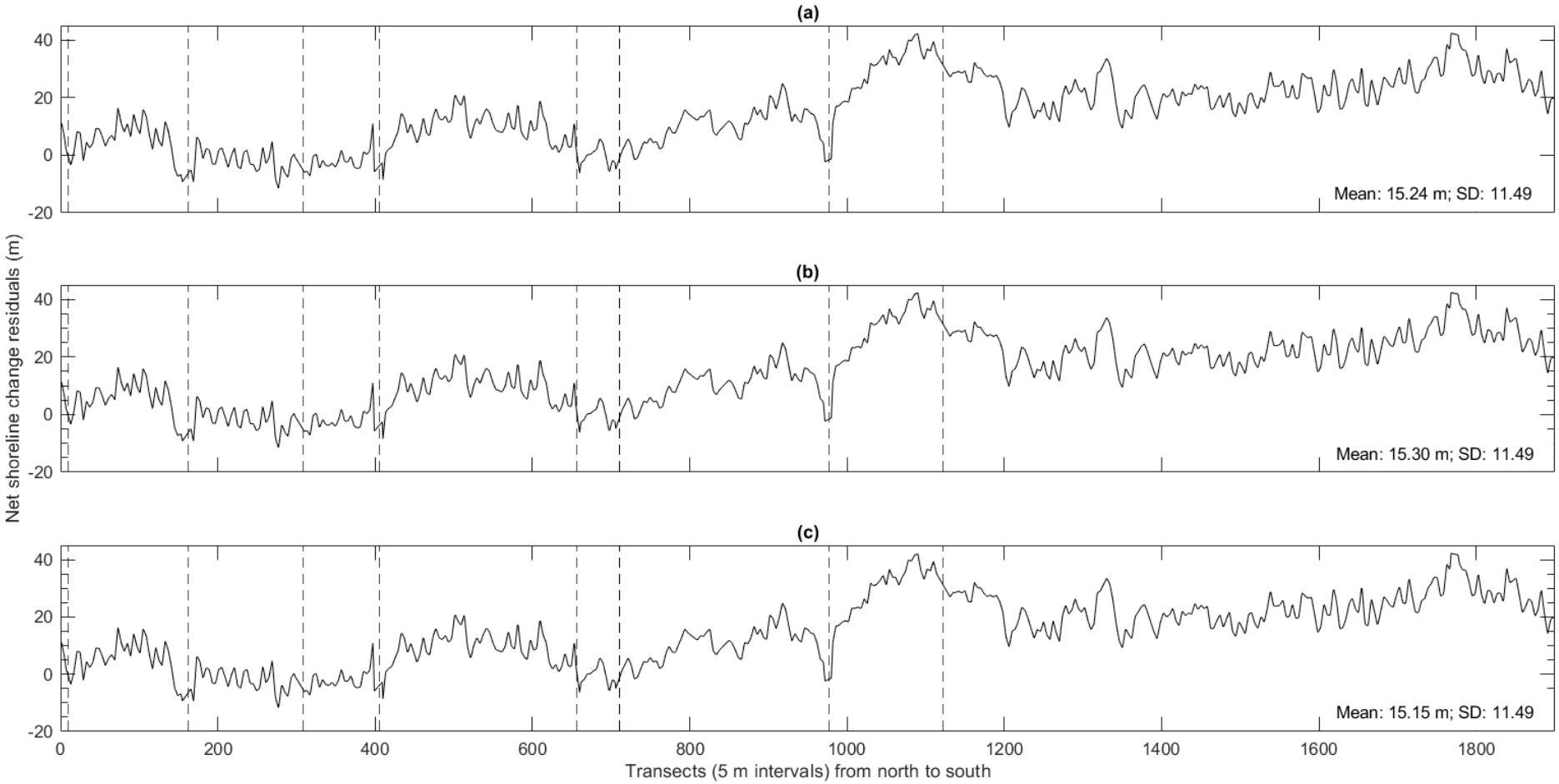

Fig. A3.9 The Bruun Rule net shoreline change residuals in response to SLR estimations from unadjusted tide data (a), seasonally adjusted tide data (b), and NOAA tide predictions (c) in the Southern California test site. Vertical dashed lines indicate groyne locations. SD is the standard deviation. Net shoreline change residuals in (a) to (c) are the difference between net shoreline change observed and predicted from 01-Jan-2009 to 02-Aug-2011. Net shoreline change residuals obtained in groyne transects are excluded from the above plots and statistics.

A4 MIKE21 sensitivity to wind data temporal resolution

A4 graphically illustrates the sensitivity of MIKE21 net littoral drift and net shoreline change predictions to coarsening wind time series data in each test site.

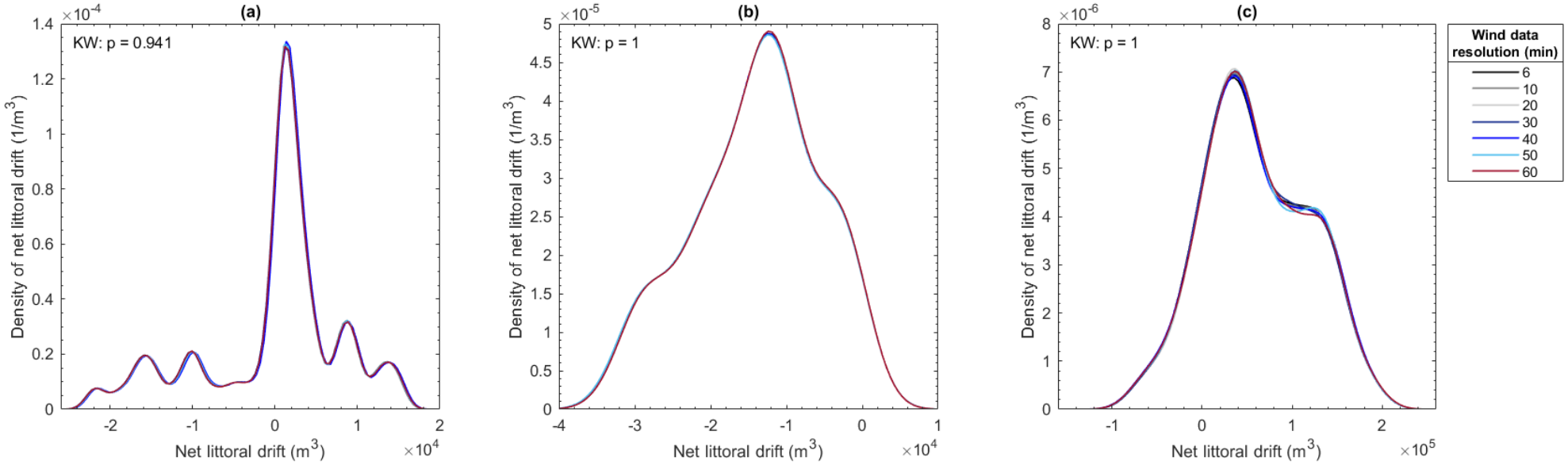

Fig. A4.1 Kernel density plots of net littoral drift predictions in response to coarsening wind data resolution in the New York (a), Puerto Rico (b), and Southern California (c) test site. Net littoral drift predictions in Fig. A4.1 are from 01-Jan-2014 to 01-Feb-2016 in the New York test site, 10-Oct-2014 to 31-Mar-2016 in the Puerto Rico test site, and 01-Jan-2009 to 02-Aug-2011 in the Southern California test site. The Kruskal-Wallis (KW) test indicates no significant differences in net littoral drift predictions from coarsening wind data in each test site.

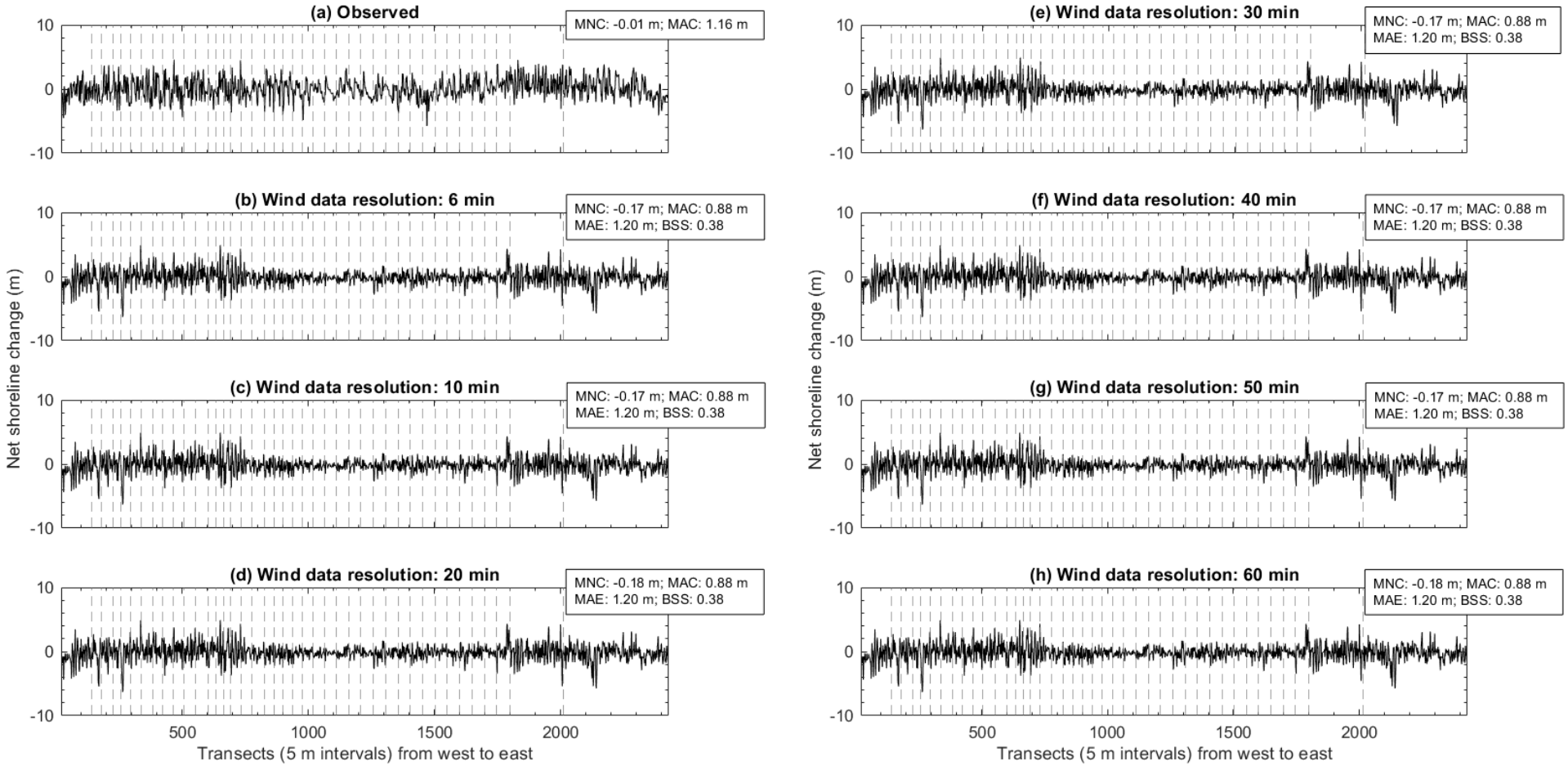

Fig. A4.2 Net shoreline change (01-Jan-2014 to 01-Feb-2016) observed and predicted in response to coarsening wind data in the New York test site. Vertical dashed lines indicate groyne locations. MNC is mean net change, MAC is mean absolute change, MAE is mean absolute error, and BSS is Brier Skill Score. Net shoreline change observed and predicted in groyne transects are excluded from the above plots and statistics.

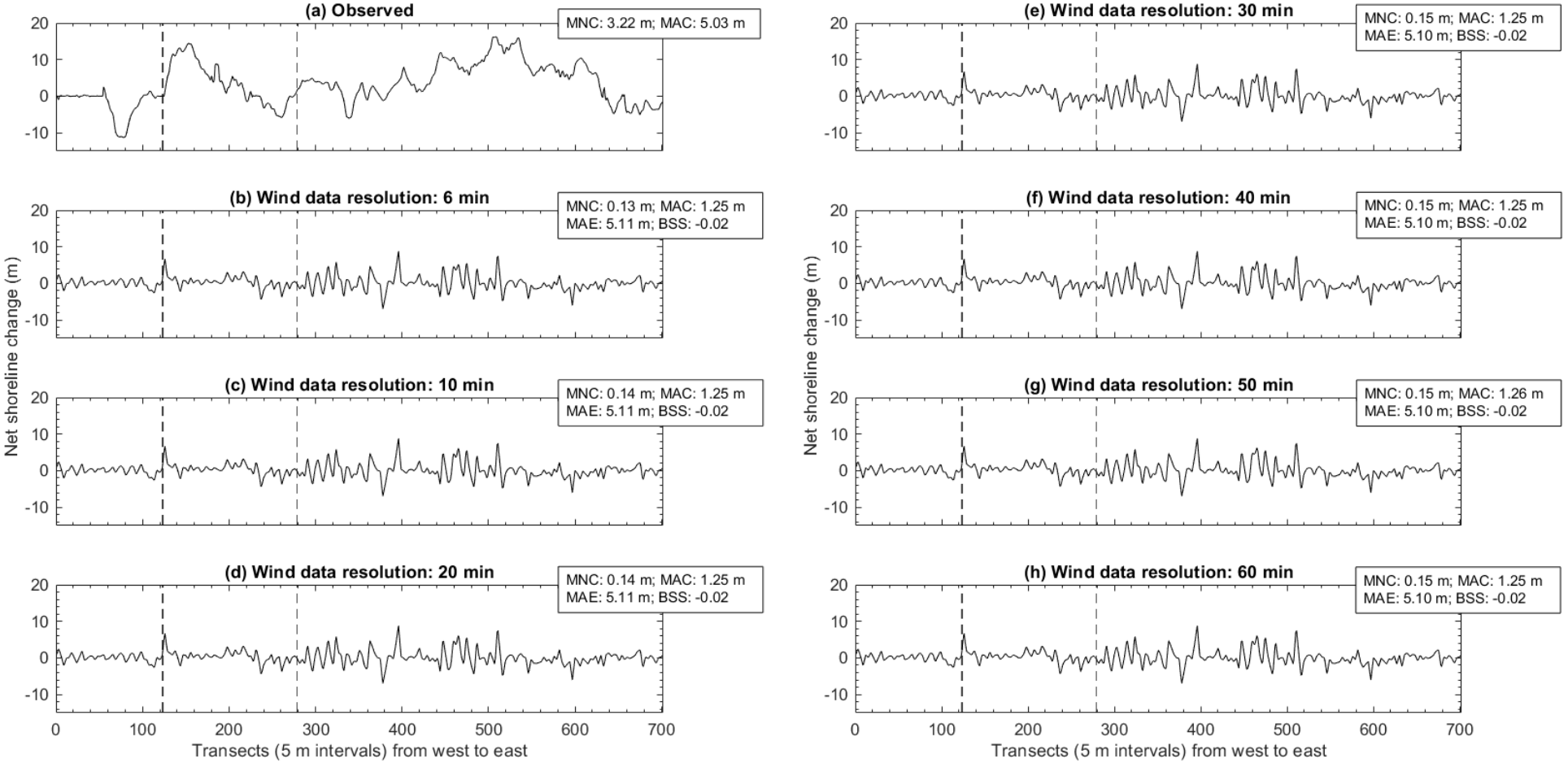

Fig. A4.3 Net shoreline change (10-Oct-2014 to 31-Mar-2016) observed and predicted in response to coarsening wind data in the Puerto Rico test site. Vertical dashed lines indicate groyne locations. MNC is mean net change, MAC is mean absolute change, MAE is mean absolute error, and BSS is Brier Skill Score. Net shoreline change observed and predicted in groyne transects are excluded from the above plots and statistics.

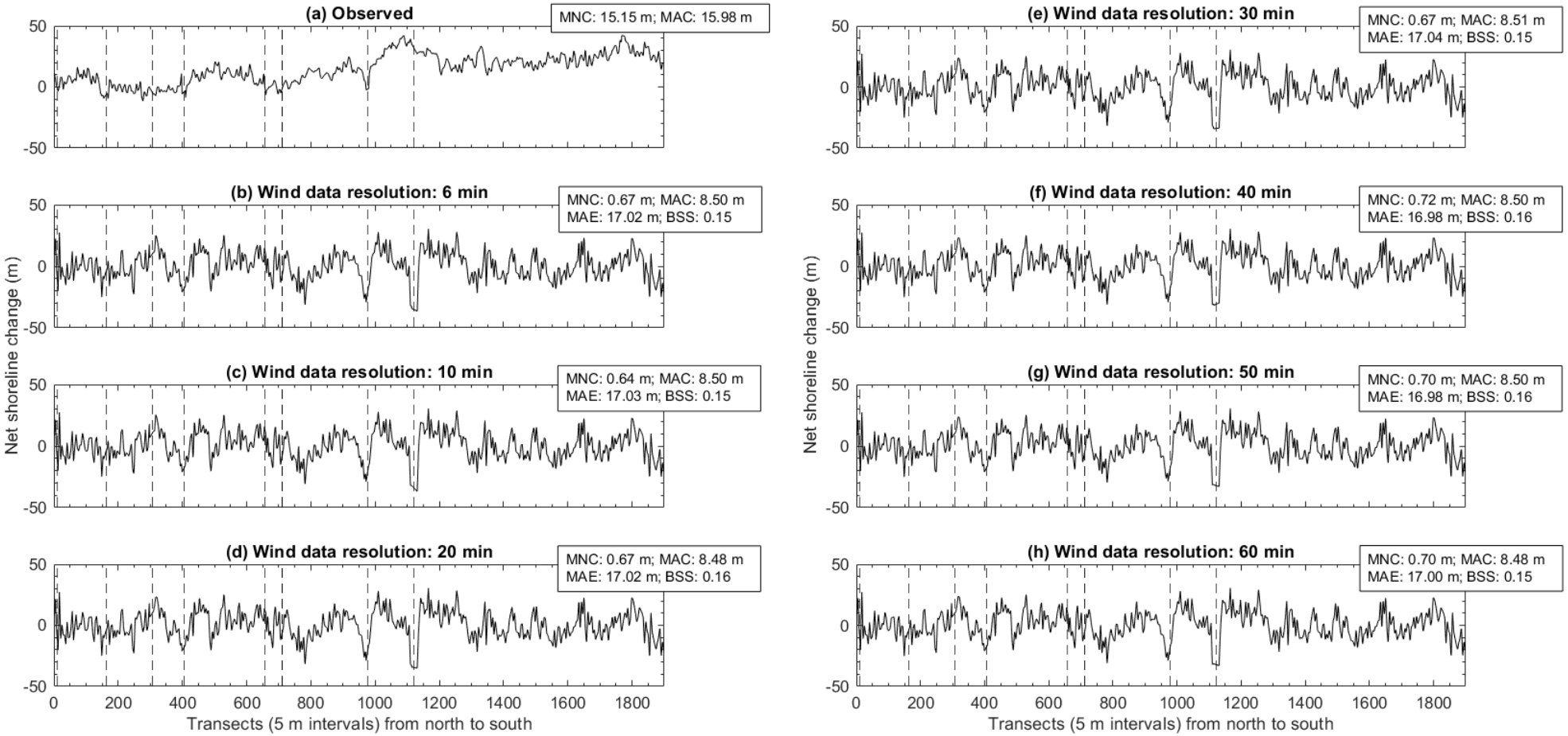

Fig. A4.4 Net shoreline change (01-Jan-2009 to 02-Aug-2011) observed and predicted in response to coarsening wind data in the Southern California test site. Vertical dashed lines indicate groyne locations. MNC is mean net change, MAC is mean absolute change, MAE is mean absolute error, and BSS is Brier Skill Score. Net shoreline change observed and predicted in groyne transects are excluded from the above plots and statistics.

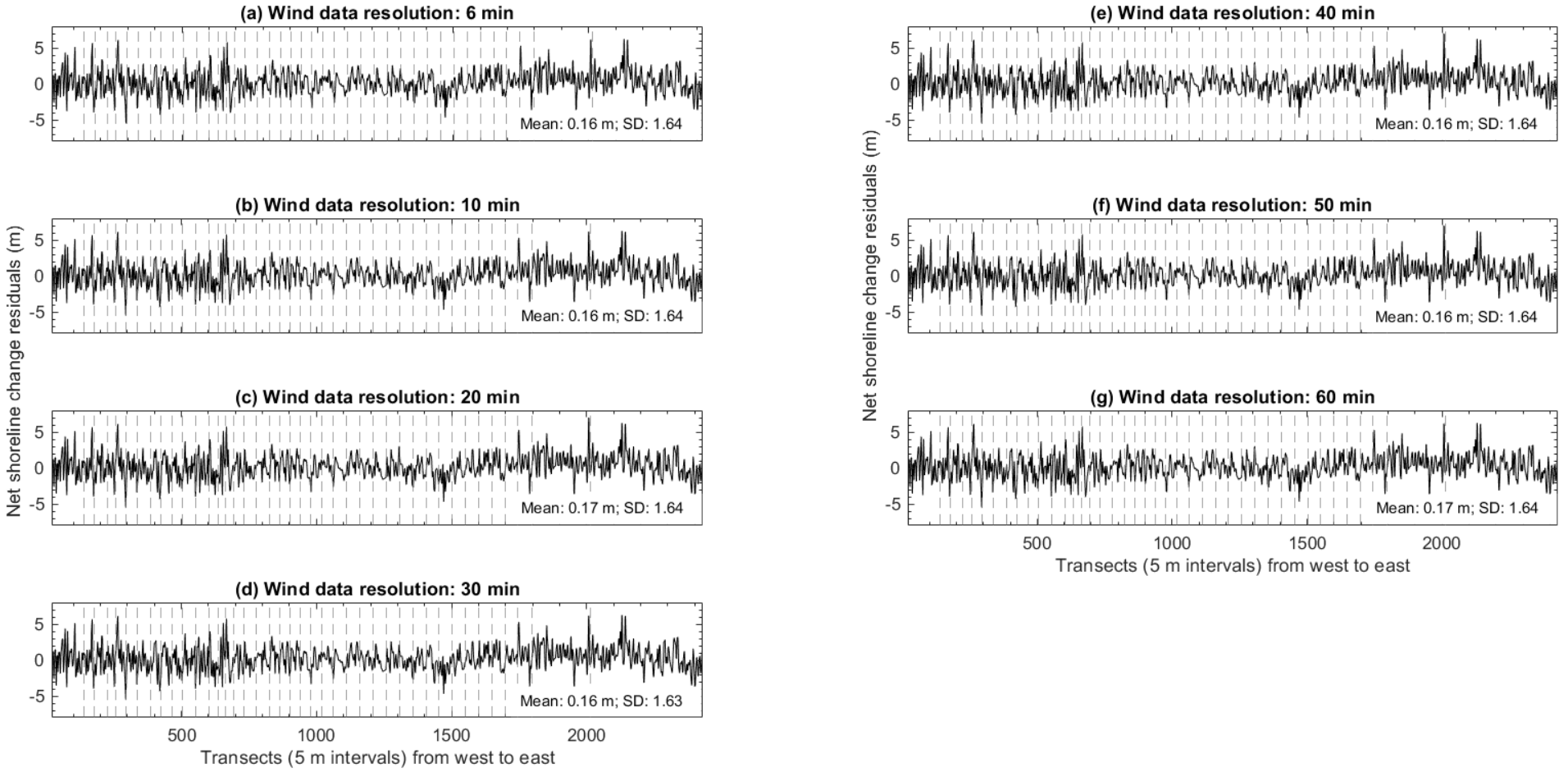

Fig. A4.5 Net shoreline change residuals from coarsening wind data in the New York test site. Vertical dashed lines indicate groyne locations. SD is the standard deviation. Net shoreline change residuals in (a) to (g) are the difference between net shoreline change observed and predicted from 01-Jan-2014 to 01-Feb-2016. Net shoreline change residuals obtained in groyne transects are excluded from the above plots and statistics.

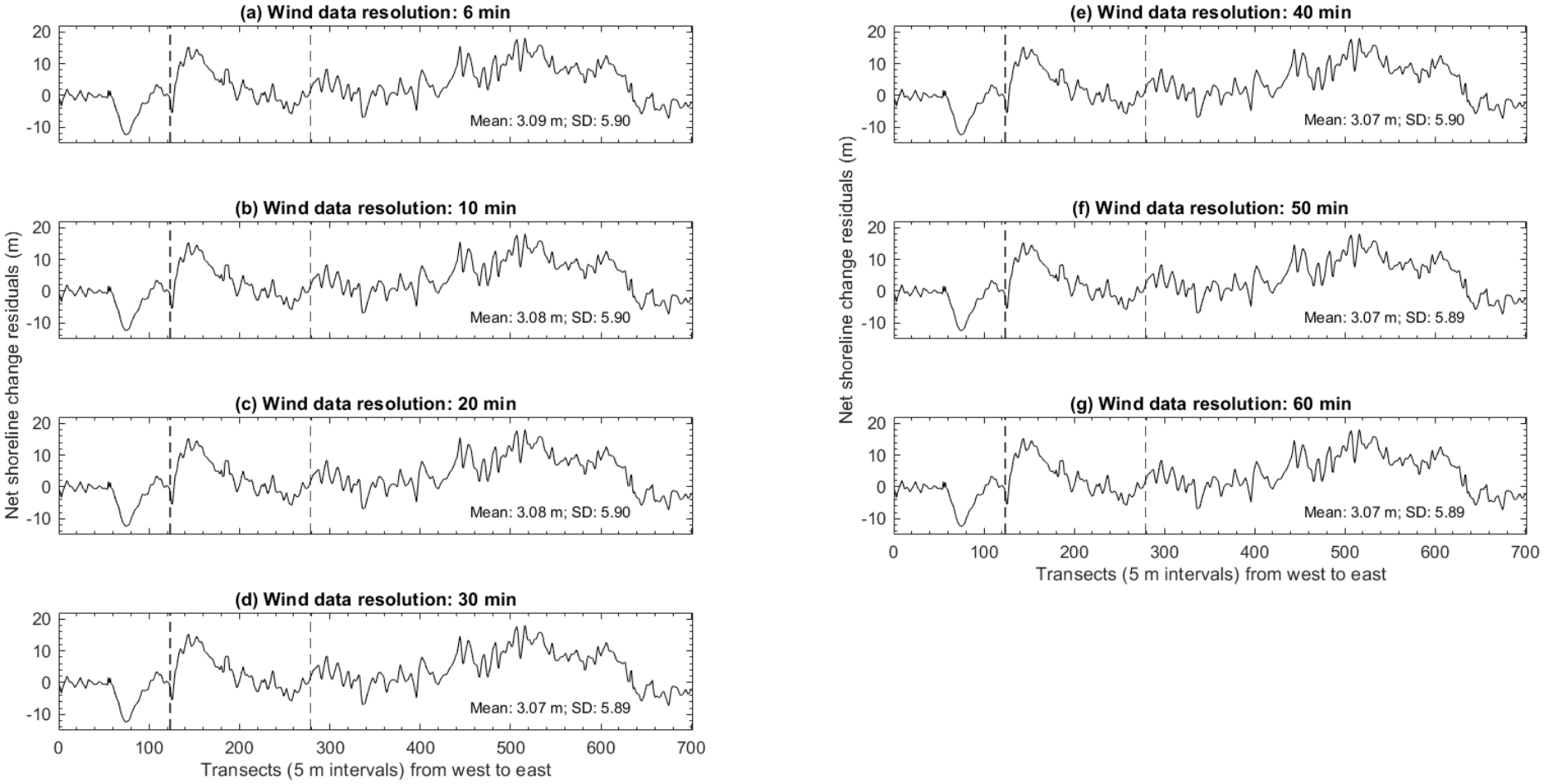

Fig. A4.6 Net shoreline change residuals from coarsening wind data in the Puerto Rico test site. Vertical dashed lines indicate groyne locations. SD is the standard deviation. Net shoreline change residuals in (a) to (g) are the difference between net shoreline change observed and predicted from 10-Oct-2014 to 31-Mar-2016. Net shoreline change residuals obtained in groyne transects are excluded from the above plots and statistics.

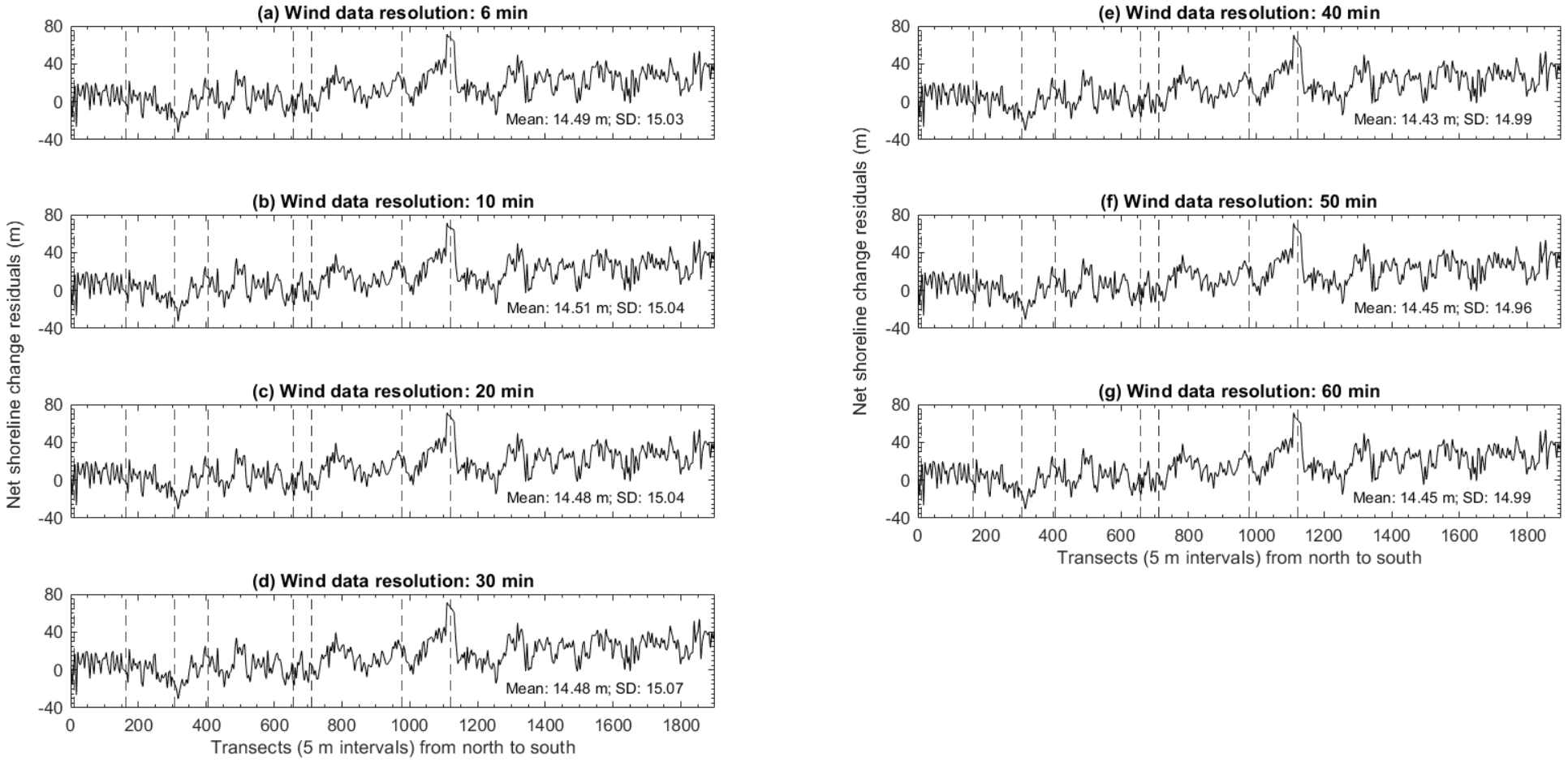

Fig. A4.7 Net shoreline change residuals from coarsening wind data in the Southern California test site. Vertical dashed lines indicate groyne locations. SD is the standard deviation. Net shoreline change residuals in (a) to (g) are the difference between net shoreline change observed and predicted from 01-Jan-2009 to 02-Aug-2011. Net shoreline change residuals obtained in groyne transects are excluded from the above plots and statistics.

A5 MIKE21 sensitivity to wave climate data temporal resolution

A5 graphically illustrates the sensitivity of MIKE21 net littoral drift and net shoreline change predictions to coarsening wave climate data in each test site.

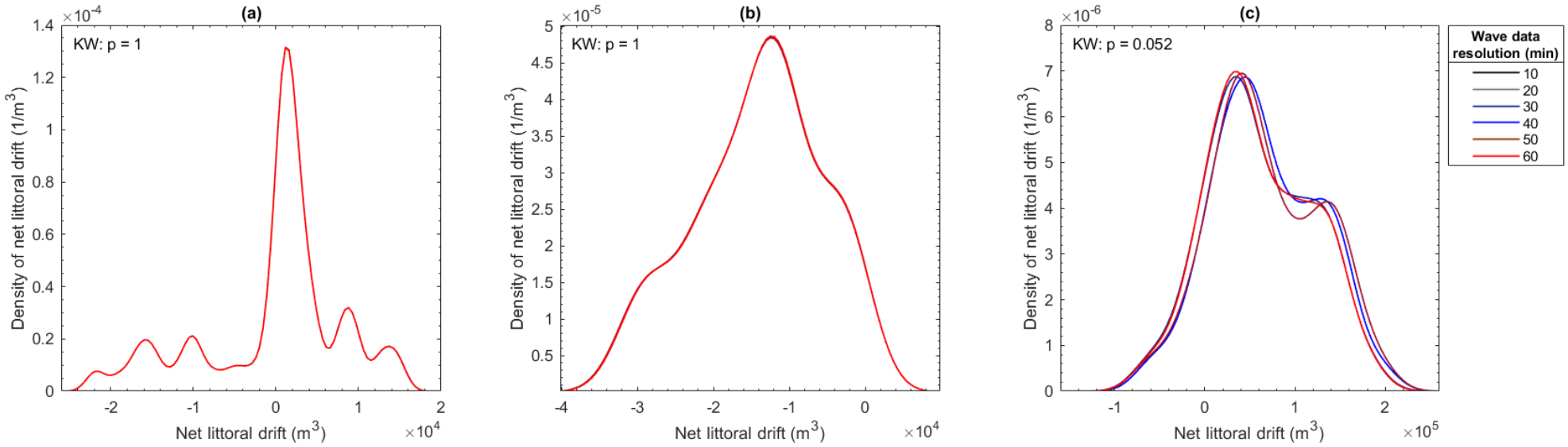

Fig. A5.1 Kernel density plots of net littoral drift predictions in response to coarsening wave climate data resolution in the New York (a), Puerto Rico (b), and Southern California (c) test site. In Fig. A5.1, net littoral drift predictions are from 01-Jan-2014 to 01-Feb-2016 in the New York test site, 10-Oct-2014 to 31-Mar-2016 in the Puerto Rico test site, and 01-Jan-2009 to 02-Aug-2011 in the Southern California test site. The Kruskal-Wallis (KW) test indicates no significant differences in net littoral drift predictions from coarsening wave climate data in each test site.

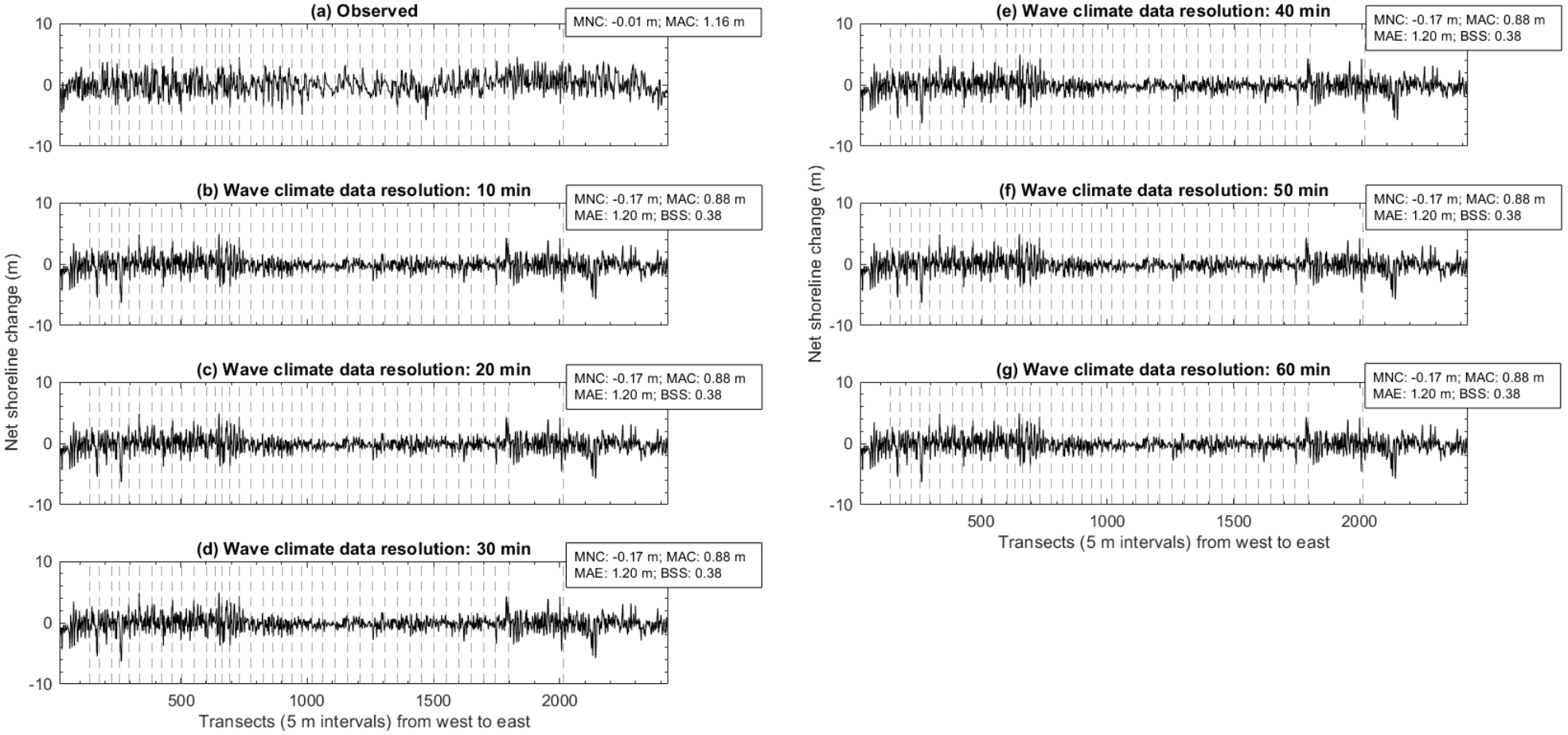

Fig. A5.2 Net shoreline change (01-Jan-2014 to 01-Feb-2016) observed and predicted in response to coarsening wave climate data in the New York test site. Vertical dashed lines indicate groyne locations. MNC is mean net change, MAC is mean absolute change, MAE is mean absolute error, and BSS is Brier Skill Score. Net shoreline change observed and predicted in groyne transects are excluded from the above plots and statistics.

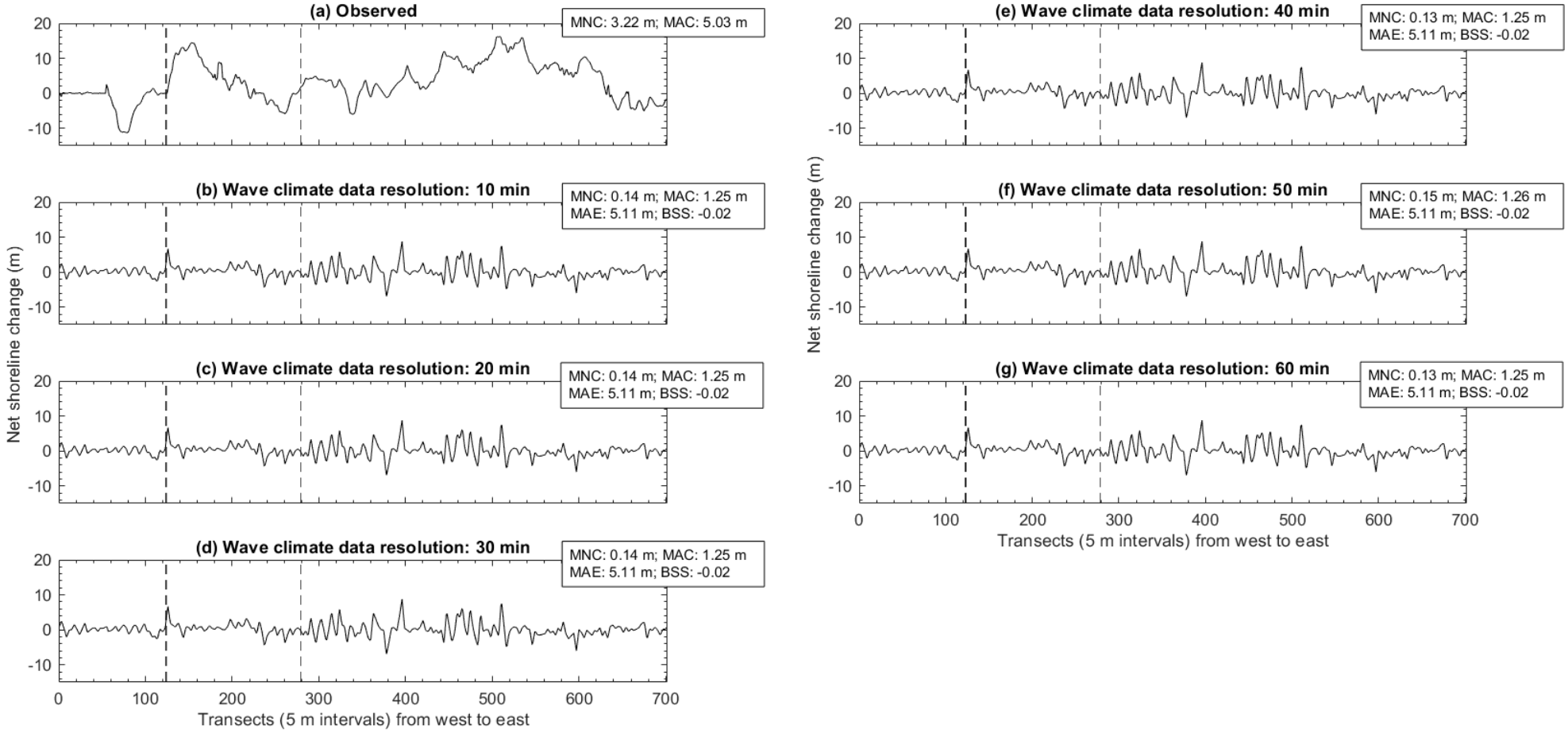

Fig. A5.3 Net shoreline change (10-Oct-2014 to 31-Mar-2016) observed and predicted in response to coarsening wave climate data in the Puerto Rico test site. Vertical dashed lines indicate groyne locations. MNC is mean net change, MAC is mean absolute change, MAE is mean absolute error, and BSS is Brier Skill Score. Net shoreline change observed and predicted in groyne transects are excluded from the above plots and statistics.

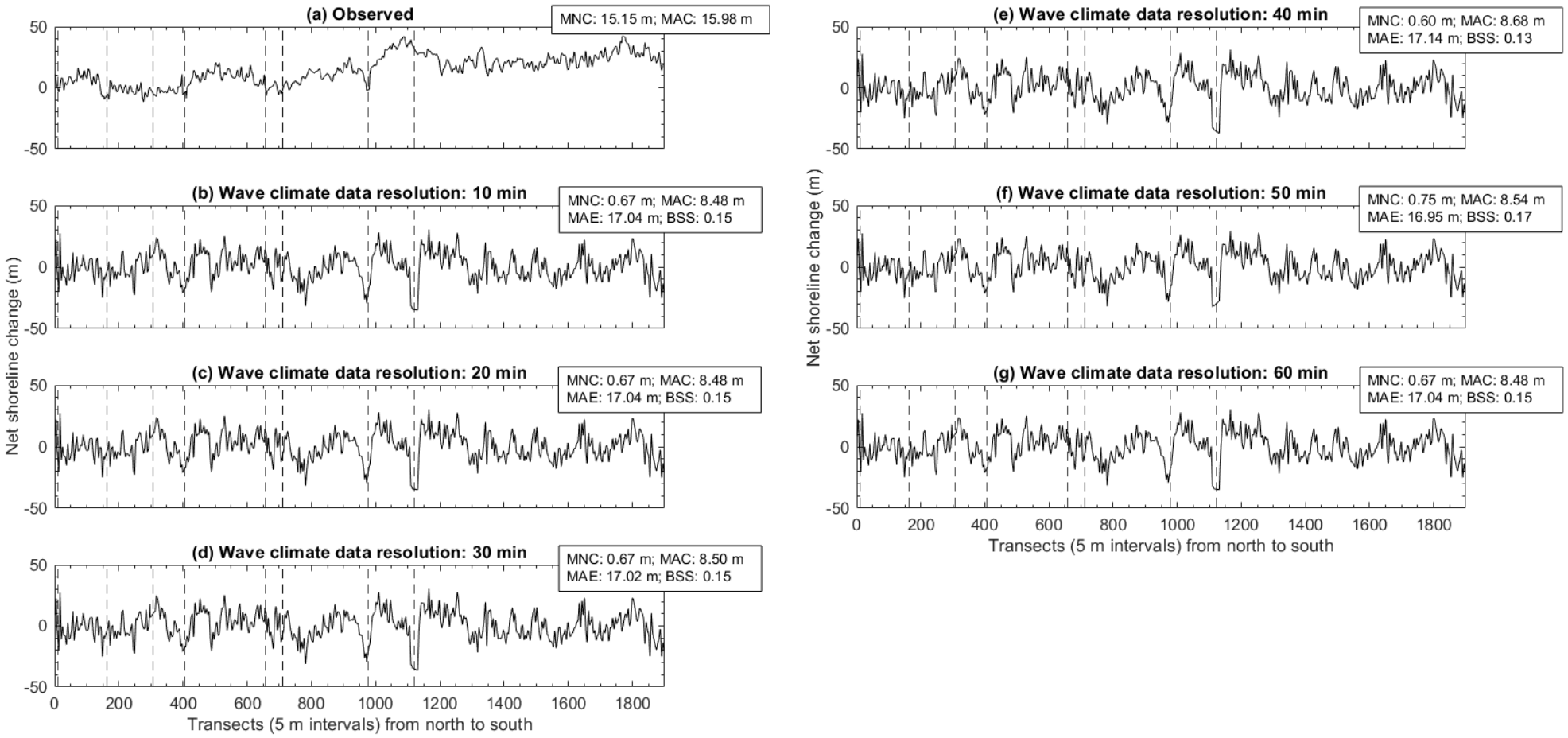

Fig. A5.4 Net shoreline change (01-Jan-2009 to 02-Aug-2011) observed and predicted in response to coarsening wave climate data in the Southern California test site. Vertical dashed lines indicate groyne locations. MNC is mean net change, MAC is mean absolute change, MAE is mean absolute error, and BSS is Brier Skill Score. Net shoreline change observed and predicted in groyne transects are excluded from the above plots and statistics.

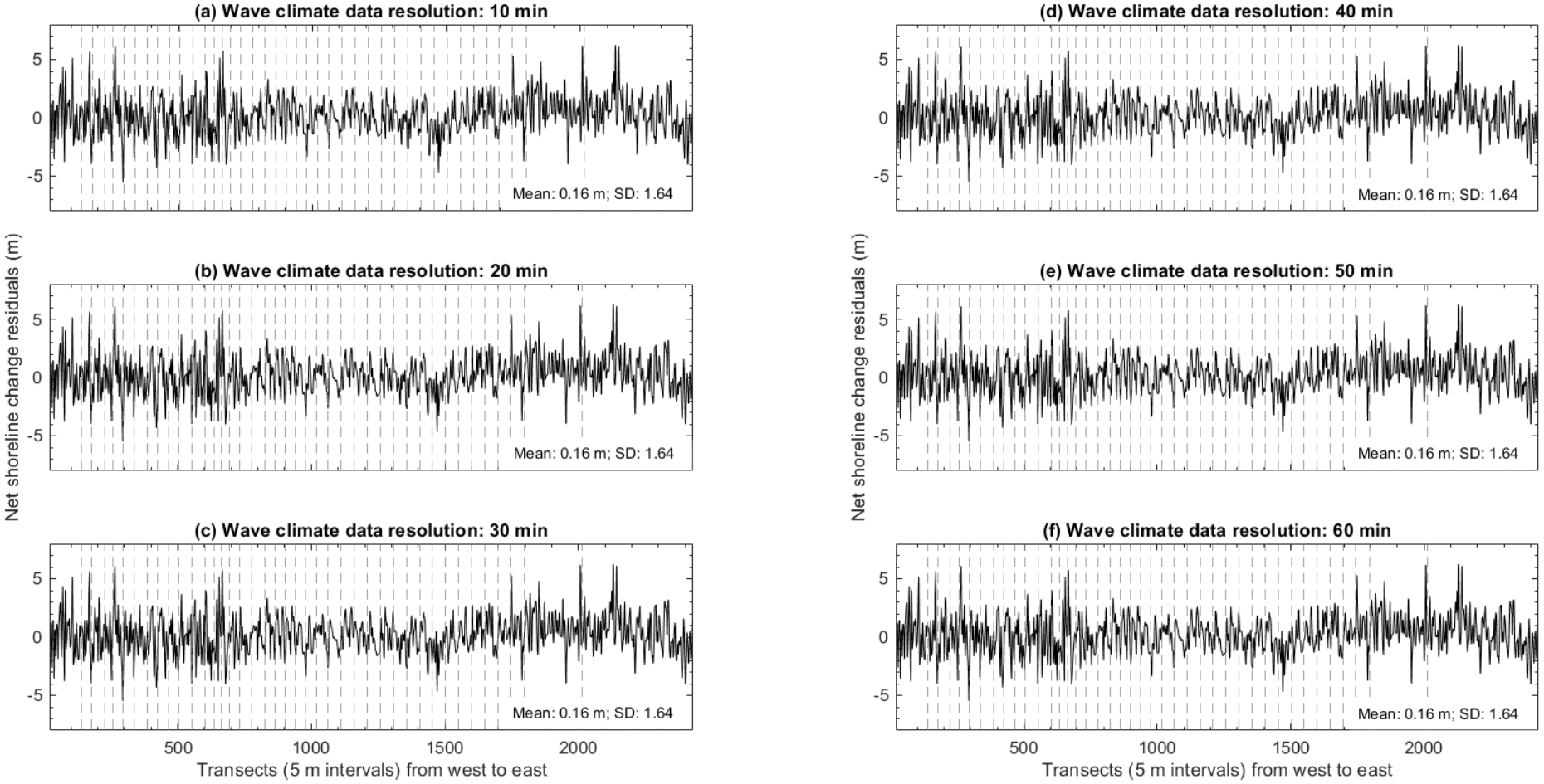

Fig. A5.5 Net shoreline change residuals from coarsening wave climate data in the New York test site. Vertical dashed lines indicate groyne locations. SD is the standard deviation. Net shoreline change residuals in (a) to (f) are the difference between net shoreline change observed and predicted from 01-Jan-2014 to 01-Feb-2016. Net shoreline change residuals obtained in groyne transects are excluded from the above plots and statistics.

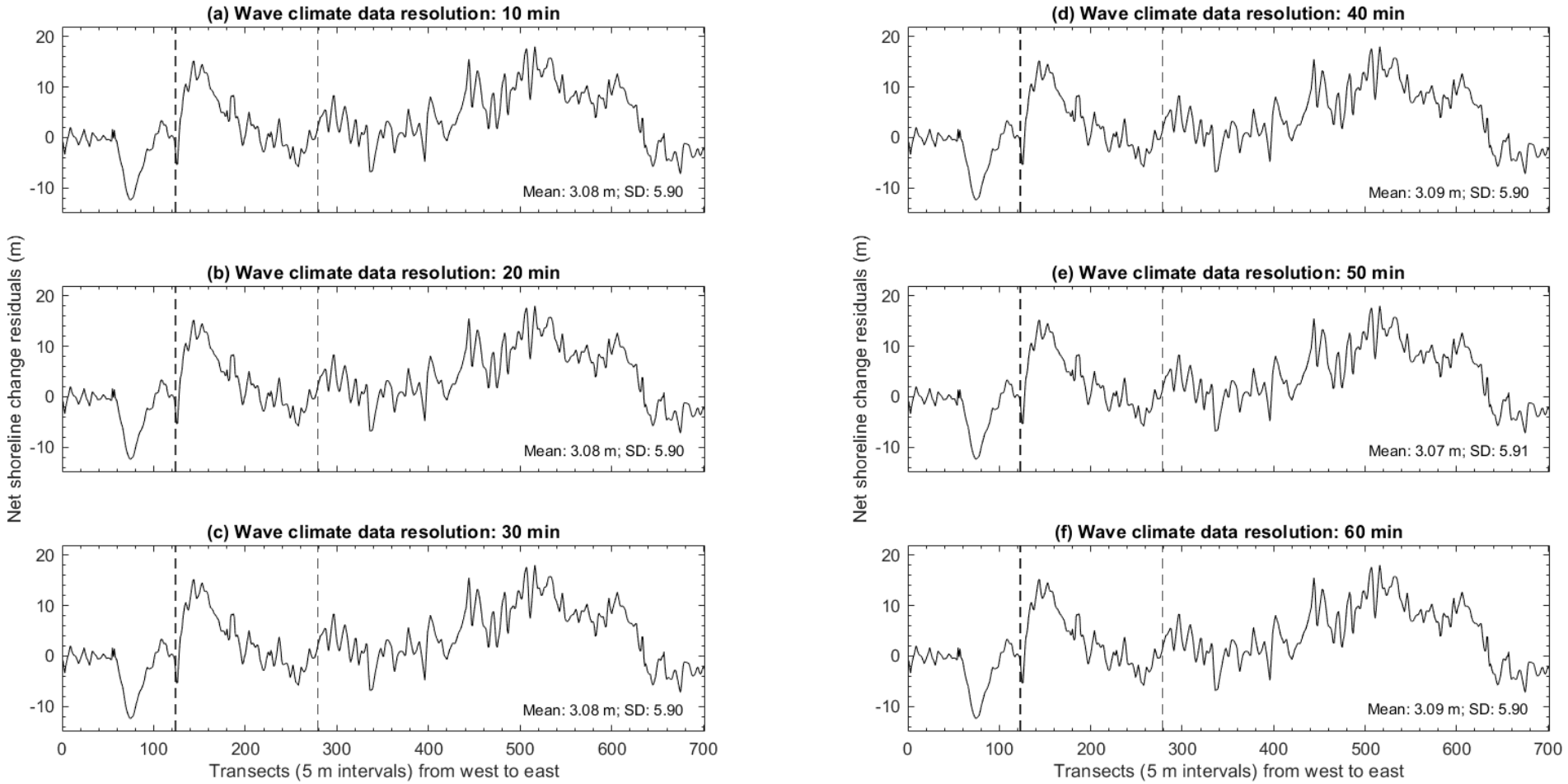

Fig. A5.6 Net shoreline change residuals from coarsening wave climate data in the Puerto Rico test site. Vertical dashed lines indicate groyne locations. SD is the standard deviation. Net shoreline change residuals in (a) to (f) are the difference between net shoreline change observed and predicted from 10-Oct-2014 to 31-Mar-2016. Net shoreline change residuals obtained in groyne transects are excluded from the above plots and statistics.

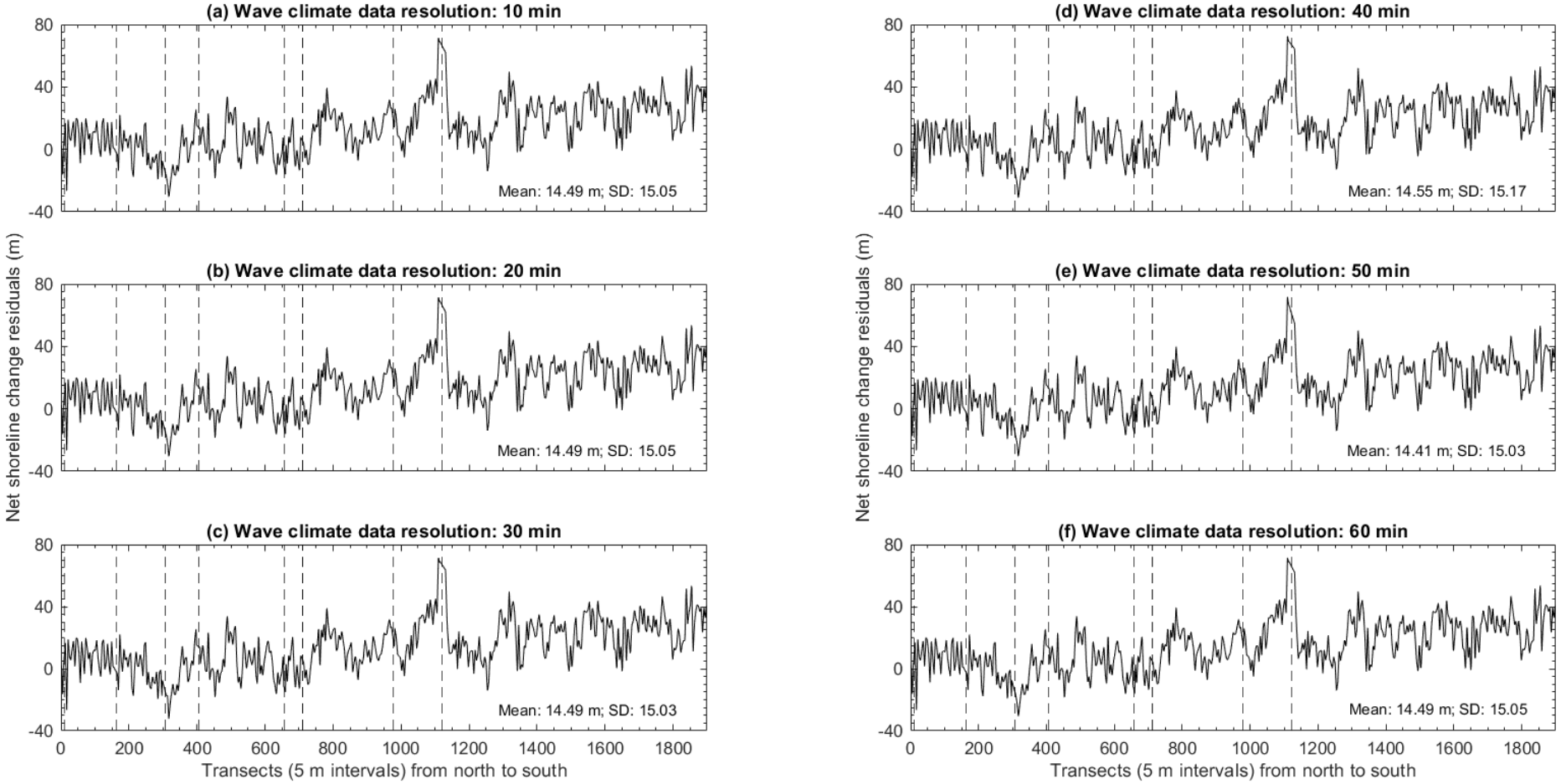

Fig. A5.7 Net shoreline change residuals from coarsening wave climate data in the Southern California test site. Vertical dashed lines indicate groyne locations. SD is the standard deviation. Net shoreline change residuals in (a) to (f) are the difference between net shoreline change observed and predicted from 01-Jan-2009 to 02-Aug-2011. Net shoreline change residuals obtained in groyne transects are excluded from the above plots and statistics.

A6 MIKE21 sensitivity to Manning's n reciprocal ($m^{1/3}/s$)

A6 graphically illustrates the sensitivity of MIKE21 net littoral drift and net shoreline change predictions to increasing Manning's n reciprocals ($m^{1/3}/s$) in each test site.

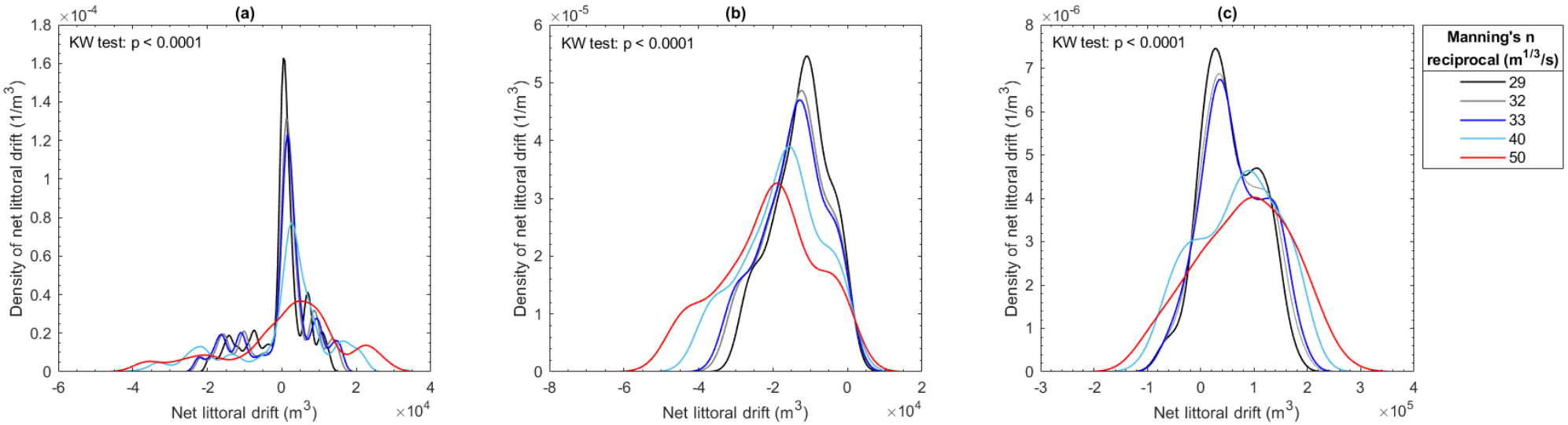

Fig. A6.1 Kernel density plots of net littoral drift predictions in response to increasing Manning's n reciprocals ($m^{1/3}/s$) in the New York (a), Puerto Rico (b), and Southern California (c) test site. In Fig. A6.1, net littoral drift predictions are from 01-Jan-2014 to 01-Feb-2016 in the New York test site, 10-Oct-2014 to 31-Mar-2016 in the Puerto Rico test site, and 01-Jan-2009 to 02-Aug-2011 in the Southern California test site. The Kruskal-Wallis (KW) test indicates that net littoral drift predictions from increasing Manning's n reciprocals ($m^{1/3}/s$) are significantly different in each test site. A post hoc Dunn's test reveals that net littoral drift predictions are significantly different from Manning's n reciprocals > 32 $m^{1/3}/s$ in the New York test site and > 33 $m^{1/3}/s$ in the Puerto Rico and Southern California test sites.

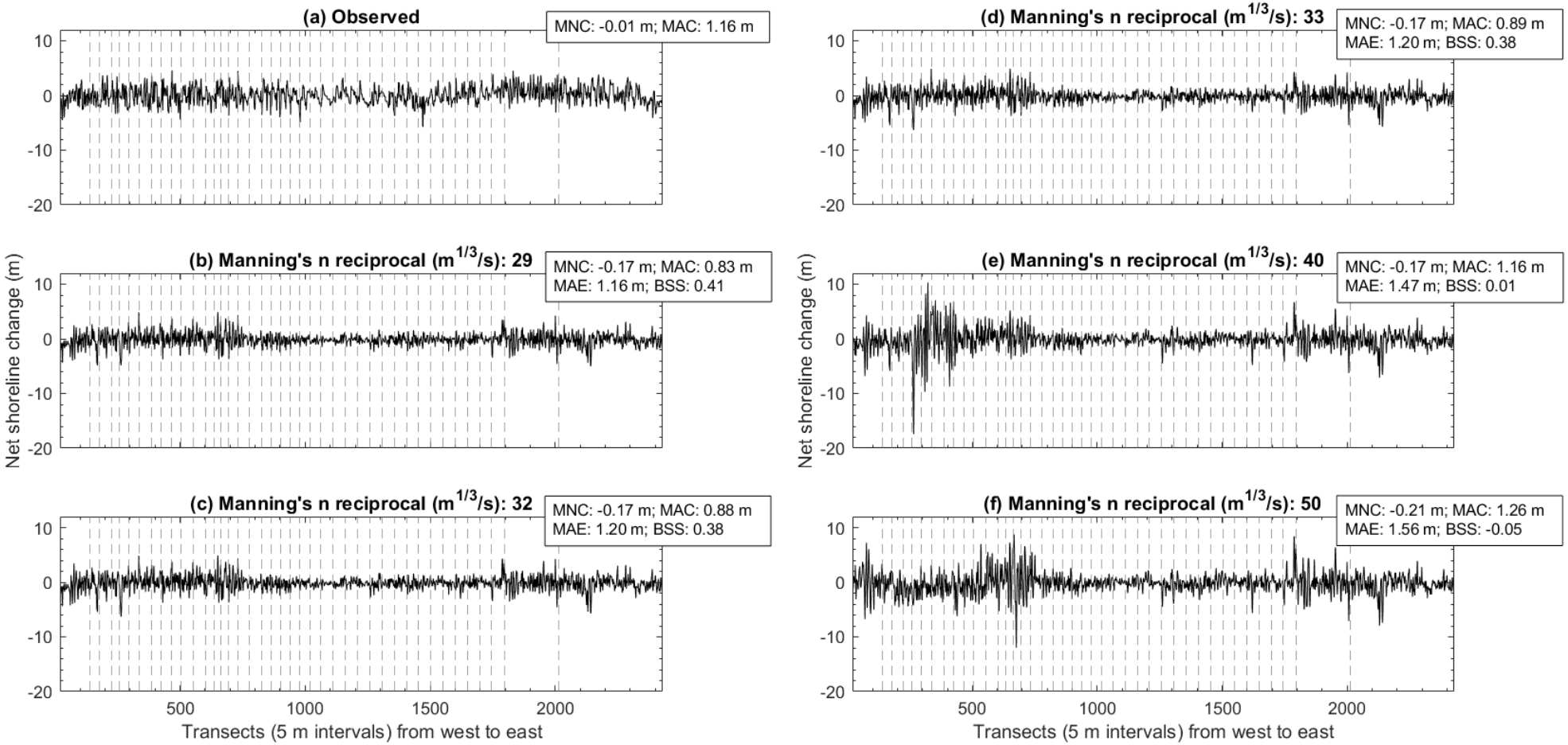

Fig. A6.2 Net shoreline change (01-Jan-2014 to 01-Feb-2016) observed and predicted in response to increasing Manning's n reciprocals ($m^{1/3}/s$) in the New York test site. Vertical dashed lines indicate groyne locations. MNC is mean net change, MAC is mean absolute change, MAE is mean absolute error, and BSS is Brier Skill Score. Net shoreline change observed and predicted in groyne transects are excluded from the above plots and statistics.

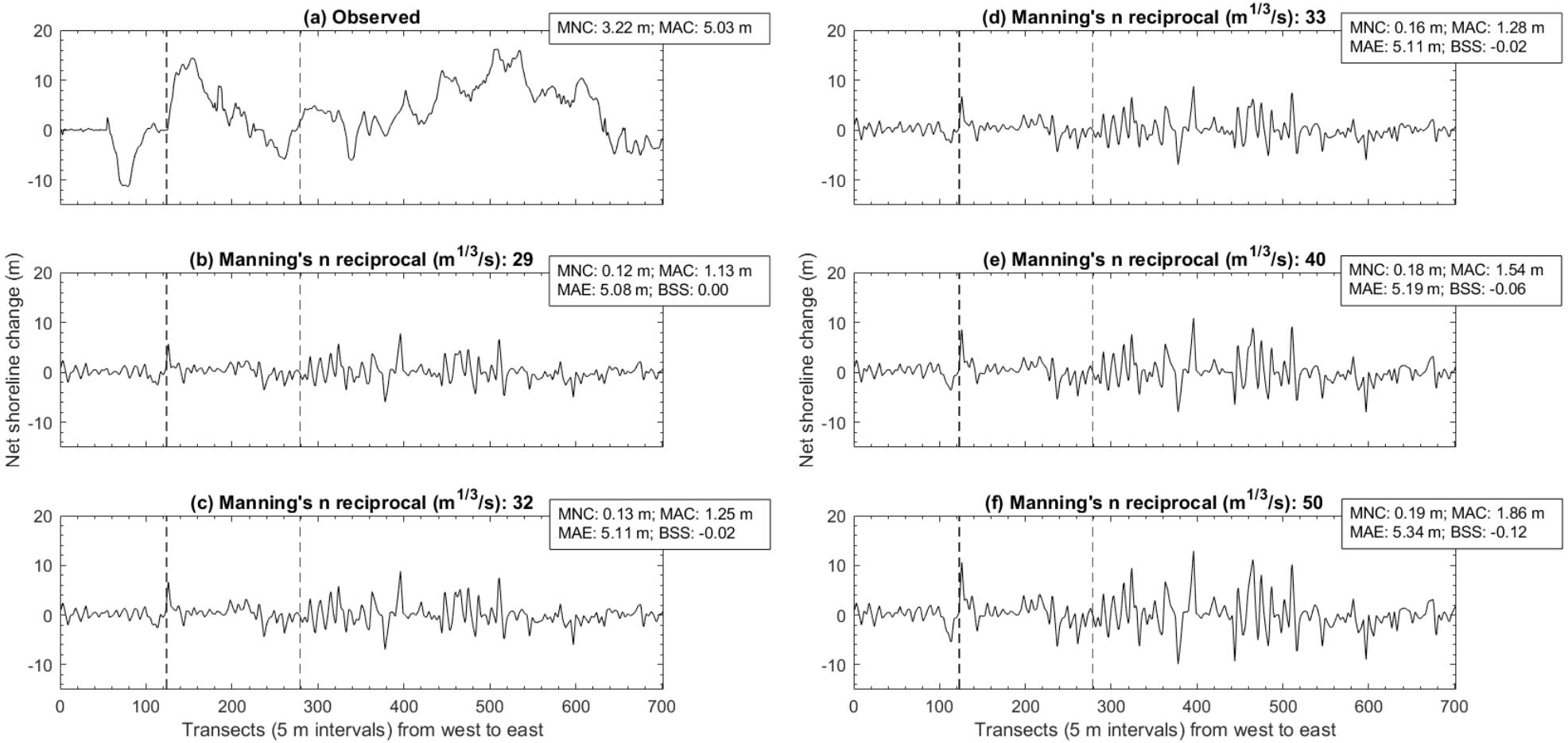

Fig. A6.3 Net shoreline change (10-Oct-2014 to 31-Mar-2016) observed and predicted in response to increasing Manning's n reciprocals ($m^{1/3}/s$) in the Puerto Rico test site. Vertical dashed lines indicate groyne locations. MNC is mean net change, MAC is mean absolute change, MAE is mean absolute error, and BSS is Brier Skill Score. Net shoreline change observed and predicted in groyne transects are excluded from the above plots and statistics.

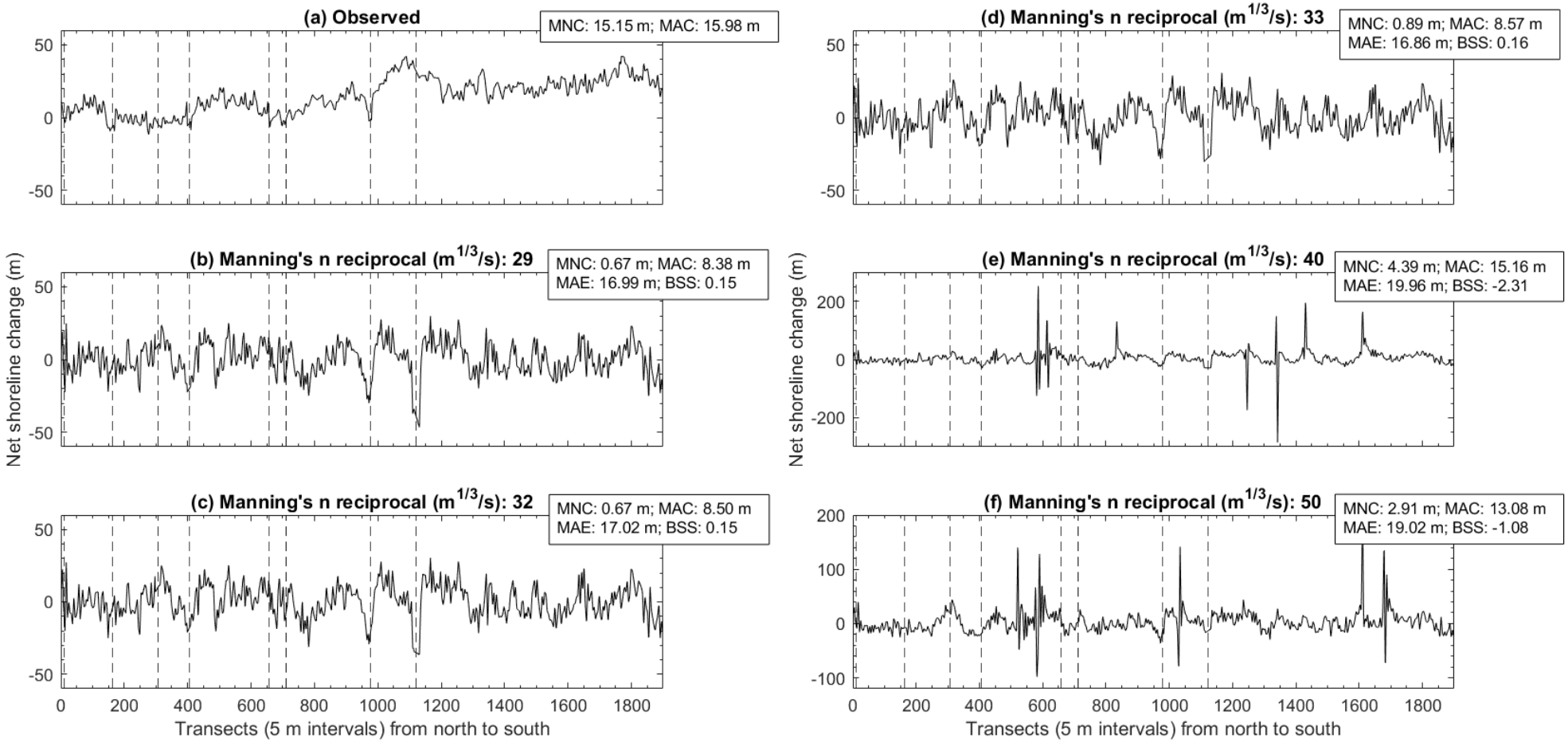

Fig. A6.4 Net shoreline change (01-Jan-2009 to 02-Aug-2011) observed and predicted in response to increasing Manning's n reciprocals ($m^{1/3}/s$) in the Southern California test site. Vertical dashed lines indicate groyne locations. MNC is mean net change, MAC is mean absolute change, MAE is mean absolute error, and BSS is Brier Skill Score. Note the difference in y axis in (e) and (f). Net shoreline change observed and predicted in groyne transects are excluded from the above plots and statistics.

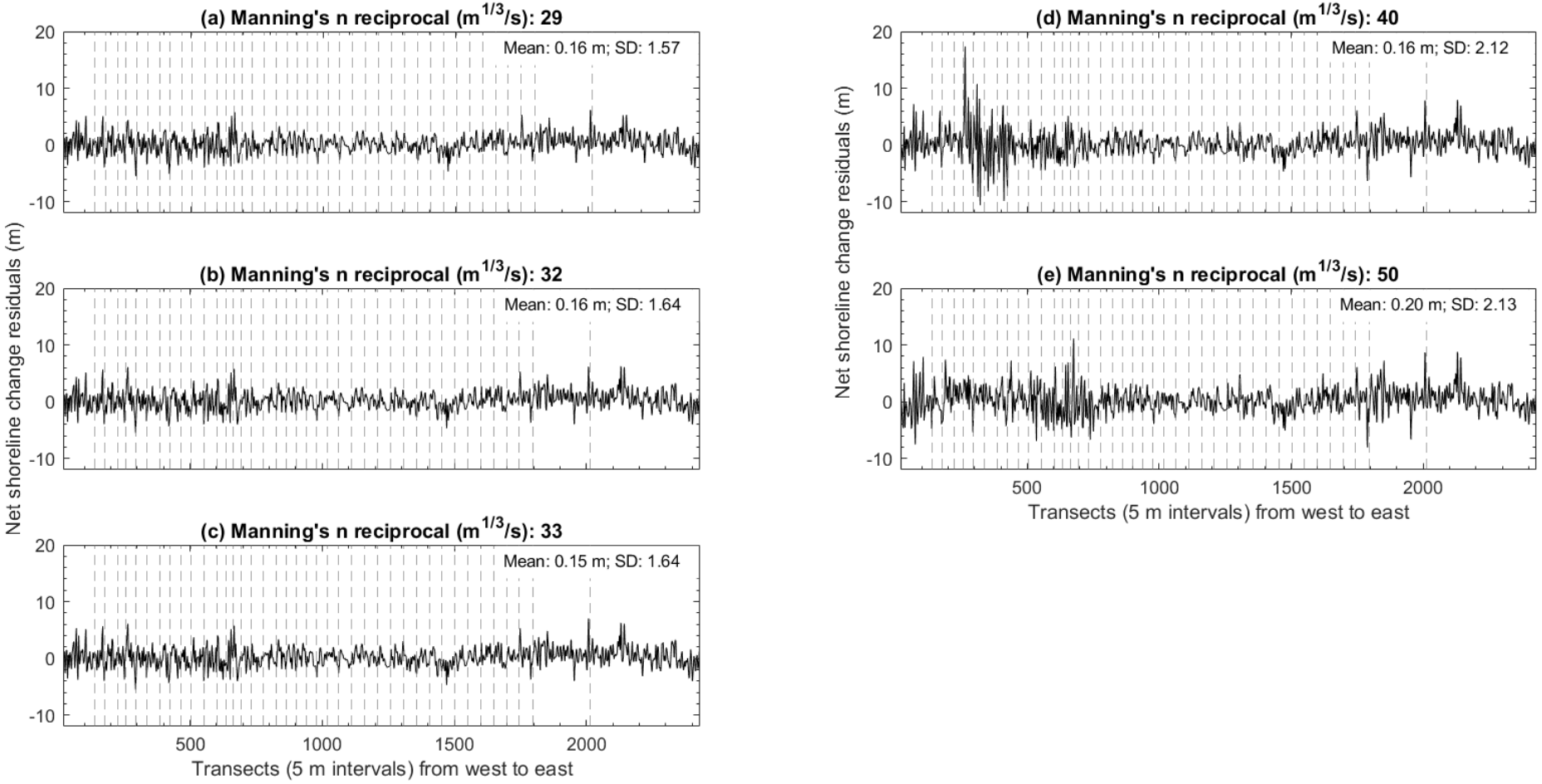

Fig. A6.5 Net shoreline change residuals from increasing Manning's n reciprocals ($m^{1/3}/s$) in the New York test site. Vertical dashed lines indicate groyne locations. SD is the standard deviation. Net shoreline change residuals in (a) to (e) are the difference between net shoreline change observed and predicted from 01-Jan-2014 to 01-Feb-2016. Net shoreline change residuals obtained in groyne transects are excluded from the above plots and statistics.

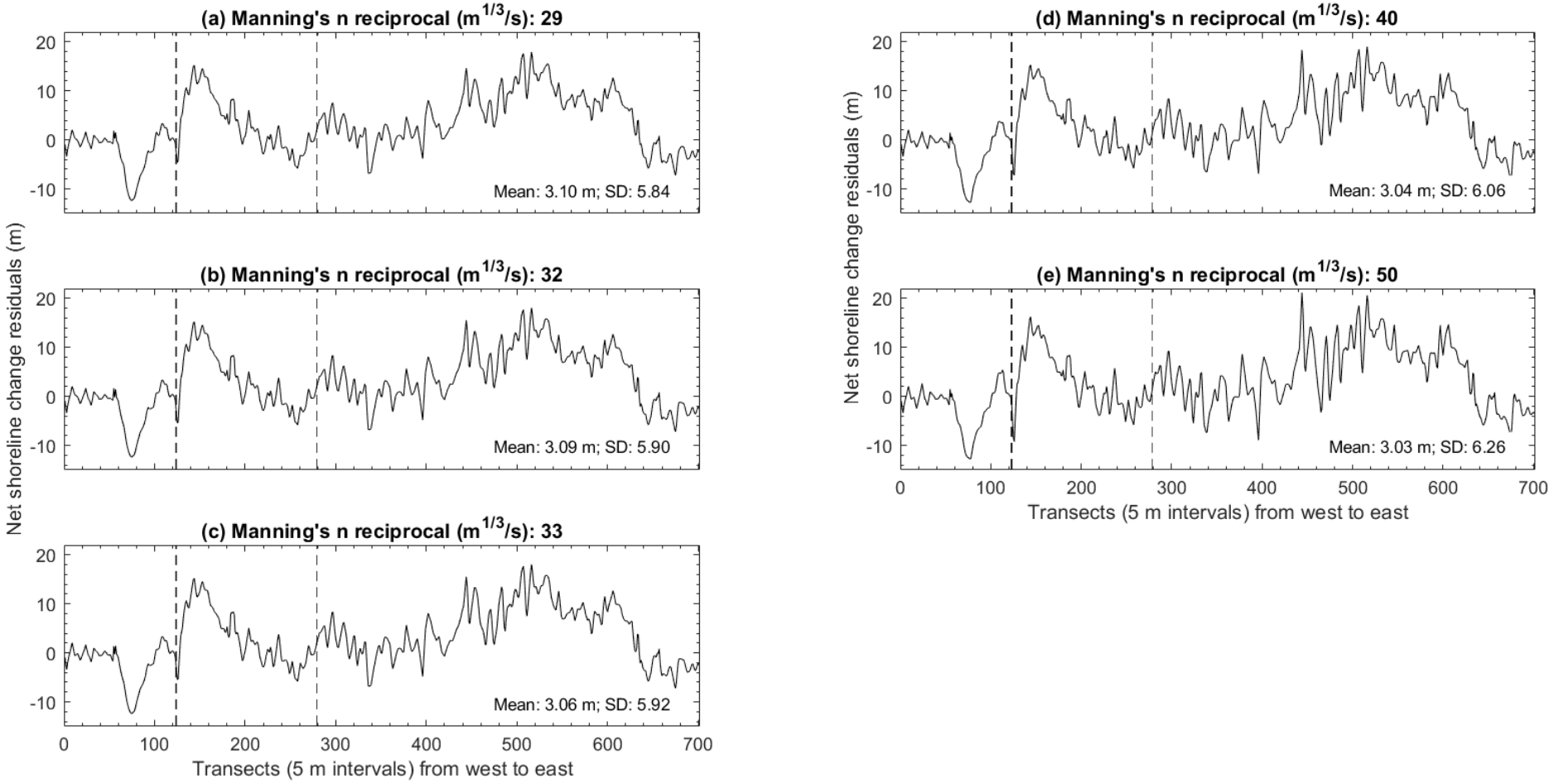

Fig. A6.6 Net shoreline change residuals from increasing Manning's n reciprocals ($m^{1/3}/s$) in the Puerto Rico test site. Vertical dashed lines indicate groyne locations. SD is the standard deviation. Net shoreline change residuals in (a) to (e) are the difference between net shoreline change observed and predicted from 10-Oct-2014 to 31-Mar-2016. Net shoreline change residuals obtained in groyne transects are excluded from the above plots and statistics.

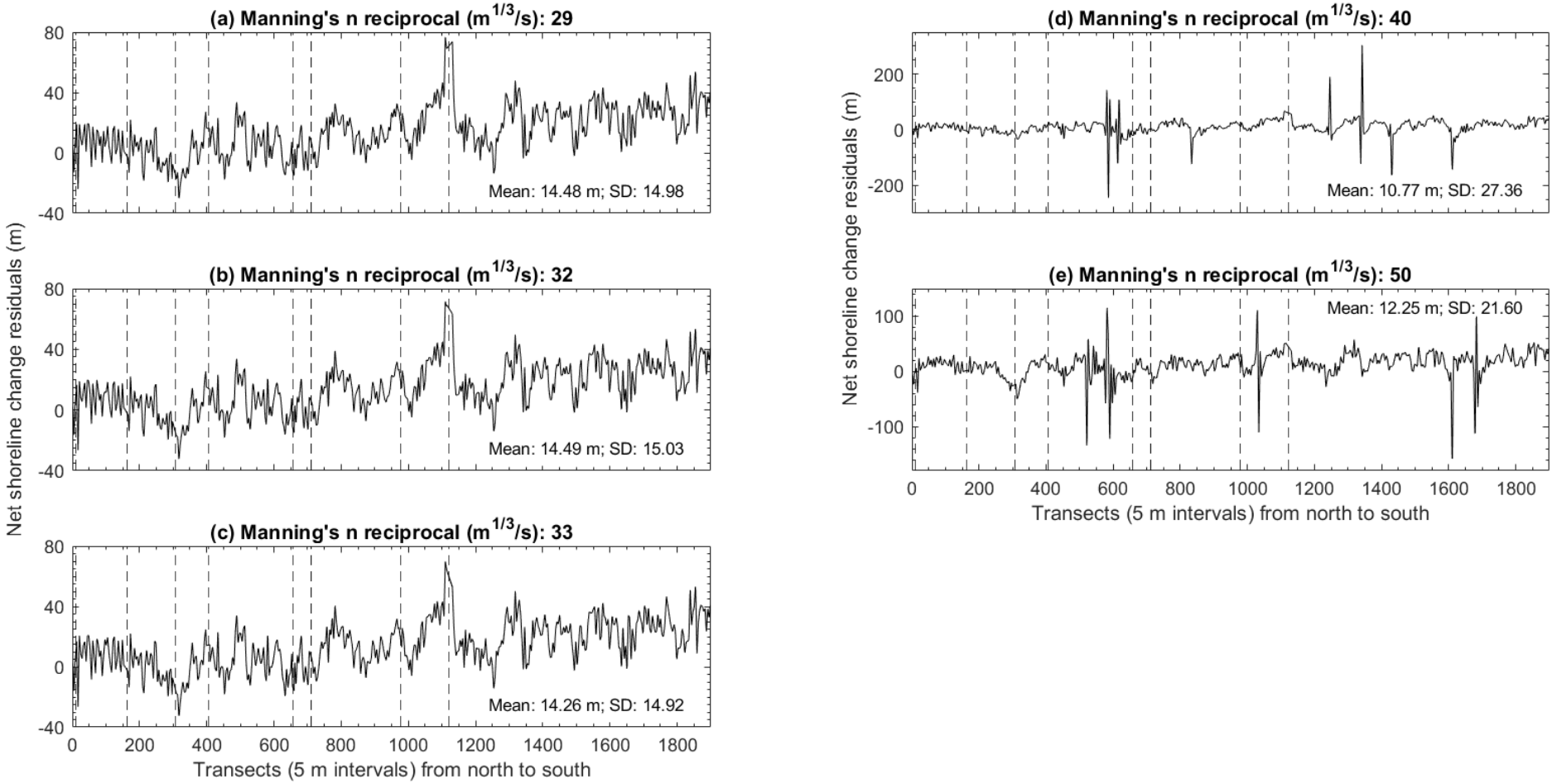

Fig. A6.7 Net shoreline change residuals from increasing Manning's n reciprocals ($m^{1/3}/s$) in the Southern California test site. Vertical dashed lines indicate groyne locations. SD is the standard deviation. Net shoreline change residuals in (a) to (e) are the difference between net shoreline change observed and predicted from 01-Jan-2009 to 02-Aug-2011. Note the difference in y axis in (d) and (e). Net shoreline change residuals obtained in groyne transects are excluded from the above plots and statistics.

A7 MIKE21 sensitivity to sand porosity

A7 graphically illustrates the sensitivity of MIKE21 net littoral drift and net shoreline change predictions to increasing sand porosity in each test site.

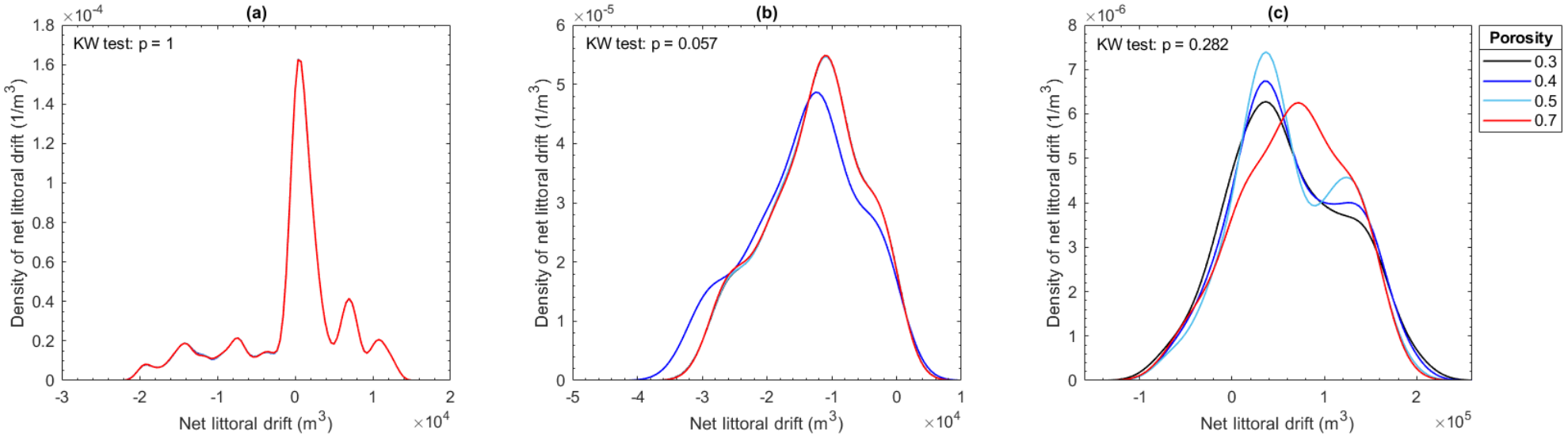

Fig. A7.1 Kernel density plots of net littoral drift predictions in response to increasing sand porosity in the New York (a), Puerto Rico (b), and Southern California (c) test site. In Fig. A7.1, net littoral drift predictions are from 01-Jan-2014 to 01-Feb-2016 in the New York test site, 10-Oct-2014 to 31-Mar-2016 in the Puerto Rico test site, and 01-Jan-2009 to 02-Aug-2011 in the Southern California test site. The Kruskal-Wallis (KW) test indicates no significant differences in net littoral drift predictions from increasing sand porosity in each test site.

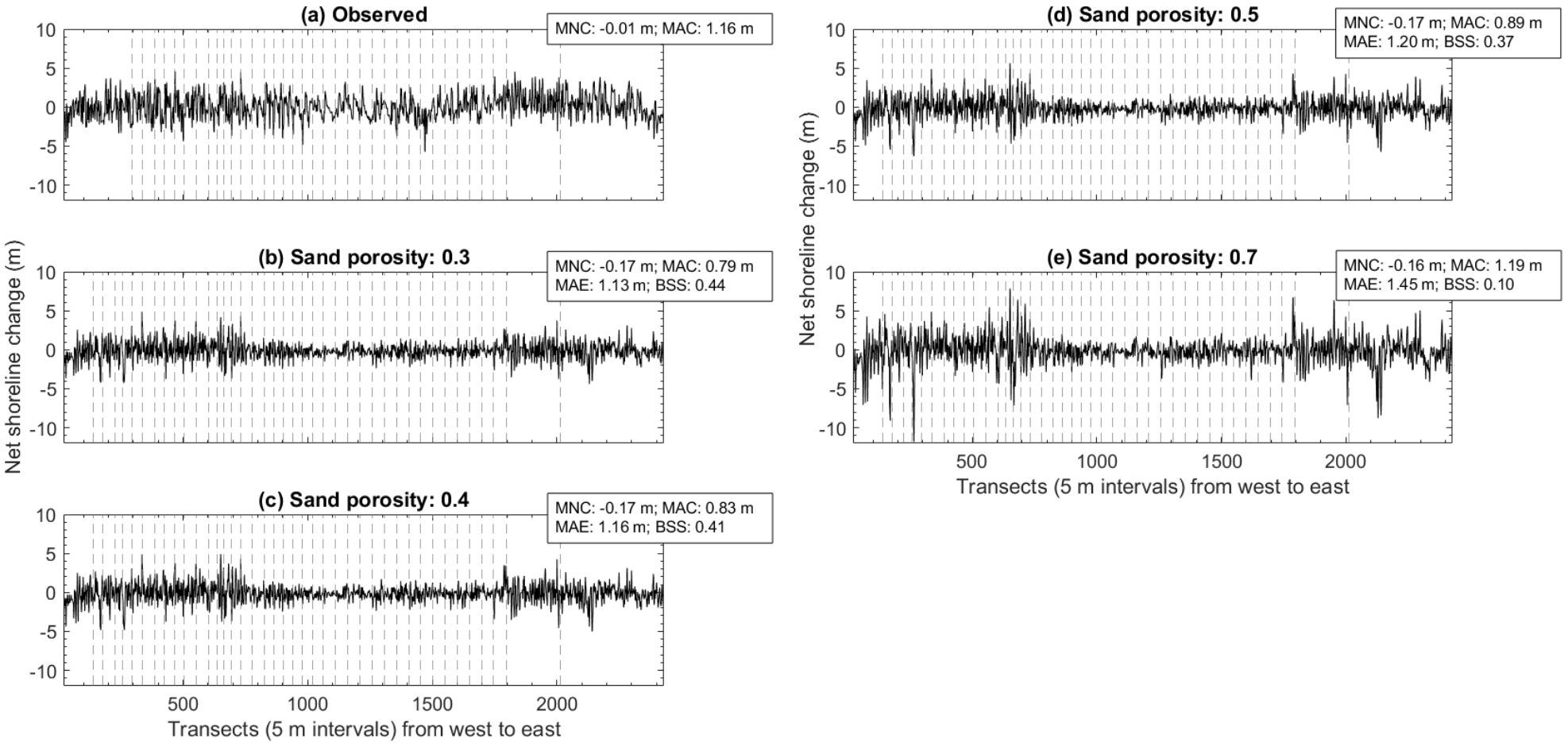

Fig. A7.2 Net shoreline change (01-Jan-2014 to 01-Feb-2016) observed and predicted in response to increasing sand porosity in the New York test site. Vertical dashed lines indicate groyne locations. MNC is mean net change, MAC is mean absolute change, MAE is mean absolute error, and BSS is Brier Skill Score. Net shoreline change observed and predicted in groyne transects are excluded from the above plots and statistics.

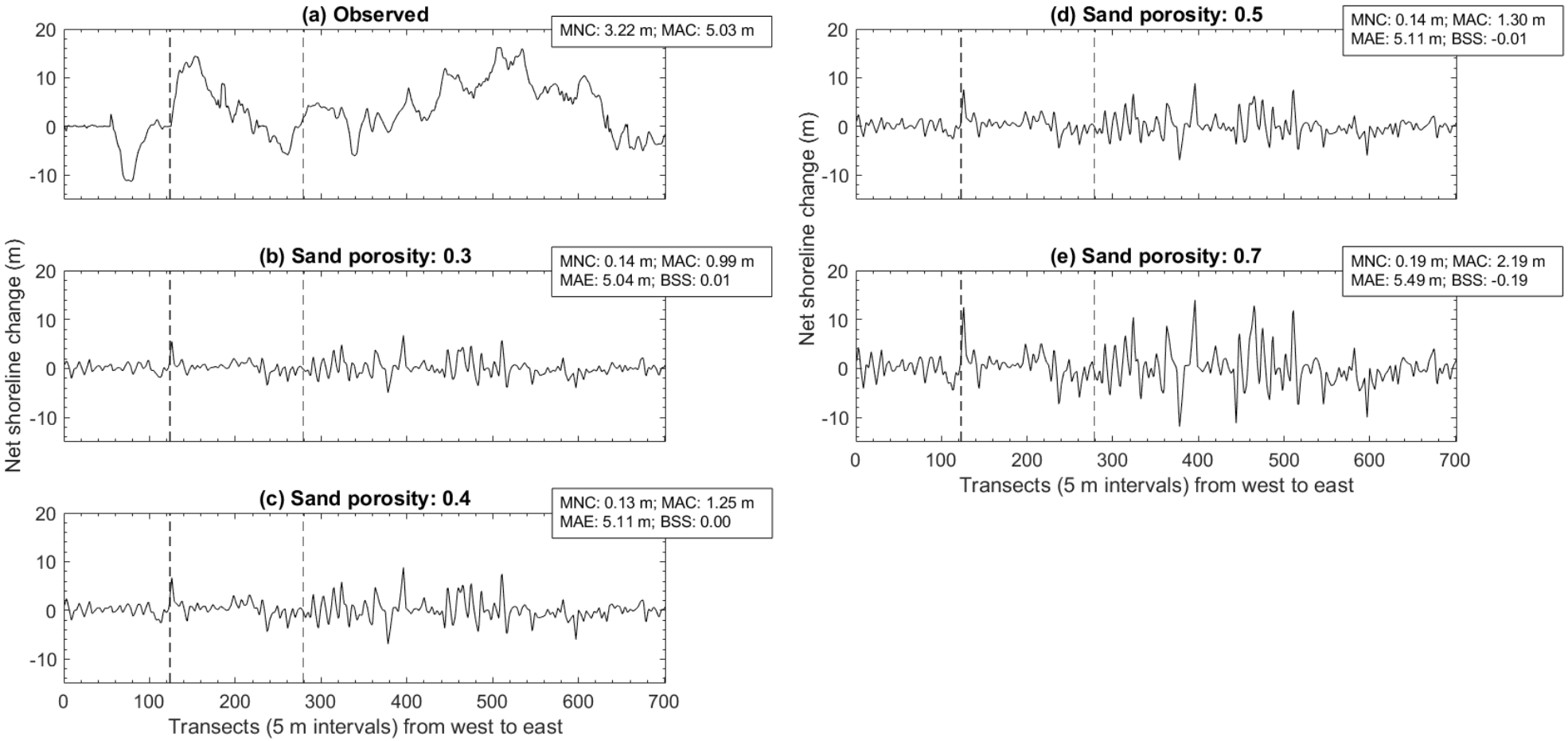

Fig. A7.3 Net shoreline change (10-Oct-2014 to 31-Mar-2016) observed and predicted in response to increasing sand porosity in the Puerto Rico test site. Vertical dashed lines indicate groyne locations. MNC is mean net change, MAC is mean absolute change, MAE is mean absolute error, and BSS is Brier Skill Score. Net shoreline change observed and predicted in groyne transects are excluded from the above plots and statistics.

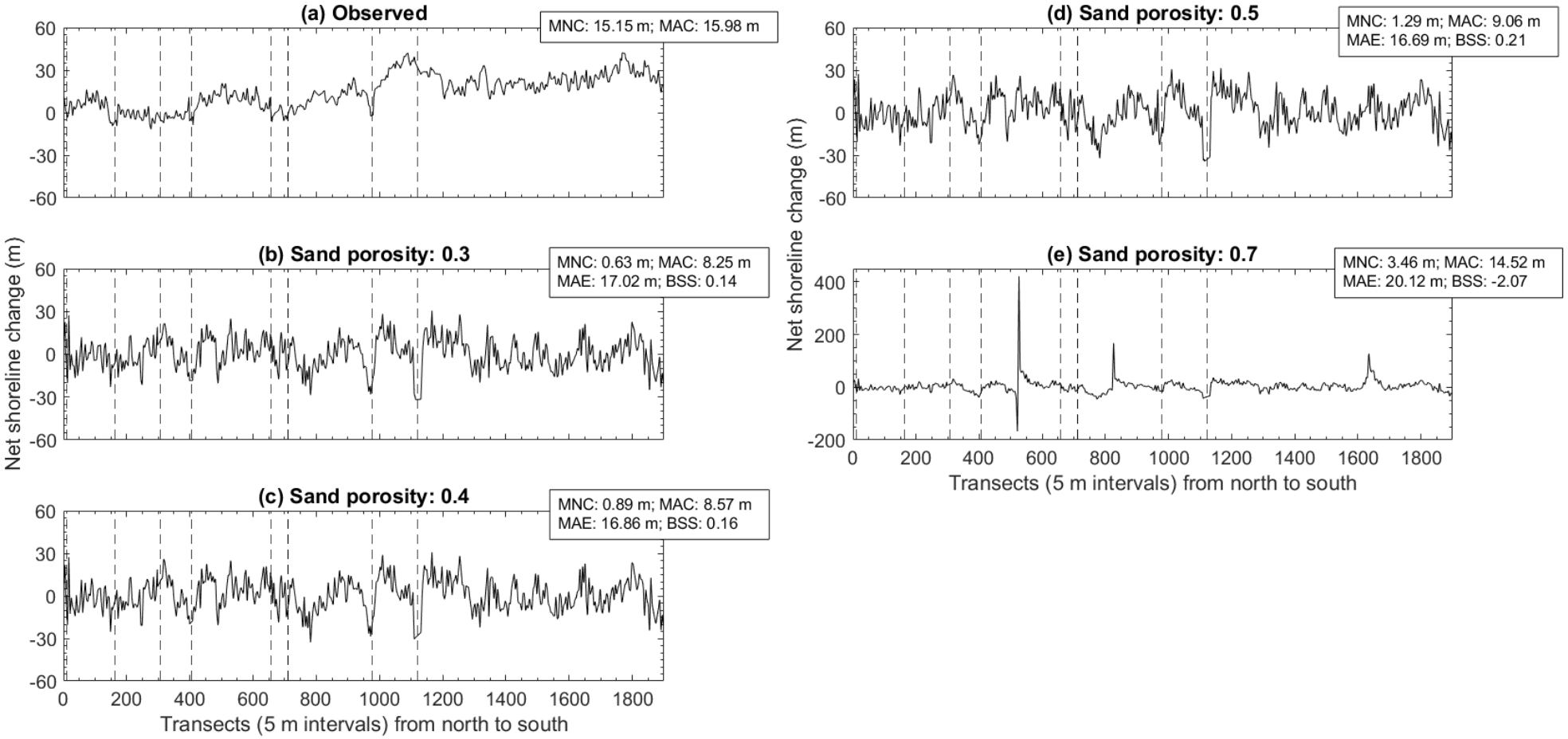

Fig. A7.4 Net shoreline change (01-Jan-2009 to 02-Aug-2011) observed and predicted in response to increasing sand porosity in the Southern California test site. Vertical dashed lines indicate groyne locations. MNC is mean net change, MAC is mean absolute change, MAE is mean absolute error, and BSS is Brier Skill Score. Note the difference in y axis in (e). Net shoreline change observed and predicted in groyne transects are excluded from the above plots and statistics.

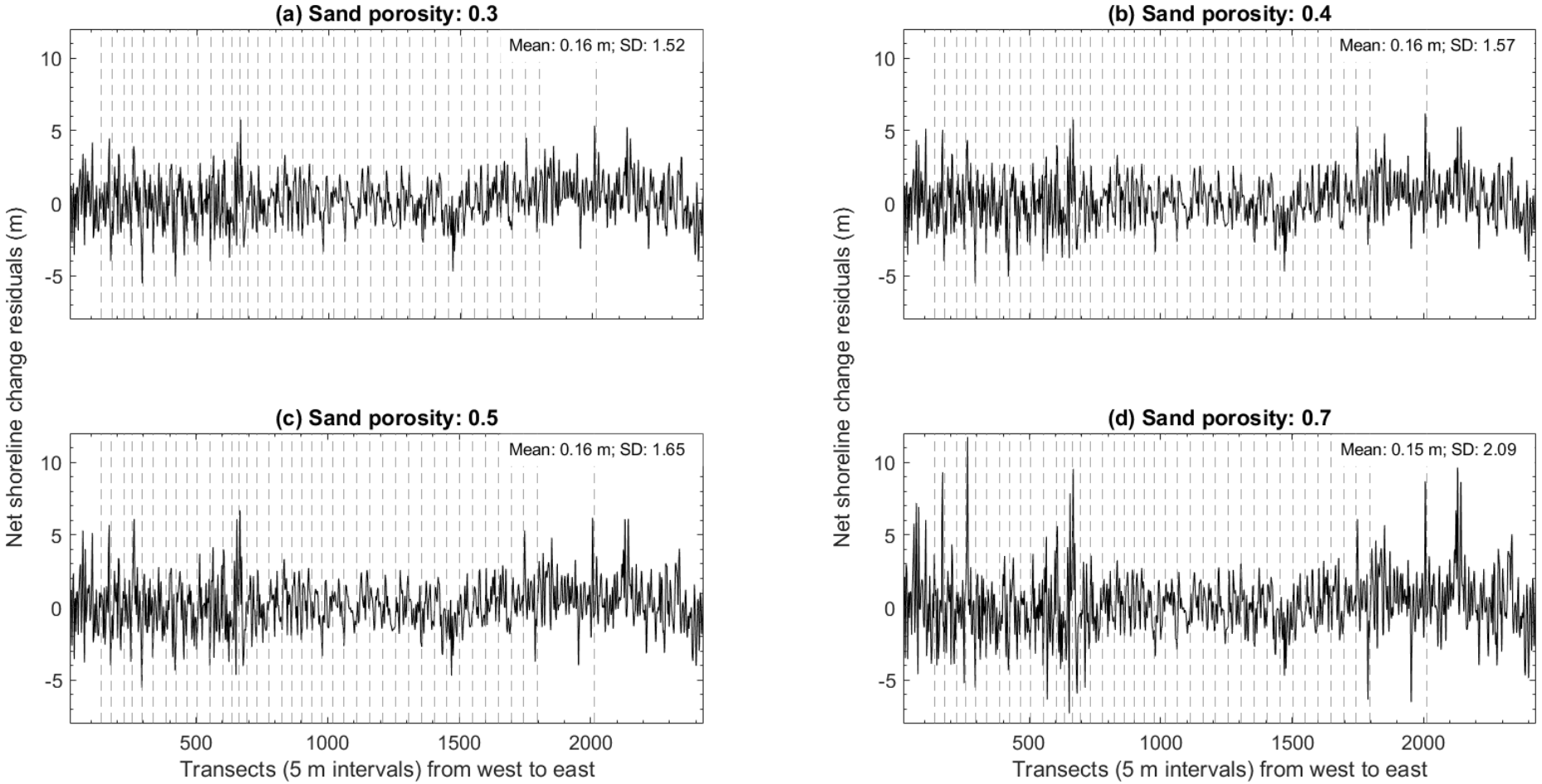

Fig. A7.5 Net shoreline change residuals from increasing sand porosity in the New York test site. Vertical dashed lines indicate groyne locations. SD is the standard deviation. Net shoreline change residuals in (a) to (d) are the difference between net shoreline change observed and predicted from 01-Jan-2014 to 01-Feb-2016. Net shoreline change residuals obtained in groyne transects are excluded from the above plots and statistics.

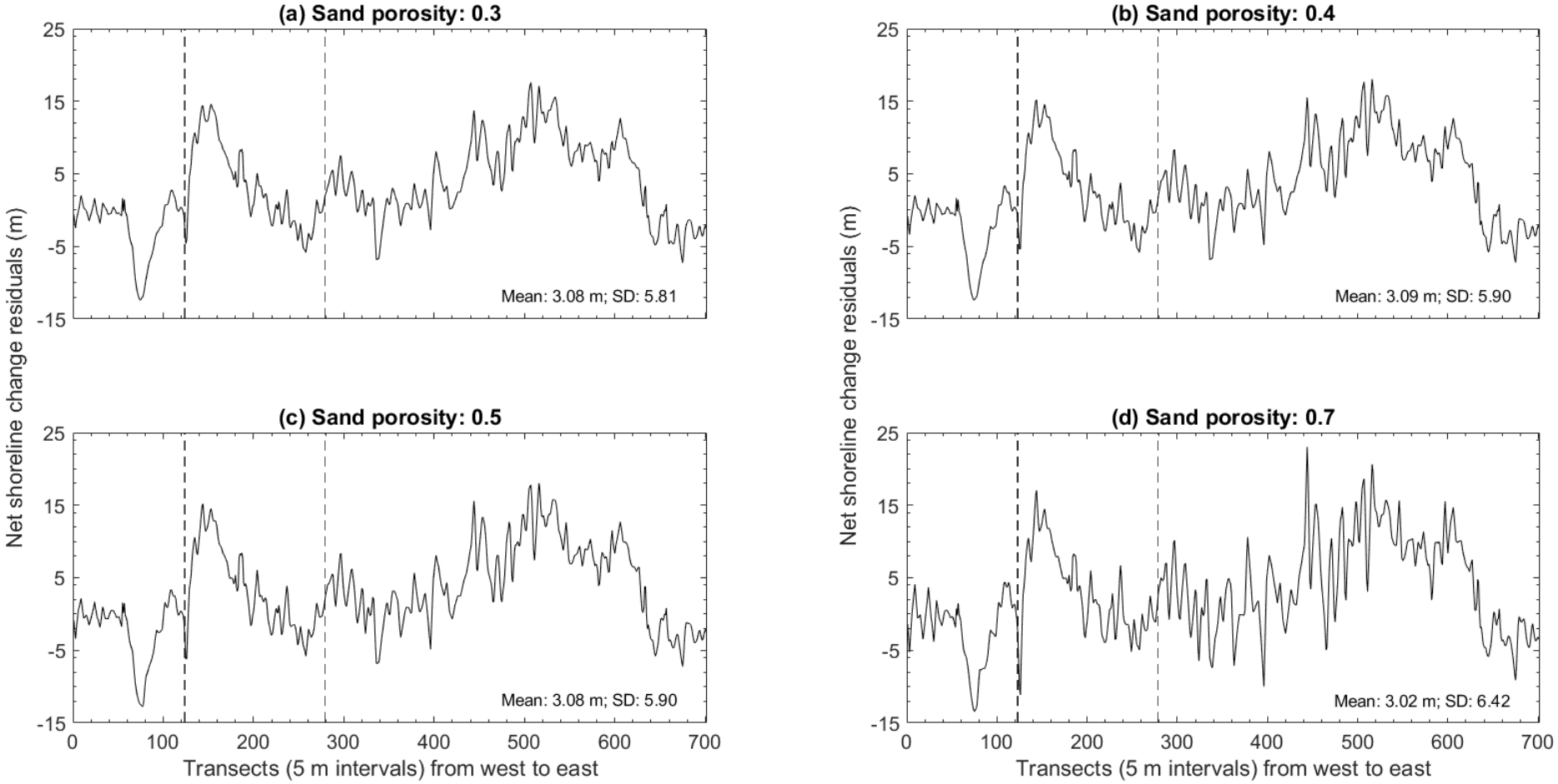

Fig. A7.6 Net shoreline change residuals from increasing sand porosity in the Puerto Rico test site. Vertical dashed lines indicate groyne locations. SD is the standard deviation. Net shoreline change residuals in (a) to (d) are the difference between net shoreline change observed and predicted from 10-Oct-2014 to 31-Mar-2016. Net shoreline change residuals obtained in groyne transects are excluded from the above plots and statistics.

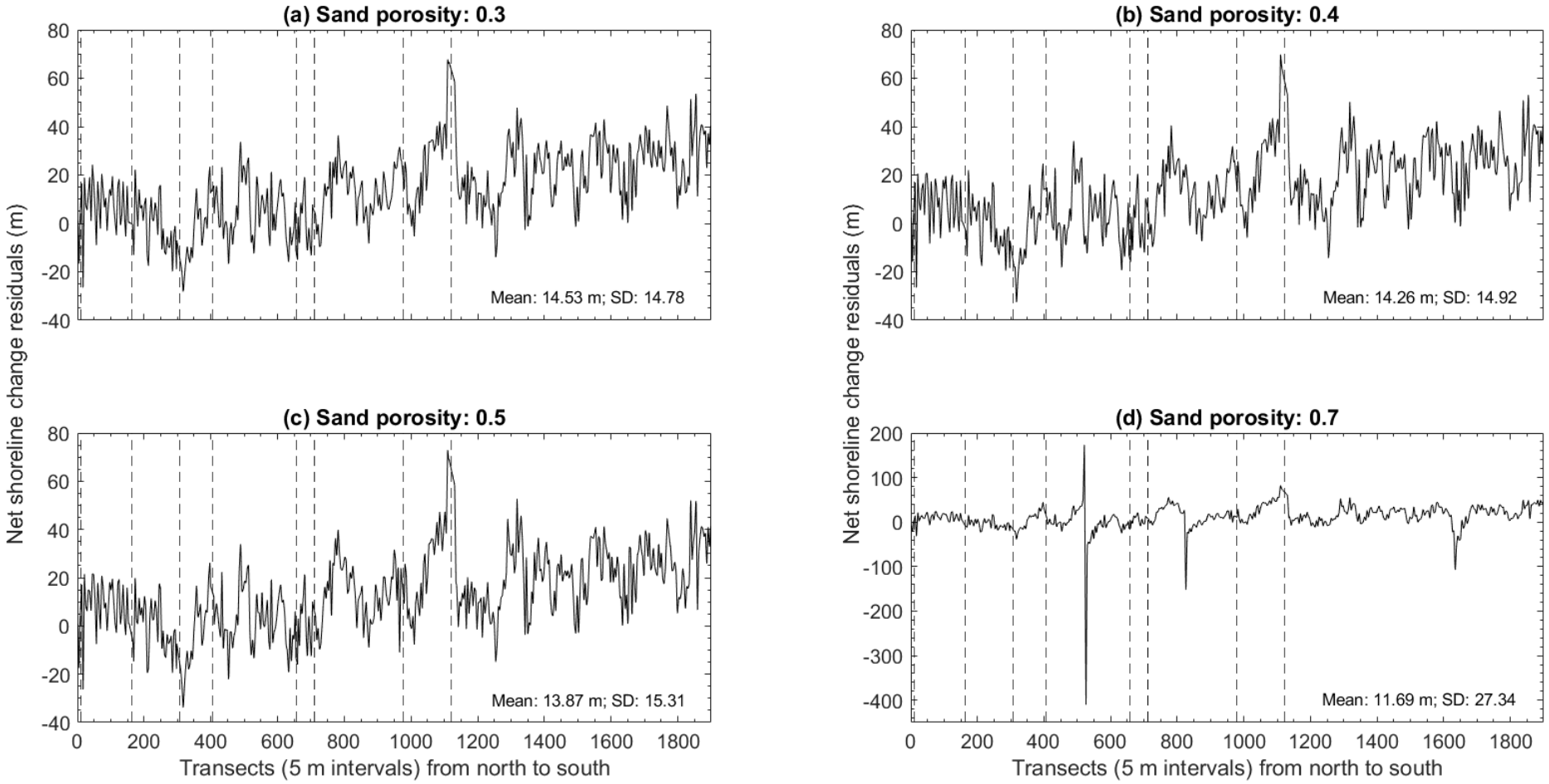

Fig. A7.7 Net shoreline change residuals from increasing sand porosity in the Southern California test site. Vertical dashed lines indicate groyne locations. SD is the standard deviation. Net shoreline change residuals in (a) to (d) are the difference between net shoreline change observed and predicted from 01-Jan-2009 to 02-Aug-2011. Note the difference in y axis in (d). Net shoreline change residuals obtained in groyne transects are excluded from the above plots and statistics.

A8 MIKE21 sensitivity to sand grain diameter (mm)

A8 graphically illustrates the sensitivity of MIKE21 net littoral drift and net shoreline change predictions to increasing sand grain diameters (mm) in each test site.

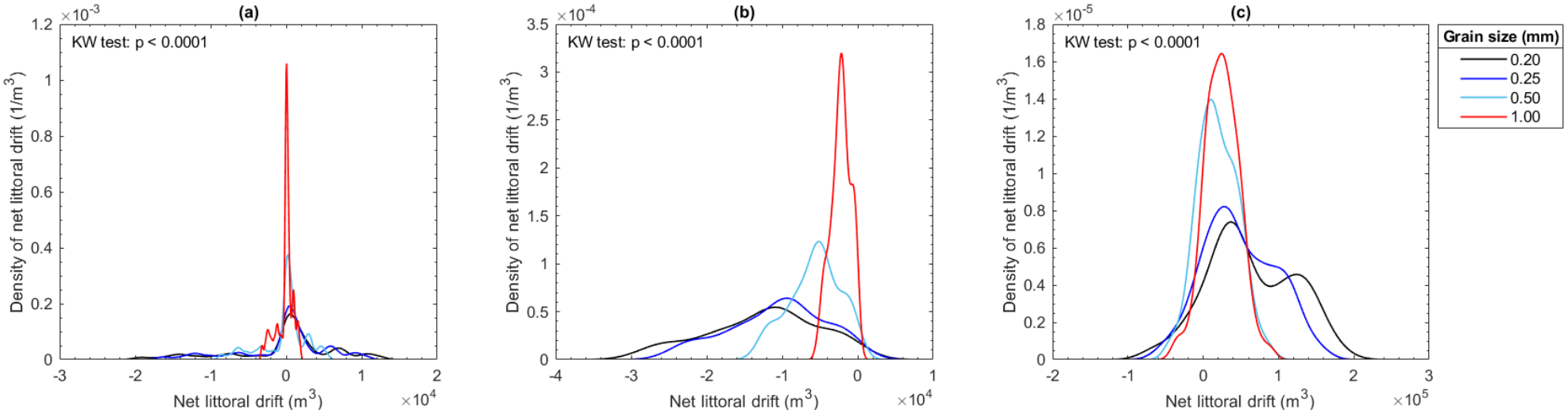

Fig. A8.1 Kernel density plots of net littoral drift predictions in response to increasing sand grain diameters (mm) in the New York (a), Puerto Rico (b) and Southern California (c) test site. In Fig. A8.1, net littoral drift predictions are from 01-Jan-2014 to 01-Feb-2016 in the New York test site, 10-Oct-2014 to 31-Mar-2016 in the Puerto Rico test site, and 01-Jan-2009 to 02-Aug-2011 in the Southern California test site. The Kruskal-Wallis (KW) test indicates significant differences in net littoral drift predictions from increasing sand grain diameters in each test site. A post hoc Dunn's test reveals that net littoral drift predictions are not significantly different from sand grain diameters ranging from 0.2 to 0.25 mm and 0.25 to 0.5 mm in the New York test site, 0.2 to 0.25 mm in the Puerto Rico test site, and 0.5 to 1 mm in the Southern California test site.

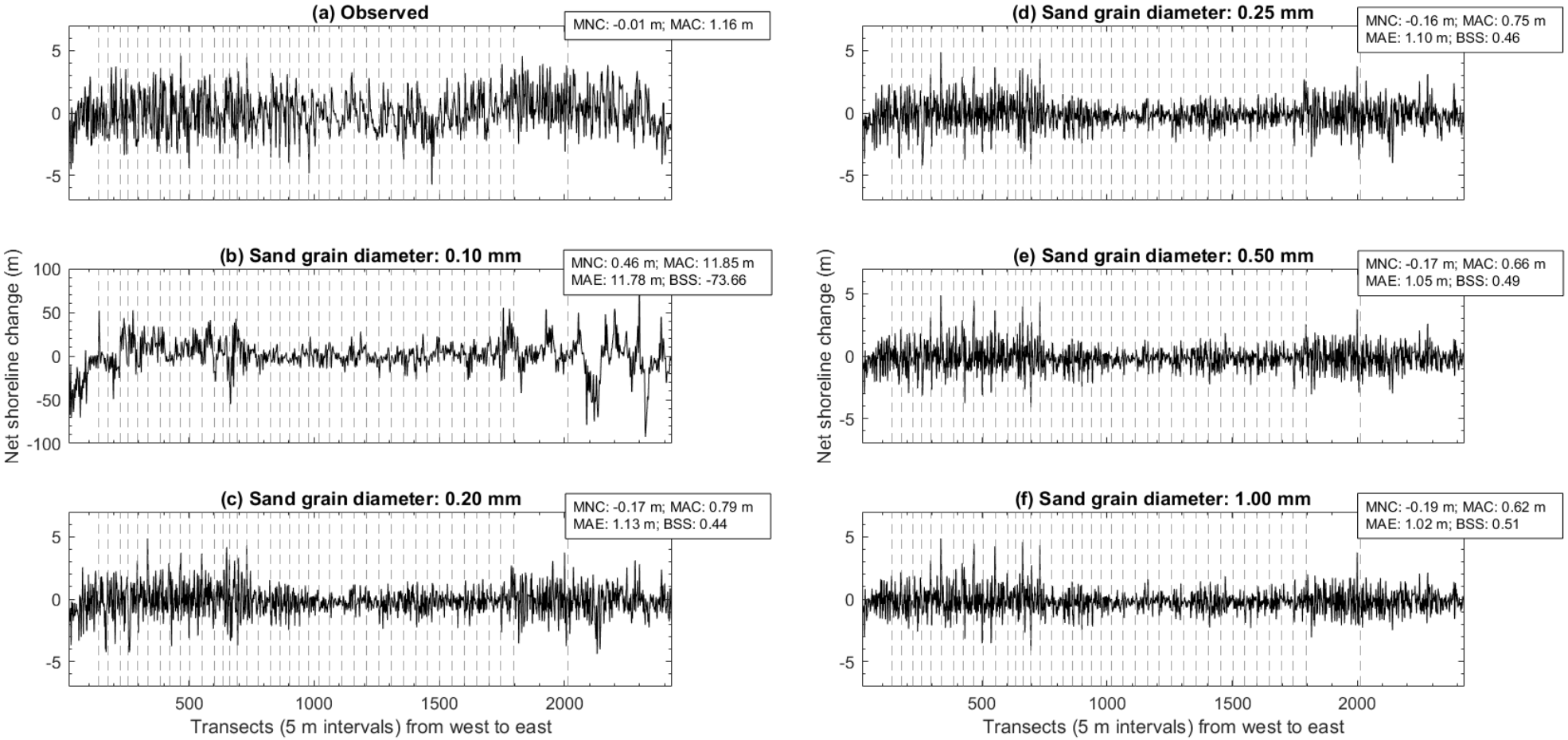

Fig. A8.2 Net shoreline change (01-Jan-2014 to 01-Feb-2016) observed and predicted in response to increasing sand grain diameters (mm) in the New York test site. Vertical dashed lines indicate groyne locations. MNC is mean net change, MAC is mean absolute change, MAE is mean absolute error, and BSS is Brier Skill Score. Note the difference in y axis in (b). Net shoreline change observed and predicted in groyne transects are excluded from the above plots and statistics.

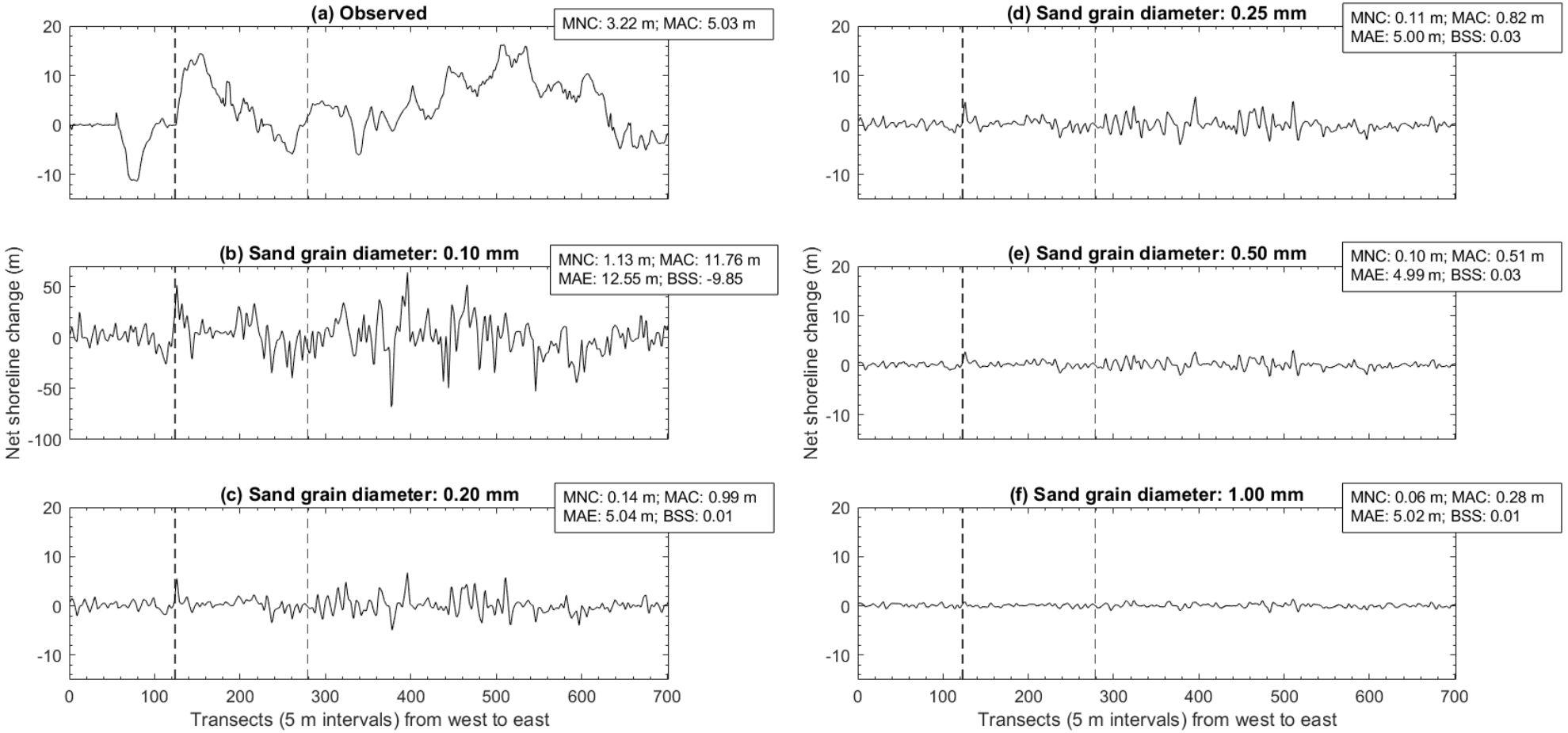

Fig. A8.3 Net shoreline change (10-Oct-2014 to 31-Mar-2016) observed and predicted in response to increasing sand grain diameters (mm) in the Puerto Rico test site. Vertical dashed lines indicate groyne locations. MNC is mean net change, MAC is mean absolute change, MAE is mean absolute error, and BSS is Brier Skill Score. Note the difference in y axis in (b). Net shoreline change observed and predicted in groyne transects are excluded from the above plots and statistics.

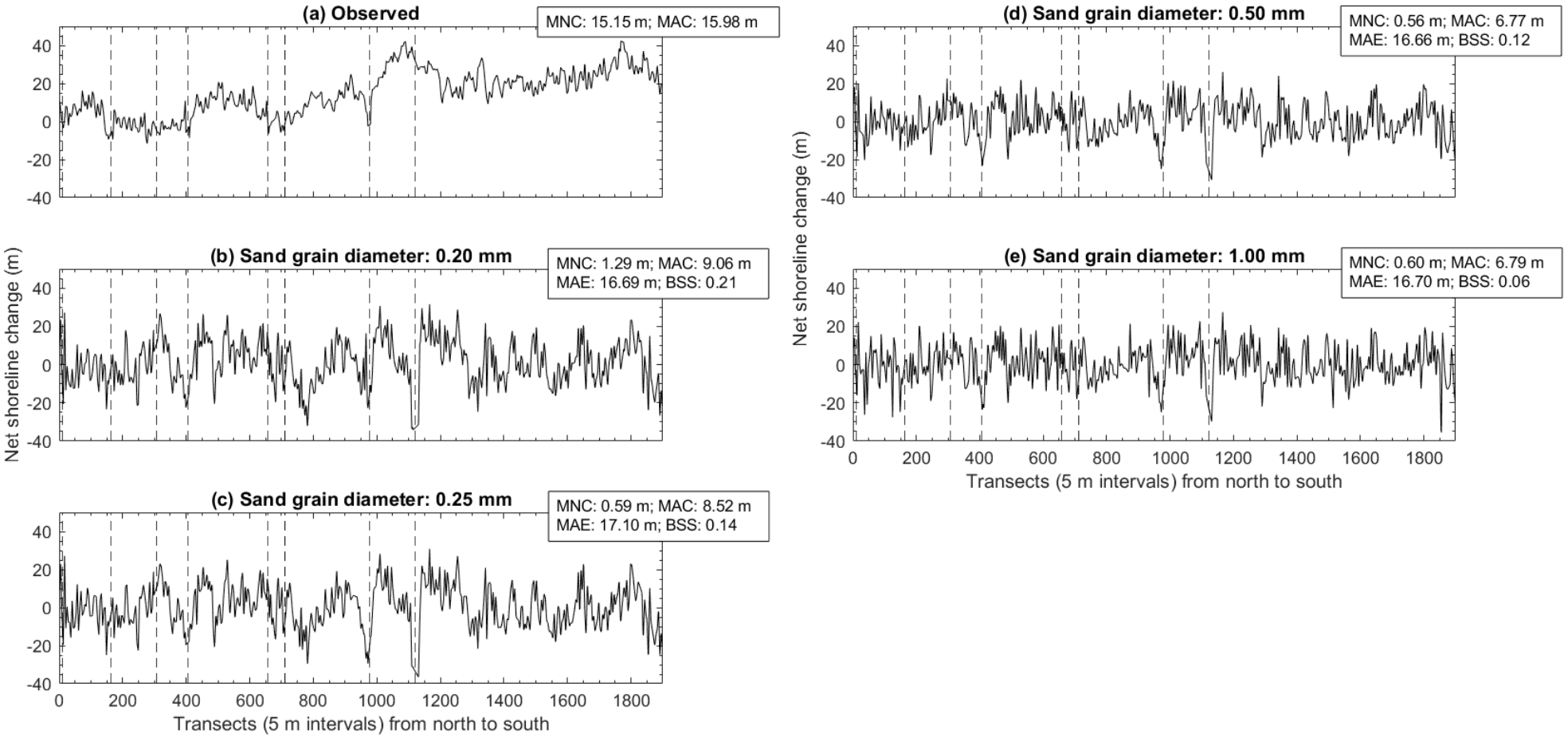

Fig. A8.4 Net shoreline change (01-Jan-2009 to 02-Aug-2011) observed and predicted in response to increasing sand grain diameters (mm) in the Southern California test site. Vertical dashed lines indicate groyne locations. MNC is mean net change, MAC is mean absolute change, MAE is mean absolute error, and BSS is Brier Skill Score. Net shoreline change observed and predicted in groyne transects are excluded from the above plots and statistics.

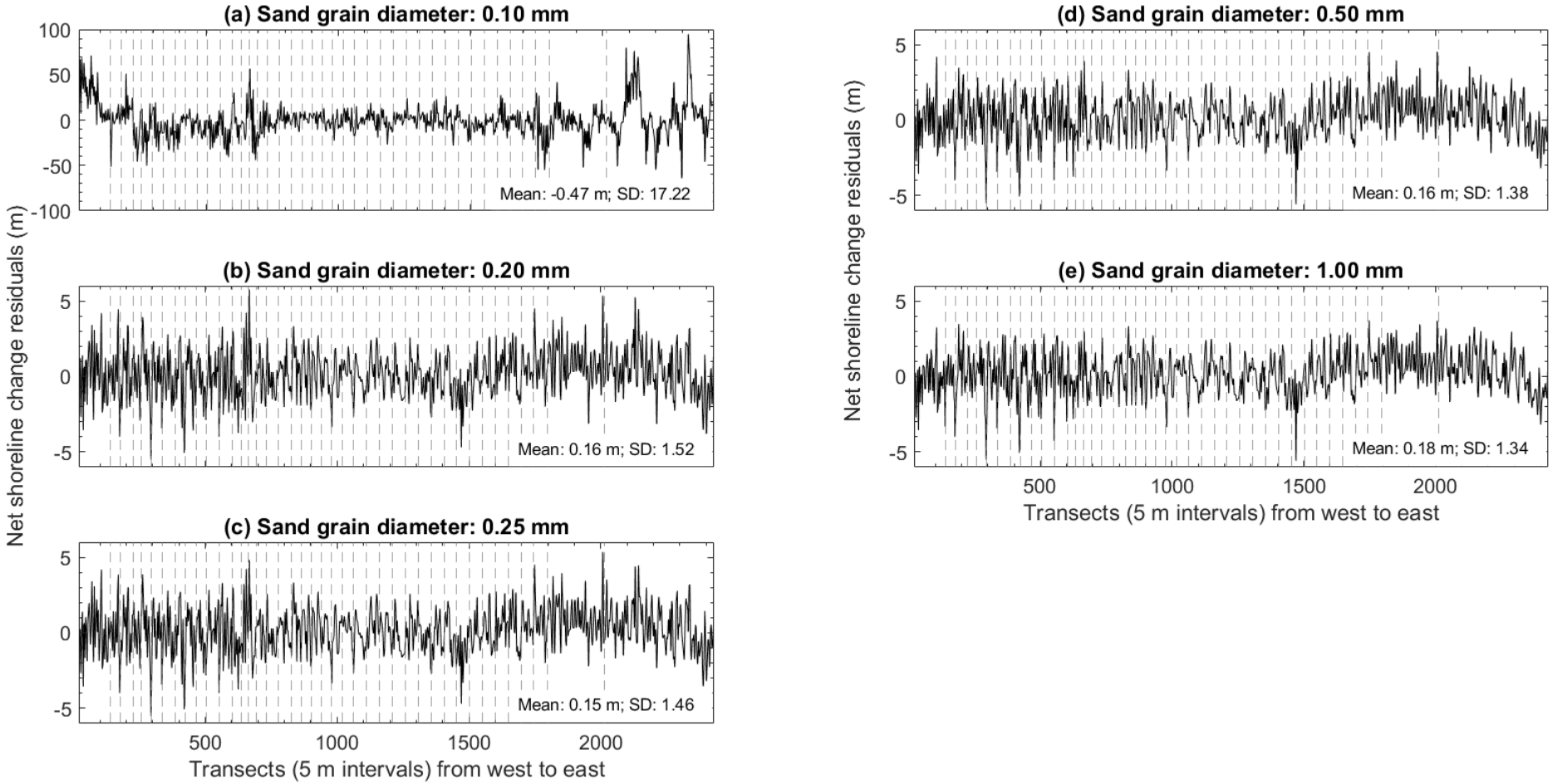

Fig. A8.5 Net shoreline change residuals from increasing sand grain diameters (mm) in the New York test site. Vertical dashed lines indicate groyne locations. SD is the standard deviation. Net shoreline change residuals in (a) to (e) are the difference between net shoreline change observed and predicted from 01-Jan-2014 to 01-Feb-2016. Note the difference in y axis in (a). Net shoreline change residuals obtained in groyne transects are excluded from the above plots and statistics.

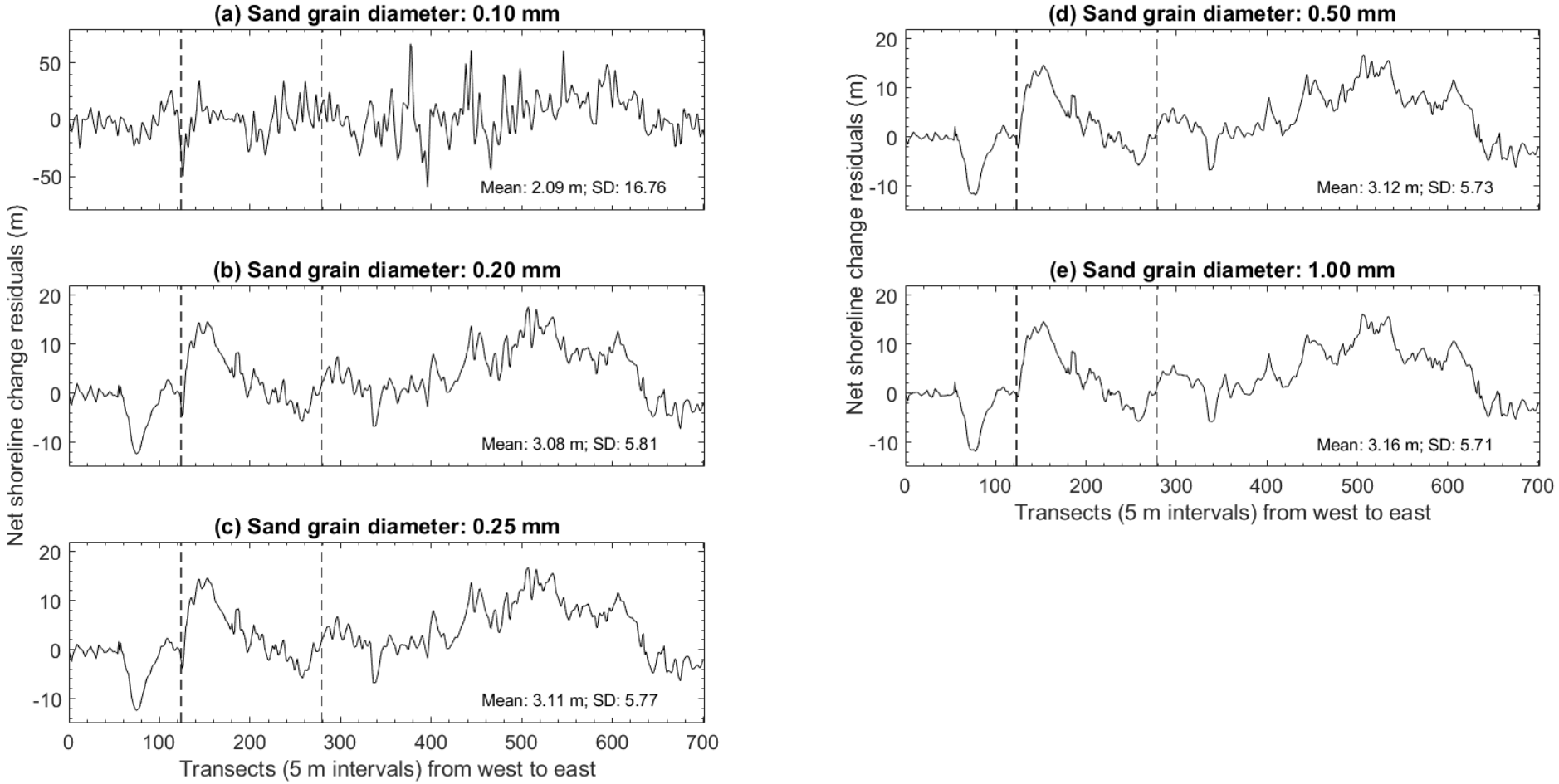

Fig. A8.6 Net shoreline change residuals from increasing sand grain diameters (mm) in the Puerto Rico test site. Vertical dashed lines indicate groyne locations. SD is the standard deviation. Net shoreline change residuals in (a) to (e) are the difference between net shoreline change observed and predicted from 10-Oct-2014 to 31-Mar-2016. Note the difference in y axis in (a). Net shoreline change residuals obtained in groyne transects are excluded from the above plots and statistics.

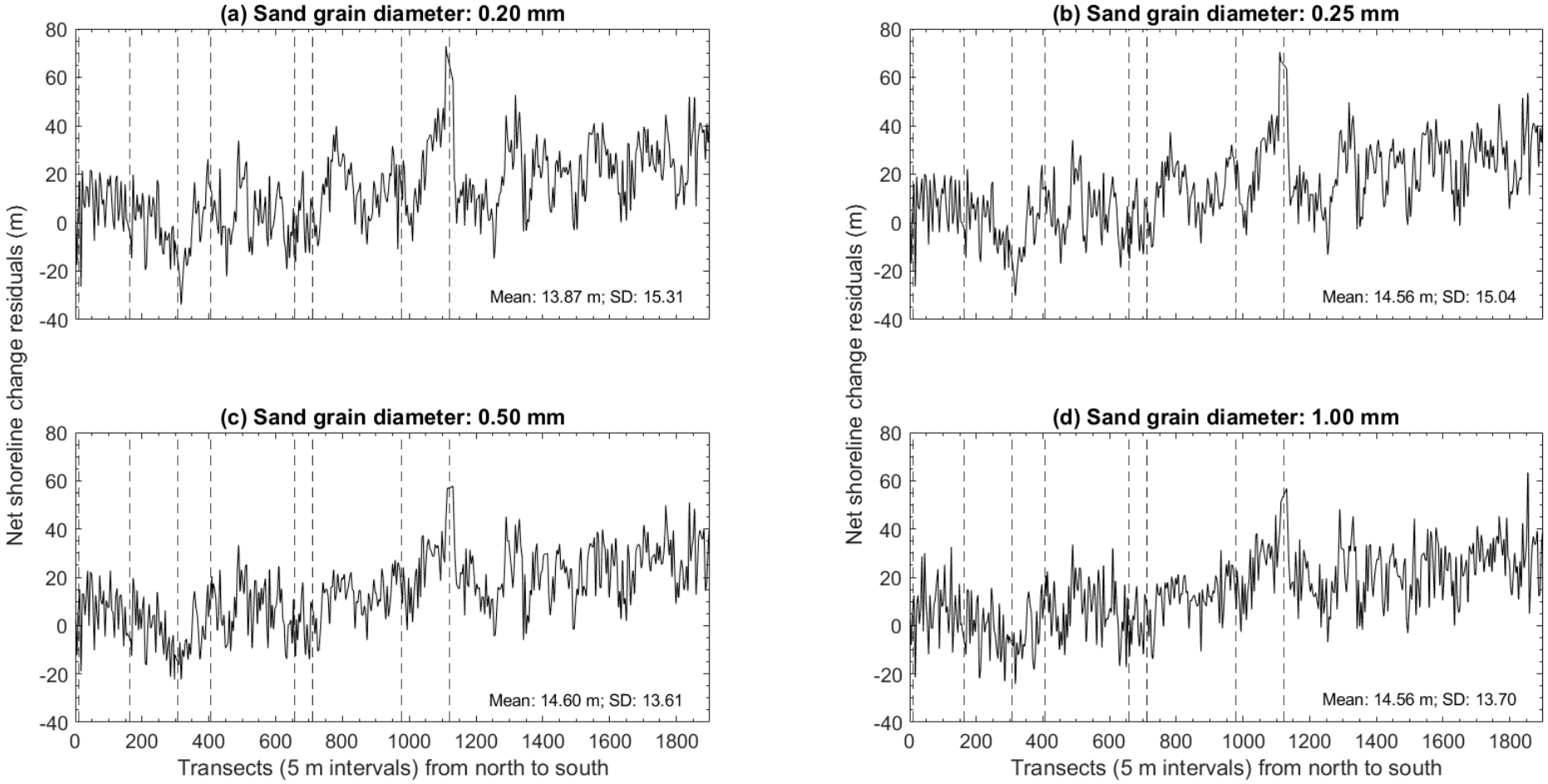

Fig. A8.7 Net shoreline change residuals from increasing sand grain diameters (mm) in the Southern California test site. Vertical dashed lines indicate groyne locations. SD is the standard deviation. Net shoreline change residuals in (a) to (d) are the difference between net shoreline change observed and predicted from 01-Jan-2009 to 02-Aug-2011. Net shoreline change residuals obtained in groyne transects are excluded from the above plots and statistics.

A9 MIKE21 sensitivity to sediment grading coefficient

A9 graphically illustrates the sensitivity of MIKE21 net littoral drift and net shoreline change predictions in response to an increase in each test site's sediment grading coefficient.

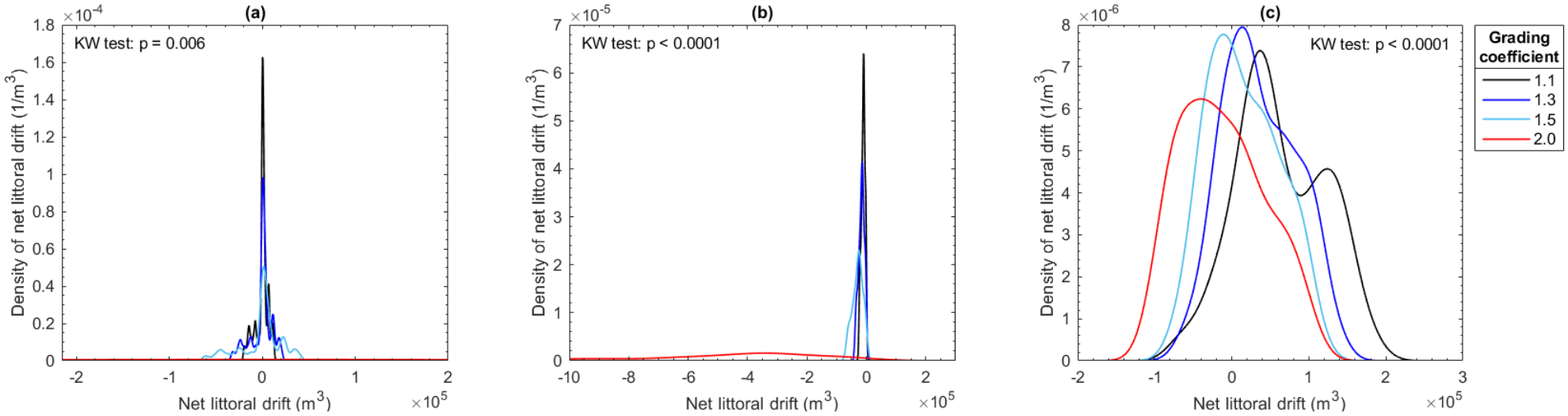

Fig. A9.1 Kernel density plots of net littoral drift predictions in response to an increase in sediment grading coefficient in the New York (a), Puerto Rico (b), and Southern California (c) test site. In Fig. A9.1, net littoral drift predictions are from 01-Jan-2014 to 01-Feb-2016 in the New York test site, 10-Oct-2014 to 31-Mar-2016 in the Puerto Rico test site, and 01-Jan-2009 to 02-Aug-2011 in the Southern California test site. The Kruskal-Wallis (KW) test indicates significant differences in net littoral drift predictions from an increase in each test site's sediment grading coefficient. A post hoc Dunn's test reveals that net littoral drift predictions from each change in sediment grading coefficient are significantly different.

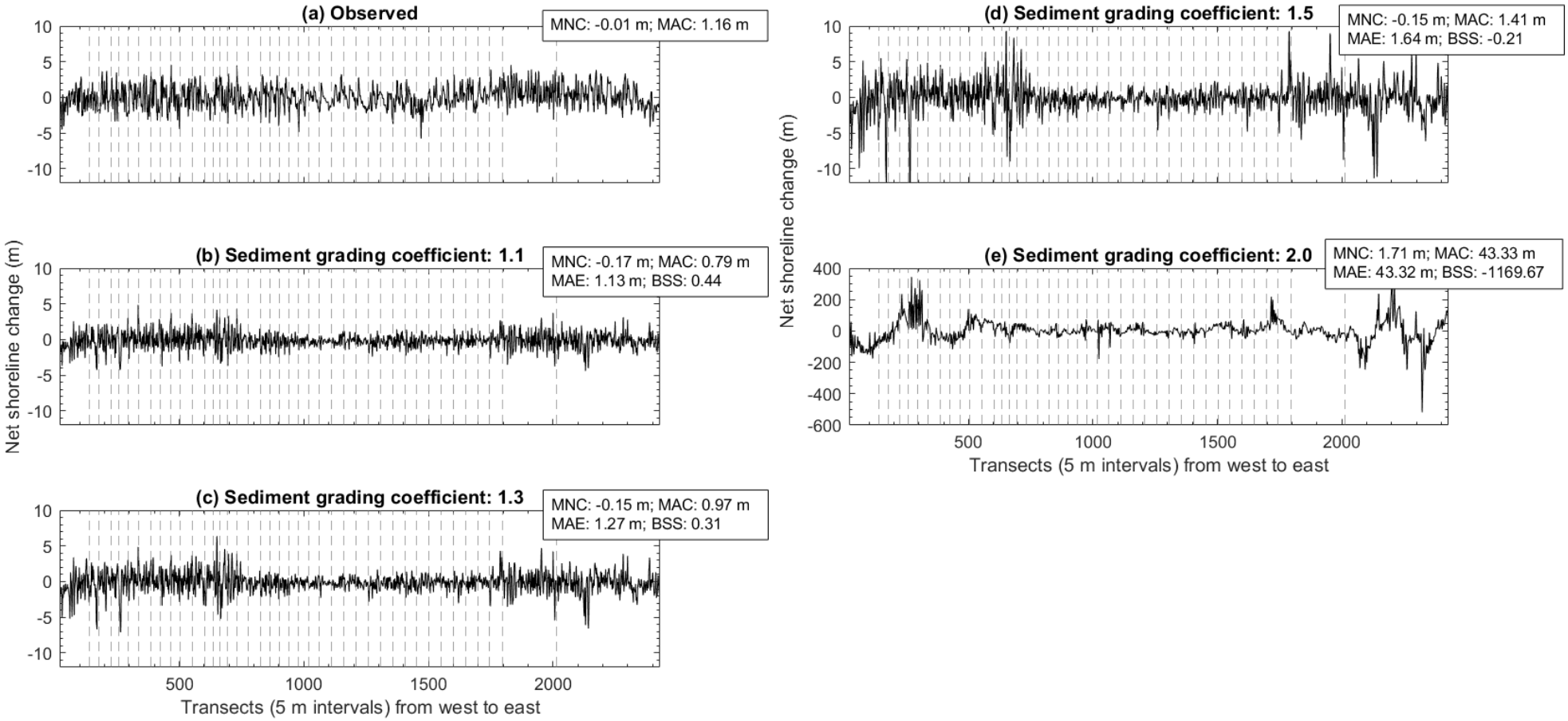

Fig. A9.2 Net shoreline change (01-Jan-2014 to 01-Feb-2016) observed and predicted in response to an increase in sediment grading coefficient in the New York test site. Vertical dashed lines indicate groyne locations. MNC is mean net change, MAC is mean absolute change, MAE is mean absolute error, and BSS is Brier Skill Score. Note the difference in y axis in (e). Net shoreline change observed and predicted in groyne transects are excluded from the above plots and statistics.

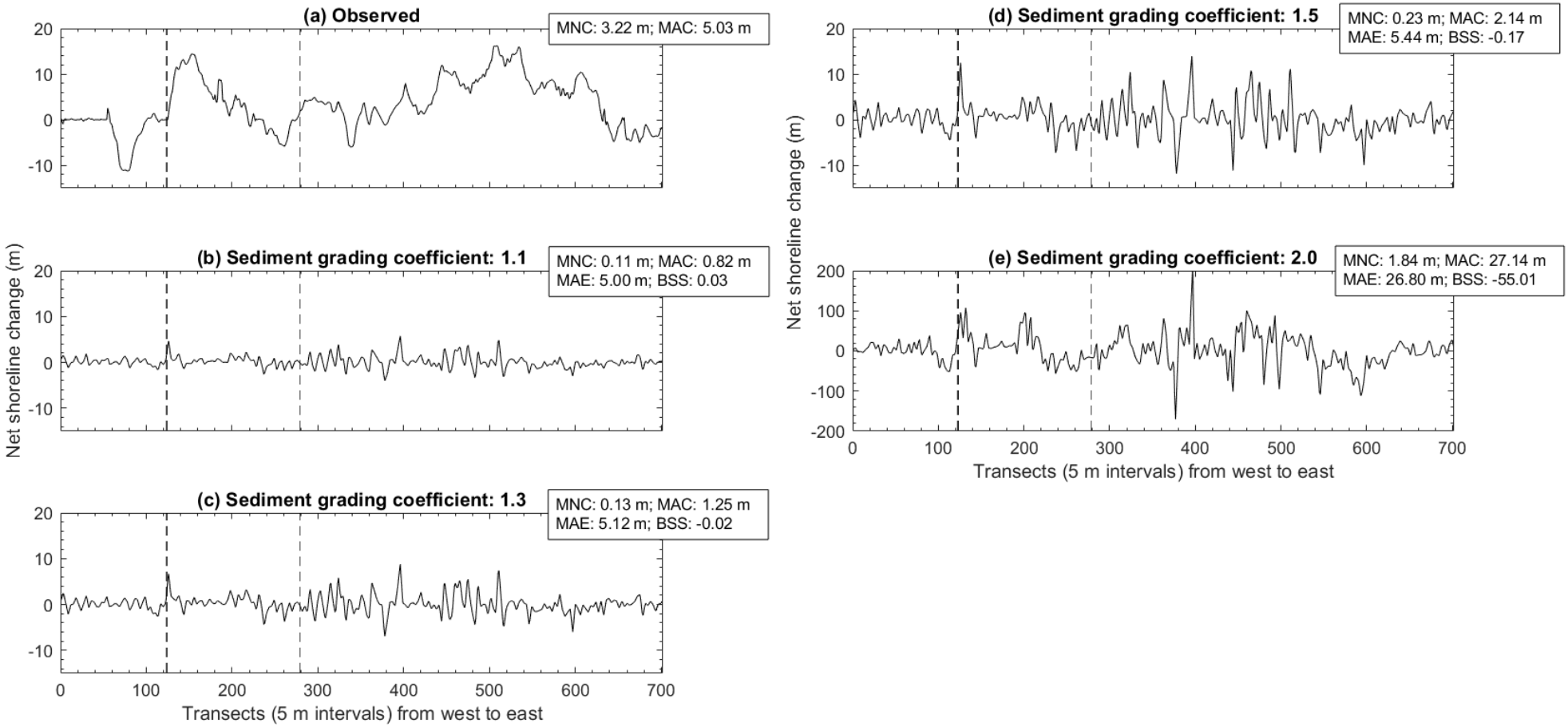

Fig. A9.3 Net shoreline change (10-Oct-2014 to 31-Mar-2016) observed and predicted in response to an increase in sediment grading coefficient in the Puerto Rico test site. Vertical dashed lines indicate groyne locations. MNC is mean net change, MAC is mean absolute change, MAE is mean absolute error, and BSS is Brier Skill Score. Note the difference in y axis in (e). Net shoreline change observed and predicted in groyne transects are excluded from the above plots and statistics.

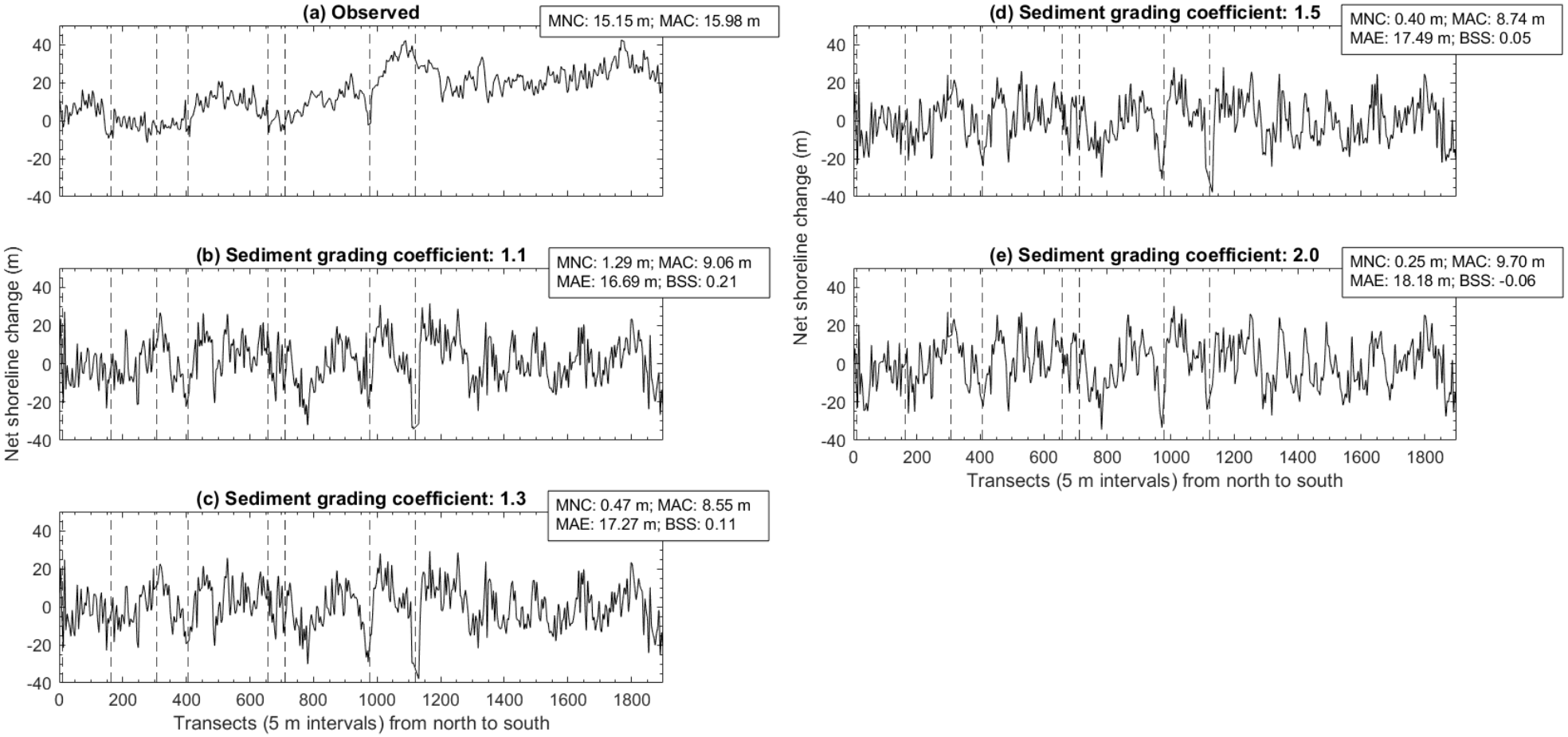

Fig. A9.4 Net shoreline change (01-Jan-2009 to 02-Aug-2011) observed and predicted in response to an increase in sediment grading coefficient in the Southern California test site. Vertical dashed lines indicate groyne locations. MNC is mean net change, MAC is mean absolute change, MAE is mean absolute error, and BSS is Brier Skill Score. Net shoreline change observed and predicted in groyne transects are excluded from the above plots and statistics.

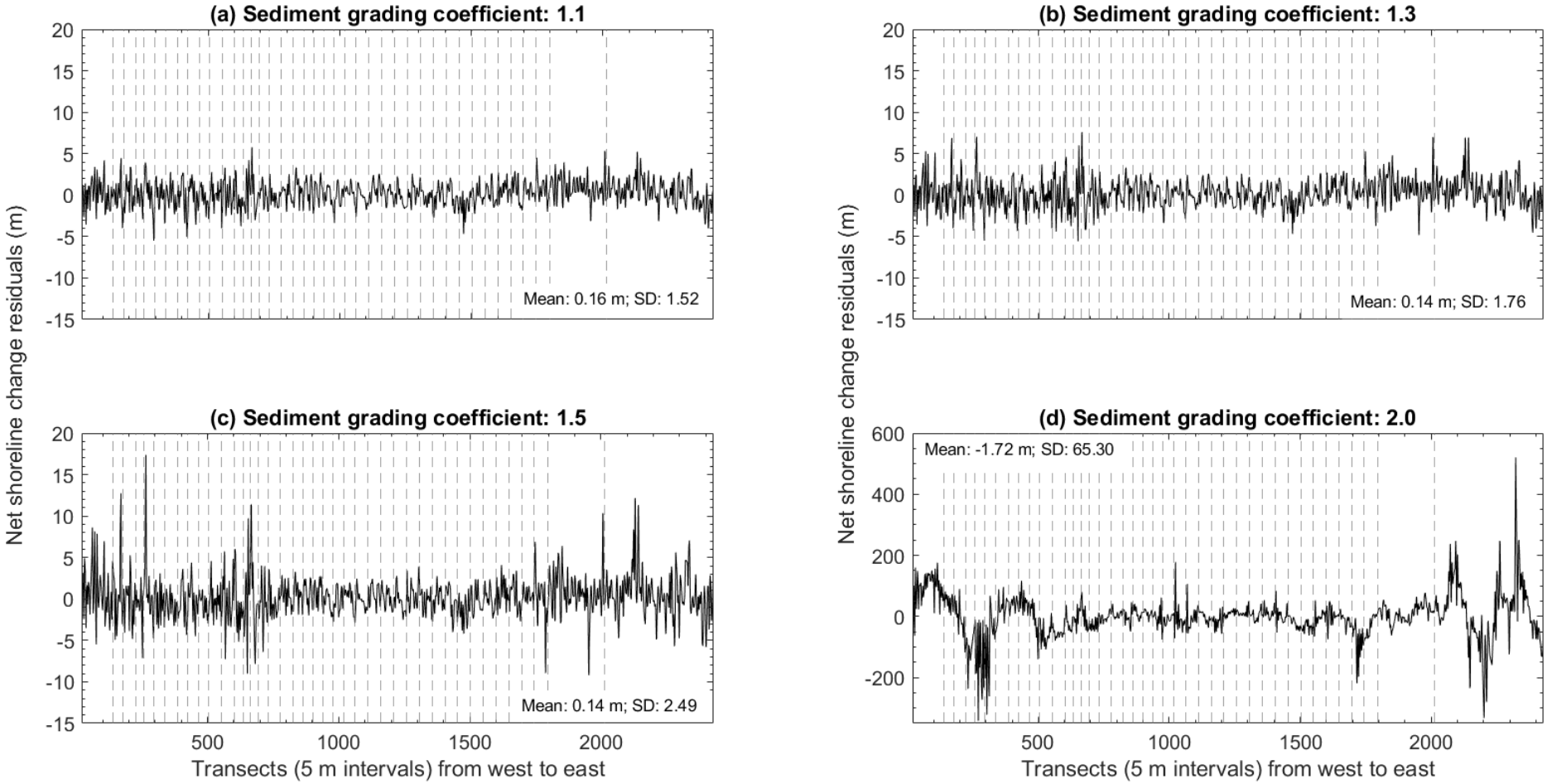

Fig. A9.5 Net shoreline change residuals from an increase in sediment grading coefficient in the New York test site. Vertical dashed lines indicate groyne locations. SD is the standard deviation. Net shoreline change residuals in (a) to (d) are the difference between net shoreline change observed and predicted from 01-Jan-2014 to 01-Feb-2016. Note the difference in y axis in (d). Net shoreline change residuals obtained in groyne transects are excluded from the above plots and statistics.

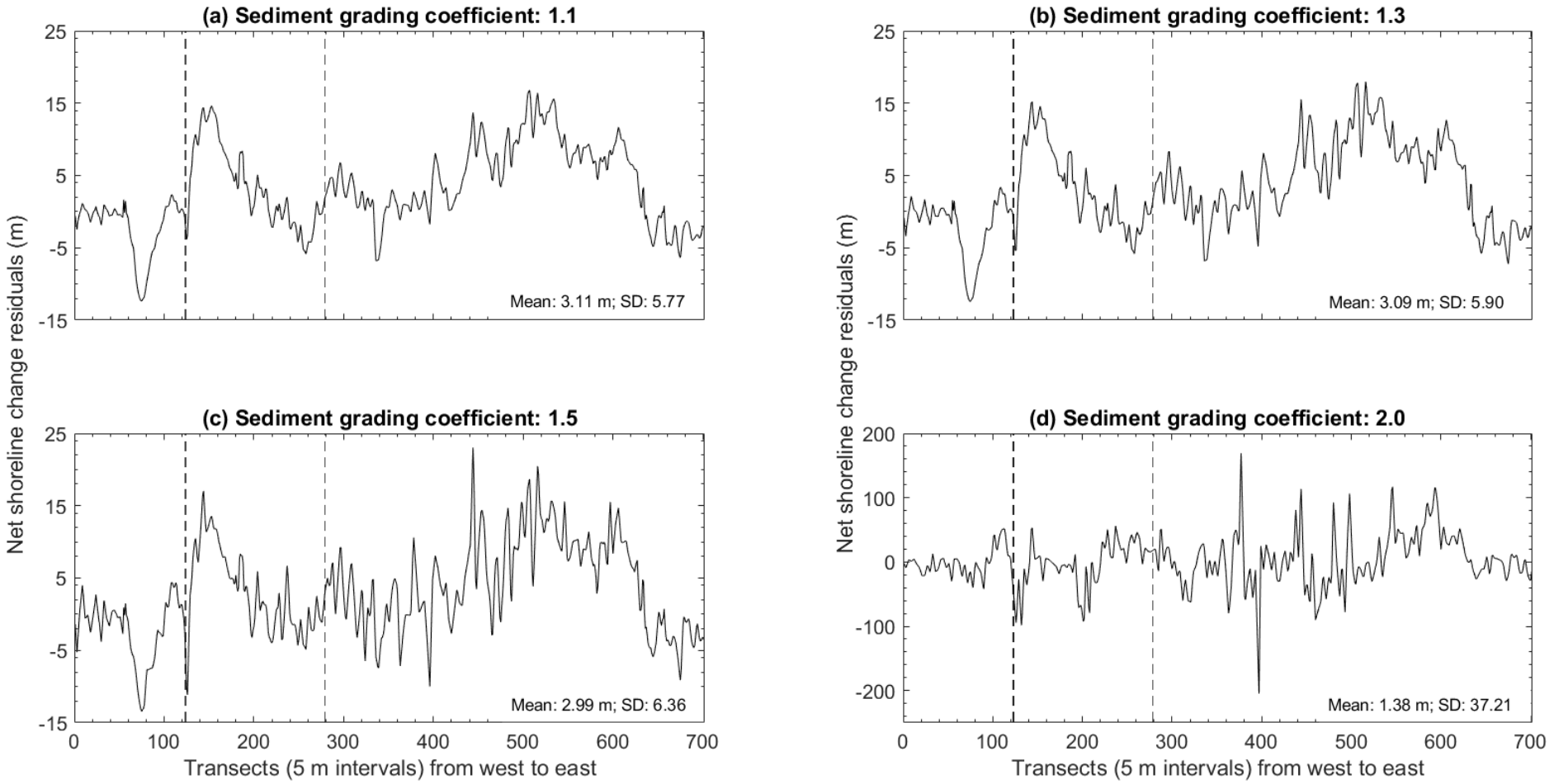

Fig. A9.6 Net shoreline change residuals from an increase in sediment grading coefficient in the Puerto Rico test site. Vertical dashed lines indicate groyne locations. SD is the standard deviation. Net shoreline change residuals in (a) to (d) are the difference between net shoreline change observed and predicted from 10-Oct-2014 to 31-Mar-2016. Note the difference in y axis in (d). Net shoreline change residuals obtained in groyne transects are excluded from the above plots and statistics.

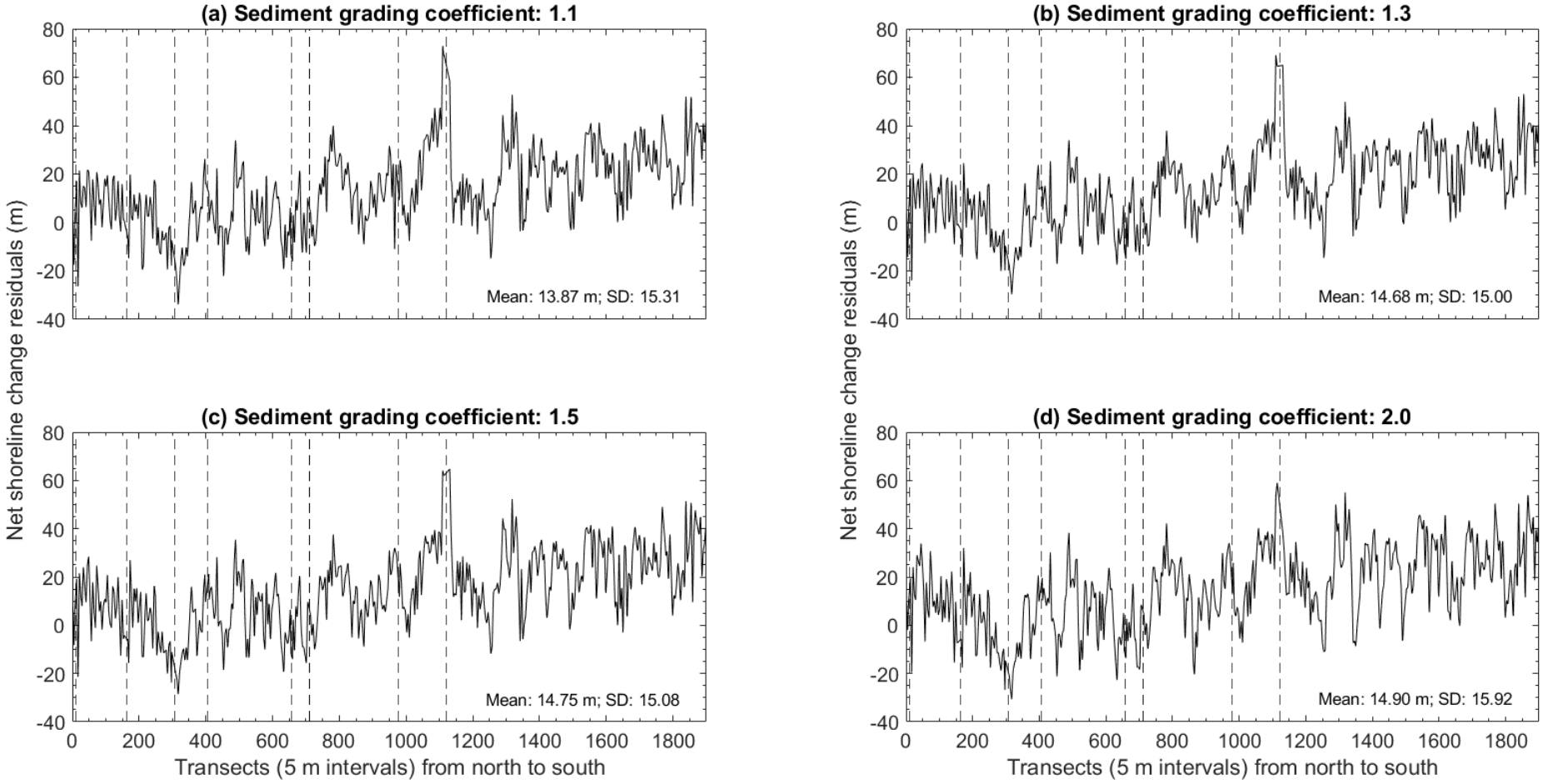

Fig. A9.7 Net shoreline change residuals from an increase in sediment grading coefficient in the Southern California test site. Vertical dashed lines indicate groyne locations. SD is the standard deviation. Net shoreline change residuals in (a) to (d) are the difference between net shoreline change observed and predicted from 01-Jan-2009 to 02-Aug-2011. Net shoreline change residuals obtained in groyne transects are excluded from the above plots and statistics.

A10 MIKE21 sensitivity to weir coefficient ($m^{1/2}/s$) of hard defences

A10 graphically illustrates the sensitivity of MIKE21 net littoral drift and net shoreline change predictions to increasing weir coefficients ($m^{1/2}/s$) in each test site.

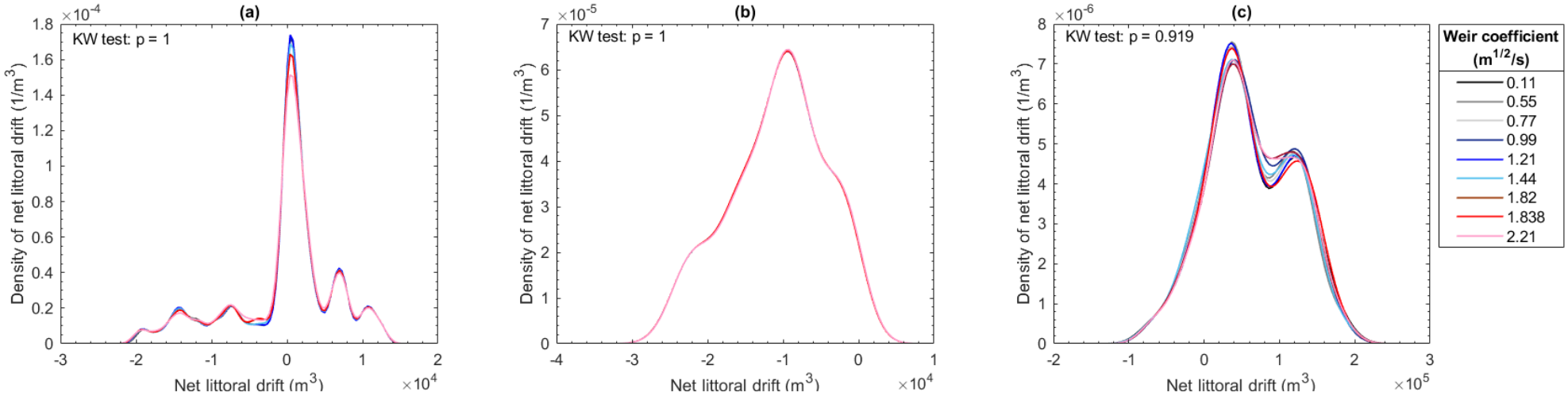

Fig. A10.1 Kernel density plots of net littoral drift predictions in response to increasing weir coefficients ($m^{1/2}/s$) in the New York (a), Puerto Rico (b), and Southern California (c) test site. In Fig. A10.1, net littoral drift predictions are from 01-Jan-2014 to 01-Feb-2016 in the New York test site, 10-Oct-2014 to 31-Mar-2016 in the Puerto Rico test site, and 01-Jan-2009 to 02-Aug-2011 in the Southern California test site. The Kruskal-Wallis (KW) test indicates no significant differences in net littoral drift predictions from increasing weir coefficients ($m^{1/2}/s$) in each test site.

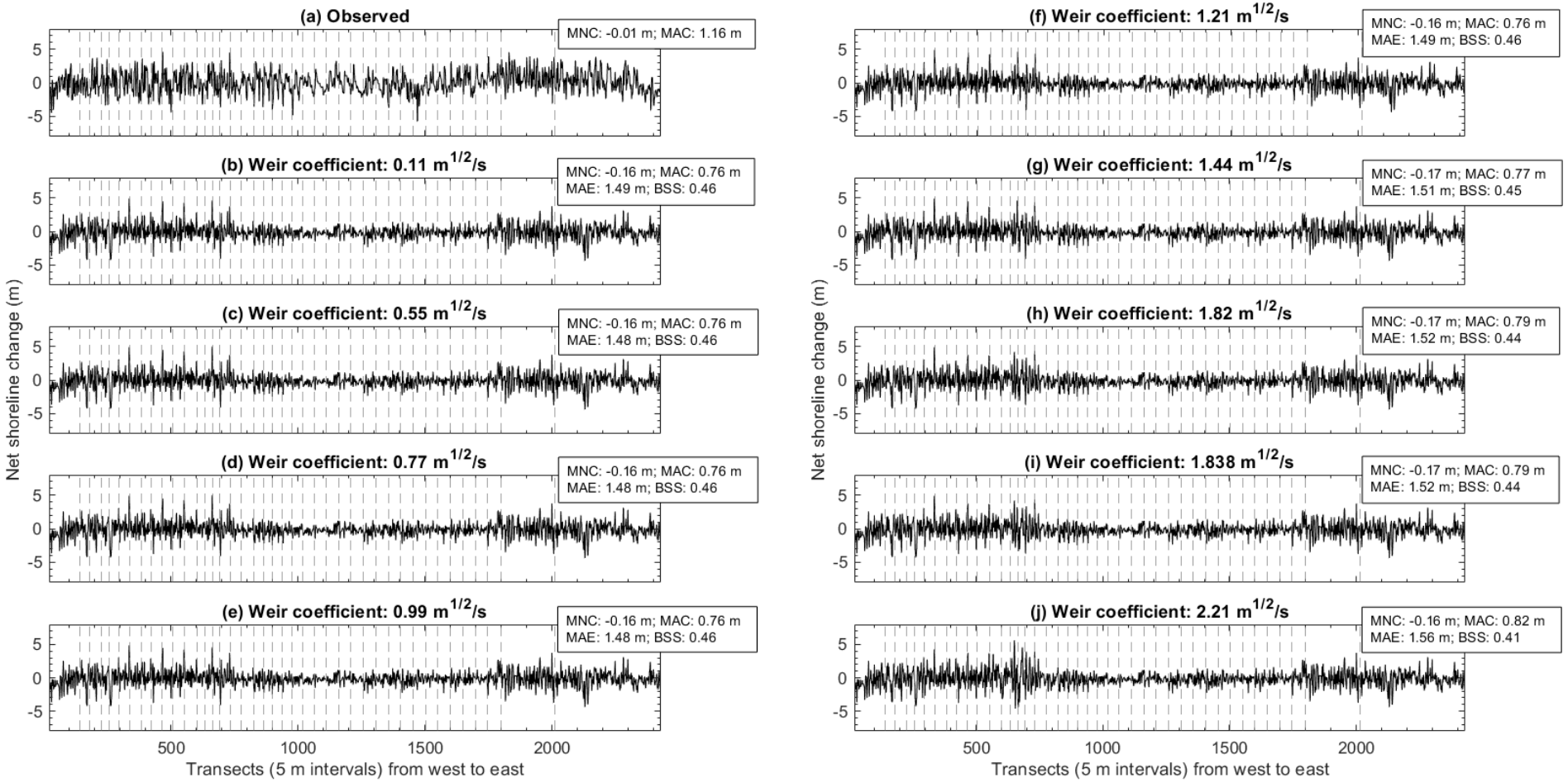

Fig. A10.2 Net shoreline change (01-Jan-2014 to 01-Feb-2016) observed and predicted in response to increasing weir coefficients ($m^{1/2}/s$) in the New York test site. Vertical dashed lines indicate groyne locations. MNC is mean net change, MAC is mean absolute change, MAE is mean absolute error, and BSS is Brier Skill Score. Net shoreline change observed and predicted in groyne transects are excluded from the above plots and statistics.

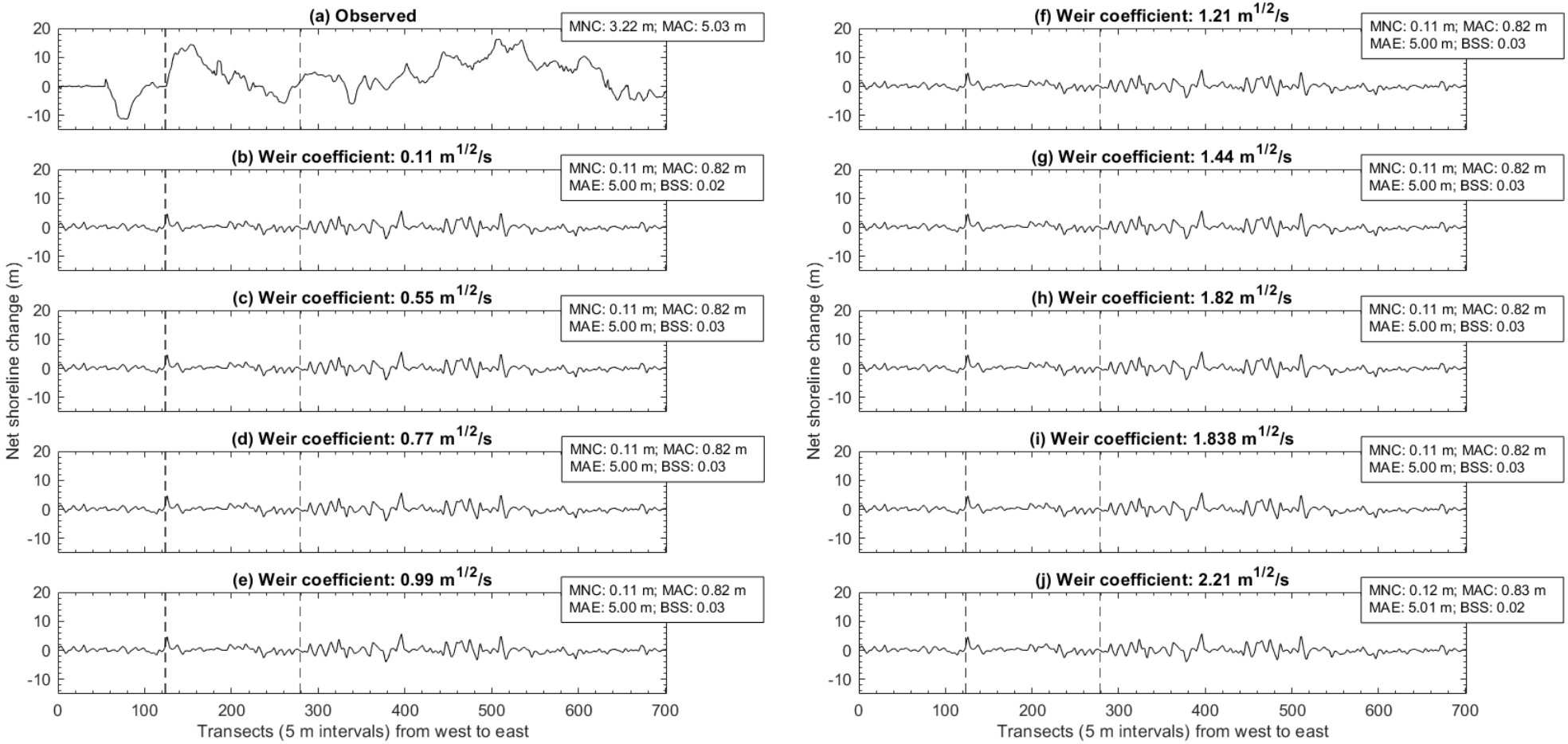

Fig. A10.3 Net shoreline change (10-Oct-2014 to 31-Mar-2016) observed and predicted in response to increasing weir coefficients ($m^{1/2}/s$) in the Puerto Rico test site. Vertical dashed lines indicate groyne locations. MNC is mean net change, MAC is mean absolute change, MAE is mean absolute error, and BSS is Brier Skill Score. Net shoreline change observed and predicted in groyne transects are excluded from the above plots and statistics.

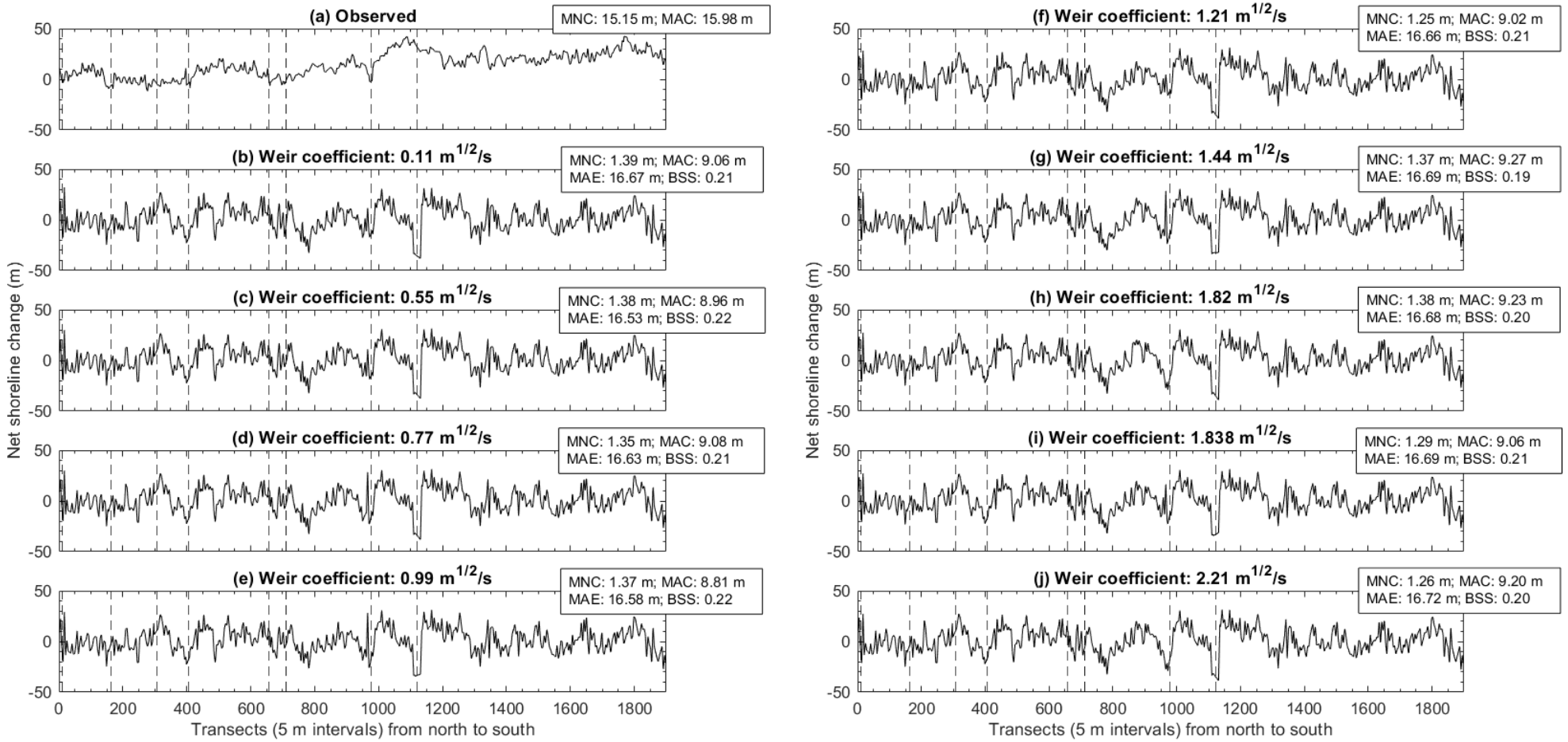

Fig. A10.4 Net shoreline change (01-Jan-2009 to 02-Aug-2011) observed and predicted in response to increasing weir coefficients ($m^{1/2}/s$) in the Southern California test site. Vertical dashed lines indicate groyne locations. MNC is mean net change, MAC is mean absolute change, MAE is mean absolute error, and BSS is Brier Skill Score. Net shoreline change observed and predicted in groyne transects are excluded from the above plots and statistics.

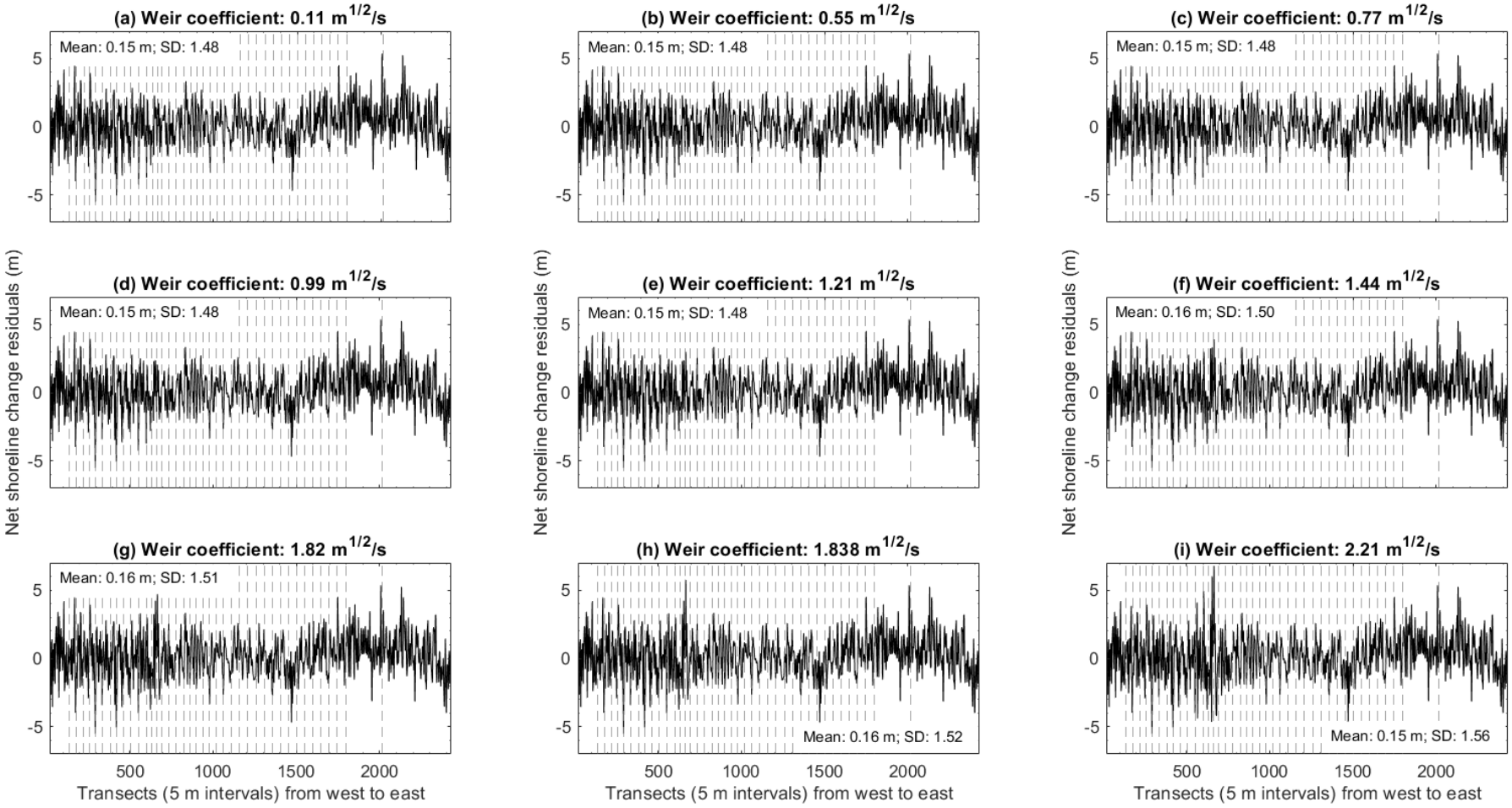

Fig. A10.5 Net shoreline change residuals from increasing weir coefficients ($m^{1/2}/s$) in the New York test site. Vertical dashed lines indicate groyne locations. SD is the standard deviation. Net shoreline change residuals in (a) to (i) are the difference between net shoreline change observed and predicted from 01-Jan-2014 to 01-Feb-2016. Net shoreline change residuals obtained in groyne transects are excluded from the above plots and statistics.

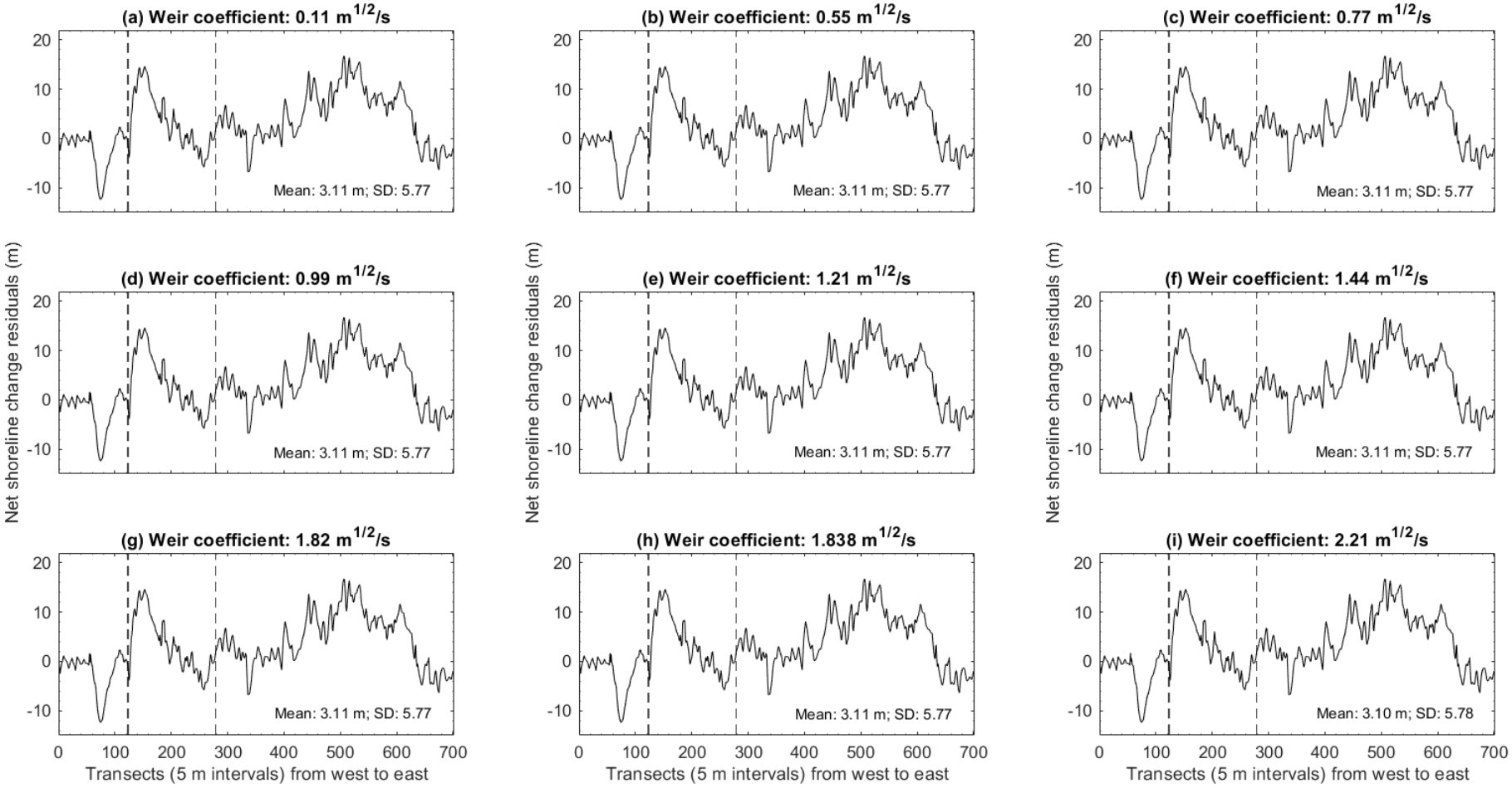

Fig. A10.6 Net shoreline change residuals from increasing weir coefficients ($m^{1/2}/s$) in the Puerto Rico test site. Vertical dashed lines indicate groyne locations. SD is the standard deviation. Net shoreline change residuals in (a) to (i) are the difference between net shoreline change observed and predicted from 10-Oct-2014 to 31-Mar-2016. Net shoreline change residuals obtained in groyne transects are excluded from the above plots and statistics.

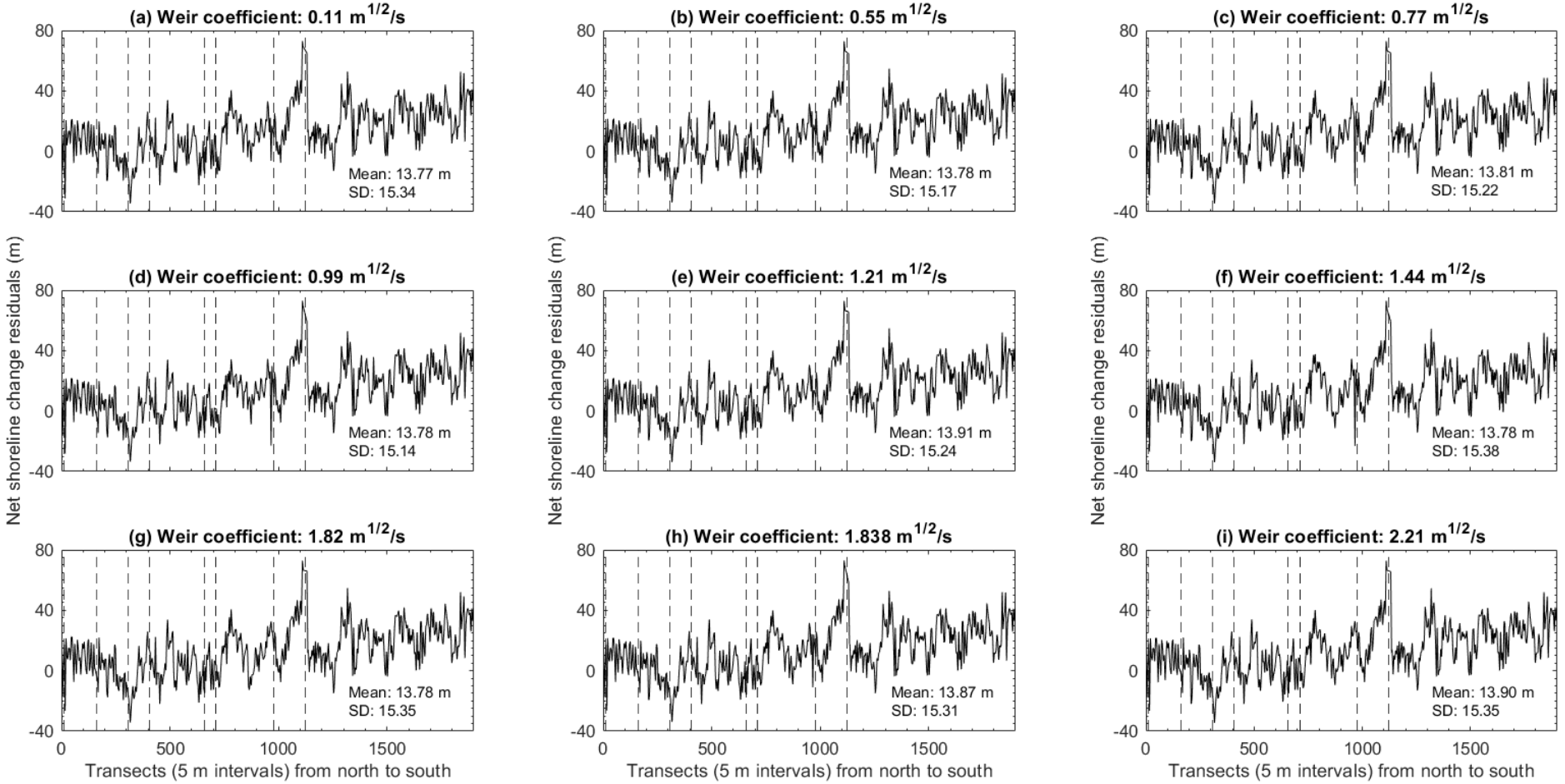

Fig. A10.7 Net shoreline change residuals from increasing weir coefficients ($m^{1/2}/s$) in the Southern California test site. Vertical dashed lines indicate groyne locations. SD is the standard deviation. Net shoreline change residuals in (a) to (i) are the difference between net shoreline change observed and predicted from 01-Jan-2009 to 02-Aug-2011. Net shoreline change residuals obtained in groyne transects are excluded from the above plots and statistics.